/
Article / Book Information

（ ）	
Title(English)	Physical modelling of wave propagation from ground vibration and vibration countermeasures
（ ）	
Author(English)	
（ ）	: （ ）, : , : 5392 , :2003 3 26 , : , :
Citation(English)	Degree:Doctor (Engineering), Conferring organization: Tokyo Institute of Technology, Report number: 5392 , Conferred date:2003/3/26, Degree Type:Course doctor, Examiner:
（ ）	
Type(English)	Doctoral Thesis

PHYSICAL MODELLING OF

WAVE PROPAGATION FROM GROUND VIBRATION AND

VIBRATION COUNTERMEASURES

ITOH Kazuya

DISSERTATION

submitted in partial fulfillment of the requirements for the degree of

DOCTOR OF ENGINEERING

at

TOKYO INSTITUTE OF TECHNOLOGY

2003

ACKNOWLEDGMENTS

<div align="right">Kazuya ITOH</div>

ABSTRACT

In today's world, the railways have become one of the most advanced and fast developing branches of transportation. In recent years, development of railways for high-speed train is growing rapidly throughout Europe, North America, and East Asia. The dramatic increase in speeds of modern passenger trains poses an environmental problem. If a high-speed train is running in the urban area, ground vibration and noise generated by passages of high-speed train will become the high incidence of environmental problem. There have been only a few studies conduced on how to use countermeasures to reduce the vibration and even fewer have been adopted in the field. In order to reduce vibration induced by high-speed train, several issues such as generation of vibration at the source, propagation of vibration through the media in the foundation, and the interaction between waves and structures must be considered. As for this problem, most of the previous studies had been numerical analysis or field measurement. However, the results of field measurement could not take advantage of numerical analysis because a complex boundary condition and very local soil parameters were contained. In order to estimate vibration reduction installing the wave barrier by numerical analysis, it is necessary to get the physical data which has clear boundary conditions and soil parameters. For this purpose the centrifuge model test was carried out in this study. It uses small-scale models subjected to a centrifugal acceleration of many times the gravitational acceleration to simulate prototype problems that are difficult to test at full scale. In this study, the newly development of two kind of systems, which can simulate wave propagation from the surface ground vibration and its countermeasures, are described. In addition, to investigate the effect of produced wave barrier on the reduction of vibration, the measurements of ground vibration were carried out before and after the measures.

This thesis is divided into 7 chapters including the introduction and the conclusions.

Chapter 1 is the introduction of this thesis.

Chapter 2 describes the literature review of studies on the ground vibration problems. The initial part of this chapter presents wave propagation studies to various approaches, numerically,

theoretically, and experimentally. The review of vibration regulations and vibration countermeasures at the transmitting path and at the vibration source is also described in this chapter.

Chapter 3 describes development of equipment for centrifuge testing. The experimental techniques theory of centrifuge modelling is briefly reviewed.

Chapter 4 describes development of the multiple ball-dropping system to study wave generation and propagation from surface ground vibration source in a centrifuge. This system can simulate not only point load but also quasi-moving loads caused by high-speed trains ruing through a viaduct. The effectiveness of a range of wave barriers was investigated using various geometry and materials, and it was found that softer barriers are generally superior to stiffer barriers, and that the geometry of the barrier significantly affects the motion of the barrier. In addition, this chapter describes the results of a series of centrifuge model tests to investigate the effect of a vibration reduction method which uses a crumb rubber-modified asphalt (CRMA) layer at the vibration source and an EPS barrier at the transmitting path. It was found through centrifuge tests that CRMA, which is a material with high shear stiffness and damping ratio, can reduce the vibration away from the source especially when working together with EPS barrier. It was also suggested that the superposition of the waves could be applicable to cases of moving load, provided that the factor of safety for bearing capacity of foundation is sufficiently high.

Chapter 5 describes newly development of the Centrifugal Vibration Testing System to investigate wave generation and propagation from shallow foundation in a centrifuge. The effectiveness of a range of wave barriers was investigated using various materials, frequencies, and distances from source. It was discovered that the range over one wave length depth had effectiveness in reducing vibration in both softer and stiffer barriers, and the range under the wave length depth had effectiveness in reducing vibration with softer barrier by the inputted frequency as the case may be. In addition, the effect of vibration countermeasures at the vibration source on the reduction of vibration was investigated using various materials and frequencies. It was found that CRMA can reduce the vibration away from the source.

Chapter 6 considers newly development of wave barrier materials, new process for making wave barrier, and effect of making wave barrier on the reduction of vibration. The first of this chapter describes the development of wave barrier, which is called "EPS beads modified cement-improved

column". This wave barrier can be satisfied with some performance requirements (e.g. reliability of reducing vibration, pump-ability, economically etc.). After that the way of making wave barrier is described. The rest part of this chapter gives the effect of wave barrier on the reduction of vibration, and it was found that the effectiveness in reducing vibration with high frequency.

Chapter 7 is the conclusions derived from this study.

CONTENTS

6. Field Test of Isolation of Ground Vibration by EPS beads Modified Cement-Improved Column

LIST OF FIGURES

LIST OF TABLES

CHAPTER 1

INTRODUCTION

1.1 BACKGROUND AND OBJECTIVES OF RESEARCH

Ground-borne vibration has existed ever since the development of urban road and railway network. Vibration generated by the moving traffic propagates through the ground and into buildings, resulting in unacceptable levels of internal noise and vibration. In the late 1950's and 1960's, serious industrial pollution overrode Japan in the period of rapid economic growth. Then, Japanese environmental policies was enacted "Basic Law for Environmental Pollution Control" to combat this situation in 1967. For the purpose of this law, "environmental pollution" means, among interference with environmental conservation, air pollution, water pollution, soil contamination, noise, vibration, ground subsidence and offensive odors affecting an extensive area as a result of business and other human activities, which cause damage to human health or the living environment. These were called "The Seven Typical Pollution". Based upon the basic law, specific laws which related to each problem above were established, as shown in Table 1.1. The number of the complaint due to pollution in 1972 is shown in Figure 1.1 (Environmental Dispute Coordination Commission, 2000). At that time, vibration and noise were totaled together, and this type of pollution occupied more than 30 % of all the complaints. In 1976, the Vibration Regulation Law which regulates some environmental vibrations was established. It controls ground vibrations which stem from factors, such as workplaces, construction work and road traffic, but does not control vibrations from railways. Figure 1.2 shows trends of complaint numbers of seven pollution by the fiscal year from 1972 to 1999 (Environmental Dispute Coordination Commission, 2000). From the viewpoint of vibration and noise, the number of complaint decreases gradually with time. However there was the high rate to occupy in the all from 1972 to 1996. The ground vibration problem has emerged as environmental pollution such as an unpleasantness given to the human being.

Others
9216

Air pollution
11873

Offensive odors
17516

Ground subsidence
68

Water pollution
13453

Soil contamination
593

Noise, Vibration
23812
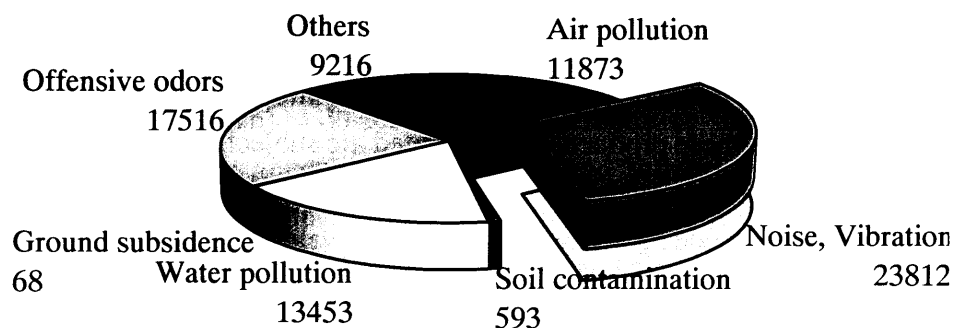
Figure 1.1 The number of the complaint due to pollution in 1972 (Environmental dispute coordination commission, 2000)

Table 1.1 The enforcement date of each regulation law

Pollution	Main Law	Effective on
Air pollution	Air Pollution Control Law	June 10, 1968
Water pollution	Water Pollution Control Law	December 25, 1970
Soil contamination	Agricultural land soil pollution prevention Law	December 25, 1970
Noise	Noise Regulation Law	June 10, 1968
Vibration	Vibration Regulation Law	June 10, 1976
Ground subsidence	Industrial Water Law	June 11, 1956
Offensive odors	Offensive Odor Control Law	June 1, 1971
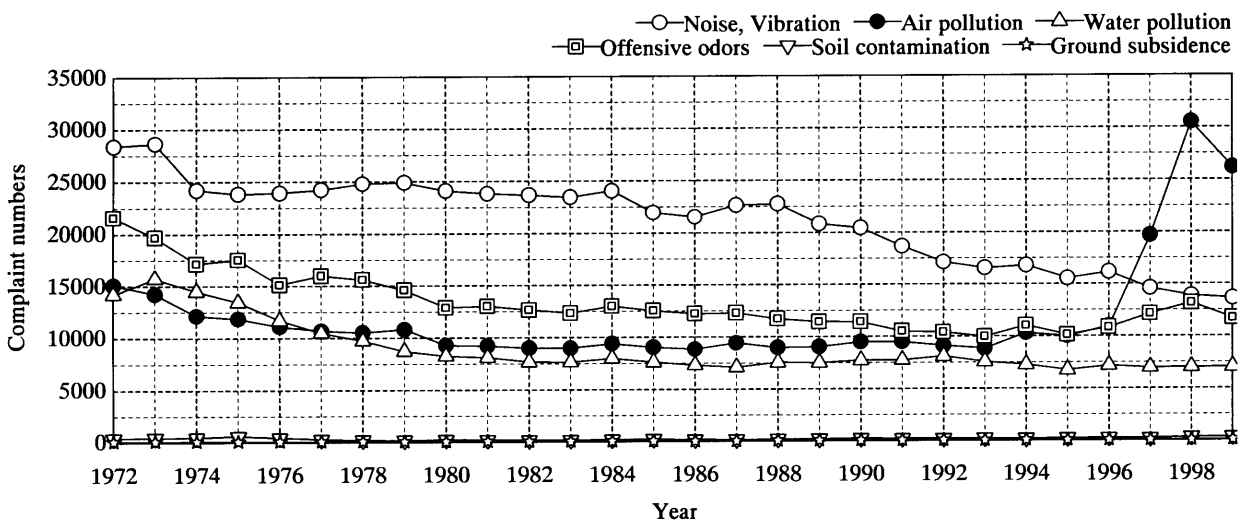
Figure 1.2 The trend of complaint number of seven pollution by the fiscal year from 1972 to 1999 (Environmental dispute coordination commission, 2000)

In addition, we have newly two problems in resent years. One is the problems about regulations requiring strict tolerances for vibration. Because the fabrication of precision electronic products, such as semiconductors and liquid crystal displays, requires extremely precise work, so the building that house factories where these products are fabricated are subject to regulations requiring strict tolerances for vibration. With the recent rapid increase in precision engineering and combined with an advance to larger-sized products, technology must be developed to provide economic solutions to protect the factories.

The other is the problem caused by high-speed train. Because development of railway tracks for high-speed trains is growing rapidly throughout Europe, North America, and East Asia. Figure 1.3 shows European high-speed network in 2002 (International union of railway, 2002). The thick
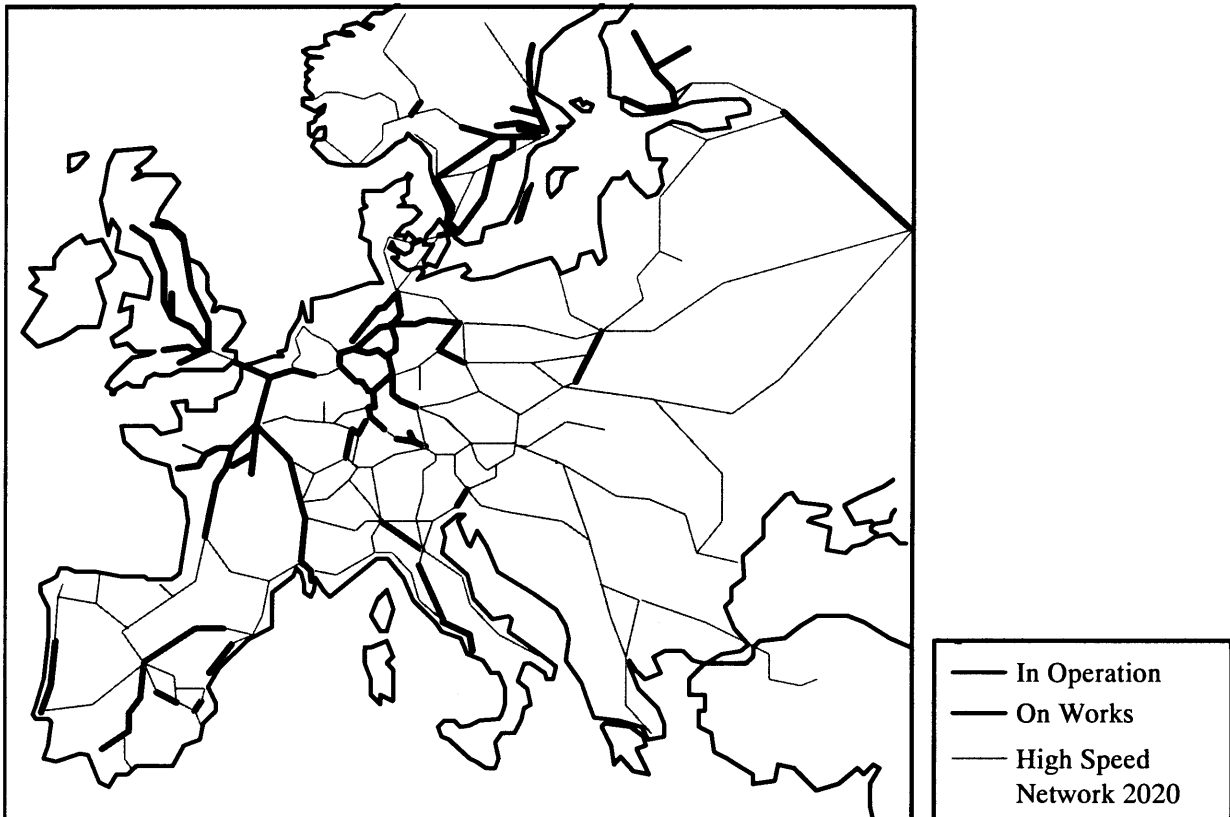
Figure 1.3 European high-speed train network in 2002 (International Union of Railway, 2002)

black lines are high-speed railways that are already in operation, the thick gray lines are those under construction, and thin gray lines are the ones to be finished by 2020. If the European high-speed union carries out future projects, the high-speed train network will be comfortable and convenient to the passenger's trip. In resent years, interest in high-speed train has increased significantly in the U.S.A. Amtrak has already started high-speed train service from Boston – New York – Washington D. C in 1999. Figure 1.4 presents the U.S. national plan using high-speed train (US Department of Transportation, 2002). For example, California high-speed rail authority is planning a 1100 km, $25 billion project linking San Francisco – Los Angeles – San Diego at a maximum speed of 350 km/h. In Japan, the Shinkansen network totals over 1850 km connecting Japan's major metropolitan areas and carries over 300 million passengers every year. Other Asian nations are now pursuing high-speed systems of their own. A new high-speed rail system is under construction in Korea and in Taiwan with another one under design in China. Especially, there is necessity for Taiwan High-Speed train (Taiwan Shinkansen) to do countermeasures requiring strict tolerances for vibration, because the train passes two science parks (Hsinchou and Tainan) as shown in Fig. 1.5. In the future, magnetically levitated (maglev) railway which is able to run with a speed of over 500 km/h as 'high-speed train in the future plan of 21 century' has made practicable in Germany and in Japan. High-speed trains are a safe, efficient, reliable and pleasurable way to travel between destinations that are generally from 100 km to 500 km apart. It must be the next major transportation means for passengers in the world. However ground vibration which is caused by high-speed train generates more pollution to the humans who live along railway lines.

Figure 1.4 The U.S. national plans using high-speed train (US Department of Transportation, 2002)
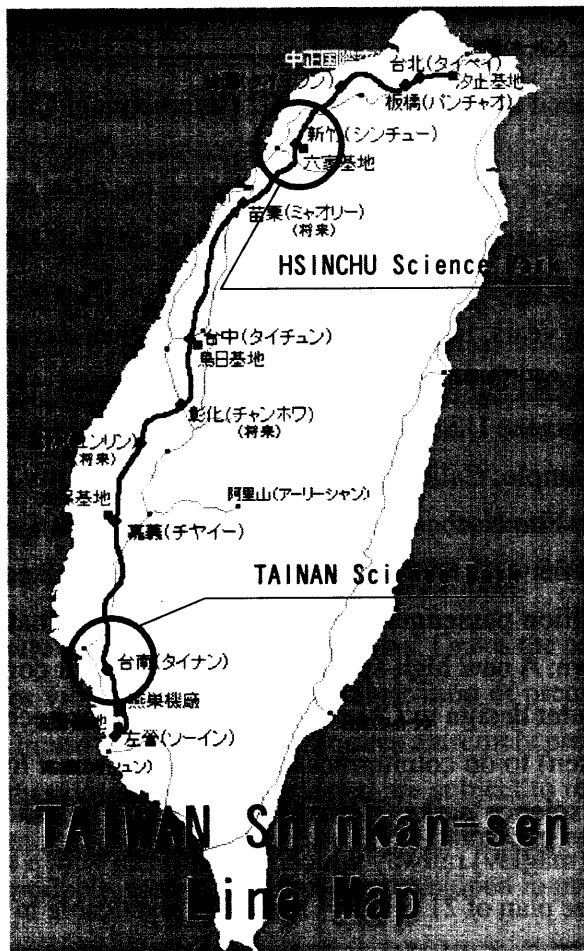
Figure 1.5 Relationship between Taiwan Shinkansen line map and location of two science parks

Basically three different approaches to the problem of ground-borne vibration control can be recognized, i.e. theoretical, numerical and experimental methods. While most of the available formulas for prediction of vibration levels are empirical, and based on field measurements, some interesting and important aspects can be described by analytical models. But prior attempts to study effective parameters in wave isolation problem have been inconclusive because the data examined lacked variables vital to the vibration reduction. The objectives of the research presented in this dissertation are:

1. To reappraise the ground vibration problems and vibration countermeasures proposed by past researchers through the literature review, and to recognize necessity to carry out the centrifuge model test.

2. To develop the system to simulate the wave propagation from vibration source at the ground surface in order to verify the behavior of wave propagation and the effect of various countermeasure methods on the reduction of vibration. In this study, new systems which can generate the various vibration forms, such as impact point load, moving load, and cyclic load, are developed.

3. To propose the effective parameters deduced from centrifuge model test, in which the parameters of various countermeasures at the transmitting path (material, embedded depth, geometry, and radius of barrier) and the vibration source (material) are varied.

4. To propose an effective method to construct wave barrier at a construction site adjacent to public transportation structures such as train lines. In this study, new development of wave barrier material to be satisfied with requirements such as reliability of the reducing vibration, pump-ability, and economically, etc. and a newly developed method for making wave barrier, which can excavate the ground and construct wave barrier at the same time, are investigated.

1.2 ORGANIZATION OF THE DISSERTATION

This dissertation consists of seven chapters:

Chapter 1: *Introduction* - includes background and objectives of the research and the organization of the dissertation.

Chapter 2: *Literature Review of Ground Vibration Problems* – describes the literature review of studies on the ground vibration problems. The initial part of this chapter presents wave propagation studies to various approaches, numerically, theoretically, and experimentally. The review of vibration regulations and vibration countermeasures at the transmitting path and at the vibration source is also described in this chapter.

Chapter 3: *Centrifugal Modelling Test* – reviews briefly theory of centrifuge modelling and then, developed of equipment for centrifuge testing and the experimental techniques are described.

Chapter 4: *Wave Propagation and its Isolation Method using Multiple Ball-Dropping System* – presents details of newly developed the multiple ball-dropping system, and centrifuge model test results on wave propagation in various input point loads and vibration countermeasures which use various materials at the transmitting path and the vibration source are presented.

Chapter 5: *Wave Propagation and its Isolation Method using Centrifugal Vibration Testing System* – describes details of newly developed the shaker system, and centrifuge model test results on wave propagation in various inputted frequencies and two types vibration countermeasures, which are vibration reduction methods at the transmitting path and the vibration source, are presented.

Chapter 6: *Field Test of Isolation of Ground Vibration by EPS beads Modified Cement-Improved Column* – describes details of newly mixed wave barrier materials called "EPS beads modified cement-improved column". After that a field test is presented, to investigate the effect of produced wave barrier on the countermeasures with "EPS beads modified cement-improved column".

Chapter 7: *Conclusions* - includes a summary of the dissertation and its major findings.

CHAPTER 2

LITERATURE REVIEW OF GROUND VIBRATION PROBLEMS

2.1 HISTORIES OF GROUND VIBRATION PROBLEMS

Ground vibration problems deal with various kinds of vibration sources on the surface ground. Some of more well-known studies on wave propagation in elastic solid are summarized in Table 2.1 (Ohbo, 1980). Various closed form solutions have been used for studying the problems of wave generation and propagation since Cauchy (1830). Among these researches, Lamb (1904) particularly solved those of elastic wave in half-space elastic body from a free surface vibration source. One of the applications of elastic wave propagation theory to seismology is to synthesize a seismogram. This kind of study is known as the Lamb's problem. He laid the basis on the elastic theory and subsequently extensive analytical and numerical studies have been undertaken. A noteworthy early example was Biot (1956), who carried out systematic analyses about propagation of elastic waves in a fluid-saturated porous solid. Halpern and Christiano (1986) and Syo and Kitamura (1988) have used his theoretical framework in their analyses.

2.2 REVIEW OF WAVE PROPAGATION STUDIES

Ground transmitted waves generated by machine foundations, traffic, or blasting may produce excessive ground vibrations which cause distress to adjacent structures and people. This can be a major problem in not only densely populated urban areas but also structures housing sensitive machinery. Especially, development of high-speed train is growing rapidly throughout Europe, North America, and East Asia (above Fig.1.3 and Fig. 1.4). Train speeds have now increased to over 300 km/h (=83.3 m/s), and demands for even higher speeds to shorten travel time are rising. This requires straight configuration railway lines that may render crossing soft soil areas unavoidable. Peat, organic clays, and soft marine clays may have shear-wave velocities as low as 30-40 m/s. Sites with such low shear-wave velocities are particularly susceptible to excessive vibration from high-speed trains. Such large motions are not only worrisome for their environmental impacts and human disturbance, but also raise concerns about the running safety of the trains, degradation of the embankment and foundation soil, fatigue failure of the rails, and disruption of power supply to the trains.

This section divides the past researches into four approaches; numerical approach, field measurement, physical modeling, and empirical/theoretical prediction of the wave propagation, here after.

Table 2.1 Historically famous studies and their contents (after Ohbo, 1980)

Year	Name	Contents
1830	Cauchy	Investigation of the propagation of plane wave through a crystalline medium
1831	Poisson	Solving the initial value problem by synthesis of simple harmonic solution, and finding the two types of waves such as P- and S-waves, and P-waves speed is $\sqrt{3}$ times the S-waves speed for his restricted model.
1839	Green	Investigation of the propagation of a plane waves through a crystalline medium.
1849	Stokes	Investigation of elastic wave motion due to a body force in an infinite medium.
1887	Rayleigh	Mathematical finding of the surface wave generated by a pair of P- and SV-waves.
1904	Lamb	The first study of the propagation of four pulses, such as surface normal line and point load sources, and the buried line and point sources of dilatation, in an elastic half space.
1911	Love	Mathematically prediction of the surface wave generated by an SH-wave.
1925 1930	Nakano	Investigation of Rayleigh wave in a half space due to internal source of two- (1925) and three-dimensional (1930) model.
1932	Smirnov Sobolov	Application of the functional analysis to transient elastodynamic problems.
1939	Cagniard	Application of the complex analysis to transient elastodynamic problems.
1949	Lapwood	Investigation of Lamb's formal solutions involving internal step input excitation.

2.2.1 *Numerical approach*

A number of researchers have used various numerical techniques to study the wave propagation problem. A good review of this literature is given by Ahmad and Al-Hussaini (1991) and Hung and Yang (2001). The investigation about newly numerical techniques and moving load simulation are introduced in this section. Further, wave propagation simulations using numerical approaches have been also used in the fields of earthquake engineering and seismology problems. In there fields, new numerical techniques have been developed to estimate the earthquake ground motion in 3D

· local models excited by external sources in resent years. The pseudospectral method (e.g., Kosloff et al., 1984; Reshef et al., 1988; Furumaru et al., 1998) is a high-accuracy numerical modelling technique that requires less computer memory and computation time than the traditional techniques such as the finite difference method. Takenaka et al. (1999) proposed an efficient approach of an economical pseudospectral method for calculation of wave fields in models symmetric with respect to vertical plane or two orthogonal vertical planes. On the other hands, all-in-one method, which is including source, path and site effect, leads to extreme needs of computer memory and time. An effective bypass is combining appropriate techniques for particular problems with hybrid methods. Hatayama and Fujikawa (1998) used boundary element method (BEM) with normal modes to evaluate the excitation of secondary surface waves in 3D basin models without waves that present in the complete 3D excitation of the secondary surface waves. Zhang et al. (1998) presented a 2.5D elastodynamic scattering formulation that evaluates the 3D response of 2D scatterers, including topography. Oprsal and Zahradnik (2001) developed a 3D FD displacement hybrid method for an irregular rectangular grid. Their hybrid method saves computer memory and time, especially in cases with high frequency content, high material parameters contrasts, and large scale difference between the local and regional models.

Railway-induced ground vibrations are one of the major sources of noise and vibration pollution in urban area. For quantitative evaluation and prediction of the vibration levels induced by trains, theoretical studies on moving load problems are necessary. Modelling the wave field generated by moving source and its influence on building is a major update issue in evaluating vibration generated by car and train traffics. In the past moving sources have been studied for simple problems. Eason (1965) studied the three dimensional steady state problems for a uniform half-space subjected to forces moving at uniform speeds. Besides the point force, Eason also considered the case of moving forces distributed over a circular or rectangle area. The governing equation was solved by means of integral transform, with the resulting multiple integrals reduced to single finite integrals for the subsonic case. Gakenheimer and Miklowitz (1969) derived an expression for the transient displacements in the interior of an elastic half space under a normal point load that was suddenly applied and then moved at a constant speed along the free surface. All the subsonic, transform, transonic, and supersonic cases were studied, with the inverse transform evaluated using the Cagniard-deHoop's method (deHoop 1959). The steady-state response for the same problem was also given by Fryba (1972) in an integral form. Using a method similar to Eason's studied the response due to an oblique moving point load applied on the free surface. For more complex model, therefore, it is necessary to develop an effective numerical method. In these days, numerical methods such as a finite element method (FEM) or a BEM may be available for the problem with arbitrary geometrical shapes. Takemiya and Goda (1997) analyzed an embankment type track over lying layered soils for a harmonic moving load of a constant speed on it using the hybrid solution method which was obtained by using the BEM for the layered soils and the FEM for the embankment. Their computer simulation cleared the vibration features of embankment ant the nearby ground with respect to the dynamic interaction between embankment and underlain layered soils, and the wave dispersion characteristics of the layered soils. Generally, the numerical method applied to a

full scale of three dimensional problems still requires huge capacity and time in computation (e.g. Chouw and Pflanz, 2000). As for this problem, Hirose and Hoshi (2001) and Hirose (2002) developed a quasi two dimensional boundary element method. Although a moving load has a three dimensional effect, a track ground system such as track or tunnel structures can usually be treated as a two dimensional model with a uniform cross section along the moving direction of a train. Such a problem can be formulated in a quasi two dimensional space, where three dimensional solutions are obtained as superposition of two dimensional ones with respect to wavenumbers in the direction of the moving load.

2.2.2 *Field measurement*

By means of filed measurements, the response of exciting installations can be obtained directly. When sufficient measurements are taken, a data base can be compiled, based on which the results can be analyzed statistically. These results serve as a basis for predicting vibration levels for similar installations. Okamura and Kuno (1991) studied the effects of various factors on railway noise and vibration through a regression analysis of field data obtained at 79 sites along 8 traditional railway lines in an urban area in Japan. Among the six factors they used to explain the vibration peak level, i.e., the distance, railway structure, train type, railway speed, train length and background vibration, they found that the influence of distance was the greatest. The second prominent factor was background vibration, which was considered to be a characteristic of the soil properties at each site. They also reported that the influence of train speed was not so obvious. This observation can be attributed to the fact that the field data were collected from traditional railways, whose running speeds were generally under 100 km/h, far lower than the Rayleigh wave speed for typical soils. Regarding the influence of railway structures, the vibration levels for the concrete bridges and retaining walls are lower than those for at-grade structures. As for field data caused by high speed train, Dagrande and Lombaert (2000) presented a few of the field data that had been obtained in studies done on Belgian railway. Field tests of the Thalys HST (high-speed train) track between Burusseals and Paris have been used to measure free field vibration and track response during passage of a Thalys HST at speeds varying between 223 km/h and 314 km/h. A major shortcoming of the present data set is that, due to time and budget limitations, no in situ experiments have been made to determine the subgrade stiffness of the track. Only limited data are also available on the stratification of the soil and the variation of dynamic soil characteristics with depth, especially material damping.

2.2.3 *Physical modeling approach*

Compared with the numerical approaches, there were few researchers who took experimental approaches in this problem. Because while full-scale field tests are practically too expensive to be carried out, small-scale model test results obtained in 1 G environments often pose a question of how to interpret their data and to deduce the implications under prototype situations. One obvious reason is that small-scale model test in 1 G is impossible to satisfy scaling laws and to produce stress levels that full-scale test might experience. In order to correctly model the prototype behavior
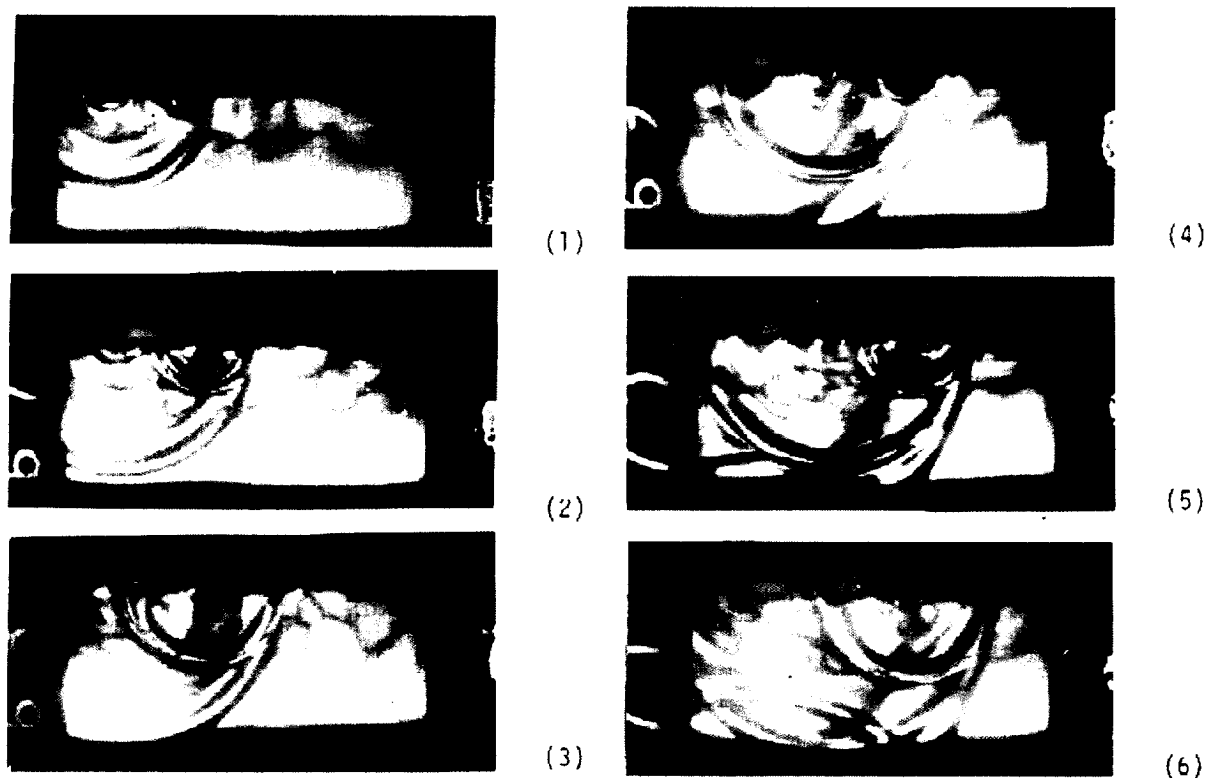
Figure 2.1 Accumulation of lateral waves originated with time differences corresponding to train loads running (after Morichi and Tamura, 1974)

by physical modeling, scaling laws must be established for the model and the prototype, taking into account three groups of equations governing the physical phenomena: equations of motion, constitutive relations of materials involved and initial and boundary conditions. Using low elastic material such as gelatine gel, past researchers had observed wave propagation at a small-scale model test in 1 G. At the beginning, the interesting research which simulated moving load at 1 G was presented by Morichi and Tamura(1974). Then after that, the details of past researches in centrifuge model test were focused in this section.

(1) 1G model test

Morichi and Tamura (1974) developed that the model experimental method effective for the clarification of phenomenon of wave propagation. Gelatine gel has so high Photoelastic sensitivity that we cannot find the other materials comparable to it at presents. Characteristic of their paper is the simulation caused by moving load. The specimen made of gelatin gel was impacted laterally with pendulums at four places separated by 50 mm with the time difference simulating a running train. The accumulation of propagate lateral waves is shown in Fig. 2.1. The clear accumulation of lateral waves at the wave front is observed. The accumulation of displacements was surely given numerically by meaning displacements electrically. It demonstrates experimentally that, if the velocity of moving load coincides that of wave propagation, the large motion could be caused under the moving load. Further it is demonstrated that such a phenomenon as for complicated boundary condition could be analyzed with this experimental work.
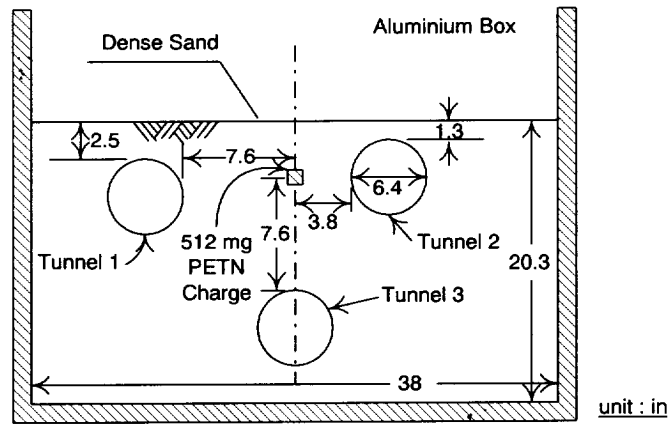
Figure 2.2 Experimental arrangement using centrifuge model test (after Kutter, 1988)
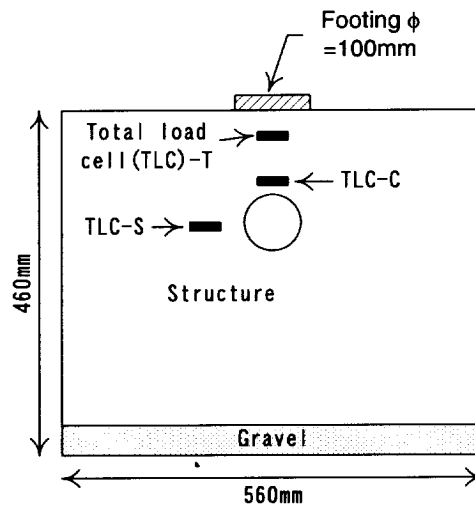
Figure 2.3 Experiment arrangement using centrifuge model test (after Davis, 1991)

(2) Centrifuge model test

The technique of centrifuge modeling has been previously used in investigations of blast loading. Kutter et al. (1988) reported an investigation to establish the feasibility of using centrifuge model tests to study the effect of blast included loading on buried structures (Fig. 2.2). Since gravity influences the cratering process, and consequently influences the soil structure interaction, it is important to conduct scale-model tests of this type of event in a centrifuge. Blasting point by their experiment was installed a few meters below the ground surface in all cases, while the experiment by Davies (1991) described the impulsive loading which was provided by a mass impacting at the surface of the soil (Fig. 2.3). Brass cylinders modeling flexible pipeline in prototype were located in either dry or saturated sand and loaded with an impulse provided by a mass impacting on a target at the soil surface. Their researches have explored wave propagation and its reduction method caused by blast loading, but these conclusions may be limited for the cases where ground vibration problems induced by high speed train are concerned, because the stress (acceleration) level is different from those of blast loading as shown in Fig. 2.4.

Semblat and Luong (1988) and Luong (1994) presented experimental procedures describing a drop-ball arrangement, which is able to generate in-flight stress waves propagating though a centrifugal soil mass and wave reflections on model boundaries are taken into account and re-
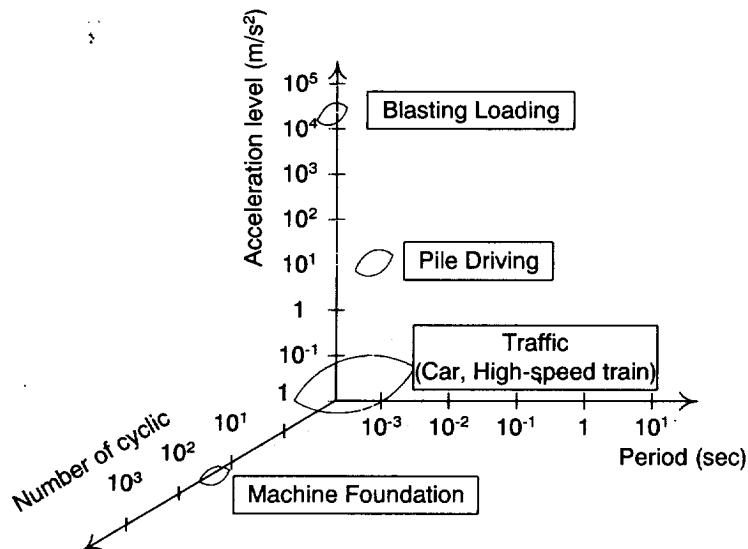
Figure 2.4 Characteristics of the acceleration level, cyclic number, and period by various vibration sources
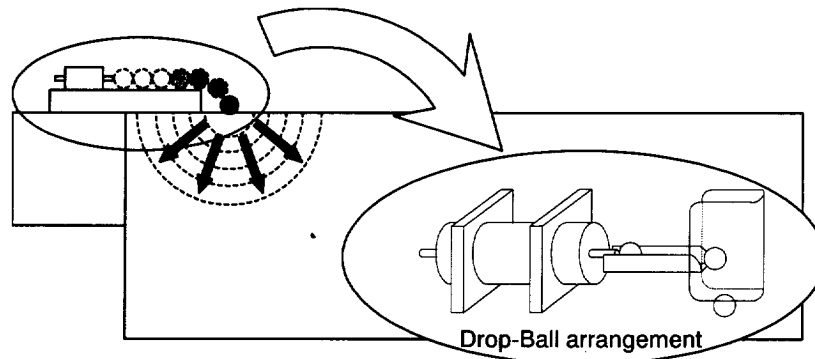
Figure 2.5 Drop-Ball arrangement system (after Semblat and Luong, 1988)

moved by homomorphic filtering. Their purpose was to generate a wave field of short duration using a simple experimental system as shown in Fig. 2.5. An actuator pushed a spherical ball (500 g), which then fell onto the medium surface (air-dried Fontaineblean sand of unit weight γ_d = 16.5 kN/m^3). The ground motions were detected by three dimensions piezo-electric accelerometers. And their measurement points were at ten different locations, out of which five accelerometers were installed 11 m, 24 m, 37 m, 50 m, and 63 m away from source at 3m deep and 15m deep in the ground at prototype scale. But they did not directly measure input accelerations.

Experiments by Semblat and Luong (1988), Luong (1994), and Siemer and Jessberger (1994) produced a shock wave on the surface ground, while the system developed by Cheney et al. (1988, 1990) induced vertical dynamic cyclic loads on circular bearing plate (ϕ = 2.54, 3.56, 4.57 mm) on a body of dry Monterey sand of unit weights γ_d = 16.5, 15.7, and 14.8 kN/m^3 (Fig. 2.6). Cheney et al. employed the use of Duxseal in treating the boundaries of their container and evaluated its effectiveness of alleviating the reflection problem for a class of foundation vibration problems.

Four research groups had been observed centrifugal simulation of wave propagation using
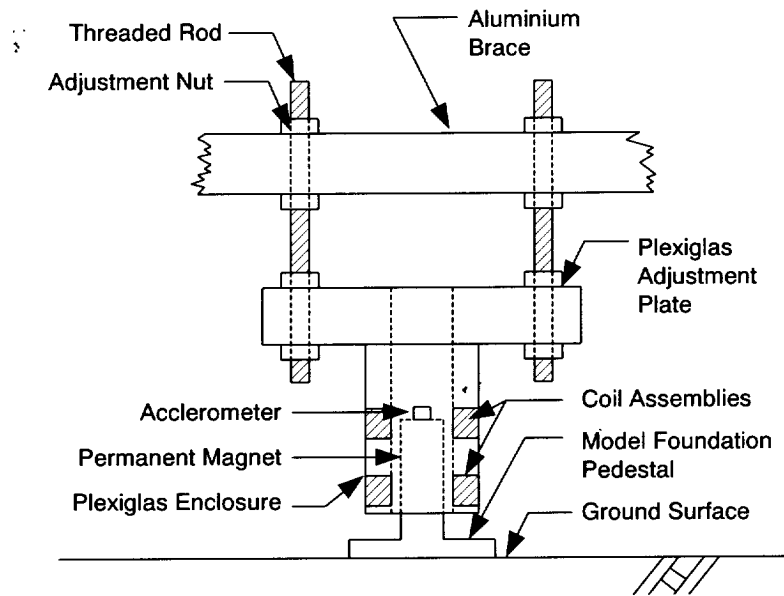
Figure 2.6 Centrifugal dynamic loading system (after Cheney et al., 1988)

each developed wave generator. However, their researches could not be satisfied with the objective of this research. For example, the experiment by Kutter et al. (1988), and Davies (1991) may be limited for the cases where ground vibration problems induced by high speed train are concerned, because the stress level is different from those of blast loading. Again, the experiments by Semblat and Luong (1988) and Luong (1994) did not get information of input acceleration directory. Additionally, the experiment by Cheney et al. (1988, 1990) did not measure the wave propagation.

Consequently, newly systems which are satisfied with these requirements have developed in this study. Chapter 4 describes the development of the Multiple Ball-Dropping System which can measure the input acceleration and simulate wave propagation by not only point load but also quasi-moving load caused by high-speed train running through viaducts. And in Chapter 5, it focuses on the development of Centrifugal Vibration Testing System, which can measure the inputted acceleration directory and generate cyclic load at ground surface by various wide range frequencies.

2.2.4 *Prediction of the wave propagation*

Vibration attenuation became a concern when heavy industrial machinery and equipment induced vibration and shock pulse into the soil. Since that time, it has been concerned not only with vibrations, but also with damping of ground vibrations which is dissipation of energy. The energy density in each wave decreases with distance from the source. This decrease in energy density or decrease in displacement amplitude is called geometrical damping. It can be shown that the amplitude of body waves decreases in proportion to the ratio of $1/r$ (r is the distance from the input source) except along the surface of the half-space, where the amplitude decrease as $1/r^2$. The amplitude of the Rayleigh wave decrease as $1/\sqrt{r}$. The decrease in amplitude of the vertical various waves with

- 14 -

distance due to geometry alone can be expression as follows:

$$A(r) = A(r_1) \left\{ \frac{r_1}{r} \right\}^n \quad \text{.. (2.1)}$$

where $A(r)$ = amplitude acceleration at distance r from source, $A(r_1)$ = amplitude acceleration at distance r_1 from source, r = distance from soured to point in question, r_1 = distance from source to point of known amplitude, and n = wave type (n = 1/2 means surface wave and n = 2 means body wave at the surface of the half-space). Considering geometrical damping alone, it can seen a large degree of isolation can be achieved by locating as far as possible from a known vibration source. Because soil is not perfectly elastic, there is another consideration which influences the attenuation of the waves. In real earth materials, energy is lost by material damping. Both geometrical and material damping can be expressed for various wave types, half space attenuation by the following (Bornitz, 1931):

$$A(r) = A(r_1) \left\{ \frac{r_1}{r} \right\}^n \times \exp\left[-\alpha(r - r_1) \right] \quad \text{... (2.2)}$$

with $\alpha = \dfrac{2\pi f h}{V}$ (Kushida, 1997)

where f = input frequency, V = wave velocity, h = damping ratio. This theoretical attenuation predicted by Eq. (2.2) is seen to be of value to judge the wave types in centrifuge model test and field test. This equation uses as one of the judgments which identify the kind of waves in Chapter 4, 5, and 6.

Due to the lack of a comprehensive understanding of excitation generation mechanisms related to railway trains and the difficulty in determining accurate values for soil properties, modelling an entire system precisely is not an easy task. One way is to construct a simplified but reasonable model for predicting the responses based on some empirical and theoretical results. Most of the prediction models are composed of several separable independent formulas, each of which serve as a control parameter and can affect, to a certain extent, the final response. A simple prediction model such as this can be used to provide tentative estimations when one cannot afford to conduct extensive individual measurements immediately. Gutowski and Dym (1976) and Verhas (1979) combined the measurement and theory into a predictive model, which was given in a simplified form of an attenuation function by taking into account the effects of material attenuation and geometrical attenuation. Madshus et al. (1996) proposed a semi-empirical model for predicting low frequency vibration, based on a large number of vibration measurements obtained in Norway and Sweden. This model includes five separable statistically independent factors, i. e., the train type specific vibration level, speed factor, distance factor, track quality factor, and building amplification factor.

Empirical equations are used for practical assessment of expected soil vibrations from industrial and construction source and they usually allow calculation of only vertical amplitude of the
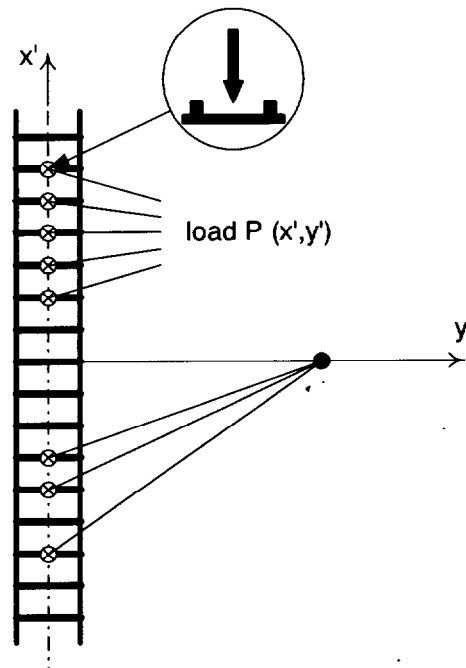
Figure 2.7 Scheme used for the evaluation of the convolution integral (after Lai et al., 2000)

peak part of vibration records and they are not always with required accuracy. These equations cannot incorporate specific differences of soil conditions at each site because heterogeneity and spatial variation of soil properties strongly affect characteristics of propagated waves in soil from construction and industrial vibration source. Lai et al. (2000) made to assess the ability of a well-known source model, namely the Krylov's model, to predict railway-induced ground vibrations. The propagation problem solved using the rigorous approach associated to the formalism of the dynamic Green's functions in vertically heterogeneous, viscoelastic media. According to this formalism the vibration field at receiver was computed through a convolution integral between the overall distribution of forces along the tack and the corresponding dynamic Green's function (see Fig. 2.7). The results of these numerical simulations were compared with experimental measurements performed during the passage of high speed trains in Italy. Good agreement between the simulated and the experimental data was found for frequencies below 8-10Hz. Svinkin (1996, 2001) proposed the application of the impulse response function concept to solve the geotechnical problems of prediction of ground and structure vibration before installation of a vibration source. The obtained results demonstrated the accuracy and efficiency of the method for the predicting soil and structure vibrations prior to installation of foundations under machines with impact loads. In particular, this method was most useful under non-uniform and complicated soil conditions for determination and verification of safe distances from dynamic source for facilities sensitive to vibrations. Yoshioka et al. (1980) originated a simple prediction method by a weight dropping experiment and a microbus running test. Their method was based upon measurement of transfer functions and was verified at Ohgusa viaduct in Tohkaido Shinkansen line. The input information was the vibration data in terms of maximum acceleration, spectra, waveforms, and vibration levels.

In this study, the results of wave propagation in centrifuge model test were compared by applying a simple prediction method produced by Yoshioka et al. (1980), in Chapter 4.

2.3 REVIEW OF VIBRATION REDUCTION METHOD

In order to reduce train induced vibrations at a distance from the track, several issues such as generation of the waves at the source, propagation of them through the media, and interaction of the waves with the structure at receiver must be considered. At each of the links mentioned, countermeasures could be taken to reduce the vibrations and their effects. Therefore this review study covers all these issues.

Waves are attenuated by two mechanisms: *radiation damping* and *material damping*. The former is sometimes referred to as geometric damping and is due to the geometric spreading of wave fronts as they propagate away from a source, thereby dispersing energy over an increasing area. This attenuation is independent of frequency but affects Rayleigh waves the least because they are essentially confined to the surface. Material damping describes the frictional energy dissipation that occurs during the passage of a wave when the ground undergoes cyclic shear or compression, and higher frequencies are attenuated the most over a given distance. The first part of this section provides outlines of vibration regulation / law / standard / manual in the world. The rest of this section reviews the various approaches of achieving this and details the vibration reduction method specially.

2.3.1 Vibration regulation / law / standard / manual

Japan has the only vibration regulation law against the environmental pollution in the world. However a number of standards aim to define acceptable vibration levels for buildings. In the UK, the British Standard BS 6472 and the International Standard ISO 2631-2 are used extensively. In the U. S. A., as to ground vibration caused by high-speed train, U. S. Department of Transportation made a manual which provided procedures for the assessment of potential vibration impacts.

(1) *Japanese standards and regulations*

The Vibration Regulation Law was enacted in 1976 in an effort to implement regulations necessary to control vibrations. The purpose of this Law is to preserve living environment and contribute to protection of the people's health by regulating vibration generated by the operation of factories and other types of work sites as well as construction work affecting a considerable area, and by providing requests regarding road traffic vibration. The outline of this law is as follows:

a) Regulation on noise caused by business activities at factories and other business establishments
The Vibration Regulation Law identified ten specified facilities producing significant vibration by certain types of metal processing machinery and regulating vibration from factories and business establishments equipped with such facilities. Control standards shown in Table 2.2 are applied at the boundary line of factory or business establishment property

b) Regulation of vibrations from construction work
Targeting 4 types of vibration during construction work producing significant noise, such as drilling, and vibration levels must be less than 75 dB at the boundaries of the work site. In addition, a

Table 2.2 Regulatory Standards for Vibration Emitted from Specified Factories (Summary)

Time Area	Daytime (dB)	Nighttime (dB)	Applicable Areas
I	60 – 65	55 - 60	Areas where maintenance of quiet is particularly needed to preserve a good living environment and where quiet is needed for as they are used for residential purposes.
II	65 - 70	60 – 65	Areas used for commercial and industrial as well as residential purposes where there is a need to preserve the living environment of local residents and areas mainly serving industrial purposes which are in need of measures to prevent the living environment of local residents from deteriorating.

Note: Vibration level shall be measured at the boundary line of the specified factory.

Table 2.3 Request Limits for Motor Vehicle Vibration

Type of Restriction	Area Classified	
Standard value	I & II	85dB
Work prohibited time	I	7 p.m. - 7 a.m
	II	10 p.m. - 6 p.m.
Maximum Working duration	I	10 hours per day
	II	14 hours per day
Maximum consecutive working days	I & II	6 days
Work prohibited days	I & II	Sundays and holidays

Table 2.4 Request Limits for Motor Vehicle Vibration (Summary)

Time / Area	Daytime (dB)	Nighttime (dB)	Applicable Areas
I	65	60	Areas where maintenance of quiet is particularly needed to preserve a good living environment and where quiet is called for as they are used for residential purposes.
II	70	65	Areas used for commercial and industrial as well as residential purposes where there is a need to preserve the living environment of local inhabitants and areas mainly serving industrial purposes which are in need of measures to prevent the living environment of local residents from deteriorating.

time regulation is applied to such construction work as shown in Table 2.3.

c) Regulation of vibrations from road traffic

Control standards shown in Table 2.4 are applied at the boundary line of road traffic.

In this law, although it is not universally accepted, the vibration acceleration level (VAL) which depends on decibel notation is in common use for vibration. Decibel notation (dB) serves to compress the range of numbers required to describe vibration. The VAL is defined as;

$$VAL = 20 \times \log \frac{A}{A_0} \quad (dB) \quad \dots\dots\dots\dots\dots\dots\dots\dots\dots\dots\dots\dots\dots\dots\dots\dots\dots\dots\dots\dots\dots\dots\dots (2.3)$$

where, A is the root mean square (RMS) acceleration amplitude, and A_0 is the standard acceleration amplitude. In Japan the standard, A_0, is 10^{-5} m/s^2 provided by the Japanese Legal Metrology. However the standard of VAL at ISO 1683-1983 (Acoustics-Preferred reference quantities for acoustic levels), A_0, is 10^{-6} m/s^2.

The Shinkansen vibration is under the control of the recommendation issued by the Environment Agency of Japan since 1976. It requires that measures have to be taken urgently to reduce the vibration in areas where vertical vibration levels exceed 70 dB. The Environmental Impact Assessment Law is also established in 1997, in which the train included ground vibration is one of the items to be assessed in the planning stage of new construction and large scale improvement of railways.

(2) International Standard ISO 2631-2

This standard applies to the human response to vibrations and shocks. In the 8-64 Hz octave band,

the "threshold of perception" is 2×10^{-4} m/s; "probable disturbance" occur at 10^{-3} m/s; "moderate disturbance" occurs at $4\text{-}10 \times 10^{-4}$ m/s

(3) U. K standards and legislation

Vibration at properties is normally assessed, in the UK, by reference to BS6472 (human response) and BS7385 (building damage). At present, railways rarely generate levels of vibration which exceed the guidelines within these standards. However, guidelines based on lower vibration levels than those currently stated may eventually emerge, as BS6472 is due for review, and the closely related International Standard, ISO2631, is being modified at present. For both noise and vibration, Local Authorities are able to use the powers provided by the Environmental Protection Act 1990 to issue an "abatement notice" against a railway operation where they are satisfied that a statutory nuisance exists. No noise or vibration levels are specified. Contravention of the notice is an offence under the Act. In any proceedings it is a defence to demonstrate that best practicable means are being used to control the nuisance. Magistrates' Courts also have similar powers under the Act, allowing them to act on behalf of individuals complaining of a nuisance.

(4) High-speed ground transportation noise and vibration impact assessment (the manual by U. S.
Department of Transportation)

This manual provided procedures for the assessment of potential noise and vibration impacts resulting from proposed high-speed ground transportation projects, including high-speed rail using traditional steel-wheel on steel-rail technology and magnetically levitated systems. This manual provided the criteria for ground-born vibration and noise as shown in Table 2.5.

Although it is not a universally accepted notation, the abbreviation "VdB" is used in this manual for vibration decibels to reduce the potential for confusion with sound decibels. Vibration velocity level in decibels is defined as:

$$L_v = 20 \times \log\left(\frac{v}{v_{ref}}\right) \quad (VdB)$$

where L_v is the velocity level in decibels, v is the RMS velocity amplitude, and v_{ref} is the reference velocity amplitude. Common vibration source and the human and structural response to ground vibration are illustrated in Fig. 2.8.

Many countries or governments have made a manual to vibration regulation law / standard. However, harsh reality that vibration level goes over the level of their standard exists at some locations. Thus, in order to reduce the vibration at some location where vibration level goes over the level, some researchers investigated the issue of vibration countermeasures. As to vibration countermeasures, some of references cover two different countermeasures which are from the vibration source and the transmitting path in the pages that follow.

- 20 -

Table 2.5 Ground-borne vibration and noise impact criteria in U. S. Department of Transportation (after U. S. Department of Transportation)

Land Use Category	Ground-Borne Vibration Impact Levels (VdB re 1 micro inch/sec)		Ground-Borne Noise Impact Levels (dB re 20 micro Pascals)	
	Frequent[1] Events	Infrequent[2] Events	Frequent[1] Events	Infrequent[2] Events
Category 1: Buildings where vibration would interfere with interior operations.	65 VdB[3]	65 VdB[3]	N A[4]	N A[4]
Category 2: Residences and buildings where people normally sleep.	72 VdB	80 VdB	35 dBA	43 dBA ·
Category 3: Institutional land uses with primarily daytime use.	75 VdB	83 VdB	40 dBA	48 dBA

Notes:
1. *Frequent Events* is defined as more than 70 vibration events per day.
2. *Infrequent Events* is defined as fewer than 70 vibration events per day.
3. This criterion limit is based on levels that are acceptable for most moderately sensitive equipment such as optical microscopes. Vibration-sensitive manufacturing or research will require detailed evaluation to define the acceptable vibration levels. Ensuring lower vibration levels in a building often requires special design of the HVAC systems and stiffened floors.
4. Vibration-sensitive equipment is not sensitive to ground-borne noise.

Human/Structural Response	VELOCITY LEVEL*	Typical Sources (50 ft from source)
Threshold, minor cosmetic damage fragile buildings →	100 ←	Blasting from construction projects
		← Bulldozers and other heavy tracked construction equipment
Difficulty with tasks such as → reading a VDT screen	90	
		← High speed rail, upper range
Residential annoyance, infrequent → events (e.g., commuter rail)	80	← Rapid transit, upper range
		← High speed rail, typical
Residential annoyance, frequent → events (e.g., rapid transit)	70	← Bus or truck over bump
Limit for vibration sensitive → equipment. Approx. threshold for human perception of vibration	60	← Bus or truck, typical
	50	← Typical background vibration

*RMS Vibration Velocity Level in VdB relative to 10 inches/second

Figure 2.8 Typical levels of ground-bone vibration (after U. S. Department of Transportation)

Figure 2.9 Site locations (after Holm et al., 2002)

2.3.2   Vibration countermeasures at vibration source

Vibration countermeasures at vibration source differ from one target source to another. This section examines its countermeasures at vibration source caused by running high-speed train, mainly. In the railway transportation, vibration reduction methods by vibration source are mainly an improvement of vehicles, rails, ballast and track. Wilson et al. (1983) gave a list of common methods for reducing train-induced ground vibration. One of these methods that have been focused on by them is use of floating slab trackbeds, which are effective at reducing frequencies above the resonance frequency of the slab. The other methods are modifying the design of transit car bogies so that wheel forces are reduced. Countermeasures investigated include resiliently supported cross ties, soft pads and others. These measures at track mainly prove to be useful above 20 Hz, but the problem still exists in the frequency range below that. The method that they suggest for control and reduction of this part of the vibration is to modify bogie design. Reducing the unsparing mass reduces ground vibrations by about 10-15 dB. Ando et al. (1996) discussed several countermeasures against high frequency (more than 40 Hz in the case of vibration) noise and vibration from high-speed trains. The considered countermeasures are: smoothing rail tread surface, elastic rail fastening, increasing the mass of the slab and / or sleeper, and noise absorption.

Excessive vibrations were observed at a section (Ledsgard) of the West Coast Line between Gothenburg and Kungsbacka in Sweden when the traffic with high speed train started (Holm et al., 2002) as shown in Fig. 2.9. An example of this behavior, Fig. 2.10 shows the measured vertical displacement of the track for an X2 train passing at different speeds. From the figure, it can be seen that at low speeds, far below the critical speed, the displacement pattern is static. At high speeds, substantial heave is observed, in addition to attenuating performance when the last axle has passed. The Ledsgard site is near a river, the Kungsbacka, in the center of a large plain. From a geotechnical

Figure 2.10 Vertical displacement of the track for an X2 train at different speeds (after Holm et al., 2002)

Figure 2.11 Soil condition in the test section (after Holm et al., 2002)

Figure 2.12 Layout of soil improvement (after Holm et al., 2002)

Figure 2.13 Track reacceptance of the track before and after soil improvement (after Holm et al., 2002)

Figure 2.14 Vertical particle displacement amplitude at difference distance from the train speed before and after the countermeasures (after Holm et al., 2002)

point of view, the Ledsgard site is rather special, with a pocket of very soft organic soil (gyttja) of maximum 3 m thickness below a dry crust. The gyttja is underlain by soft clay and the depth to bedrock is more than 60 m. Figure 2.11 shows the soil condition in the test/measurement section. The shear wave velocity is in the order of 40 m/s in the gyttja layer. In the underlying clay, the shear wave velocity is approximately 60 m/s, increasing to 90 m/s at 14 m depth. Banverket (the Swedish National Rail Administration) initiated a research and development project and comprehensive measurements. And as the results of FDM analysis of which cord is FLAC3D, the dry deep mixing method (DMM) was chosen to reduce the vibrations. Figure 2.12 shows the layout of soil improvement with the dry DMM columns. Figure 2.13 shows the track receptance of the track before and after soil improvement. The excitation and response were measured on the rail head mainly by means of accelerometers. The receptance was extremely high before of the soil improvement. Figure 2.14 shows calculated vertical particle displacement amplitude at difference distances from the track versus train speed before and after the countermeasures. From this figure, it shows that the reduction of displacement amplitude level due to the countermeasures was very clear at high speeds (190 km/h).

As an effective measure to reduce the man made vibration, an idea of wave impeding block (WIB) was proposed (Chouw et al., 1991, Chouw and Schmid, 1993). This approach is based on vibration transmitting behavior of a soil layer over bedrock (Fig. 2.15). To obtain the effects of bedrock an obstacle consisting of stiff material is placed in the soil. The effect resulting from the presented approach is shown by comparing the screening capacity with that of a stiff wall as a vibration barrier. ·

As to the WIB mechanism, the past researchers who were using centrifugal model test are introduced as follows. Siemer and Jessberger (1994) developed a wave generation system in centrifuge similar to the "Down-Hole-Method" (Telford et al., 1985), which is able to work without the complicated core hole technique. A foundation (B60 × W60 × H25 mm) at the surface was excited dynamically by a falling mass which was held at a certain height (150mm) by an electromagnetic system as shown in Fig. 2.16. Their system enables to measure input acceleration directly.
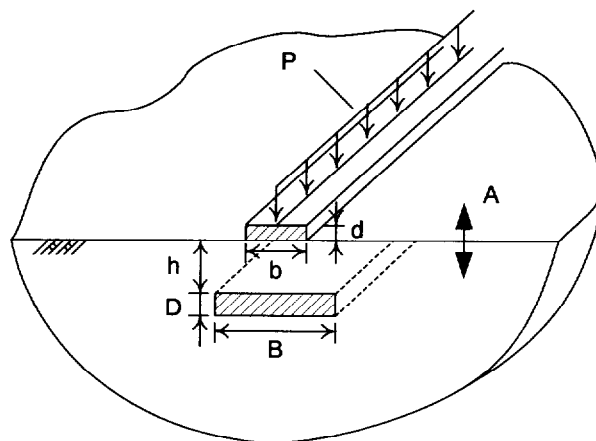
Figure 2.15 Concept of Wave Impeding Block / Barrier (WIB) (after Chouw and Schmid, 1993)
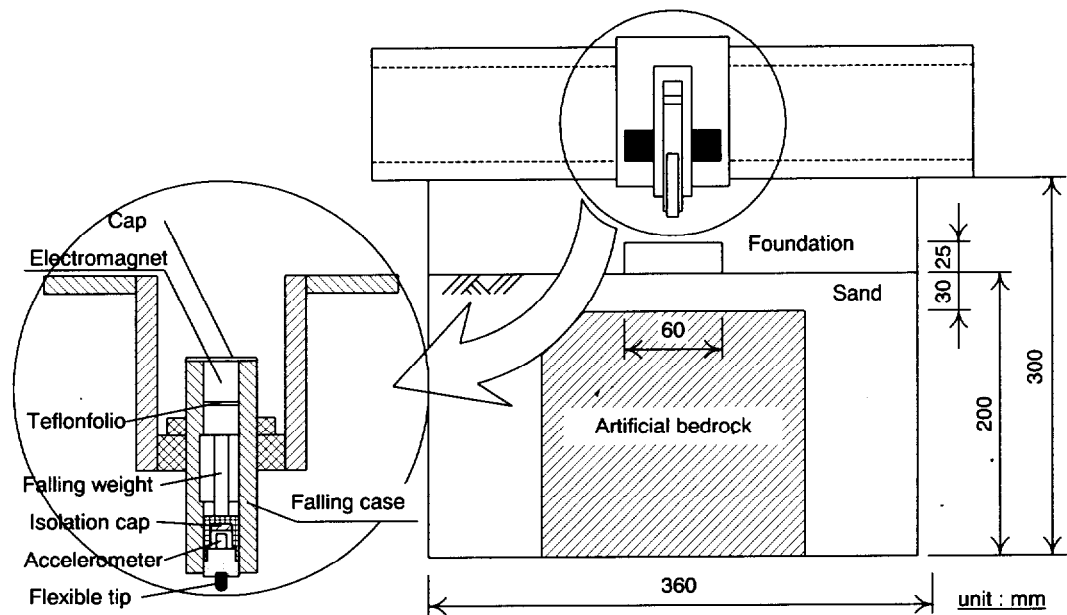
Figure 2.16 Experiment arrangement for WIB (after Siemer and Jessberger, 1994)

Their experiments were carried out to determine shear wave velocities against the depth which were related to the dynamic soil stiffness. All experiments were run at 30 G, of which air-dry sand of unit weight and the average relative density were γ_d = 16.6 kN/m³, 98% respectively. The pressure wave velocities increased with depth. These results were in agreement with a semi-empirical equation by Iwasaki and Tatsuoka (1977). As for vibration isolation method, they researched the effect on a vibration reduction when the improved artificial bedrock beneath the vibration source was built. The artificial bedrock was modeled in a concrete block (B200 × W200 × H200 mm) in their experiment. The results of their research showed that the block could reduce the vertical accelerations of about 36 %.

Vibration countermeasures at the vibration source are a more effective vibration reduction method. However it is difficult to construct the vibration reduction method at operating location. Because it is necessary to temporarily close down in order to construct vibration countermeasures. Therefore the countermeasure method of vibration source is not almost applicable to wide area construction. Most of the countermeasures about the lines in operation choose the vibration countermeasures at transmitting path, to be discussed in the next section.

2.3.3 Vibration countermeasures at transmitting path

One opinion available is to construct deep trenches or underground 'wave barriers' to impede the transmission of surface vibration. A good deal of research, both experimental and numerical, has been carried out over the last several decades to study the vibration isolation problem. Barkan (1962), Dolling (1965), Neumeuer (1963), Mc Neill et al. (1965), and Woods (1968) were the first pioneers who reported a number of practical cases of wave barriers. In the past two decades, a number of researchers have used various numerical techniques to study the vibration isolation problem. Aboudi (1973) used perturbation expansions and FDM with a special treatment of exter-

nal boundaries to evaluate the ground response of elastic half-space with a thin barrier, due to a specified time-dependent surface load. A perturbation method is used to analyze the effectiveness of thin solid barriers. The approach is to use the forced half space (without a barrier) solution as the 1st-order solution. The barrier, which should represent a small change in the elastic constants, and provided that the width is also small, enters as the perturbation; the screening results come out in the 2nd-order solution. A (time-domain) finite difference scheme is used to carry out the 1st- and 2nd-order solutions. The results indicate that a low velocity – low density barrier is more effective than a high velocity – high density barrier. Haupt (1978, 1981) also performed laboratory model experiments to study the screening performance of open trenches and concrete walls. His experimental results were in good agreement with the results of his FEM results for the open trenches and the concrete walls. By the past researches, an analytical approach has rarely been used, because closed-form solutions are extremely difficult to obtain except for very simple geometry and boundary conditions that hardly exist in practice. However, in recent years, the development of high-speed computer enables to study complicated geometry and boundary conditions. In addition, BEM has emerged as a very efficient numerical technique for solving a wide range of engineering problems. It has certain inherent advantages and suites for wave propagation problems in soils involving semi-infinite domain. Using BEM algorithm, physical explanations regarding wave phenomena depending on barrier dimensions, barrier properties and source dimensions have been given by Ahmad and Al-Hussaini (1991), Ahmad et al. (1996) and Al-Hussaini and Ahmad (1996). Their analysis provided results that agree reasonably well with published numerical and experimental results by others (Haupt, 1981; Woods, 1968). In order to study the influence of different parameters on the effectiveness of open and in-filled trench barriers, extensive numerical analyses have been conducted. The dimensionless parameters conceived include frequency of vibration, geometrical parameters (barrier dimensions, barrier location, source size, angular extent of partial circle barrier, extent of screened zone) and material properties (wave propagation velocity, density, damping, Poisson's ratio). The important findings from this numerical study are (1) Soft (bentonite) barriers yields higher reduction in vertical ground vibration compared to stiff (concrete) barriers, (2) The influence of barrier depth is found to depend mainly on shear wave velocity ratio between barrier and soil and to a lesser on the barrier width, and (3) An efficient numerical technique can be an effective alternative for thoroughly investigating the vibration isolation phenomena.

Noteworthy examples from mainly an experimental point of view are described as follows. Woods (1968) conducted a series of field tests to evaluate the screening effect of open trenches for both active and passive isolation cases. Active isolation, as shown schematically in Fig. 2.17, is the employment of barrier close to or surrounding the source of vibrations to reduce the amount of wave energy radiated away from the source. Passive isolation, as shown schematically in Fig. 2.18 is the employment of barriers at points remote from the source of vibrations but near a site where the amplitude of vibration must be reduced. Both types of foundation isolation problems were investigated. He suggested that the minimum trench depth should be 0.6 λ_R to achieve isolation and 1.33 λ_R for passive isolation to achieve an average reduction of 75 % in vertical ground vibrations, where λ_R is the Rayleigh wavelength. Woods's experiment for active isolation has defined the
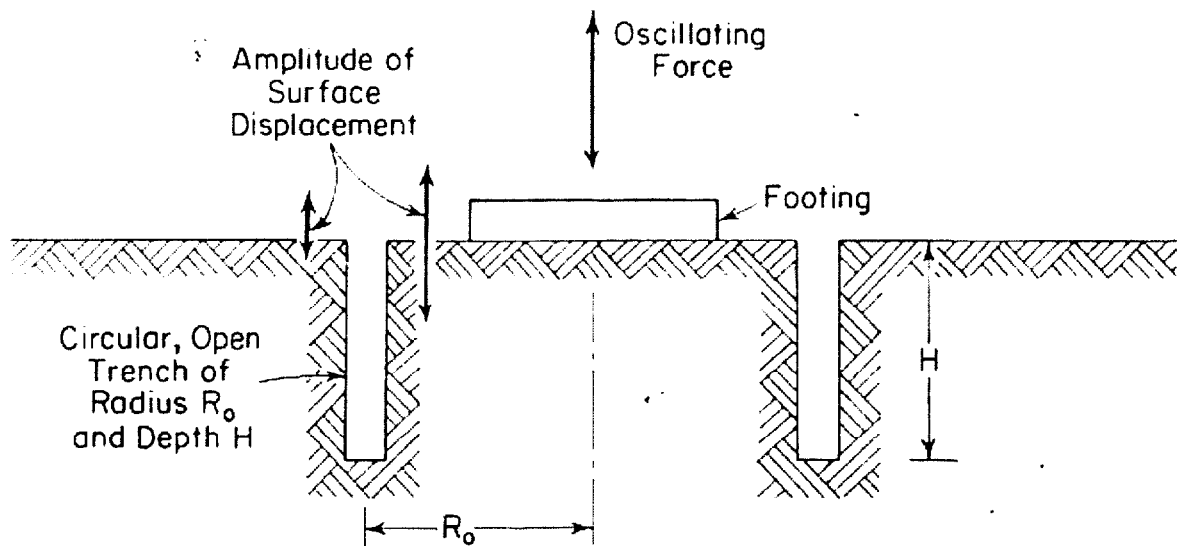
Figure 2.17 Schematic of vibration isolation using a circular trench surrounding the source of vibration – active isolation (after Woods, 1968)
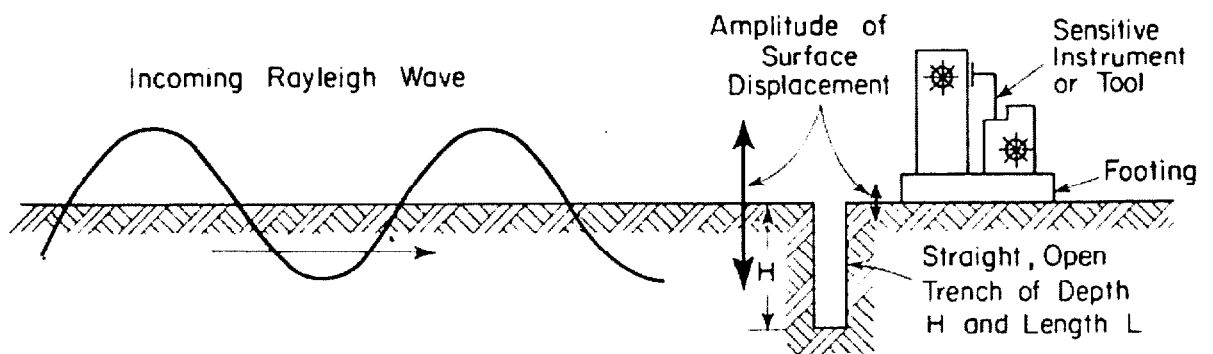
Figure 2.18 Schematic of vibration isolation using a straight trench to create a quiescent zone – passive isolation (after Woods, 1968)

screened zone for a partially complete circular trench as the area symmetrical about the radial line passing through the centre of the source and the centre of the trench, bounded laterally by two radial lines extending from the centre of the source through points 45 ° from each end of the trench. It was observed that semi-cylindrical shape trenches did not provide an effectively screened zone if the trenches have an angular length j less than 90 °. For passive isolation, amplitude magnification can be seen in front of and near the end of the trench. But the effect of barrier length had not been discussed. This paper distinguishes itself from the other researches because the systematic experiment has been carried out. Al-Hussaini and Ahmad (1996) have used his experiment as compared with own theoretical results.

There was the past researcher which used low elastic materials similar to Morichi and Tamura (1974) and described the effect of wave barrier such as countermeasures method at the transmitting path on the vibration. Takibuchi et al. (1977) concluded a series of 1-G model test to study the screening effect of open trenches and in-filled barriers. Steel ball having mass of 4 g and diameter of 10mm was allowed to fall freely from 80 mm onto the surface ground, directory. The material
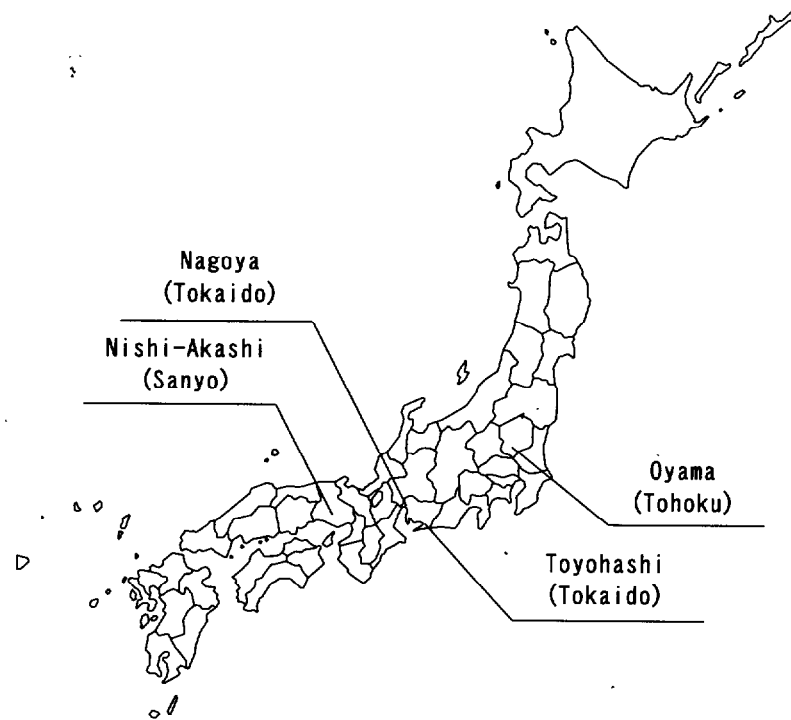
Figure 2.19 Location of the field test by Yoshioka (2000)

used was acrylic amide, diatomaceous earth, bentonite and sand. Scaling laws in this model test satisfied a geometric scale of 1/30, time scale of 1/15 and density scale of 1/1.2. Their test has defined as follows; 1) In the case of wave propagation behavior, mainly wave type was Rayleigh wave. 2) In the case of open trenches, wavelength (λ) and depth of barrier (D) were strongly related to effect of vibration isolation. In other words, higher values of D/λ were needed to effective isolation. 3) In comparison with the case of open trenches, isolation effect by in-filled barrier had half values.

The information of the effect of wave barrier on the vibration at the field test is very limited. Nevertheless, the group of Railway Technical Research Institute (RTRI, Japan) proposed a lot of information at the field test. Yoshioka and Ashiya (1991) and Yoshioka (2000) examined the isolation effect of Shinkansen-induced ground vibration by a concrete core wall-in-earth built along the way, several field measurements. These conditions in each case are listed in Table 2.6, Fig. 2.19 and Fig. 2.20. Figure 2.21 shows a comparison of overall vertical vibration level (VL-oa-z) values before and after installation of concrete wall in the ground. With this figure, all the examples show a vibration increase in front of the wall and a decrease behind it. The degree of the reduction is the largest just behind the wall and becomes smaller away from the wall. However, the reduction data are rather scattered and it cannot be said that a large size wall exhibits large effectiveness. They were able to approximately describe not only the common isolation properties independent of various conditions, but also the properties dependent on conditions of the wall, its surrounding ground and vibrations impinging into the wall.

Yoshioka and Ashiya (1991) and Yoshioka (2000) did not provide the influence of extension of wave barrier on the reduction of vibration. As for this influence, Woods (1974) and Ashiya (2001) researched experimentally and theoretically, respectively. Woods et al. (1974) carried out

Table 2.6 Parameters of each wave barriers (after Yoshioka, 2000)

ID No.	1	2	3	4	5	6	7	8
Line	Tokaido		Tohoku			Sanyo	Tokaido	
Site (Location is seen in Fig. 2.19)	Nagoya	Nagoya	Oyama	Oyama	Oyama	Nishi-Akashi	Nagoya	Toyoha shi
Track with	Ballast		Slab.				Ballast	
Structure	Rigid-frame bridge, with pile foundation							
Site Condition	(see Fig. 2.20)							
Pile length (m)	12	8	11	11	11	8	10	20
Speed (km/h)	190~200		~200			>200	>180	~210
Wall								
Position (m)	5.6	5.5	8.4	8.4	8.4	5.6	5.7	10.5
Depth (m)	3.0	3.0	5.0	5.0	10.	3.0	4.0	10.0
Thickness (m)	0.8	.8	0.4	0.8	0.4	1.2	0.8	~0.8
Extension (m)	39	21	43	43	43	80	34	110
Embedded together with	Sheet Piles		Without			rails	Deck Plates	II-type sheet
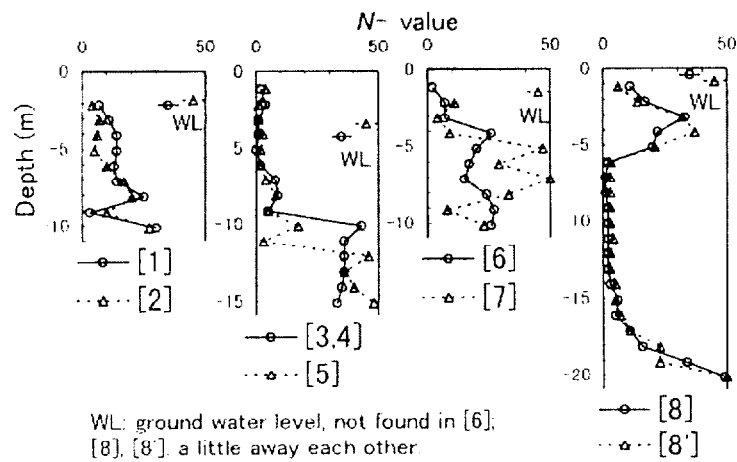
Figure 2.20 Site condition (after Yoshioka, 2000)
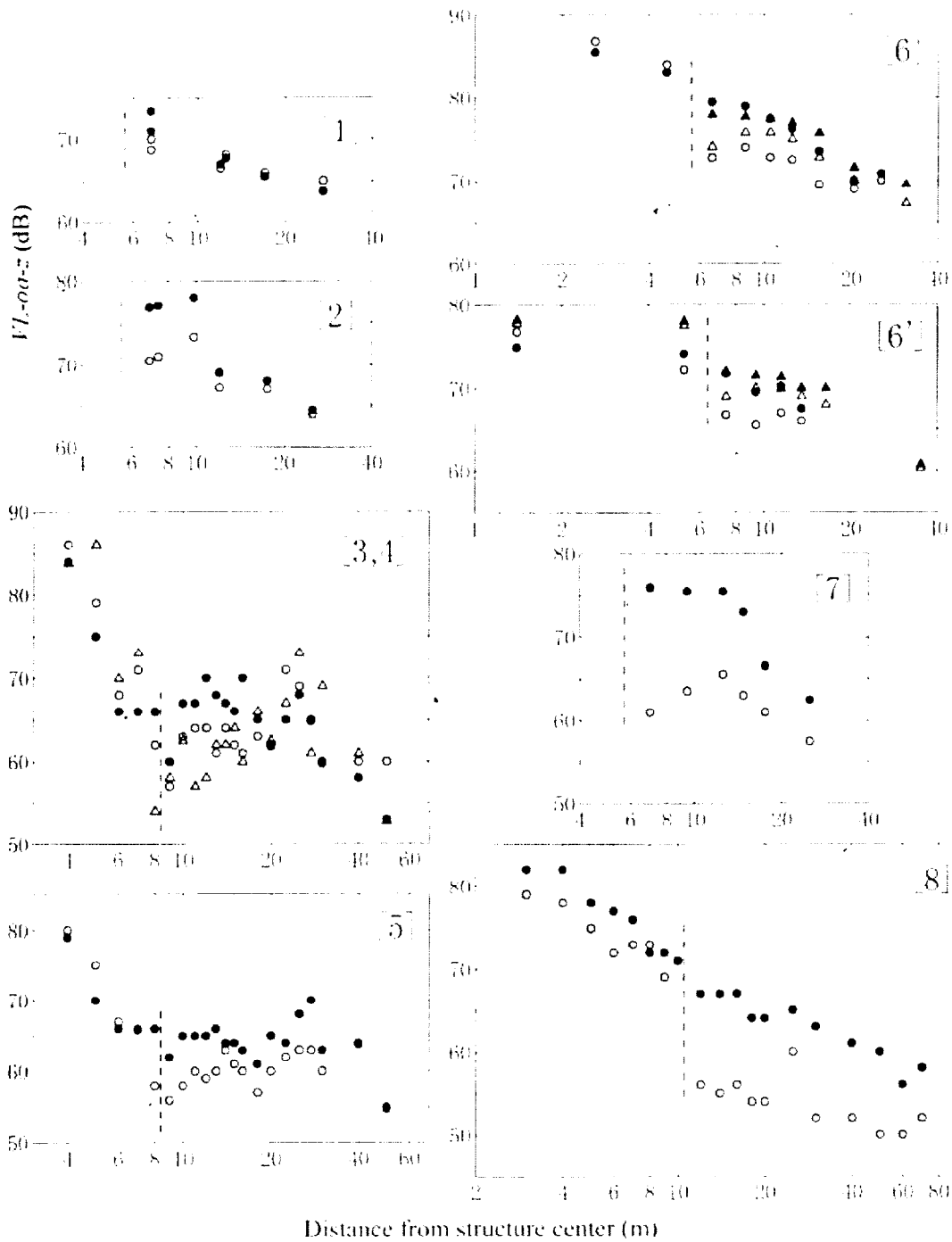
Figure 2.21 Comparison of VL-oa-z value before and after installation of concrete wall in soil
(after Yoshioka, 2000)
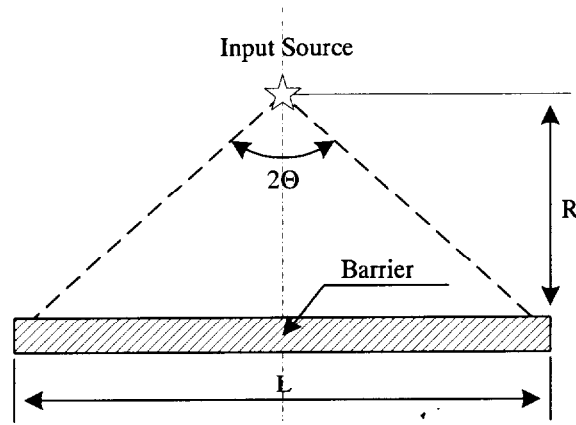
Figure 2.22 Definition of the value of Θ
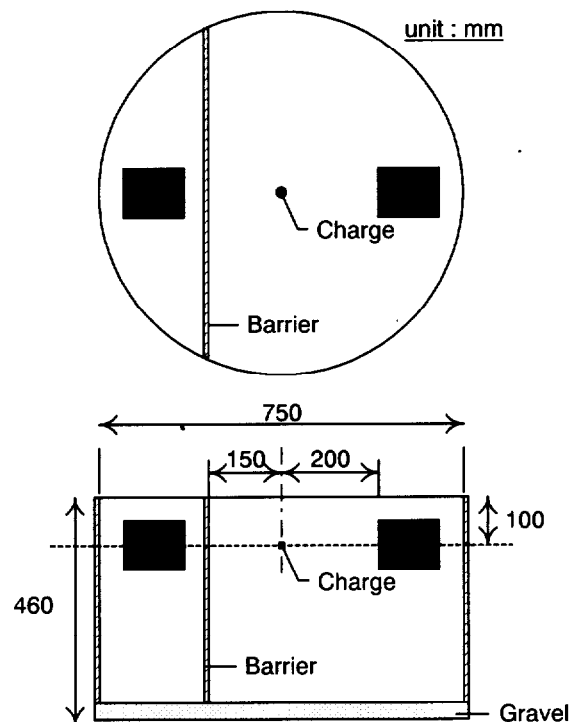
Figure 2.23 Centrifuge model protecting structure from the buried explosions by use of barrier (after Davies, 1994)

another set of field tests by using the technique of holography. The barriers were rectangular open trenches with a subtended angle of 2Θ which is dependent on the barrier length L and the perpendicular distance from the source R, as shown schematically in Fig. 2.22. 2Θ was selected as either 24 ° or 77 °. It was found that the larger the angle, Θ, the better the amplitude reduction along the centreline. But the difference of the angular length was small and the trench with 2Θ = 24 ° must be considered as being effective. Ashiya (2001) proposed to estimate the effect of trench and wall-in-ground to reduce train-induced ground vibration. His method applied Kirchhoff's theory of diffraction to the problems of Rayleigh wave incident into trench and walls in the ground. The validity of the method was examined by comparing the estimated vibration reduction effect with the results of several small-scale tests and field tests. As the results, the calculation result using this estimation method is good agreement with the result of experiment test except for some cases.

About using centrifuge model test, the reviews of past researchers are introduced as follows. Davies (1994) conducted to investigate the feasibility of protecting buried structures from the effects of buried explosives by the use of barrier which was a low acoustic impedance barrier, a stiff barrier, a composite barrier, and an air void. The detail of his experiment is seen in Fig. 2.23. Two structures, which were called "protected" and "unprotected", were subjected to blast loading in each experiment. The effectiveness of each barrier concept was assessed using the results of strain gauges and accelerometers to compare the response to loading of protected structures with similar unprotected structures. Barriers containing low acoustic materials were highly effective in attenuating propagating stress waves and reducing the magnitude of shock loading on structures. Because his object of research is about protecting buried structures from the buried explosives, the stress level is different from those of blast loading. Luong (1994) examined only one case about the wave barrier to reduce vibration caused by traffic, vibrating machines, blast, shock or impact loading which is similar to this objective. The research of wave propagation using centrifuge model test have been reported since the 1980's but has lacked systematically study about vibration countermeasures under ground vibration problems.

2.4 SUMMARY

Compared with the numerical and theoretical approaches, there were few researchers who took experimental approaches in ground vibration problem. Because while full-scale tests are practically too expensive to be carried out, small-scale model test results obtained in 1 G environments often pose a question of how to interpret their data and to deduce the implications under prototype situations. In past researchers, the technique of centrifuge modelling test, in which the scaling relationship agrees with the relevant effect of self weight induced stresses appropriate to the prototype earth structures has been used previously in investigations of blast loading and seismic. However their research did not provide systematic results and data, yet. In addition, there is not systematic research as for vibration reduction method, using a centrifuge.

Throughout the course of this chapter this study provides the systematic result which examines the effectiveness of wave barrier using various materials and geometries.

CHAPTER 3

CENTRIFUGE MODEL TEST

3.1 INTRODUCTION

The aims of the centrifugal modeling test in this study were to simulate the wave propagation caused by machine, high-speed train, and blasting and to develop the efficient design of wave barrier. All the tests described here were conducted on the Tokyo Institute of Technology Mark III Centrifuge. In this chapter, theory of centrifuge modelling is briefly reviewed and then, development of equipment for centrifuge testing and the experimental techniques are described in detail.

3.2 TOKYO INSTITUTE OF TECHNOLOGY MARK III CENTRIFUGE

The Tokyo Institute of Technology Mark III Centrifuge (Tokyo Tech Mark III Centrifuge) was used for the model test described in Chapter four and five. This centrifuge is a beam type centrifuge having a pair of parallel arms that hold platforms on which the model container and a weight for counterbalance are mounted as shown in Fig. 3.1. Radius of rotation is 2.45m, which is the distance from the rotating shaft to the platform base. The surface of the swinging platform is always normal to the resultant acceleration of the centrifugal acceleration, n G, and earth's gravity. Specifications of the centrifuge are summarized in Table 3.1.

For data acquisitions, two types of signal transmission methods are used. One is classical electrical slip ring. Transducers are connected to the slip rings through a junction box and signals are transferred to amplifiers on the laboratory floor. The other is an optical rotary joint. Transducers are connected to signal conditioners on the centrifuge. Analog signals from the transducers are amplified there and then are converted to digital signals by A/D converters. Gains and the other conditions of the signal conditioners can be controlled by a PC on the laboratory floor. The digital signals are transferred to a PC on the laboratory floor through the optical rotary joint. In most data acquisitions, an optical rotary joint was used in this study.

3.3 INSTRUMENTATION

(1) Circular container

The container, Fig. 3.2, is a steel cylindrical tub of 455 mm in diameter and 410 mm in height. The thickness of this container is 13 mm and weight is about 0.9 kN. Using this container, Okamura (1993) conducted centrifuge model tests on the bearing capacity problem. It was observed that this container has the internal diameter against about three times of the deformation area. Thus this container can accommodate loading test using the footing of 60 mm in diameter.
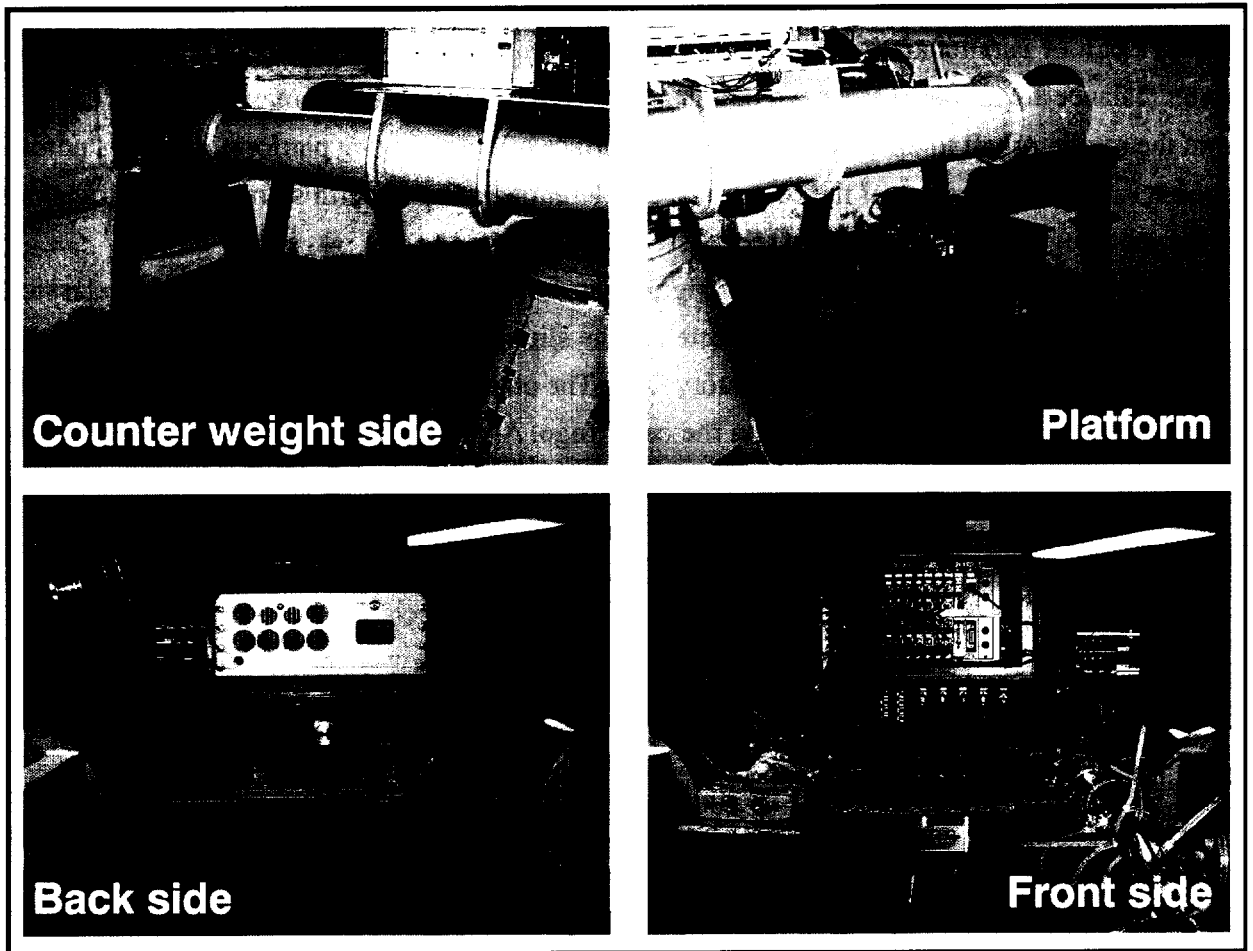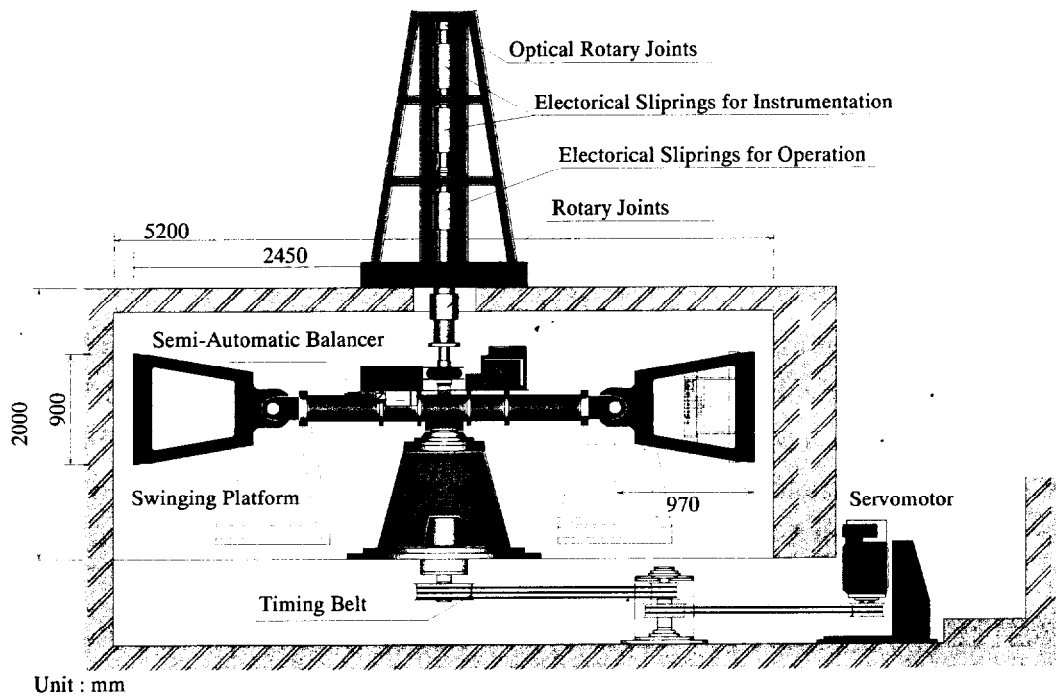
Figure 3.1 Tokyo Institute of Technology Mark-III Centrifuge

Table 3.1 Specifications of the Tokyo Tech Mark III Centrifuge

Radius	Platform radius	2.45 m
	Effective radius	2.0-2.2 m
Platform dimensions	Width	0.9 m
	Depth	0.9 m
	Maximum height	0.97 m
Capacity	Maximum payload	50 G ton
	Maximum number of rotation	300 rpm
	Maximum payload at 80 G	600 kg
Electrical slip rings	For instrumentation	72 channels
	For operation	18 channels
Optical rotary joints	Number of ports	4
Rotary joint	Number of ports for air and water	2
	Working pressure for air and water	1 MPa
	Number of ports for oil	2
	Working pressure for oil	21 MPa

unit: mm

Plane view

Cross section
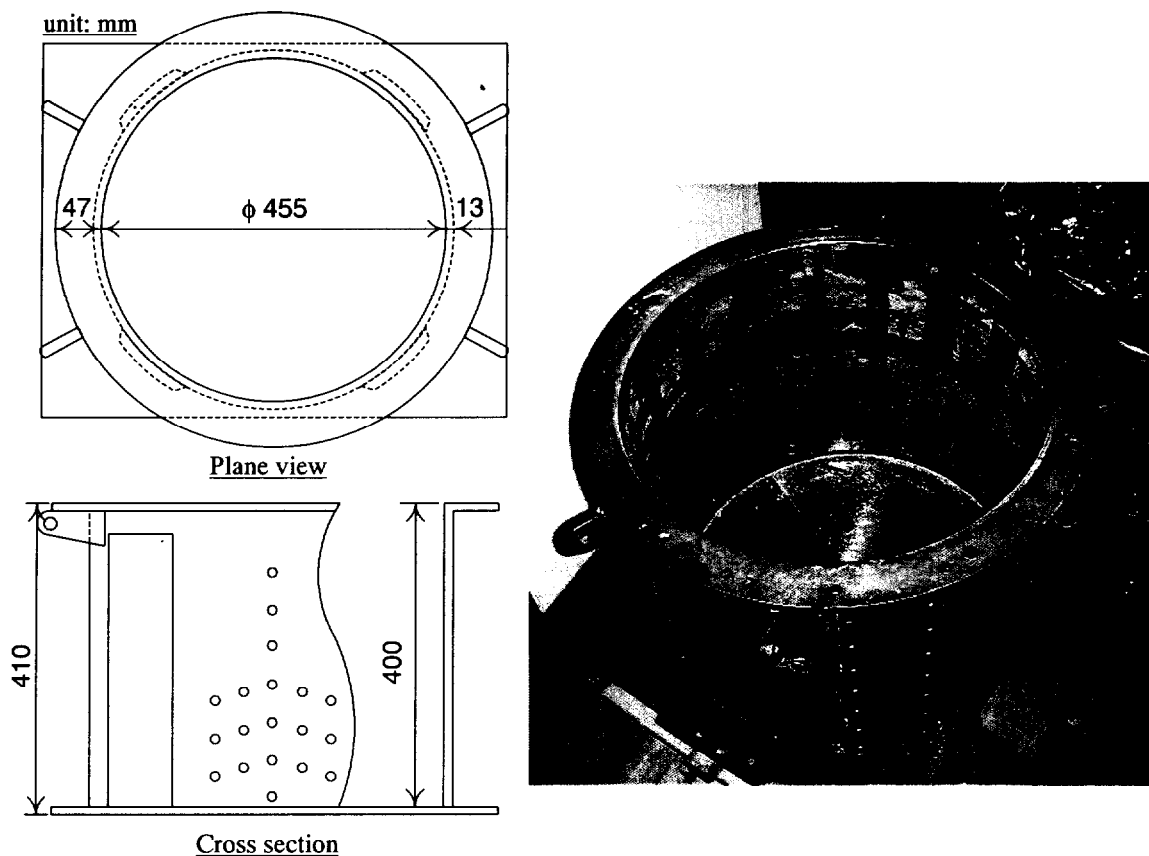
Figure 3.2 Circular container
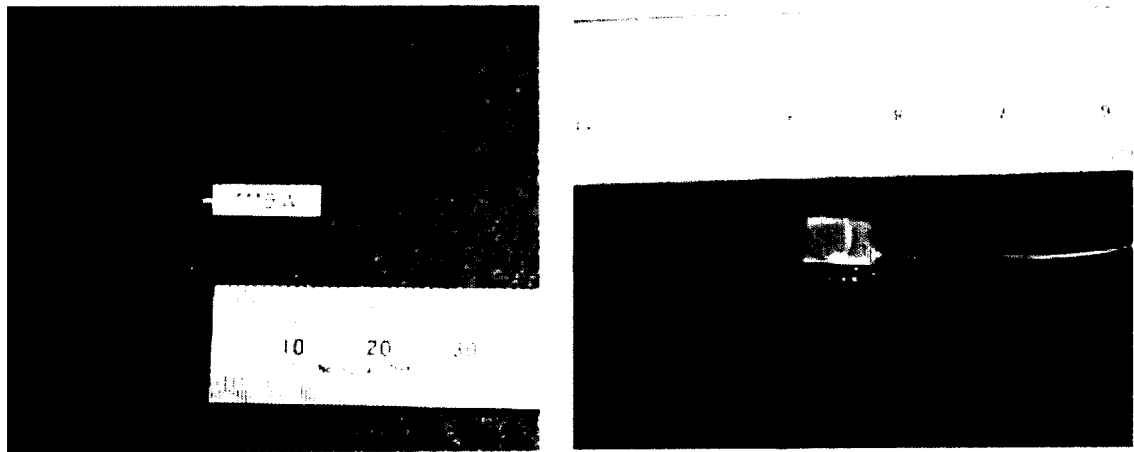
(a) CBC111BW   (b) CBC107S

Figure 3.3 Piezo-electronic accelerometers

Table 3.2 Specifications of piezo-electronic accelerometers

Model	CBC111BW	CBC107S
Electrical charge sensitivity (pC/m·s^{-2})	1.84	0.0357
Resonance frequency (kHz)	Over 4	Over 60
Size (mm)	4.0 × 13.0 × 4.0	4.6 × 5.8 × 4.3
Mass (g)	1.3	0.5

(2) Piezo-electronic accelerometer (Fig 3.3)

Piezo-electronic accelerometer which makes use of piezo characteristics is high quality, high band, light in weight, and high shock-resistant than the other types of sensor. Piezo-electric materials are those that produce a voltage when deformed (squeezed or bent) or produce a small movement when a voltage is applied. In this study, two types of piezo-electric accelerometer were used. One is the CBC111BW (Fig. 3.3(a), bent type, CBC Materials Co., Ltd.), and another one is the CBC107S (Fig. 3.3(b), squeezed type, CBC Materials Co., Ltd.). The performances of them are listed in Table 3.2. The accelerometer sensor recorded acceleration through the charge amplifier (CBC4101 (Fig. 3.4), CBC Materials Co., Ltd.). The specification of charge amplifier is listed in Table 3.3.

The original names of this piezo-electric accelerometer are yamco111BW and yamco107S, and company is Yamaichi Electronics Co., Ltd. The measurement division of Yamaichi Electronics Co., Ltd. had been transferred by Yamaichi Electronics Co., Ltd. to CBC Materials Co., Ltd. at the end of March 2002. The name of piezo-electric accelerometer is unified called like CBC107S and CBC111BW in this thesis.

(3) Photoelectric sensor (Fig 3.5)

A photoelectric sensor (PQ-01, Keyence Co., Ltd.) is a device that detects a light source. With the discovery in the early seventies of the Light Emitting Diode (LED), the problem of ambient light
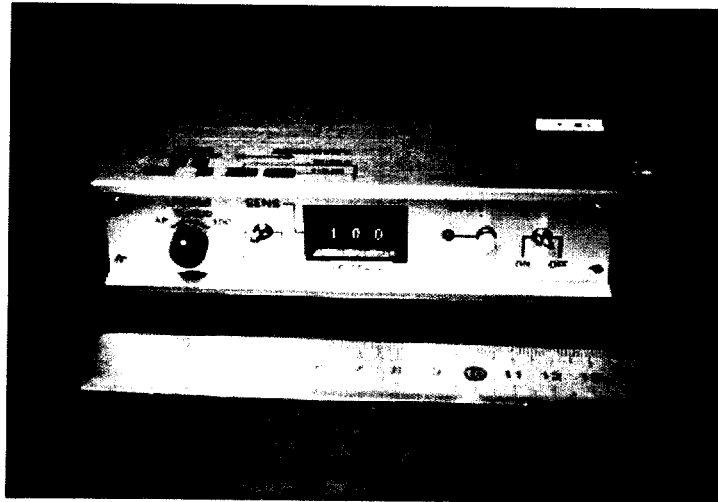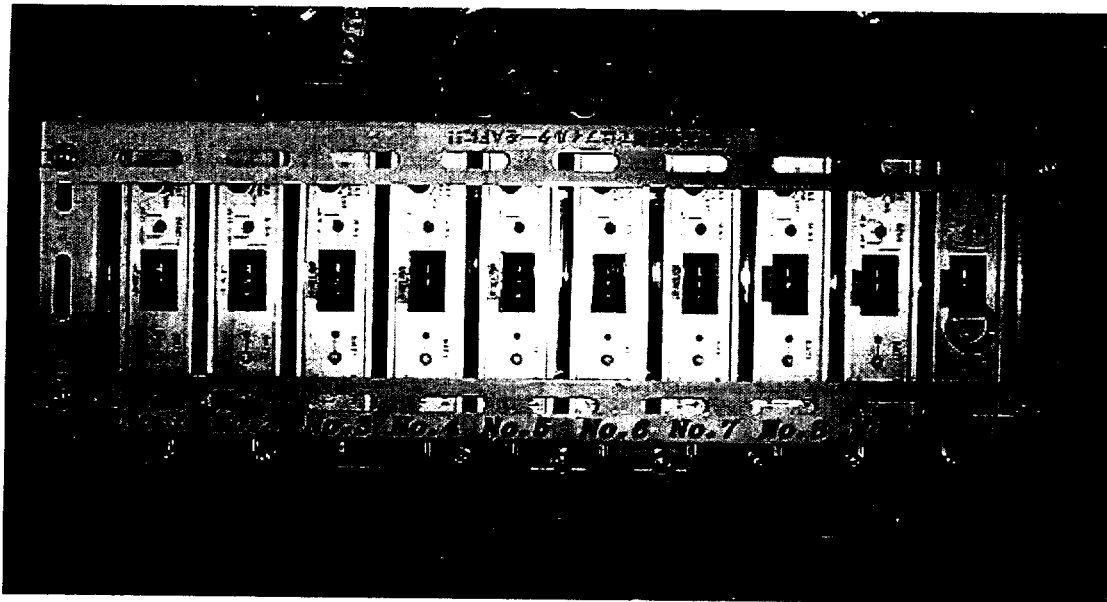
Figure 3.4 Charge amplifier CBC4101

interference was solved. A photoelectric sensor can be adjusted to respond only to the pulse of a particular LED, thus changing of any background light will not affect the sensor response. The specification of this sensor is listed in Table 3.4. This sensor supplies the output voltage, when light receiver does not catch LED from light transmitter (dark-on mode). This sensor was used to estimate the experimental falling velocity of steel ball by mounting it in the guide part of the system (Fig 3.6).

(4) Displacement transducer (Fig. 3.7)

Settlement of the sand surface was measured by a displacement transducer (Model MLT, Data Instrument Co. Ltd.) to obtain a void ratio change of the sand under the acceleration. A displacement transducer is a device for measurement of deformation electrically with by the flexible rod. Resistance is built in the main shaft. An output voltage corresponding to the deformation occurs when the flexible rod which composes the terminal moves. This transducer was contact type, however, the weight of the rod was small enough comparing with the bearing capacity of the sand used. The specification is listed in Table 3.5.

Table 3.3 Specifications of charge amplifier

Model	CBC4101
Input terminal	C25-102P
Output terminal	BNC
Output	$0.01V/m \cdot s^{-2}$ (0.1-9.99 pC/m·s^{-2}) $0.001V/m \cdot s^{-2}$ (0.01-0.099 pC/n·s^{-2}) $\pm 4V_{max}$ (peak)
Frequency characteristics	Acc: 1 Hz to 50kHz
Filter	Law pass filter Fc: 300Hz,500Hz,1kHz,AP
Maximum input electrical charge	4×10^3 pC (at 1kHz 99.9pC/m·s^{-2})
Noise level	Under 0.02pC (r. m. s.)
Mass (include dry cell) (g)	420
Size (mm)	140(W) × 40(H) × 82(D)
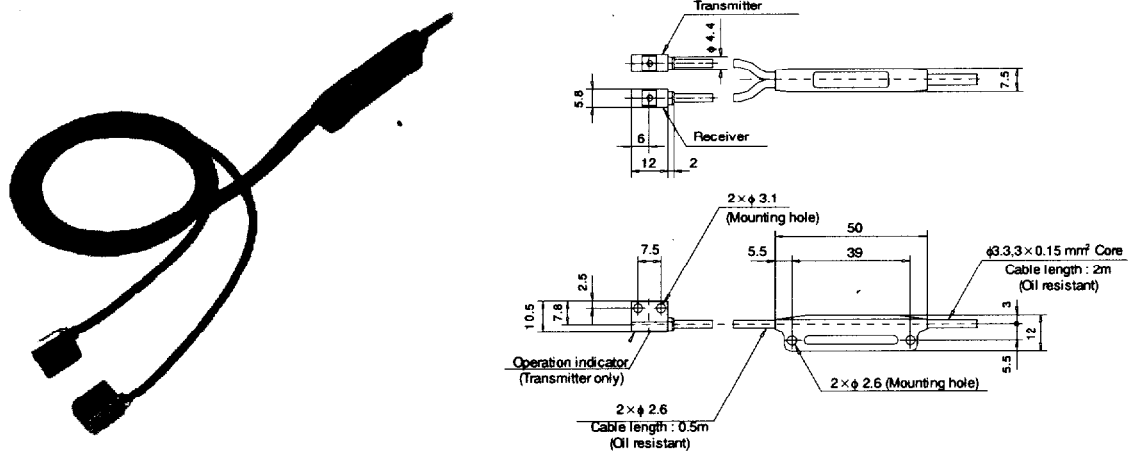
Figure 3.5 Photoelectric sensor
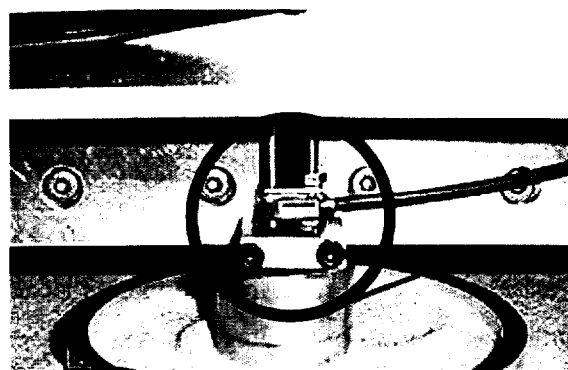
Figure 3.6 Setup photoelectric sensor

- 40 -

Table 3.4 Specifications of photoelectric sensor

Model	PQ-01
Detecting distance	0 to 100mm
Supply voltage	DC12 to 24V ± 10% Ripple (p-p) 10 % max
Current consumption	30mA max
Output mode	Dark – ON
Control output	100mA (at 40V) max
Protective circuit	Reversed polarity, overcorrect protection, surge absorber
Response time	1ms max
Detective object	Opaque materials (1.0mm dia. min)
Ambient operating illumination	Incandescent lamp	3000lx max
	Sunlight	10000lx max
Degree of protection	IP-64
Light source	Infrared LED
Detection indicator	Red LED
Materials	Amplifier: Polysulfone, Sensor: Polyallylate
Cable length	2m (Between sensor head and amplifier: 500mm each)
Weight (include cable)	Approx. 48g
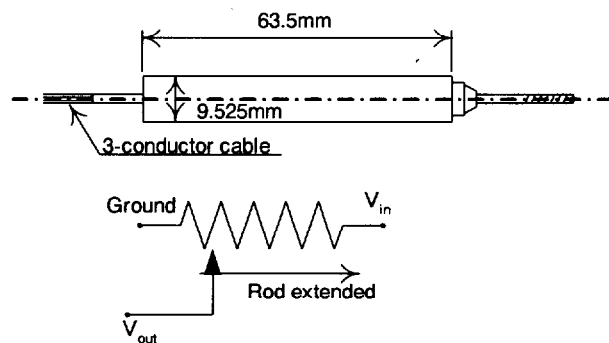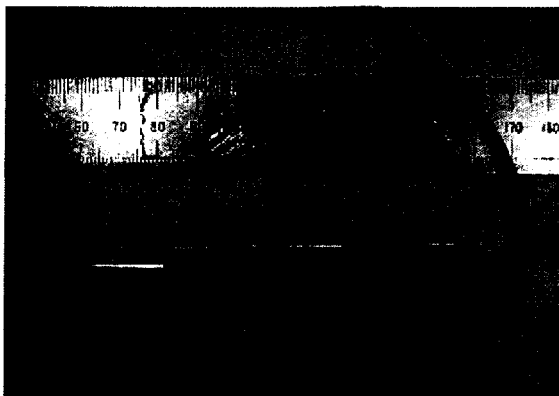
Figure 3.7 Displacement transducer

Table 3.5 Specifications of displacement transducer

Model	MLT
Measurement range	0 to 48.1 mm
Total resistance	1500 Ω / 25.4 mm
Impedance linearity	± 1.0 %
Resolution	infinity
Output rating	0.25 W / 25.4 mm
Fatigue Life	10^9

(5)   CCD camera (Fig. 3.8)

In order to observe the behavior in which a steel ball was hitting on the foundation, a CCD camera (CS6100B CCU, Tokyo Electronic Industry Co., Ltd.) was used.

(6)   Function synthesizer (Fig. 3.9)

The function synthesizer (1940S, NF Electronic Instruments Co., Ltd.) was used to generate and control the input frequencies of centrifugal vibration exciter used in Chapter 5.
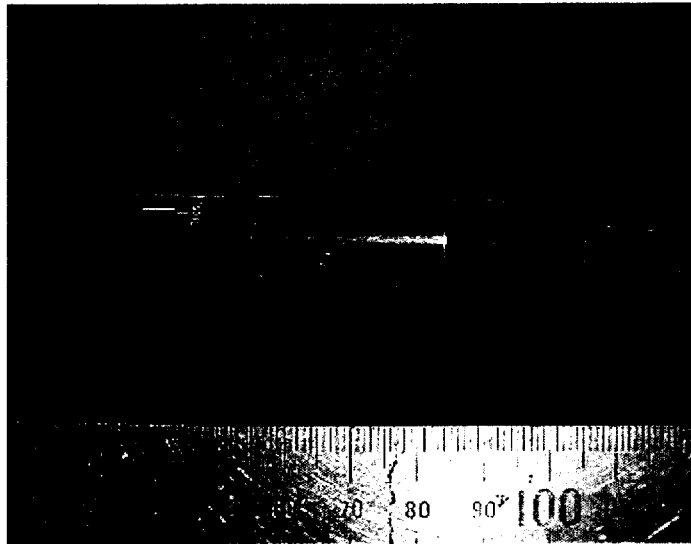
Figure 3.8 CCD camera
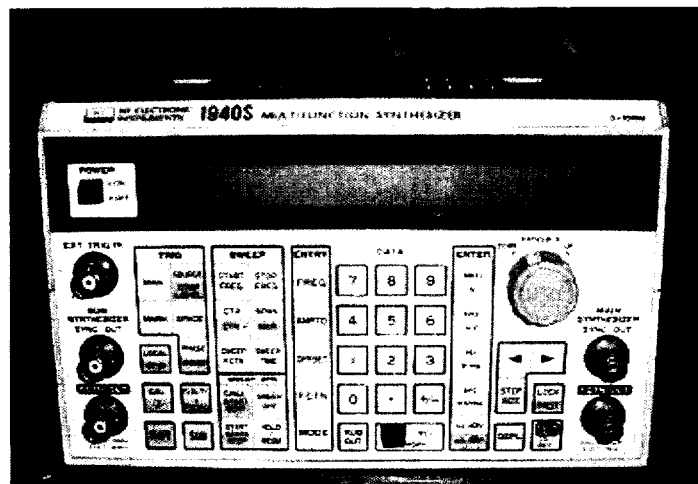
Figure 3.9 Function synthesizer

- 42 -

3.4 MATERIAL AND MECHANICAL PROPERTY OF MATERIALS USED

3.4.1 Overview of soil properties

In centrifuge experiment, the soil used was air-dried Toyoura sand in all cases. Toyoura sand that is uniform fine sand was used as Japanese standard sand in laboratory testing. Many researchers of geotechnics in Japan used Toyoura sand so that the author also used this as typical fine sand in Chapter 4 and 5. Figure 3.10 shows the magnified view of Toyoura sand particles. Figure 3.11 shows the grain size distribution of Toyoura sand. Physical properties of Toyoura sand are tabulated in Table 3.6.

In addition, Chaudhary and Kuwano (2001) investigated the yielding behavior of dense Toyoura sand (Dr = 80%) from small to large strain in a p'-constant plane with respect to anisotropy using the hollow cylinder testing system. Figure 3.12 shows a close-up of the stress-strain curves for small strain ranges. It can be observed that they were linear up to shear strain of approximately 0.002%. Up to this strain level, the secant shear modulus was constant and the same as the tangent shear modulus. The shear strain increment was elastic. But over the elastic range, the shear modu-
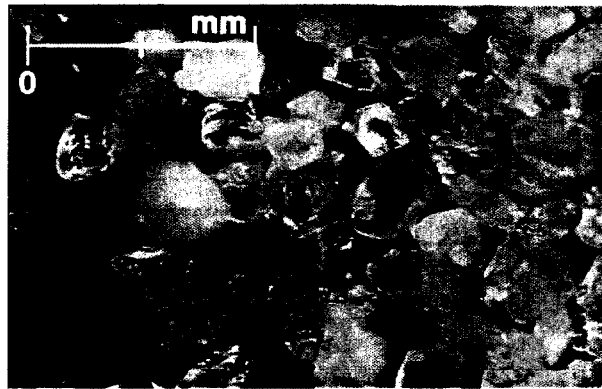
Figure 3.10 Toyoura sand particles
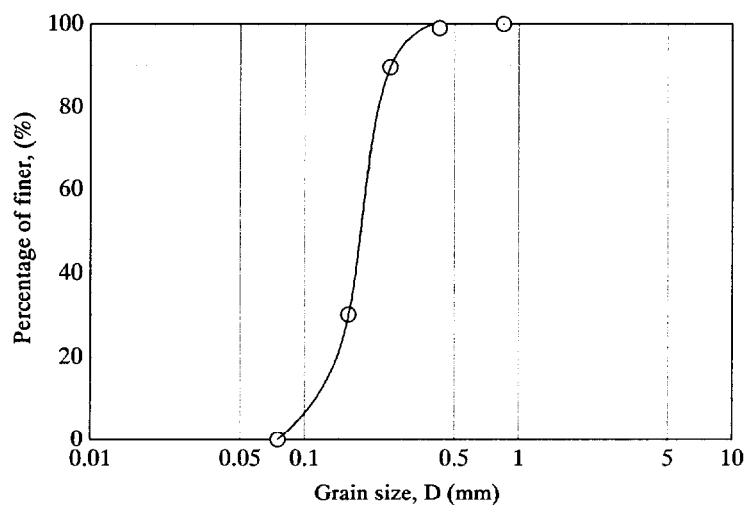
Figure 3.11 Grain size distribution of Toyoura sand

Table 3.6 Material properties of Toyoura sand

Property	Toyoura sand
Particle density ρ_s (g/cm^3)	2.645
Maximum grain size (mm)	0.85
Mean particle diameter D_{50} (mm)	0.19
30% diameter of soil particle D_{30} (mm)	0.164
10% diameter of soil particle D_{10} (mm)	0.135
Uniformity coefficient U_C	1.56
Coefficient of curvature U_C'	0.95
Maximum void ratio e_{max}	0.973
Minimum void ratio e_{min}	0.609
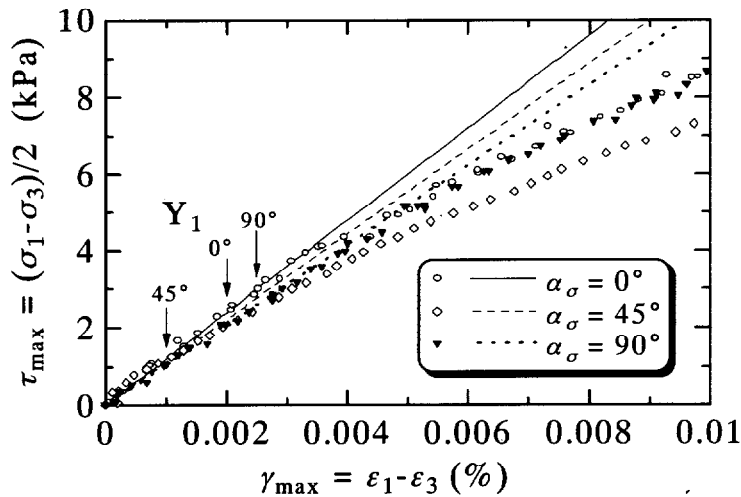
Figure 3.12 Close-up of shear stress-shear strain curve (after Chaudhary and Kuwano, 2001)

lus decreased a little by less than 10% of the initial value. The plastic shear strain increment appeared. The results from their laboratory test indicate that the plastic behavior of sand is observed at very small strain level. This behavior is a factor of knotty problems in order to simulate the wave propagation on the ground.

In the centrifuge model test, there are obvious differences in the stress field, namely in proportion to depth as the stress increases. The field of exploration geophysicist calls this type of ground condition "mirage layer" (e.g. Watanabe, 1953; Sassa et al., 1993). Let us assume that velocity is equal to this equation as follows;

$$V(z) = V_0 + kz \quad\quad\quad (3.1)$$

where $V(z)$ is velocity at depth z, V_0 is velocity at ground surface(z=0), k is coefficient of magnitude, and is depth. Figure 3.13 shows travel time curve and ray paths in the case of mirage layer. Travel time equation can be determined as follows:
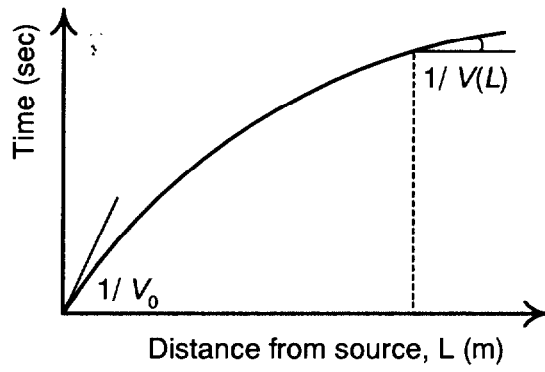
(a) Travel time curve
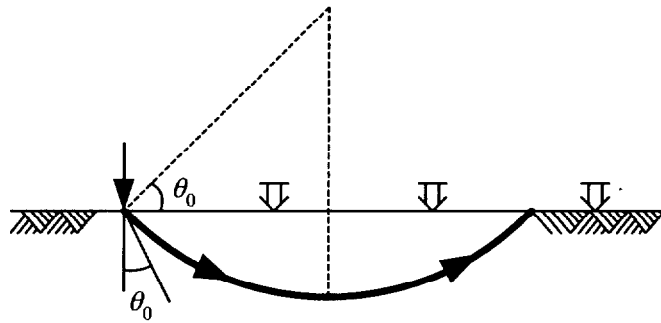
(b) Ray paths

Figure 3.13 Travel time curve and ray paths in the case of mirage layer

Figure 3.14 Triaxial apparatus for cyclic loading test within BE test

$$T(L) = \left(\frac{2}{k}\right) \sinh^{-1}\left(\frac{kL}{2V_0}\right) \quad \text{..(3.2)}$$

where, $T(L)$ is travel time at distance form source, L.

In order to investigate a variation of wave velocity of dry Toyoura sand under various pressures, Bender Element Test (BE test) was carried out. Figure 3.14 shows the test system. This system is originally used as a triaxial apparatus for cyclic loading test which can measure strain range. In addition this system can measure wave velocities in three directions (e.g. Hayano, 1999). However this study measured only one direction, vertical shear velocity. The soil used was dried Toyoura sand (D_r = 78.6 %). When the confining pressure was changed at seven cases which are 20 kPa, 30 kPa, 50 kPa, 100 kPa, 150 kPa, 200 kPa, and 250 kPa respectively, each wave velocity was measured by BE test. Figure 3.15 shows the relationship between depth and wave velocity, together with the results reported by Iwasaki and Tatsuoka (1977). In order to provide the travel time curve and ray paths under the mirage layer, this data were approximated by a linear equation, as follows:

$$V(z) = 178.94 + 9.31 \times z \quad \text{..(3.3)}$$

Upon substituting travel time given by V_0 =178.94 and k =9.31 into Eq. 3.2 yields the results as shown in Fig. 3.16 (a). Apparent in this figure are observed the convexly curve far away. However as for this experiment, measurement location is only 10 m at prototype scale, because diameter of container is 435mm. Thus this curve can approximate a linear line as shown in Fig. 3.16 (b) within this study range.
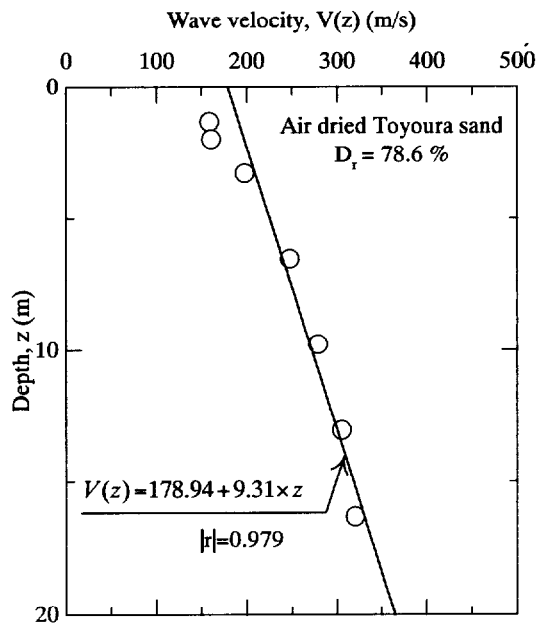
Figure 3.15 The relationship between depth and wave velocity in the case of air dried Toyoura sand (D_r = 78.6 %)
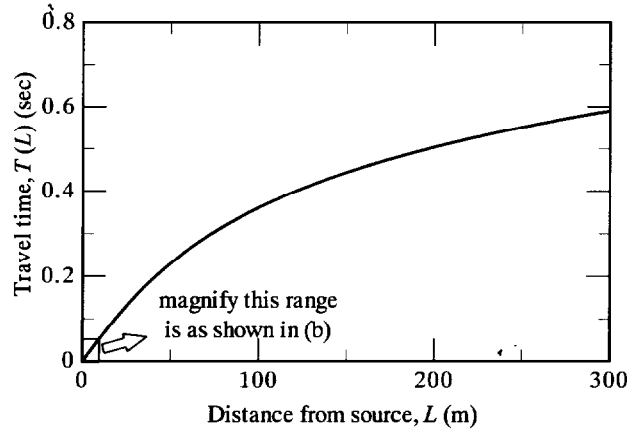
(a) General Travel time curve
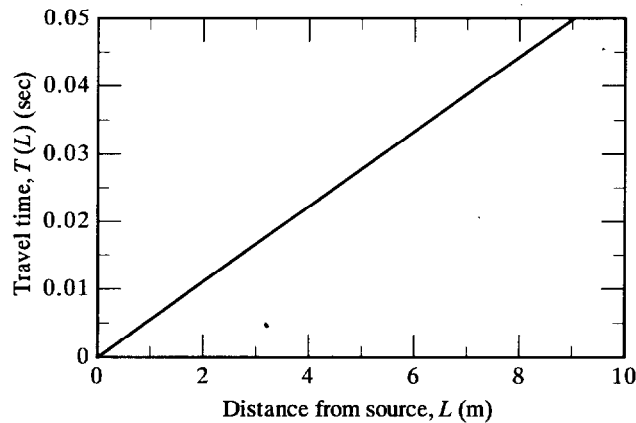
(b) Close-up of travel time curve

Figure 3.16 Travel time curve in the condition of centrifuge model test

3.4.2 Overview of materials used in centrifuge model test

(1) Materials for modelling wave barrier

In this study, aluminium, acryl, and Expanded Poly-Styrol (EPS) were used materials for modelling wave barrier (Fig. 3.17) in order to investigate the effect of stiffness or wave impedance (material) of wave barrier on the reduction of vibration. The material / mechanical properties of them are listed in Table 3.7. In their materials, the characteristics of Aluminium and Acryl have been decided by International Organization for Standardization (ISO) and Japanese Industrial Standards (JIS) as the industrial material. Additionally, the characteristics of EPS materials are standardized by JIS, and the material used is D-12 type (EPS construction method Development Organization).

(2) Material for modelling trackbed

In this experiment, natural rubber, aluminium, and Crumb Rubber Modified Asphalt (CRMA) were used materials for modelling trackbed (Fig. 3.18), in order to verify the influence of stiffness or damping ratio of trackbed on the reduction of vibration. The material / mechanical properties of modelling trackbed are listed in Table 3.7, together with other materials. As to the countermeasures
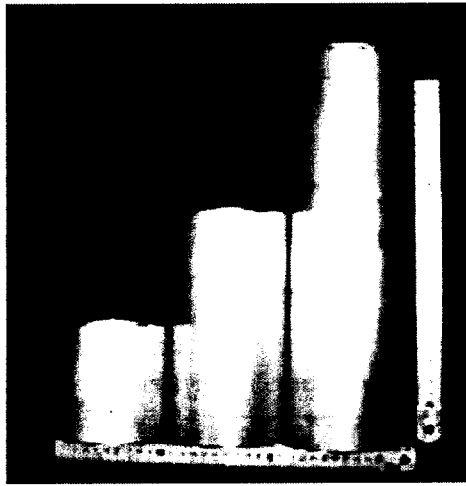
(a) Aluminium
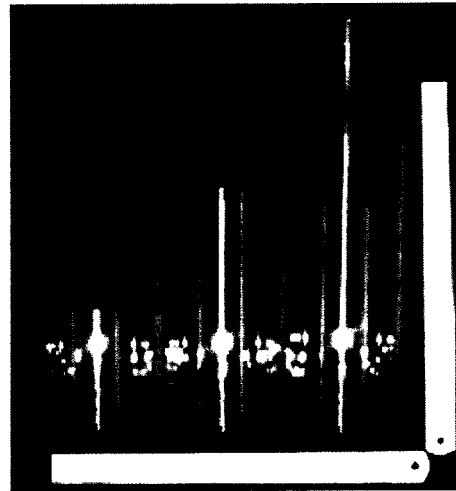
(b) Acryl
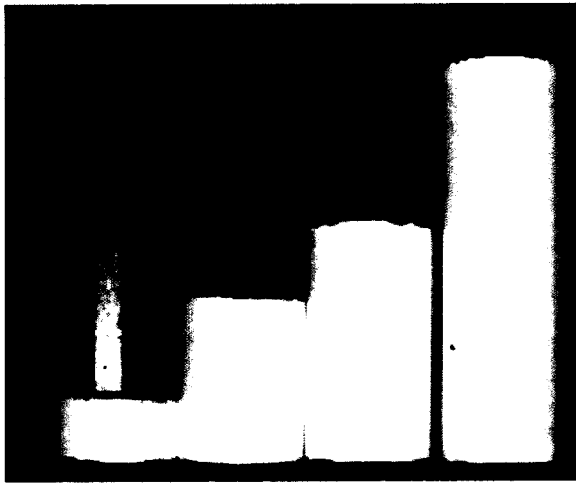
(c) EPS (cylindrical type)
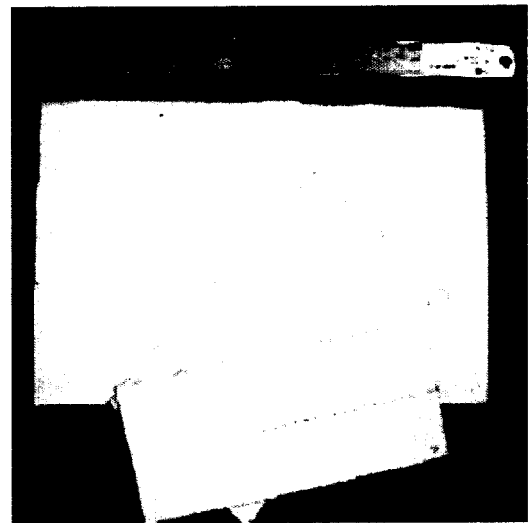
(d) EPS (rectangular type)

Figure 3.17 Used materials of countermeasures at transmitting path

at vibration source, the application of CRMA was mainly examined in Chapter 4 and 5. The idea of using waste tires to make rubber-modified asphalt started in 1940's in the United States. Rubber-modified asphalt is a bituminous mix, consisting of blended aggregates, recycled crumb rubber, and petroleum asphalt binding agents. The rubber is often obtained from used tires. Previous studies and field measurements on highways have shown that rubber-modified asphalt can significantly reduce the noise pollution that is associated with roadway traffic (Roschen, 2000). The introduction of rubber-modified asphalt into railroad track beds is expected to produce considerably more benefit in noise mitigation than on highways. There are two reasons for this. One is that there is a much stiffer contact surface on railways than on highways. The rubber tires of motor vehicles help reduce the noise induced by automobiles on highways, while on the railroad the contact surface is between the steel wheel of railway cars and the steel rail of the track. The introduction of rubber-modified asphalt pavement material is expected to significantly increase its capacity of vibration attenuation and seems to be an ideal construction material for railway trackbeds. Laboratory tests on crumb rubber-modified asphalt mixes show that adding crumb rubber to asphalt increases the damping

Table 3.7 Material and mechanical properties of modelling barrier and trackbed

	Dry unit weight γ_d (kN/m^3)	Shear modulus G (MN/m^2)	Maximum grain size (mm)	Mean particle diameter D_{50}(mm)
Aluminium	26.5	2.56×10^4	-	-
Acryl	11.8	1.21×10^3	-	-
EPS (type D-12)	0.12	1.11	-	-
Rubber (natural rubber)	9.60	1.08×10^2	-	-
CRMA prototype	23.1	9.50×10^2	15.0	3.35
CRMA 1/5 size	23.5	9.60×10^2	4.75	0.25
Toyoura sand (Dr=80%) near the surface	15.4	1.79×10	0.85	0.19

Aluminium Natural Rubber

CRMA (prototype scale) CRMA (1/5 scale)
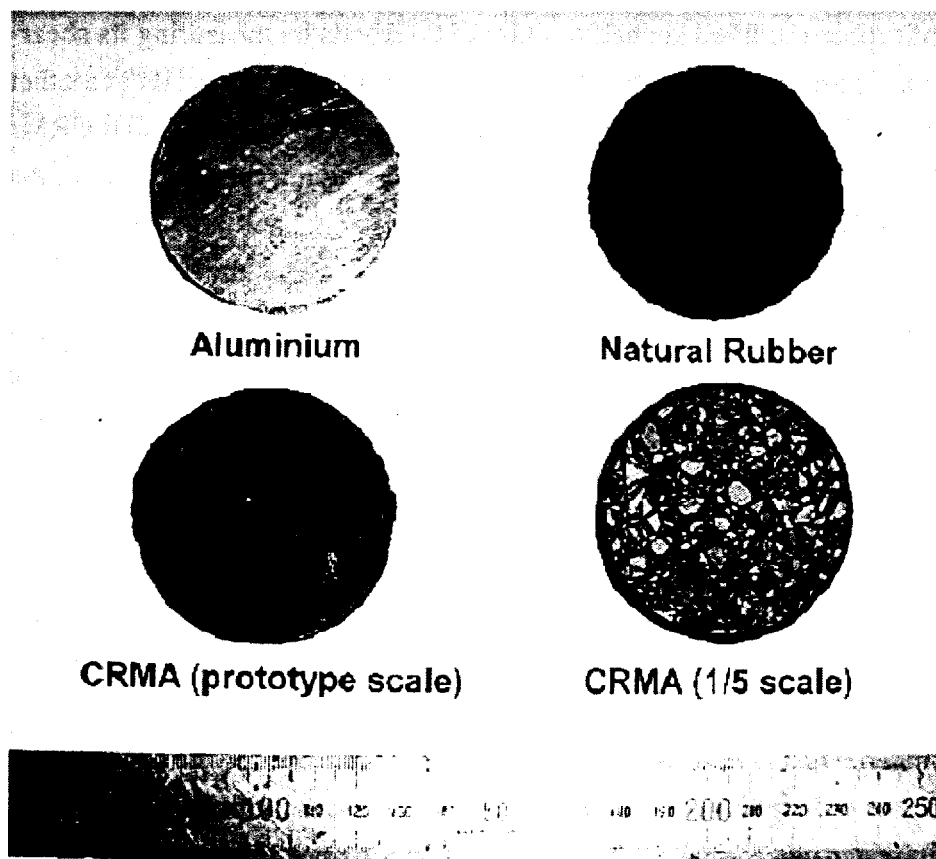
Figure 3.18 Used materials of countermeasures at vibration source
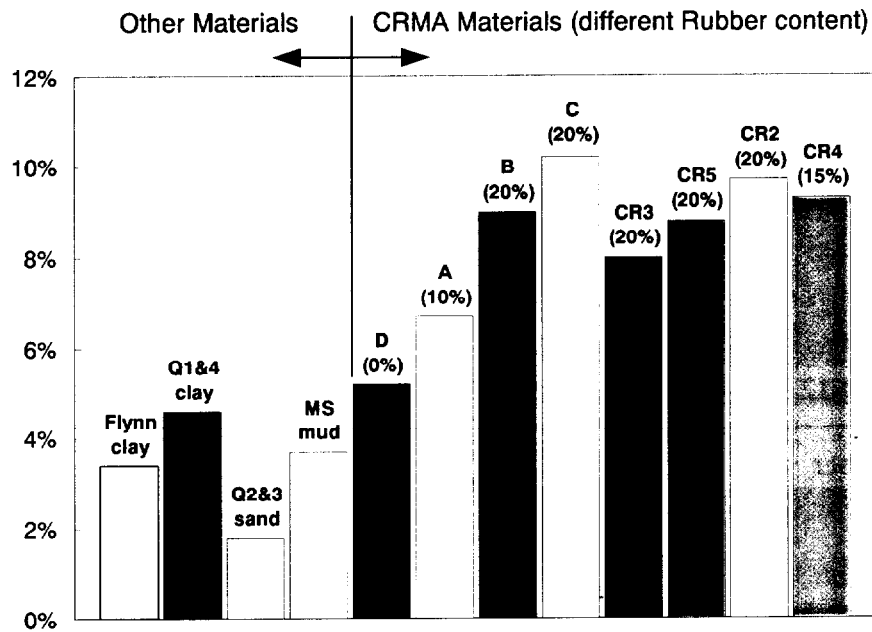
Figure 3.19 Damping ratio of CRMA materials and other materials at shear strain around 10^{-4} percent (after Zhong et al., 2002)

ratio of asphalt mix while maintaining its high stiffness (Zeng et al, 2001). Zhong et al. (2002) conducted cyclic triaxial tests in order to present the results of an investigation into the potential application of rubber-modified asphalt in railroad trackbeds by measuring its shear modulus and damping ratio. Figure 3.19 shows the damping ratio of CRMA materials and other materials at shear strain around 10^{-4} percent (Zhong et al., 2002). Their results show that CRMA sample is a material with high shear stiffness and damping ratio, making it a very attractive material for vibration attenuation of railroad trackbeds.

3.5 SIMILITUDE IN DYNAMIC CENTRIFUGE MODELLING TEST

Physical modelling is performed in order to study particular aspects of the behavior of prototypes. Full-scale testing is, in a way, an example of physical modelling where all features of the prototype being studied are reproduced at full scale. However, most physical models will be constructed at much smaller scales than the prototype precisely because it is desired to obtain information about expected patterns of response more rapidly and with closer control over model details than would be possible with full-scale testing. If the model is not constructed at full scale, we need then to have some idea about the way in which we should extrapolate the observations that we make at model scale to the prototype scale.

If the material behavior is entirely linear and homogeneous for the loads that we apply in the model and expect in the prototype then it may be a simple matter to scale up the model observations and the details of the model may not be particularly important. However, if the material behavior is nonlinear or if the geotechnical structure to be studied contains several materials which interact

with each other then the development of the underlying theoretical model will become more difficult. It then becomes even more vital to consider and understand the nature of the expected behavior so that the details of the model can be correctly established and the rules to be applied for extrapolation of observations are clear.

A true model is obtained when all the governing laws of similitude are in place. However, often for geotechnical modelling it will be necessary to make do with an adequate model which maintains 'first order' similarity.

Many researchers have discussed scaling factors for models in general and geotechnical models in particular (i.e. Craig et al., 1988; Iai, 1989; Schofield and Steedman, 1988) - some of these have been primarily concerned with the factors that are relevant to centrifuge modelling. A brief discussion is warranted here – often stiffness is not identified as a factor that needs to be considered separately and it seems to be helpful to use stiffness rather than strain as an independent quantity. There are various scaling factors that need to be chosen and there may be discussion about the most fundamental set to use. It seems that four are certainly required for the soil material (Wood et al., 2002):

Length: $\dfrac{length_{model}}{length_{prototype}} = \alpha_L$

Density: $\dfrac{density_{model}}{density_{prototype}} = \alpha_\rho$

Stiffness: $\dfrac{stiffness_{model}}{stiffness_{prototype}} = \alpha_E$

Acceleration: $\dfrac{acceleration_{model}}{acceleration_{prototype}} = \alpha_G$

There is an implicit assumption that dynamic accelerations must be scaled with the model equivalent gravitational acceleration. Other scaling factors can be deduced from these, as follows;

$$stress = \frac{force}{area} = \frac{density \times length^3 \times acceleration}{length^2} = \frac{\alpha_\rho \alpha_L{}^3 \alpha_G}{\alpha_L{}^2} = \alpha_\rho \alpha_L \alpha_G \quad \dotfill (3.4)$$

$$strain = \frac{stress}{stiffness} = \frac{\alpha_\rho \alpha_L \alpha_G}{\alpha_E} \quad \dotfill (3.5)$$

$$displacement = strain \times length = \frac{\alpha_\rho \alpha_L \alpha_G}{\alpha_E} \times \alpha_L = \frac{\alpha_\rho \alpha_L{}^2 \alpha_G}{\alpha_E} \quad \dotfill (3.6)$$

A scale factor for velocity can be proposed from the need to match scales of potential and kinetic energies, as follows;

$$velocity = \sqrt{\alpha_G \times \frac{\alpha_\rho \alpha_L^2 \alpha_G}{\alpha_E}} = \alpha_G \alpha_L \sqrt{\frac{\alpha_\rho}{\alpha_E}} \quad\text{...} \quad (3.7)$$

For dynamic events the scale factor for time and frequency are follows;

$$dynamic\ time = \frac{displacement}{velocity} = \frac{\left(\dfrac{\alpha_\rho \alpha_L^2 \alpha_G}{\alpha_E}\right)}{\left(\alpha_G \alpha_L \sqrt{\dfrac{\alpha_\rho}{\alpha_E}}\right)} = \alpha_L \sqrt{\frac{\alpha_\rho}{\alpha_G}} \quad\text{..................................} \quad (3.8)$$

$$frequency = \frac{1}{dynamic\ time} = \frac{1}{\alpha_L}\sqrt{\frac{\alpha_G}{\alpha_\rho}} \quad\text{..} \quad (3.9)$$

The shear wave velocity for the soil is dependent on the density and stiffness of the soil.

$$V_s = \sqrt{\frac{G}{\rho}} = \sqrt{\frac{\alpha_E}{\alpha_\rho}} \quad\text{..} \quad (3.10)$$

All scaling factors are listed in Table 3.8.

Table 3.8 Scale factor (after Wood et al., 2002)

Variable	Scale factor	Ng model
Length	n_l	$1/n$
Density	n_ρ	1
Stiffness	n_G	1
Acceleration	n_g	n
Stress	$n_\rho n_g n_l$	1
Strain	$\dfrac{n_\rho n_g n_l}{n_G}$	1
Displacement	$\dfrac{n_\rho n_g n_l^2}{n_G}$	$1/n$
Velocity	$n_g n_l \left(\dfrac{n_\rho}{n_G}\right)^{1/2}$	1
Dynamic time	$n_l \left(\dfrac{n_\rho}{n_G}\right)^{1/2}$	$1/n$
Frequency	$\dfrac{1}{n_l}\left(\dfrac{n_G}{n_\rho}\right)^{1/2}$	n
Shear wave velocity	$\left(\dfrac{n_G}{n_\rho}\right)^{1/2}$	1

CHAPTER 4

WAVE PROPAGATION AND
ITS ISOLATION METHOD USING
MULTIPLE BALL DROPPING SYSTEM

4.1 INTRODUCTION

This chapter presents the centrifugal modeling test which can simulate the wave generation and propagation from various types of impact loading. Those problems in a half-space elastic body from a single free surface vibration source had been solved by past researchers, numerically (e.g. Lamb, 1904; Love, 1911). As to centrifuge model test, Luong (1994), Semblat and Luong (1988), and Siemer and Jessberger (1994) produced the simulation system which generated vibration by impact loading on the ground surface. However Luong (1994) and Semblat and Luong (1988) did not measure the information (acceleration) at the input position.

This chapter describes on the development of the Multiple Ball-Dropping System, which can simulate wave propagation. In addition, this system is possible to simulate not only the point load but also the quasi-moving loads caused by high-speed trains running through viaducts (Itoh et al., 2002a, 2002b, 2002c, and 2002d). Details of the Multiple Ball-Dropping system are described, and centrifuge model test results on wave propagation in various input point loads and vibration countermeasures at transmitting path and vibration source are presented.

4.2 DEVELOPMENT OF MULTIPLE BALL-DROPPING SYSTEM

4.1.1 System description

The Multiple Ball-Dropping system was designed with the aims of

1) Measuring input force (acceleration),

2) Simulating impact point load and moving load conditions, and

3) Studying the effects of the geometry of wave isolation barriers on the reduction of vibration.

Details of this system are shown in Fig. 4.1. The concept of the ball dropping mechanism is, in principle, the same as the sand hopper commonly used in centrifuge tests, for modelling embankment construction (Kimura et al., 1982). An AC induction motor of 40W (Oriental Motor Co., Ltd. THI540A-GVHJ) drives a slider made of aluminium plate via a crankshaft. There are 20mm-square holes in the slider and when these holes overlap a series of holes made in a falling guide frame, a steel ball of 19.8 mm in diameter and 28.0 g in mass drops onto a model foundation resting on the surface of the model ground. Figure 4.2 shows the view of the model foundation. The model foundation was made of an aluminium cylinder of 30mm in diameter and 25mm in height, housing a
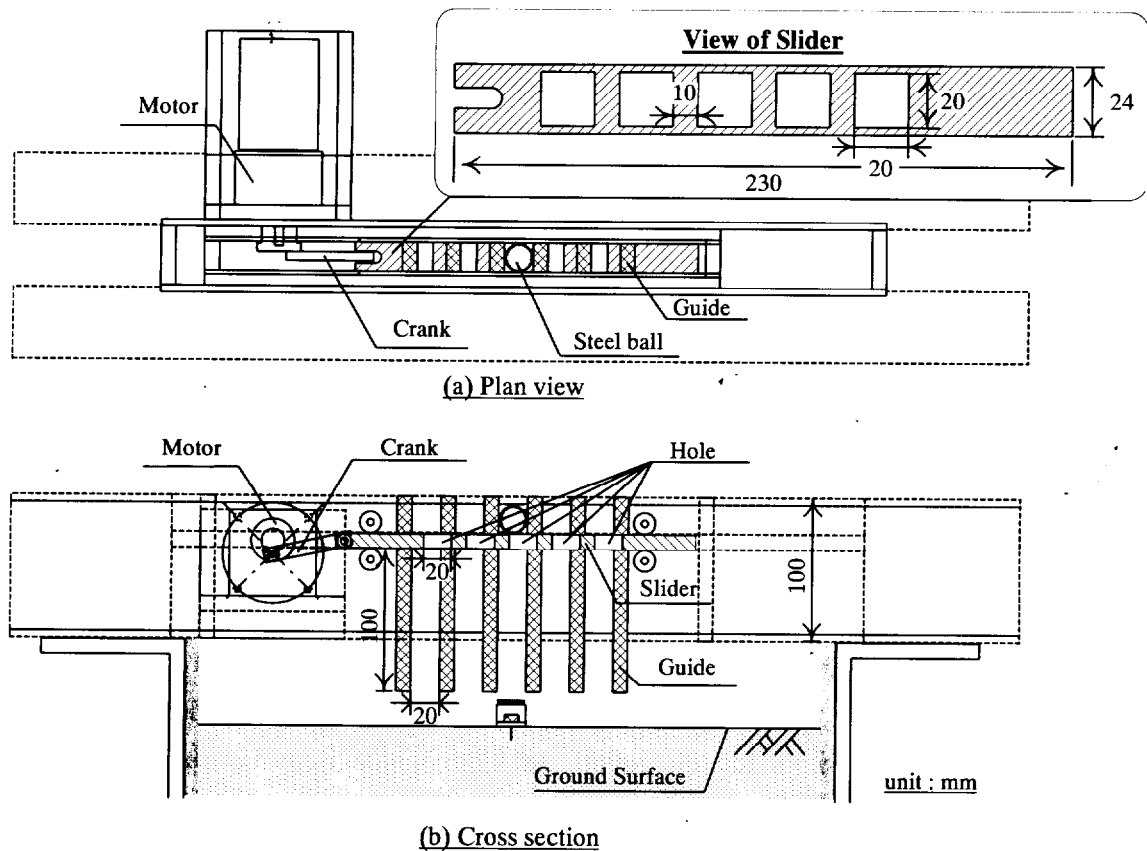
Figure 4.1 System of Multiple Ball-Dropping System
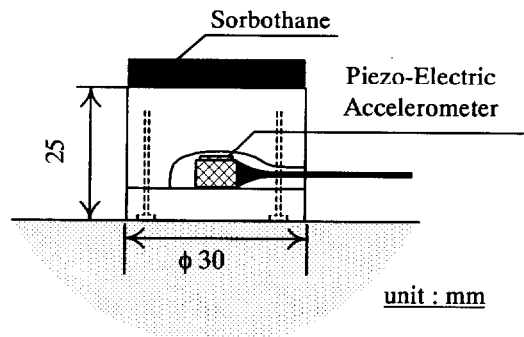
Figure 4.2 View of the model foundation

built-in piezo-electric accelerometer (CBC111BW, a resonance frequency of 4 kHz, B15 × W4 × H4 mm, CBC Materials Co., Ltd.) in order to measure the input force directly. The mass of the model foundation was 48.5 g. Proof tests revealed that the capacity of the initially built-in piezo-electric accelerometer was inadequate and the accelerometer was then upgraded to a CBC107S (a resonance frequency of 60 kHz, B6 × W5 × H5 mm, CBC Materials Co., Ltd.) for the following tests, which were more productive.

A sheet of 5 mm thick Sorbothane (Sorbothane Inc.) was glued on the surface of the model foundation in an attempt to absorb the impact shock energy partially and to suppress the bouncing of the ball, so that the ball and the model foundation could move together after impact. An in-flight
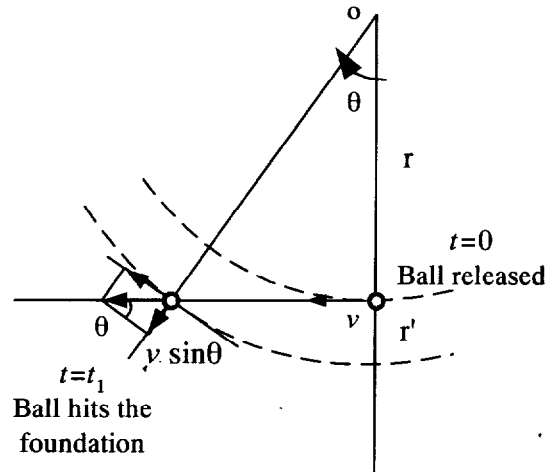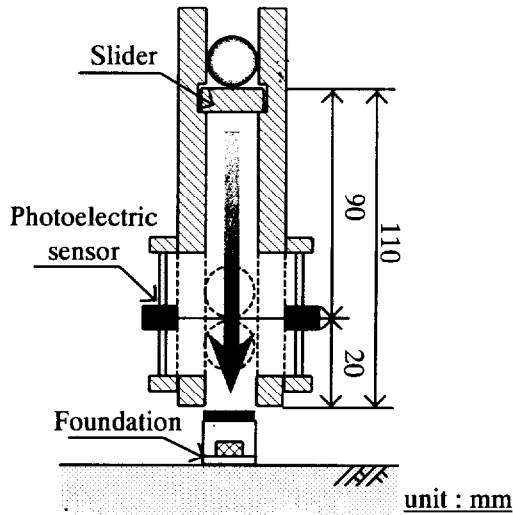
Figure 4.3 Side view of photoelectric sensors   Figure 4.4 Reference frame for a particle's mo-
mounted onto the guide frame   tion in a centrifuge

Table 4.1 Parameters for falling velocity calculations in the case of Tokyo Tech Mark-III Centrifuge

r (m)	1.826
r' (m)	0.09
ω (rad/sec)	15.31
v = r ω (m/s)	27.95

camera confirmed that the bouncing of the ball did not occur. A sheet of sandpaper (#80) was glued to the base of the model foundation to represent a rough condition. A set of photoelectric sensors (KEYENCE Co., Ltd., PQ-01) were mounted on both sides of the guide frame, as shown in Fig. 4.3, to measure the falling velocity of the steel ball.

4.1.2   Performance of Multiple Ball Dropping System

It may be interesting, first of all, to compare the theoretical velocity of a free falling mass in the centrifugal acceleration field with the velocity of a falling ball through the guide frame in the system, in which there exists only 0.2 mm gap between the ball and the guide frame.

Consider a steel ball resting on the slider of the system at a distance r from the axis of a centrifuge, which is rotating at an angular velocity of ω. A steel ball is theoretically subjected to an absolute radial acceleration of $r\omega^2$. When the steel ball is released from the initial position, it will move in a straight line tangential to its orbit if it is free to do so (Fig. 4.4). From the viewpoint of the model ground, the falling velocity of the steel ball is given below because of the effect of the Coriolis force.

$$v = r\omega \sin\theta \dotfill (4.1)$$

where v is a velocity component tangential to $r\omega^2$ orbit as the falling velocity, r is the initial position from the axis of a centrifuge and θ is the rotation angle from a point when the ball drops to the point
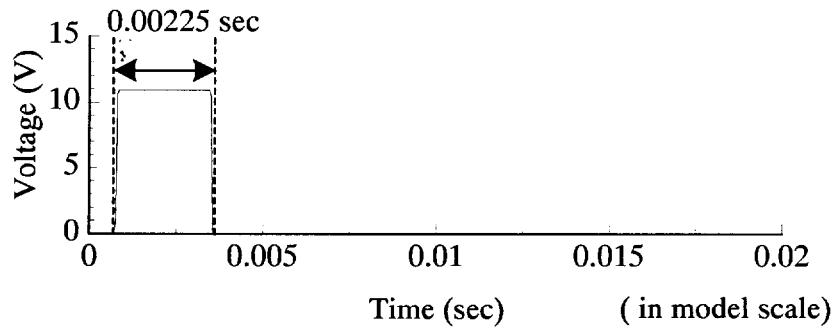
Figure 4.5 An example of voltage of photoelectric sensor with reaction time

Maximum Acceleration α_{max} (m/s^2)

Δt (sec)
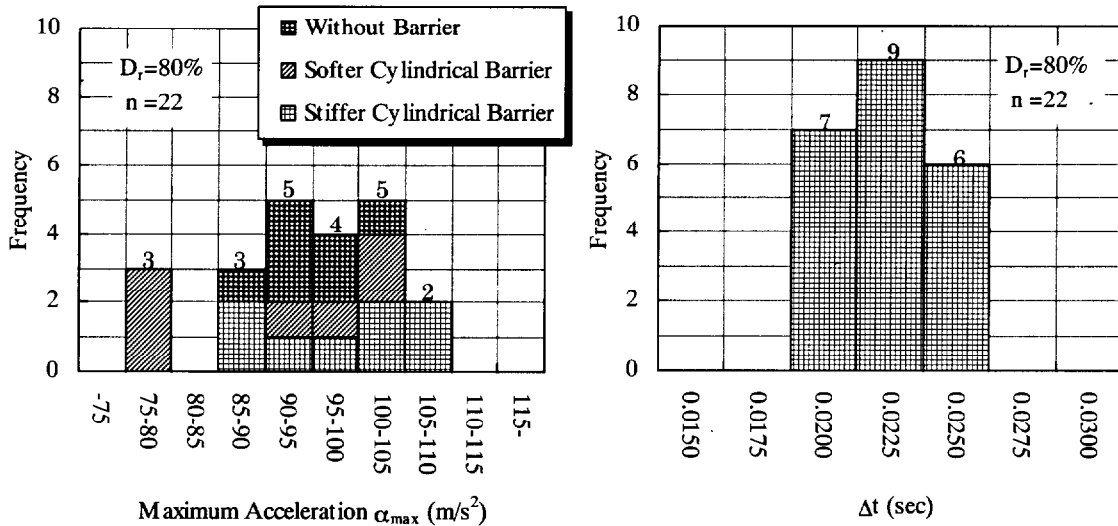
Figure 4.6 Frequency distributions of maximum acceleration α_{max} and time required to reach α_{max}, Δt

when the ball hits the foundation. Putting the experimental parameters for this particular test condition (as listed in Table 4.1) into Equation (4.1) yields the theoretical falling velocity of a ball at 90 mm beneath the initial position as follows,

$$V_{cal} = v\sin\theta = 27.5\times\sin(17.63°) = 8.47 \ (m/s) \quad\text{...}\quad (4.2)$$

The photoelectric sensors (KEYENCE Co., Ltd., PQ-01) measured the corresponding experimental falling velocity. Figure 4.5 shows an example of the relationship between reaction time and voltage of the photoelectric sensor at 90 mm under the initial position of the ball. It was found that the reaction time was 0.00225 sec in model scale, and the falling velocity was thus calculated as,

$$V_{exr} = 19.8mm / 0.00225s = 8.80 (m/s) \quad\text{..}\quad (4.3)$$

This value is very close to that of the theoretical prediction, which might imply that the motion of the ball in the system is close to that of free falling body in the centrifugal field.

Repeatability of the test is also a key issue for the reliability of the test results. Figure 4.6 shows the histogram and frequency distributions of maximum acceleration α_{max} of the input and the time required to achieve α_{max}, Δt, as are defined in Fig. 4.7. There are a total of 22 test cases, 15 of which with cylindrical barriers and 7 without barriers. Statistical values of the maximum acceleration α_{max}, are a mean of 94.52 m/s^2, with a coefficient of variation of 0.100, and the values of the

- 58 -
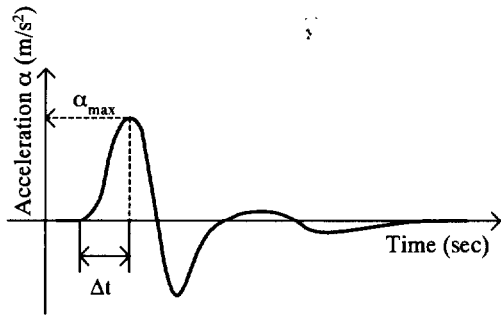
Figure 4.7 Definitions of the maximum acceleration α_{max}, and time required to reach α_{max}, Δt
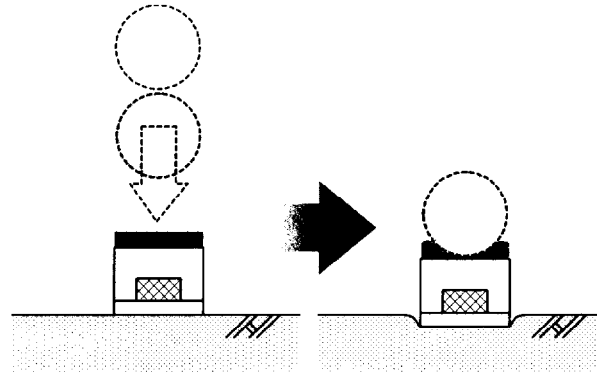
Figure 4.8 Schematic illustration of behavior of a falling steel ball and a model foundation
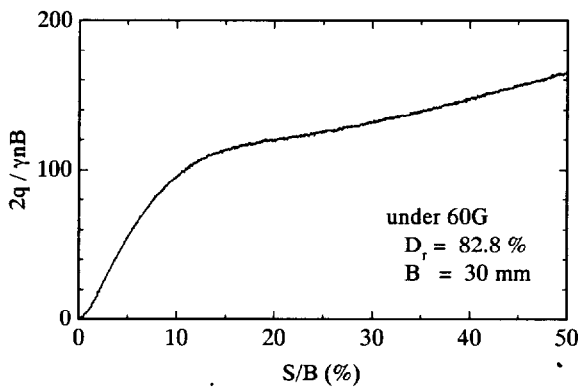
(a) Normalized load intensity – settlement curve
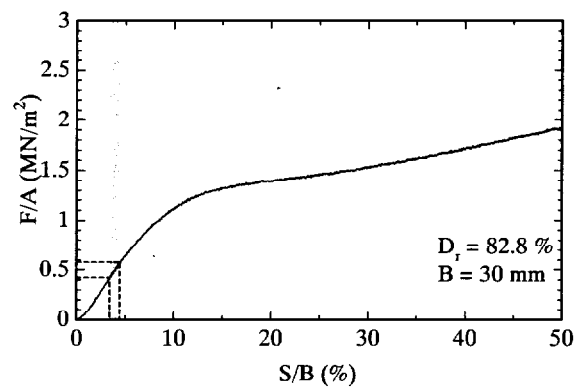
(b) Range of bearing pressure at the model foundation

Figure 4.9 An example of static loading test result in the case of D_r =82.8 % and the range of bearing pressure at the model foundation

maximum acceleration vary with the stiffness of the barrier. Generally, it may be said that the installation of a stiffer barrier results in larger maximum acceleration, probably due to the confining effect of the cylindrical barrier. For the values of Δt, a mean of 2.24×10^{-2} s, and a coefficient of variation of 0.087 were obtained. It is noted that the coefficients of variation for α_{max} and Δt are in the same order of 0.1, which clearly indicates that the multiple ball dropping system developed can produce consistent results of impact loading conditions.

The foundation is usually designed with a certain margin of safety, ensuring that working loads should be below an allowable level of bearing capacity. The force acting on the ground surface can be written as below, provided that the ball and the foundation move together as illustrated schematically in Fig. 4.8.

$$F = (M_f + M_b) \times \alpha \quad \dots \dots \dots \dots \dots \dots (4.4)$$

where F is the force acting on the ground surface, M_f the mass of the foundation (= 48.5 g), M_b the mass of the ball (= 28.0 g), α_{max} the measured maximum acceleration.

The computed results of load intensity of the foundation base, q=F/A, are within a range of

0.58 MN/m² to 0.42 MN/m², where A is the cross-sectional area of the model foundation. Figure 4.9 (a) presents a normalizêd load intensity – settlement curve for the case of static loading test in a centrifuge on circular footing of 30 mm diameter on dry sand with a relative density D_r of 82.8 % under 60 G (The Japanese Geotechnical Society, 1995). The data is directly converted into the computed results of load intensity of the foundation base – settlement curve for the conditions corresponding to the present series of tests in Fig. 4.9 (b). The shaded zone in Fig. 4.9 (b) indicates the level of load intensity in the present series, confirming that impact loads are well below the ultimate bearing capacity with a factor of safety greater than three for the cases of dense sand with a maximum relative density of 80%.

4.3 IMPACT POINT LOADING –WAVE PROPAGATION-

4.3.1 General

Sections 4.3, 4.4, and 4.5 constitute a set of physical data of propagation waves through the ground surface induced by the point load which is generated by the Multiple Ball-Dropping System. The experiment programs in all cases of point loading test are listed in Table 4.2. This section, 4.3, focuses on the behavior of wave propagation by impact point load.

4.3.2 Test procedures

A general arrangement of the model is presented in Figs. 4.10 and 4.11. The container was a steel cylindrical tub of 455mm in diameter and 400mm in height, mentioned above in Chapter 3, Section 3.3.1. One of the common problems encountered in physical modelling of vibration problems is that the walls of the container are rigid relative to the prototype ground systems and almost total reflection of the body waves would occur. Prevost and Scanlan (1983) and Cheney et al. (1990) recommended the use of Duxseal for an effective method of wall treatment for absorbing stress waves in the soil. Davies (1994) used a 12 mm thick polystyrene sheet to reduce the reflection of stress waves which reached the boundaries of the model. In this study, a sheet of sponge rubber, with a thickness of 10 mm, was glued to the internal surfaces of the sidewalls and the bottom of the
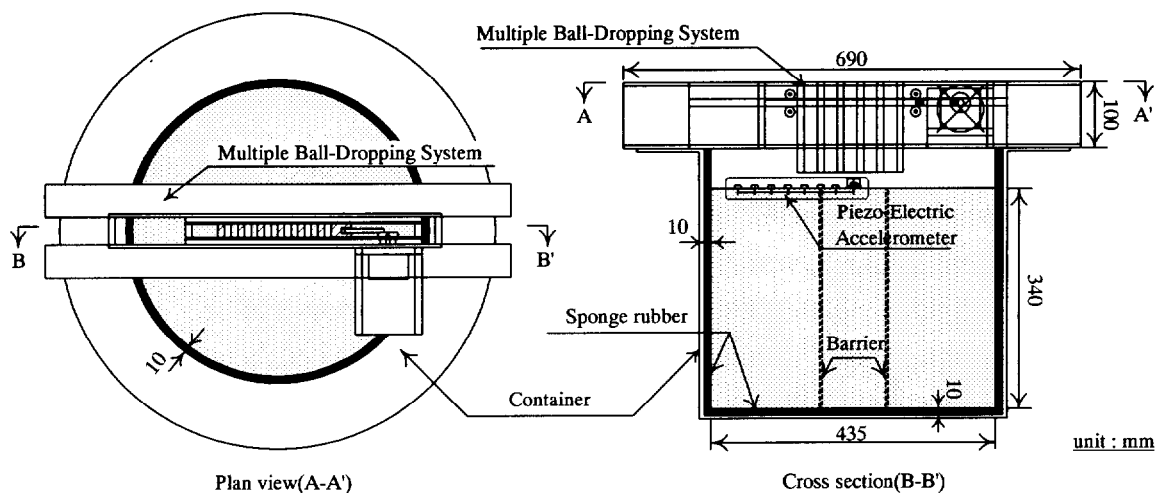
Figure 4.10 Experimental setup
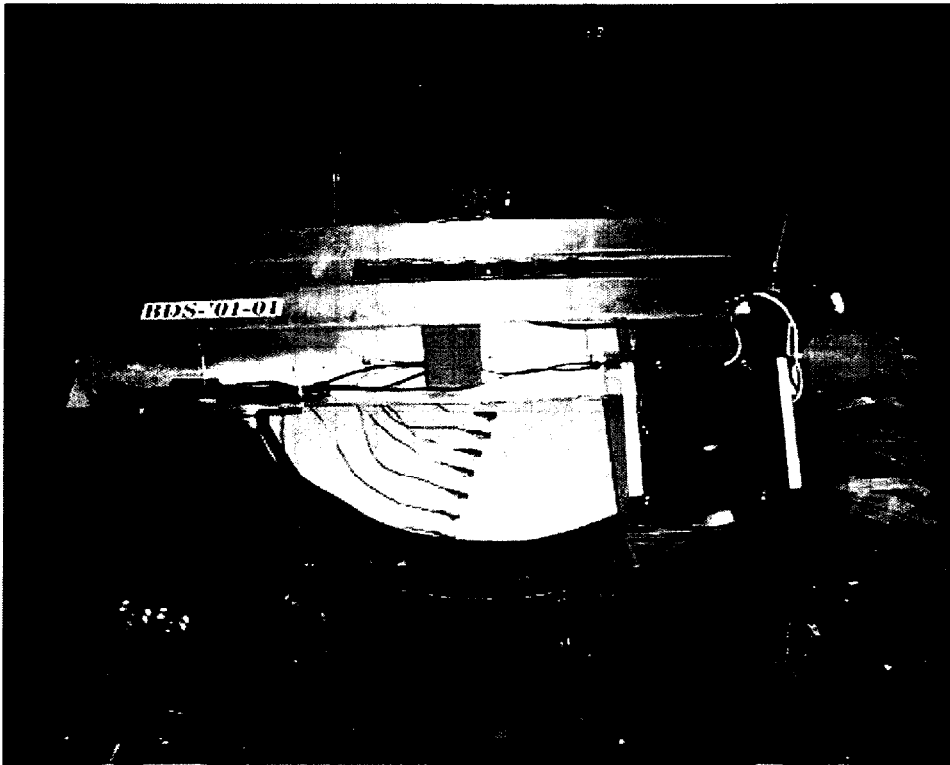
Figure 4.11 View of the Multiple Ball-Dropping System
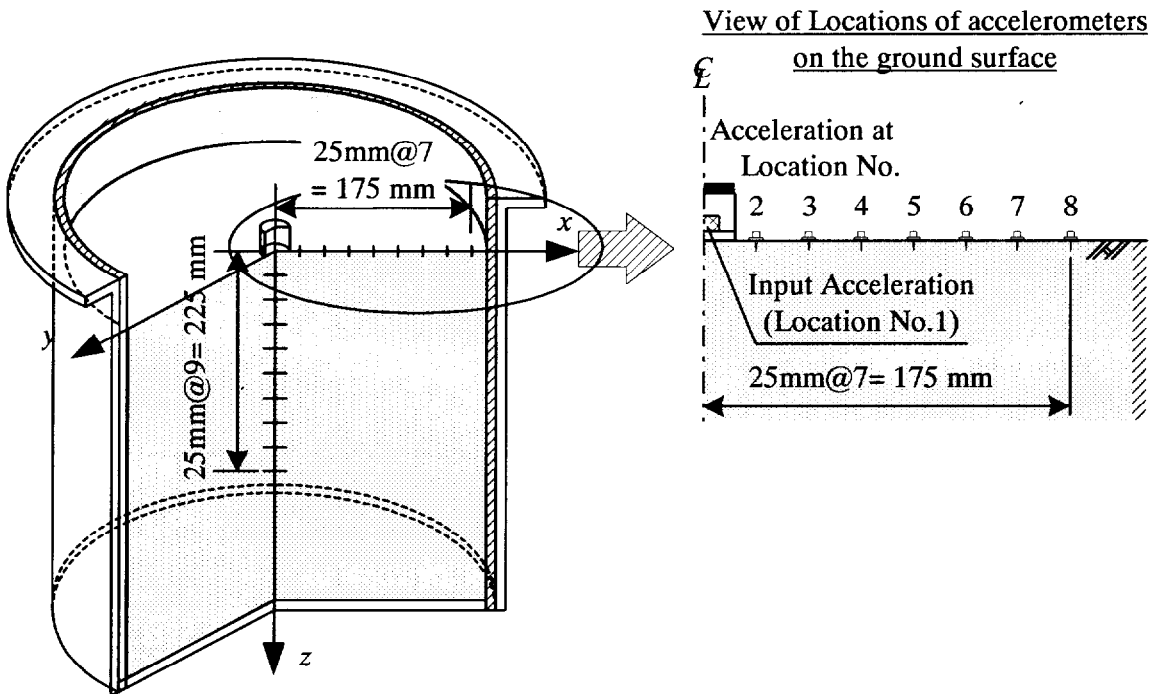
Figure 4.12 Locations of accelerometers on the ground surface and beneath the foundation

Table 4.2 Experiment programs of impact point loading tests

Test number	Normal relative density Dr (%) (real value)	Thickness of layer (mm)	Diameter of Foundation (mm)	Kind of barrier Material	Geometry	Size (diameter × depth) in mm	4.3 (1)	4.3 (2)	4.3 (3)	4.4 (1)	4.4 (2)	4.5	Note
BDS-08	80 (80.64)	340	φ30		Without barrier		O	O	O	O	O		?
BDS-02	80 (81.20)	340	φ30		Without barrier			O					Repeatability check
BDS-34	80 (78.79)	340	φ30		Without barrier		O						
BDS-33	80 (79.80)	340	φ30		Without barrier			O					
BDS-16	80 (82.20)	340	φ30		Without barrier			O					
BDS-17	80 (82.10)	340	φ30		Without barrier			O					
BDS-24	60 (60.27)	340	φ30		Without barrier			O					Repeatability check
BDS-30	60 (57.57)	340	φ30		Without barrier			O		O			
BDS-40	80 (82.71)	50	φ30		Without barrier				O				
BDS-41	80 (82.71)	50	φ30		Without barrier				O				
BDS-42	80 (82.19)	80	φ30		Without barrier				O				
BDS-43	80 (82.19)	80	φ30		Without barrier				O				
BDS-54	80 (80.20)	100	φ30		Without barrier				O	O			
BDS-11	80 (82.94)	340	φ30	Aluminium	Cylinder	φ100 × 340				O			
BDS-10	80 (82.33)	340	φ30	Aluminium	Cylinder	φ100 × 200				O			
BDS-05	80 (79.70)	340	φ30	Aluminium	Cylinder	φ100 × 100				O			
BDS-07	80 (82.28)	340	φ30	Acryl	Cylinder	φ100 × 340				O			
BDS-06	80 (80.70)	340	φ30	Acryl	Cylinder	φ100 × 200				O			
BDS-09	80 (81.82)	340	φ30	Acryl	Cylinder	φ100 × 100				O			
BDS-18	80 (79.22)	340	φ30	EPS	Cylinder	φ100 × 340				O			
BDS-19	80 (80.17)	340	φ30	EPS	Cylinder	φ100 × 200				O			
BDS-20	80 (83.22)	340	φ30	EPS	Cylinder	φ100 × 100				O	O		
BDS-21	80 (84.72)	340	φ30	EPS	Cylinder	φ100 × 50				O			
BDS-32	60 (60.82)	340	φ30	EPS	Cylinder	φ100 × 340				O			

Test number	Normal relative density Dr (%) (real value)	Thickness of layer (mm)	Diameter of Foundation (mm)	King of countermeasure material at the source	Kind of barrier			Correspond section					
					Material	Geometry	Size	4.3 (1)	4.3 (2)	4.3 (3)	4.4 (1)	4.4 (2)	4.5
BDS-29	60 (61.57)	340	φ30		EPS	Cylinder	φ100 × 200				O		
BDS-28	60 (61.57)	340	φ30		EPS	Cylinder	φ100 × 100				O		
BDS-31	60 (62.63)	340	φ30		EPS	Cylinder	φ100 × 50				O		
BDS-26	80 (82.56)	340	φ30		EPS	Rectangle	300 × 200 × 10					O	
BDS-27	80 (83.10)	340	φ30		EPS	Rectangle	210 × 200 × 10					O	
BDS-22	80 (81.50)	340	φ30		EPS	Rectangle	120 × 200 × 10					O	
BDS-51-1	80 (79.69)	320	φ60	Aluminium	Without barrier								O
BDS-51-2				Aluminium									O
BDS-51-1				CRMA (full scale)									O
BDS-51-2				CRMA (full scale)									O
BDS-51-3				Rubber									O
BDS-51-4				Rubber									O
BDS-52-1	80 (80.05)	320	φ60	CRMA (1/5 scale)	Without barrier								O
BDS-52-2				CRMA (1/5 scale)									O
BDS-52-3				Aluminium									O
BDS-52-4				Rubber									O
BDS-53-1	80 (81.20)	320	φ60	CRMA (1/5 scale)	EPS	Cylinder	φ200 × 200						O
BDS-53-2				CRMA (1/5 scale)									O
BDS-53-3				Aluminium									O
BDS-53-4				Rubber									O

container to reduce the reflection waves. As for the influence of a sheet of sponge rubber on the reduction of the reflection wave, it is examined in Section 4.3.2 (1).

The soil was air-dried Toyoura sand. The sand was poured from a certain height for consistent production of uniform deposit with an average dry unit weight γ_d of 15.4 kN/m^3 and 14.8 kN/m^3, and corresponding average relative densities of 80% and 60%, respectively. The ground surface was levelled by vacuuming. The motion of the model foundation and the ground was detected by the piezo-electric accelerometers (CBC111BW and CBC107S, CBC Materials Co., Ltd.) which provided data on the vertical accelerations at different locations on the ground surface and at different depths beneath the foundation, as shown in Fig. 4.12. This section addresses the issue as follows; 1) Effect of the side and of the bottom walls of the container on the reduction of the reflection waves, 2) Characteristics of wave propagation, 3) Influence of the layer thickness on the reflection waves. All cases were examined using the models of D_r = 80%. Moreover, as to the characteristics of wave propagation, models of D_r = 60% were also carried out. All tests were carried out under the 50 G acceleration. All the results of the centrifuge tests are presented at prototype scale, hereafter.

4.3.3 Test results and discussions

(1) *Effect of the sidewalls and the bottom of the container on the reduction of the reflection waves*
Figure 4.13 shows the time histories in the case with and without a sheet of sponge rubber which was glued to the sidewalls and the bottom of the container. Compared to the results in the case with a sheet of rubber sponge, the results in the case without it observed larger amplitude and long response. However input acceleration showed the same trend. Figure 4.14 presents how the maximum acceleration decreases with distance from the vibration source with or without a sheet of rubber sponge. The maximum acceleration was reduced by 20-40 % in the case where the container was lined with the sponge rubber, compared to the case without the sponge rubber. It is clear from these data that a sheet of sponge rubber reduces the reflection waves.

(2) *Characteristics of wave propagation*
An impact point load creates wave propagation in the surrounding ground, both on the surface of the ground and in the ground. Figure 4.15 shows a time history of vertical acceleration of the model foundation and the corresponding frequency spectrum using Fast Fourier Transform (FFT) in the case of relative density D_r of 80% (Fig. 4.15(a)) and 60% (Fig. 4.15(b)). In the case of D_r = 80%, the maximum acceleration is 87.0 m/s^2 and the dominating vibration frequency is found to be around 11.72 Hz. On the other hand, the maximum acceleration is 112.2 m/s^2 and the dominating vibration frequency is found to be around 11.33 Hz in the case of D_r = 60%. These frequencies are within a typical range of the predominant frequency of traffic vibration caused by high-speed trains and trucks (Kobayashi, 1975). Figure 4.16 presents a time history of the vertical acceleration at the ground surface 2.50m away from the source of impact point load (Location No. 3), together with the corresponding frequency spectrum using FFT in the case of relative density D_r of 80% (Fig. 4.16(a)) and 60% (Fig. 4.16(b)). At this location in the case of D_r = 80%, the first and the second dominating vibration frequencies are around 20 Hz and 80 Hz, respectively. Additionally in the case of D_r = 60%, the first and the second dominating vibration frequencies are around 17 Hz and
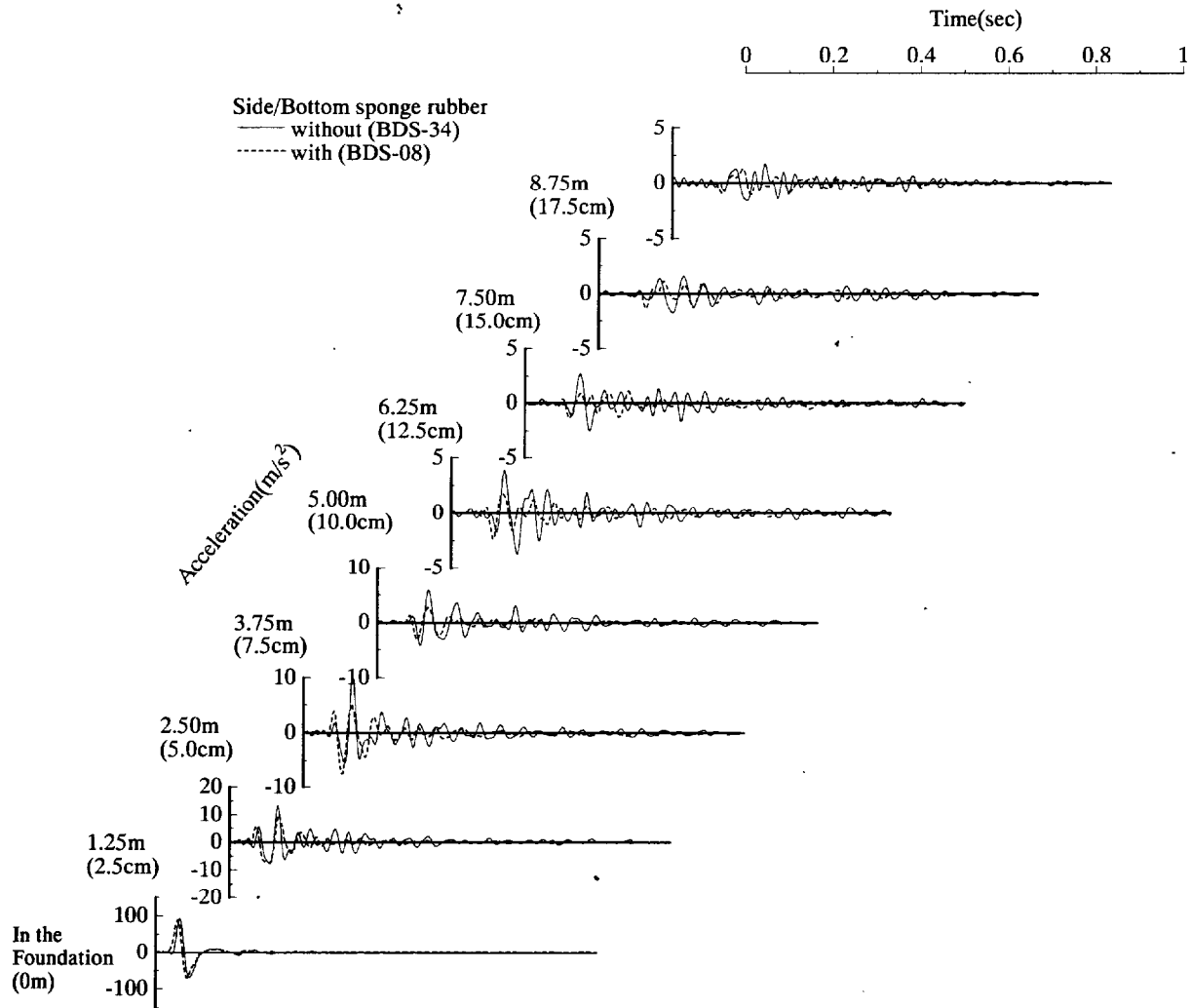
Figure 4.13 Time histories in the case with and without a sheet of sponge rubber which was glued to the sidewalls and the bottom of the container
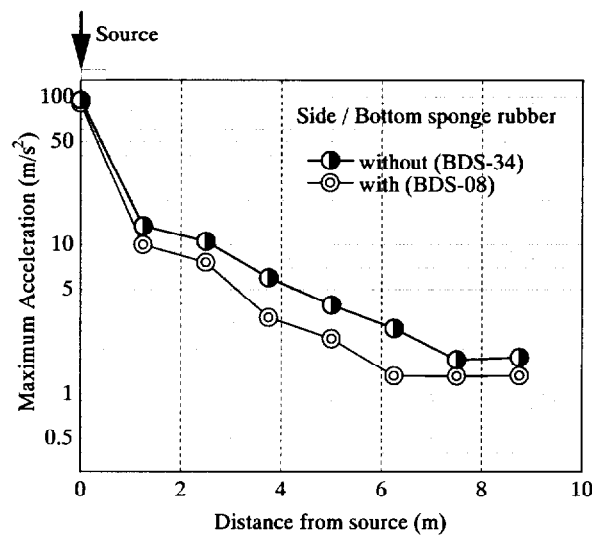
Figure 4.14 Influence of sponge rubber gluing sidewalls and bottom of the container on the reduction of reflection waves

Input Acceleration

Maximum : 87.0 m/s²
Minimum : -68.4 m/s²

Results of Fast Fourier Tansform

Predominant Frequency

11.72Hz (2.505 m/s²*sec)

Input Acceleration

Maximum : 112.2 m/s²
Minimum : -68.7 m/s²

Results of Fast Fourier Tansform

Predominant Frequency

11.33Hz (2.858 m/s²*sec)

(a) D_r = 80% (BDS-08)

(b) D_r = 60% (BDS-30)
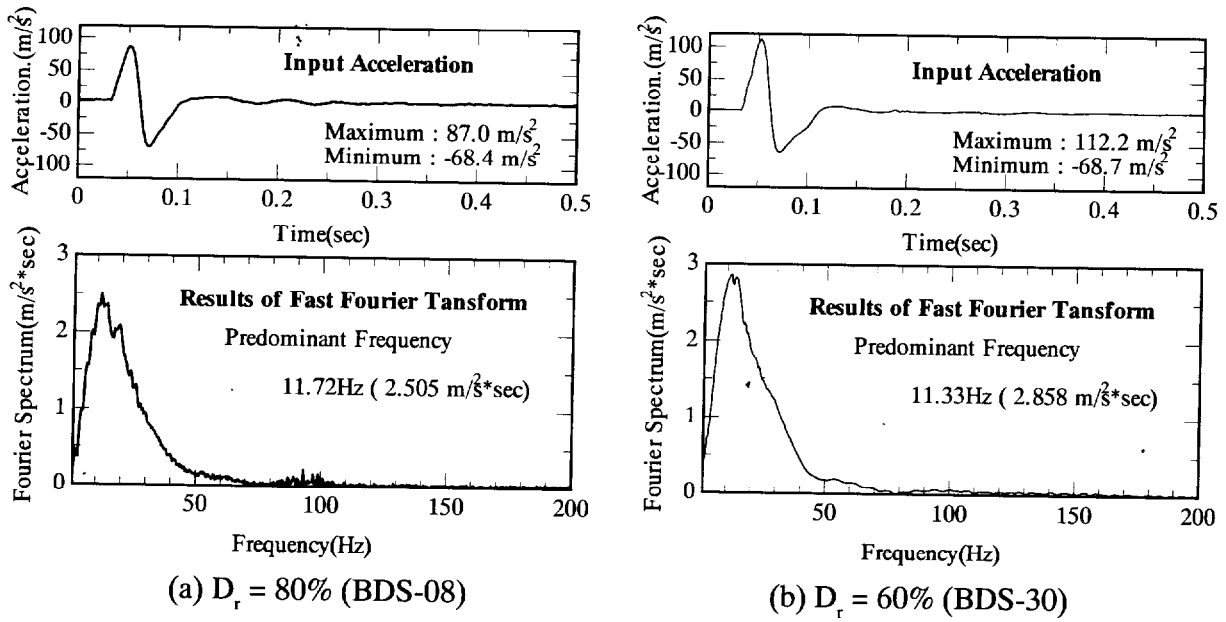
Figure 4.15 Time histories of vertical accelerations and results of FFT for input source

Acceleration at No. 3 Location

Maximum : 7.51 m/s²
Minimum : -6.78 m/s²

Results of Fast Fourier Transform

Predominant Frequency

20.73Hz (0.265 m/s²*sec)

Acceleration at No. 3 Location

Maximum : 2.21 m/s²
Minimum : -1.70 m/s²

Results of Fast Fourier Transform

Predominant Frequency

16.80Hz (0.192 m/s²*sec)

(a) D_r = 80% (BDS-08)

(b) D_r = 60% (BDS-30)
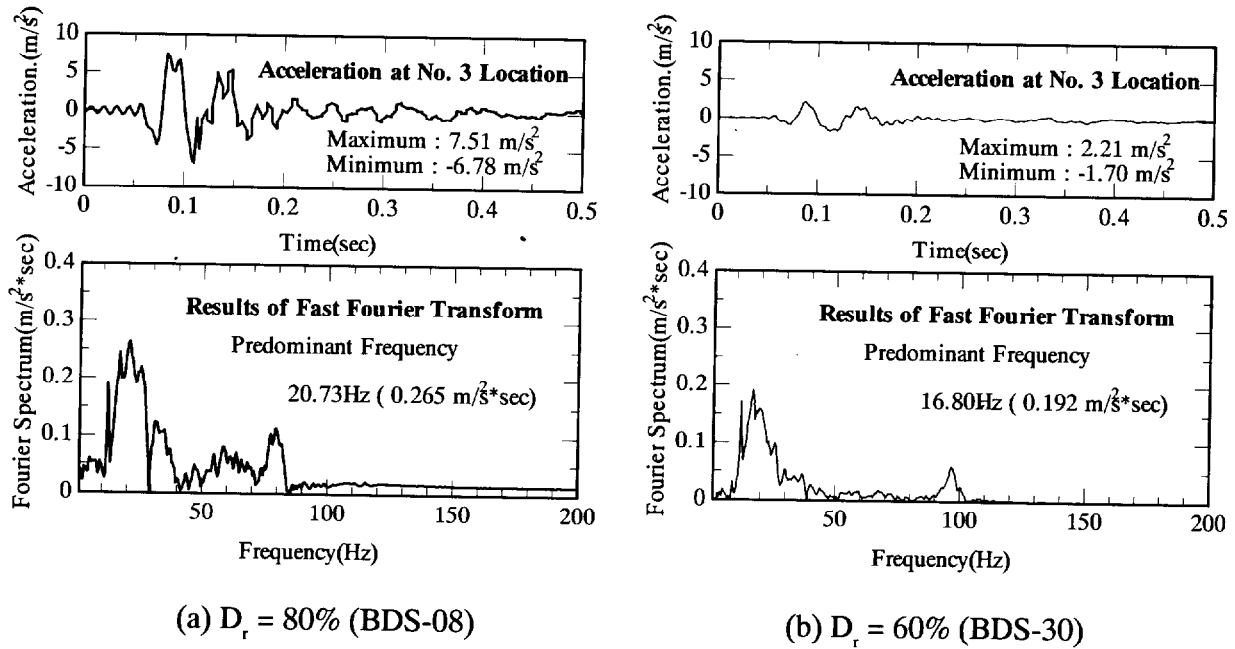
Figure 4.16 Time histories of vertical accelerations and results of FFT for the location at No. 3 (= 2.50 m away from the source of impact point load)

95 Hz, respectively. The motion of the ground surface was detected by the piezo-electric accelerometer CBC111BW which has a resonance frequency of 4 kHz. The second dominating vibration frequency 80 Hz is considered to be due to the resonance frequency of the accelerometer adopted (80 Hz × 50 = 4 kHz). For this reason, it was decided that raw data were filtered by a low pass filter of 50 Hz to eliminate the influence of the resonance frequency of the accelerometer.

Figure 4.17 presents a typical example of the filtered data, showing how the input wave propagates radially on the ground surface as well as downwards beneath the model foundation in the case of D_r = 80%. As to the movement on the ground surface, the same condition test did twice

to check the repeatability. At the same position, the movements of the dashed line are good agreement with them of solid line. These observations indicate that this experiment system has a good repeatability. It should be noted that the scaling of acceleration axis differs depending on the magnitude of the acceleration, to be able to visualize the attenuation of the wave data clearly. To determine the surface wave velocity, the difference in travel time of the first wave was obtained at two adjacent accelerometers. The average difference in travel time dt and the distance ds between the two detection points were $\delta t = 0.007$ sec and $\delta s = 1.25$ m at prototype scale respectively, giving the average surface wave velocity of

$$V = \delta s / \delta t = 178.6 \, (m/s) \quad\text{...} \quad (4.6)$$

From the predominant frequency of 20Hz and the surface wave velocity of 178.6 m/s, the surface wavelength (λ) in prototype can be calculated to be 8.93m. In addition, getting wave velocity of this test (= 178.6 m/s) is similar to that from BE test result (= 178.9 m/s) as was described in Chapter 3.

Figure 4.18 shows the observation of wave propagation on the surface ground in the case of $D_r = 60\%$. The surface wave velocity was also measured in a similar way. The average difference in travel time dt and the distance ds between the two detection points were $\delta t = 0.009$ sec and $\delta s = 1.25$ m at prototype scale respectively, giving the average surface wave velocity of

$$V = \delta s / \delta t = 141.2 \, (m/s) \quad\text{...} \quad (4.7)$$

From the predominant frequency of 16.8Hz and the surface wave velocity of 141.2 m/s, the surface wavelength (λ) in prototype can be calculated to be 8.40m.

Generally, the surface (Rayleigh) wave is of primary concern for foundation on or near the surface of the ground. In order to estimate primary wave type, Bornitz (1931) proposed a simple method for predicting the decrease in amplitude of the vertical component of the wave with distance. Figure 4.19 shows attenuation of the maximum acceleration with distance from vibration source observed in the cases of $D_r = 80\%$ and $D_r = 60\%$. These figures show the theoretical attenuation lines predicted by Eq. (2.2) alongside of the experimental data. The solid black lines represents attenuation of surface wave (n = 0.5), and the dashed and single-dotted gray lines represent attenuation of body wave (n = 2). These figures show some interesting associations that the theoretical attenuation line represented of surface wave fit each experimental data. It appears that the major tremor at the ground surface is the type of surface wave.

Furthermore, the detail of wave type which was generated by this system was checked by two methods. One is the wave particle motion that is induced by impulsive sources acting on the ground surface. The main purpose was to investigate their shape in the view of clarifying the relation between Rayleigh wave and body wave. The test was conducted with impulsive sources and a series of composite receivers, in which a vertical geophone was coupled to a horizontal one. Figure 4.20 shows the measurement locations for this series of the tests. Two direction accelerations, which are recorded to vertical and horizontal movement, set up on or under the ground. Figure 4.21 shows the wave particle motion in the case of the all recorded positions. At location No. 1 (x: 0.0m, z: -7.5m), which is placed under the impact source, wave particle path shows the primarily vertical movement because of generating P wave. At the other locations, It appears that the vertical ampli-
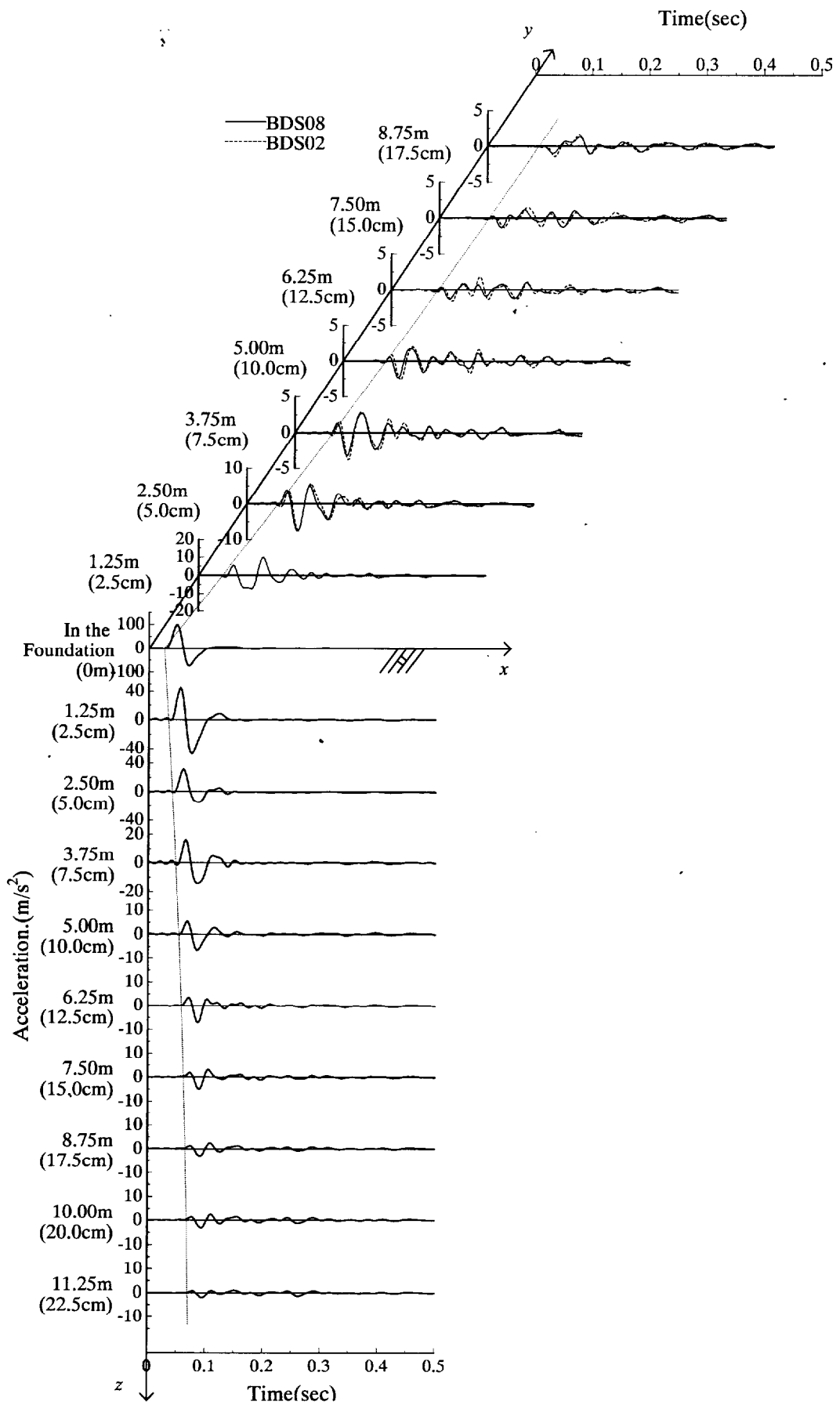
Figure 4.17 An example of wave propagation on the ground surface and beneath the foundation in the case of $D_r = 80 \%$.

Time(sec)

0   0.1   0.2   0.3   0.4   0.5

——BDS30
------BDS24

8.75m
(17.5cm)

7.50m
(15.0cm)

6.25m
(12.5cm)

5.00m
(10.0cm)

3.75m
(7.5cm)

2.50m
(5.0cm)

1.25m
(2.5cm)

In the
Foundation
(0m)
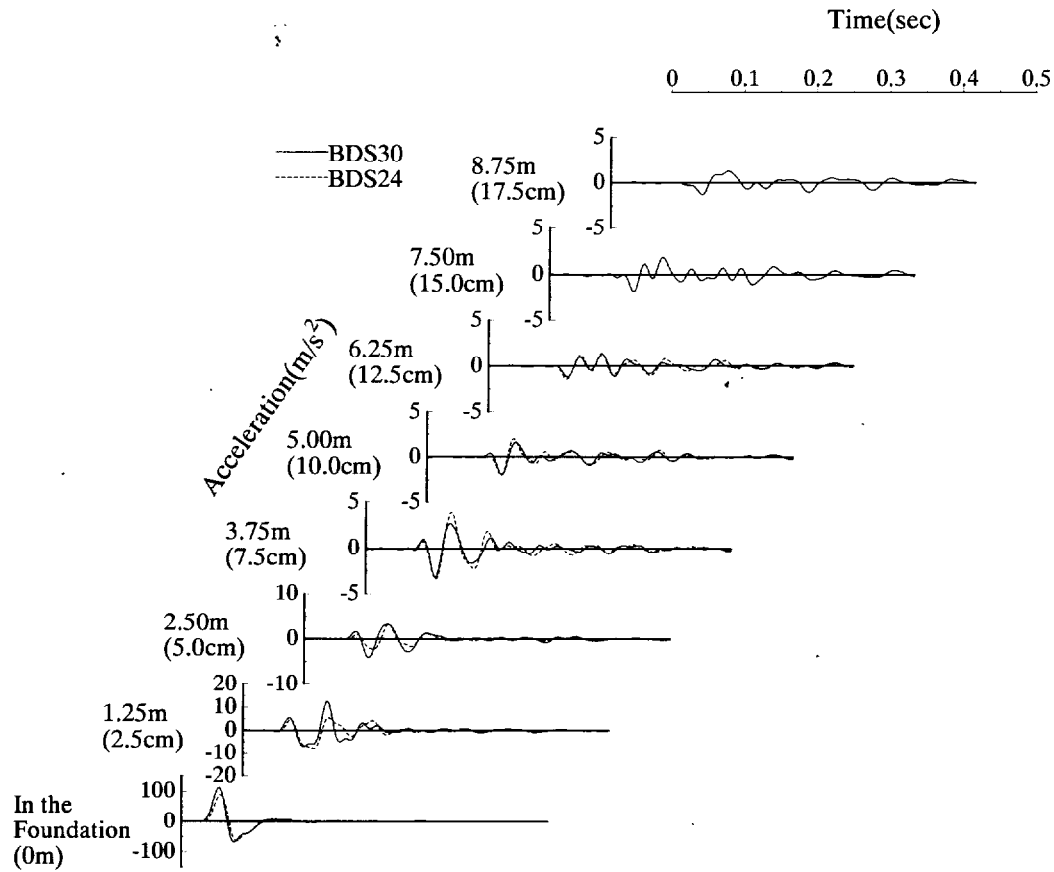
Figure 4.18 An example of wave propagation on the ground surface in the case of $D_r = 60\ \%$.
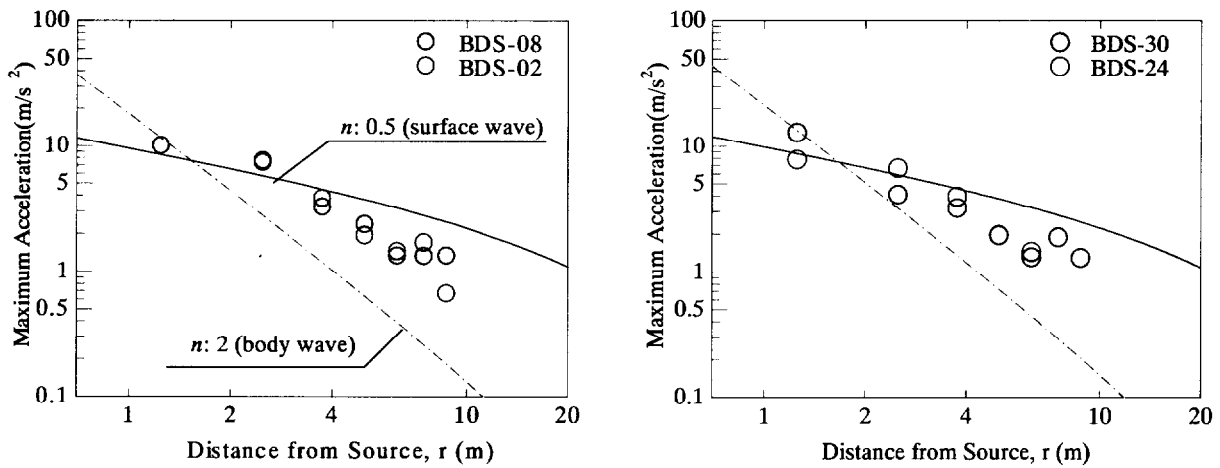
Figure 4.19 Attenuation of the maximum acceleration with distance from vibration source

tude amplifies more than the horizontal one. The elliptical path associated to surface waves has been detected in most of the recorded signals, nevertheless it was often perturbed by incoherent or coherent noise. Another is motion product. If the horizontal(H) and vertical(V) motion are multiplied, the product, H × V, defining 'away' and 'up' motions as positive, is positive for P wave and negative for S wave. Pure Rayleigh wave motion goes positive and negative at twice the original frequency. Figure 4.22 shows the motion product, H × V, in the case of the all recorded positions. It is reasonable to suppose that these figures offer support for the results from the wave particle motion. In other words, the product, H × V, at location No. 1 (x: 0.0m, z: -7.5m) is located in the positive area, and other products are moved from the positive area to the negative area, such as sine wave. As to the motion product, the result is not the twice as amplitude, because there are impurities such as body wave and reflected wave in the recorded data. However it is clear that the major tremor at the ground surface is apt to be the type of surface wave. It is clear from these results that there is not much difference between generated vibration by this experiment and real behavior.

(3) Influence of layer thickness on the reflection waves

Sometimes, seismic refraction survey is used to determine wave propagation velocities through various soil layers in the field and to obtain thicknesses of each layer. Generally, consider the case where there are two layers of soil as shown in Fig. 4.23. Let the velocities of P-wave in layers 1 and 2 be v_{p1} and v_{p2}, respectively, and $v_{p1} < v_{p2}$. When detecting instruments are placed at various distances from the source of vibration to obtain the first arrival time and the results are plotted in a form as shown in Fig. 4.23. If the upper layer of a horizontally layered halfspace has wave velocities lower than those of the second layer, three wave types which are direct wave, reflected wave, and head wave are generated. This section shows that centrifuge modelling test were carried out in order to simulate a behavior of wave propagation. Figure 4.24 gives the experimental system. In order to observe the refraction survey, a thickness of the first layer was made shallow. The spacer made by steel was used on the bottom of model container in order to adjust the first layer thickness
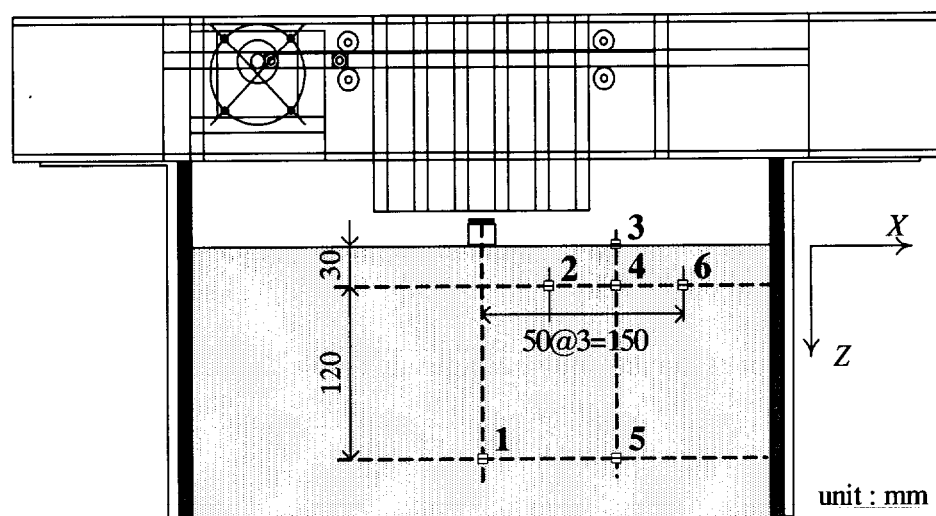
Figure 4.20 Locations of accelerometers on the ground surface and under the soil
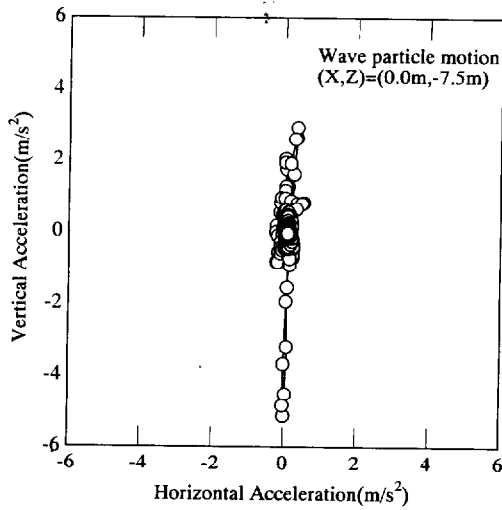
i) No. 1 (0.0 m, -7.5 m)
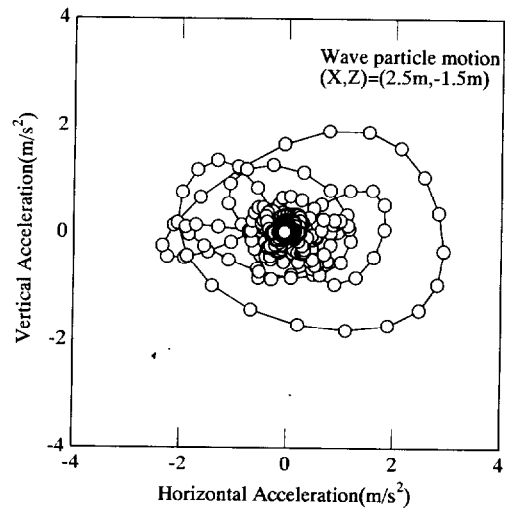
ii) No. 2 (2.5 m, -1.5 m)
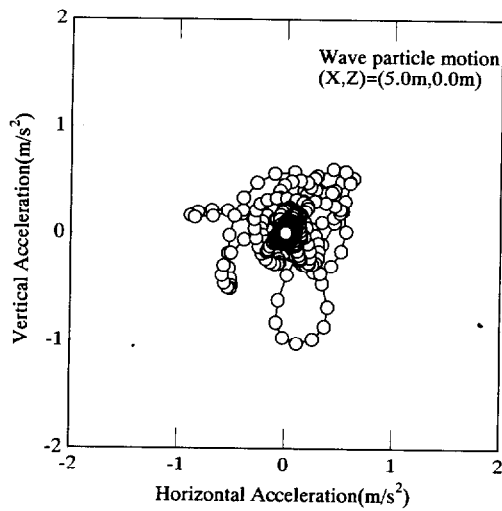
iii) No. 3 (5.0 m, 0.0 m)
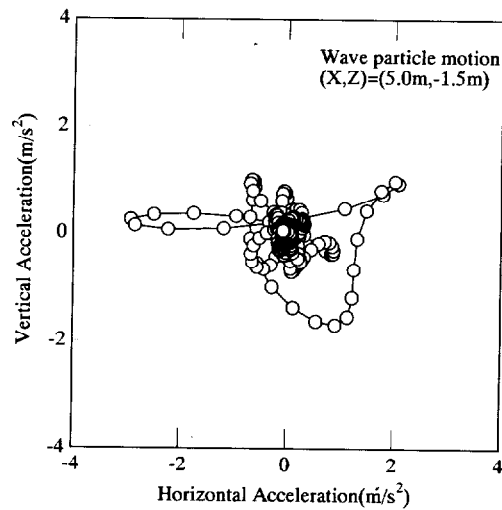
iv) No. 4 (5.0 m, -1.5 m)
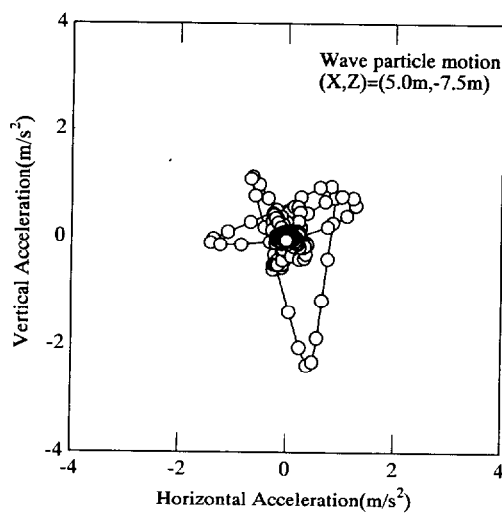
v) No. 5 (x: 5.0 m, z: -7.5 m)
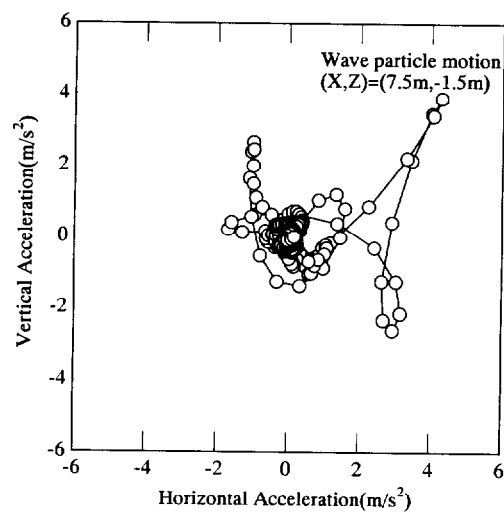
vi) No. 6 (7.5 m, -1.5 m)

Figure 4.21 Wave particle motion at the all recorded positions

i) No. 1 (0.0 m, -7.5 m)

ii) No. 2 (2.5 m, -1.5 m)

iii) No. 3 (5.0 m, 0.0 m)

iv) No. 4 (5.0 m, -1.5 m)

v) No. 5 (5.0 m, -7.5 m)

vi) No. 6 (7.5 m, -1.5 m)
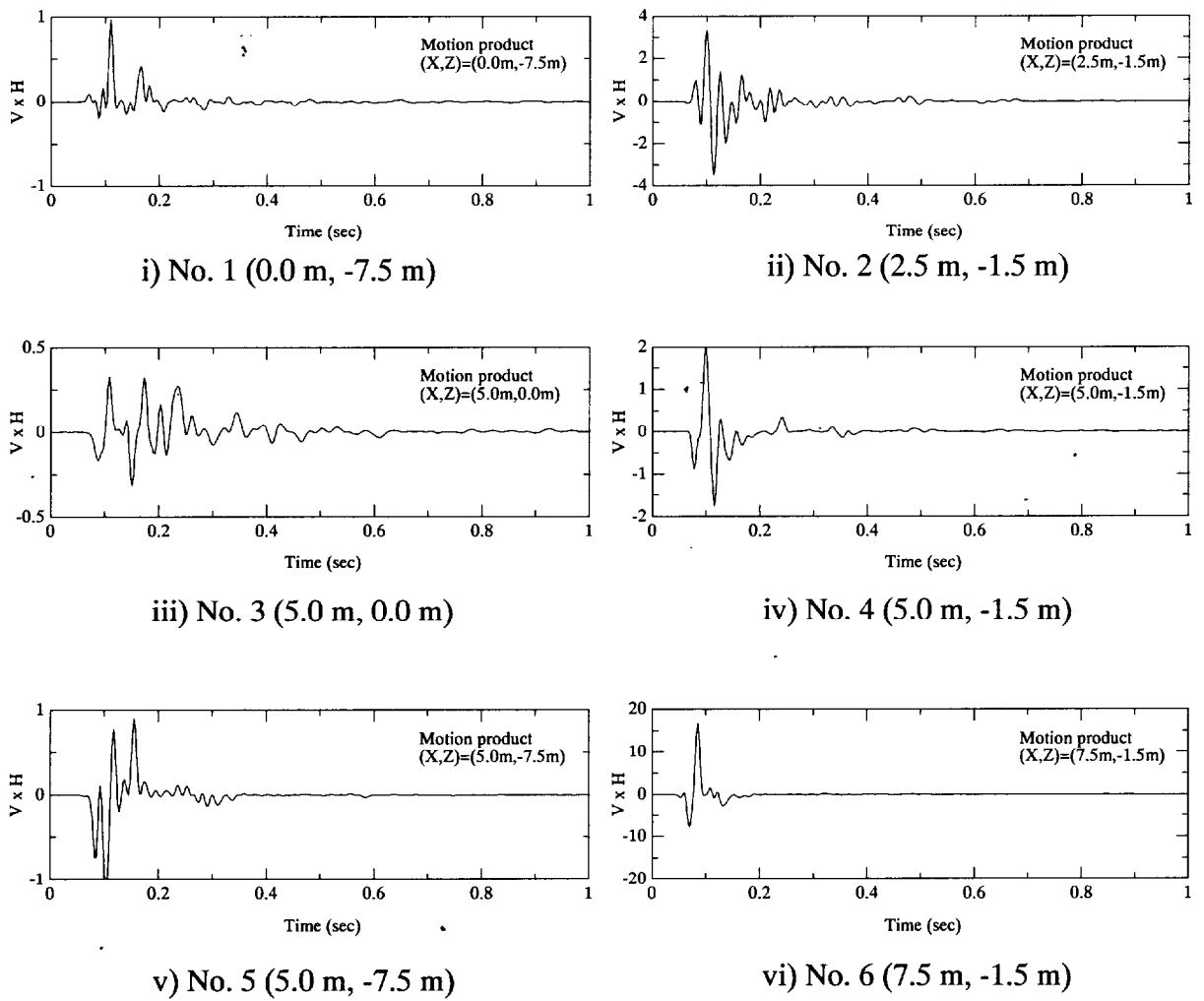
Figure 4.22 Results of the motion product method at the all positions
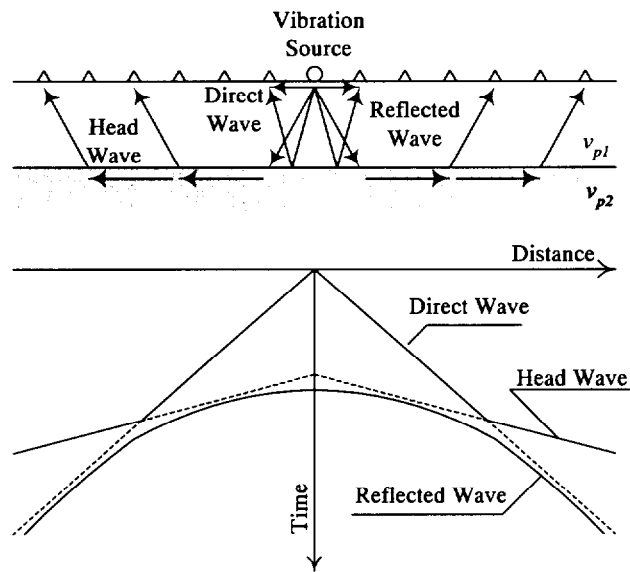
Figure 4.23 Ray paths and travel-time curves for direct, reflected, and head waves.
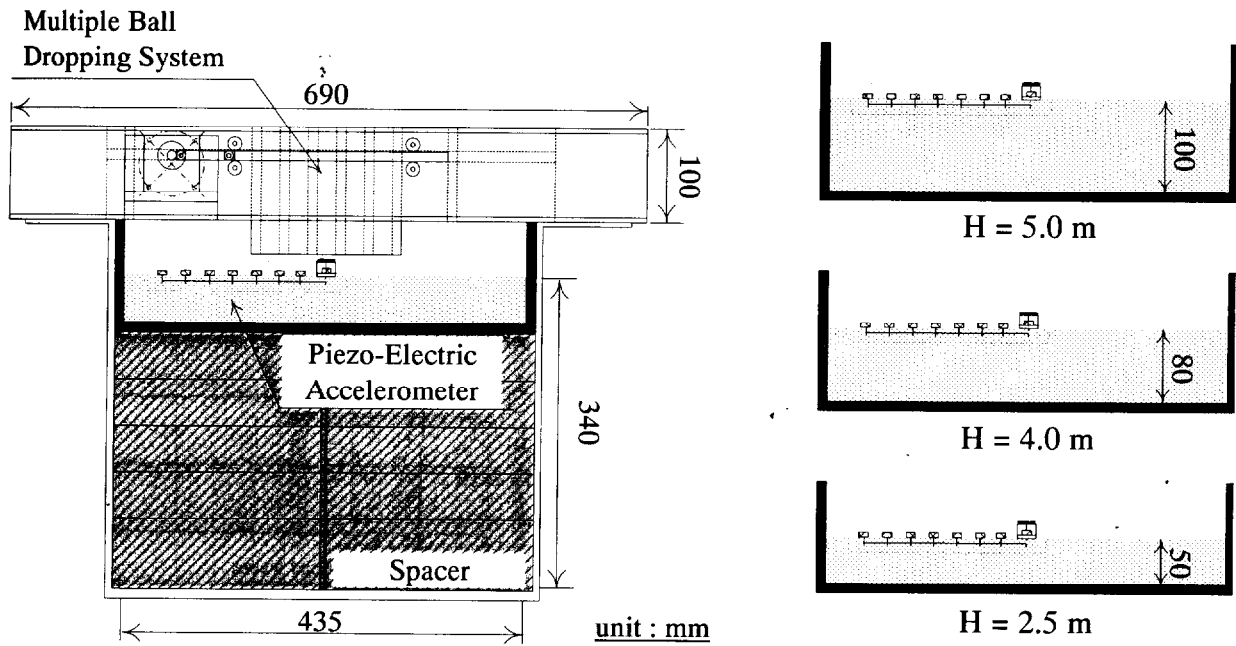
Figure 4.24 Experiment system of investigating the refraction survey

(a) Setup the spacer on the bottom of container   (b) Put the steel ring plate on the spacer

Figure 4.25 Process for making a shallow layer in order to observe the reflection survey

as shown in Figure 4.25. In order to observe the behavior of refraction survey clearly, the second layer used was steel ring plate which set up on the spacer. By the way, Toyoura sand was glued to the surface of the steel ring plate to represent a rough condition. As for the first layer, respectively 50 mm (BDS-40 and 41), 80 mm (BDS-42 and 43) and 100 mm (BDS-54) high soil layer was prepared by raining air-dried Toyoura sand which is a relative density of 80 %, as shown in Figure 4.24. The ground surface was leveled by vacuuming. Figure 4.26 shows typical examples of how the different depth of the first layer would change the wave propagation. In addition, the solid line which is the first arrival time at various distances from the source is plotted in this figure. The result of this figure clearly shows that travel time changes suddenly at the appointed location. It appears that the head wave arrives before either of the other waves because it travels for a significant time in the higher-velocity through a boundary between the first layer and the second layer. In the case of
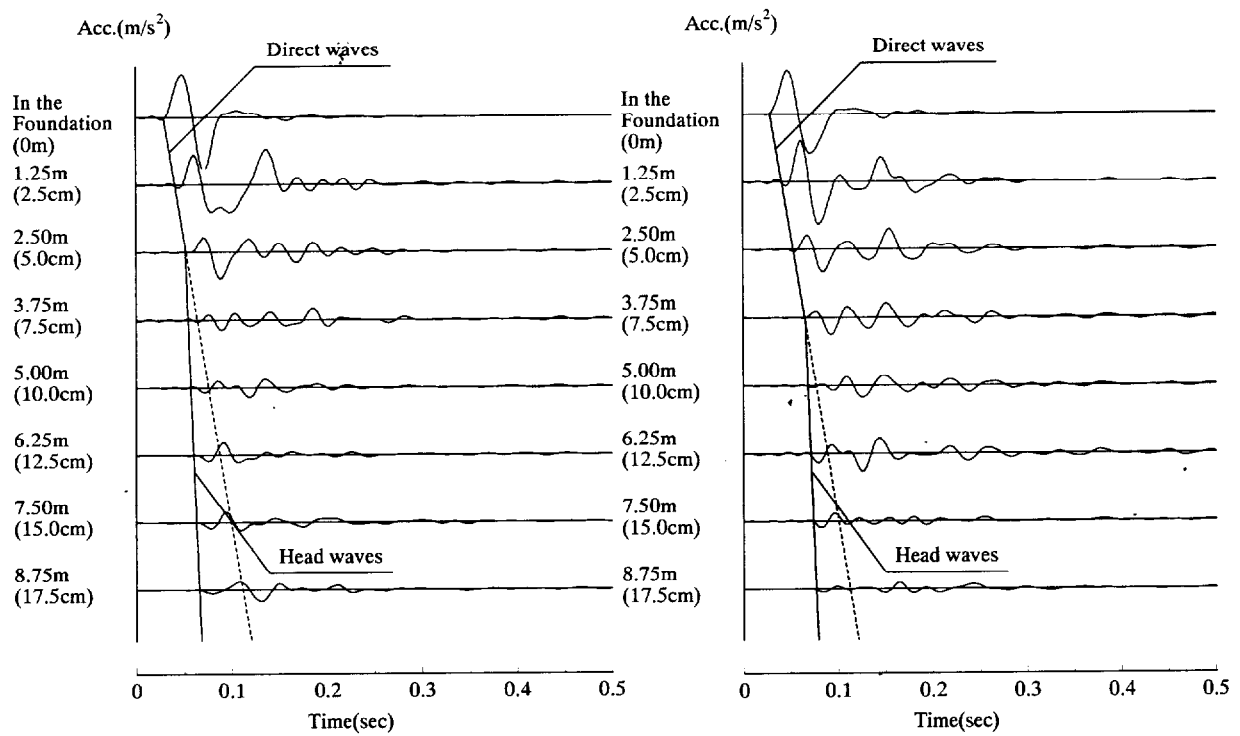
(a) Depth of the first layer H = 2.5 m (BDS-41) (b) Depth of the first layer H = 4.0 m (BDS-43)
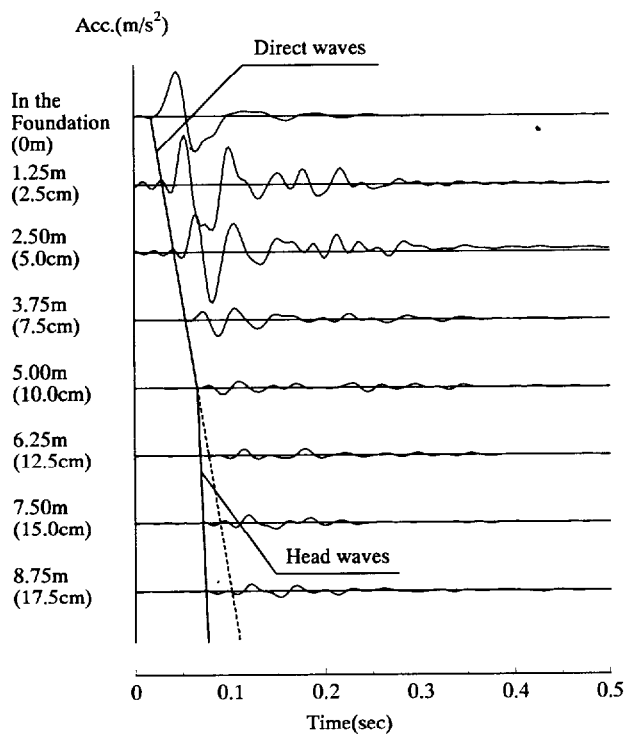
(c) Depth of the first layer H = 5.0 m (BDS-54)

Figure 4.26 The difference in refraction survey by the first layer depth
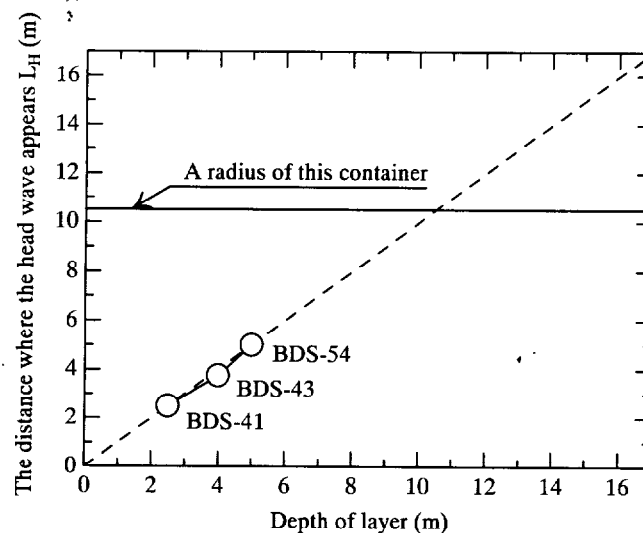
Figure 4.27 The relationship between the thickness of the first layer and the distance where the head wave appears

shallow thickness of the first layer, head wave was generated at nearer places from the source. Figure 4.27 presents the distance where the head wave appears, L_H, plotted against the thickness of the first layer H. For the thickness of layer 340mm which is mainly in this study, it seems to be lacking the influence of reflection wave from bottom of the container.

4.4 IMPACT POINT LOADING -VIBRATION COUNTERMEASURES AT TRANSMITTING PATH-

4.4.1 General

It has already been shown in Chapter 2 that there is not a systematic research as for vibration isolation method using centrifuge. This section, 4.4, did the systematic centrifugal model test and examined the effect of wave barriers of various configurations (cylinder, rectangle), embedded depth, and materials on the reduction of vibration.

4.4.2 Test procedures

The test procedures are identical with those shown by section 4.3.1. The soil used was air-dried Toyoura sand. The sand was poured from a certain height, to make a homogeneous ground with relative density of Dr = 80 %. Additionally, experiments using EPS cylindrical barrier (section 4.4.2(1)) were carried out using not only the model of D_r = 80% but also the ground of D_r = 60%. Figure 4.28 shows the measurement locations for this series of the tests. The wave barrier was located at 50mm from the center of source in the model scale. The procedures how to install the wave barrier are as follows. In the case of cylindrical wave barrier, the sand was rained into the container until a certain height before installing wave barrier. In the case of cylindrical wave barrier, the sand was rained into the container until a certain height before installing wave barrier. After that, wave barrier sets up keeping a vertical, and sand was poured again, carefully. On the other hand, in the case of rectangular wave barrier, the sand was rained into the container until certain
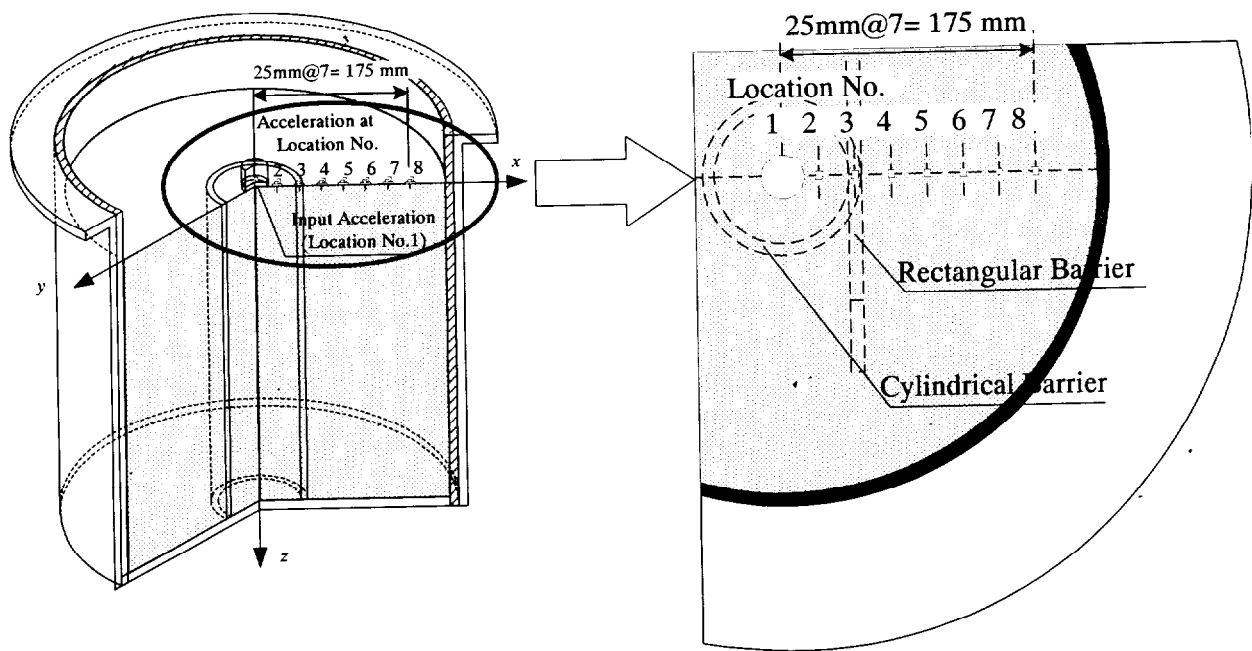
Figure 4.28 Locations of accelerometer and barrier
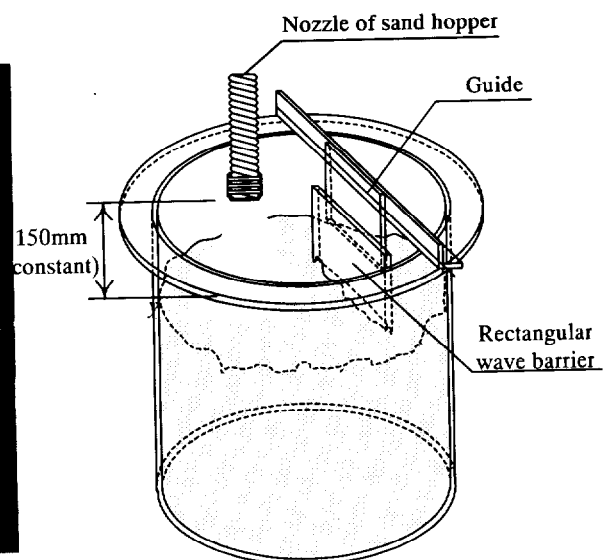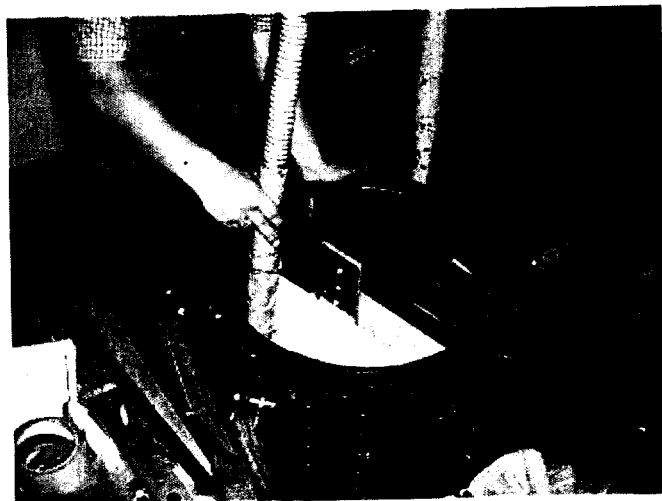
Figure 4.29 Picture and illustration of the method of installation

height. Next, in order to set wave barrier vertically, the guide was used as shown in Fig 4.29. After that, the sand was rained. All tests were carried out under the 50 G acceleration. All results are presented at prototype scale, hereafter.

4.4.3   Test results and discussions

(1)   Effect of cylindrical barrier on the reduction of vibration

The effects of an isolation method of cylindrical barrier was examined by using various barrier conditions such as embedded depth of the barrier D, wave impedance A, as illustrated in Fig. 4.30. Wave impedance A is given by
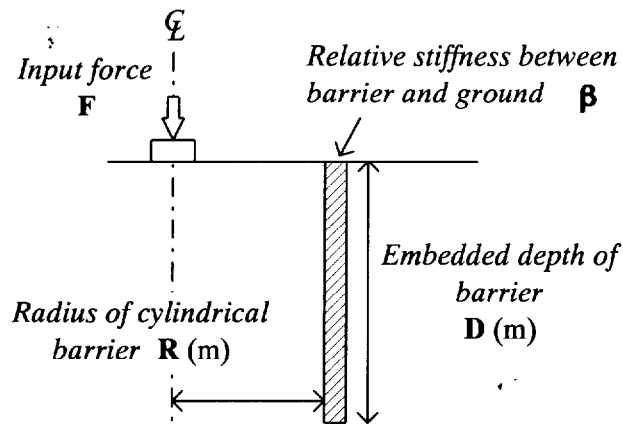
· Figure 4.30 Schematic diagram of vibration isolation by cylindrical barrier
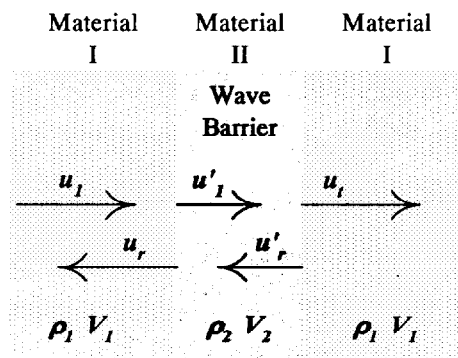
Figure 4.31 The definition of wave impedance *A*

$$A = \frac{\rho_2 V_2}{\rho_1 V_1} \qquad \qquad \qquad \text{.............(4.8)}$$

where ρ_1= density of the soil, V_1= shear wave velocity of the soil, ρ_2= density of the barrier, V_2= shear wave velocity of barrier mentioned above in Fig 4.31. The experimental conditions are listed in Table 4.3. Selected stiffer materials than soil (A<1, stiffer barrier) are aluminium and acryl, while a softer material (A>1, softer barrier) is Expanded Poly-Styrol (EPS). These mechanical properties are listed in Table 4.4. From the point of view of the wave impedance, these materials are good agreement with prototype wave barrier in practice (Takatani and Kitamura, 2001). To be more precise, wave impedance of aluminium model barrier equals that of concrete barrier in the proto-type and wave impedance of EPS model barrier nearly equals that of EPS barrier in prototype. The value of shear modulus of soil was taken from the literature (Jung, 1998).

Figure 4.32 shows typical examples of how the installation of the cylindrical barriers of various materials would change the wave propagation for the case of the embedded depth of the barrier D of 17 m. It should be noted again that the different scales of the acceleration axis are selected at various measurement points. Comparing the data obtained without a barrier with the data obtained with a barrier, it can be clearly seen that the cylindrical barriers are in fact effective; the ground motion is considerably smaller beyond the barrier. Interestingly, it is observed that the stiffer barri-

Table 4.3 Experimental program for point load test using cylindrical barrier

				Embedded depth of barrier D (m)			
				17.0	10.0	5.0	2.5
Radius of cylindrical barrier R (m)	2.50	Wave impedance A	>0 (EPS)	O	O	O	O
			<0 (Acryl)	O	O	O	-
			<<0 (Aluminium)	O	O	O	-

Table 4.4 Mechanical properties of cylindrical barriers and Toyoura sand

	Dry unit weight γ_d (kN/m^3)	Shear modulus G (MN/m^2)	Wave impedance A	Relative shear modulus between barrier and soil β
Aluminium	26.5	25.6×10^3	49.6	about 1400
Acryl	11.8	12.1×10^2	7.2	about 70
EPS	0.12	11.1×10^{-1}	0.007	about 0.10
Toyoura sand (D_r=80%) near ground surface	15.4	17.9	1	-
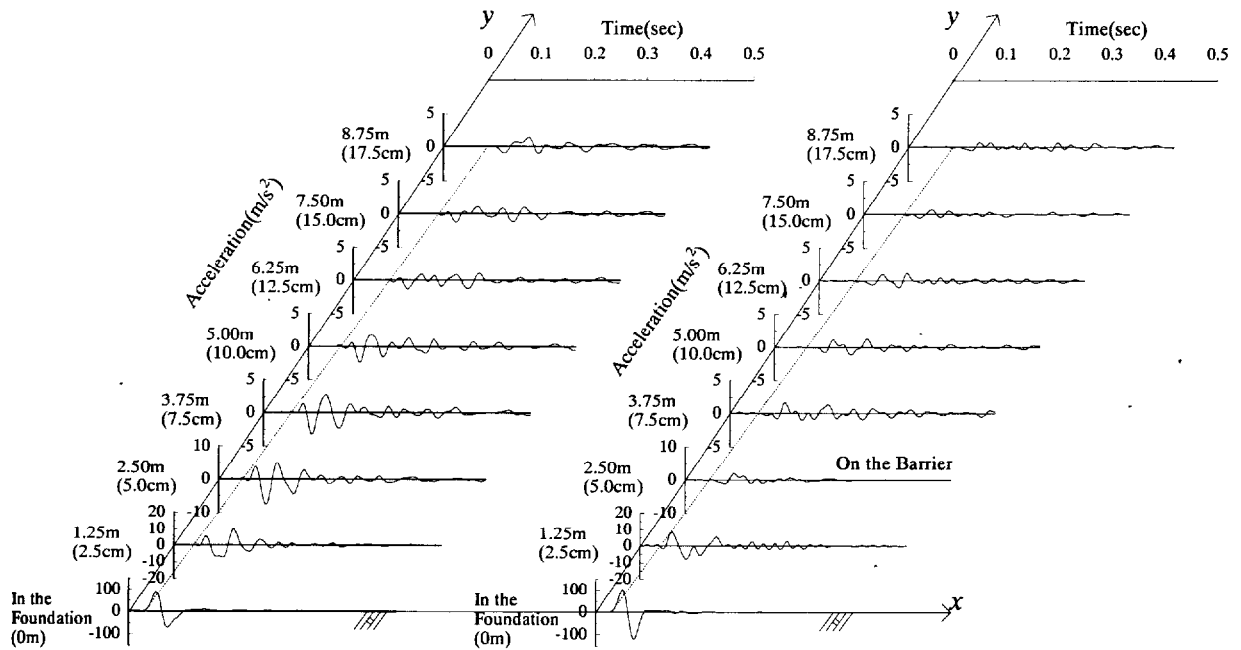
(a) Without barrier   (b) Aluminium barrier
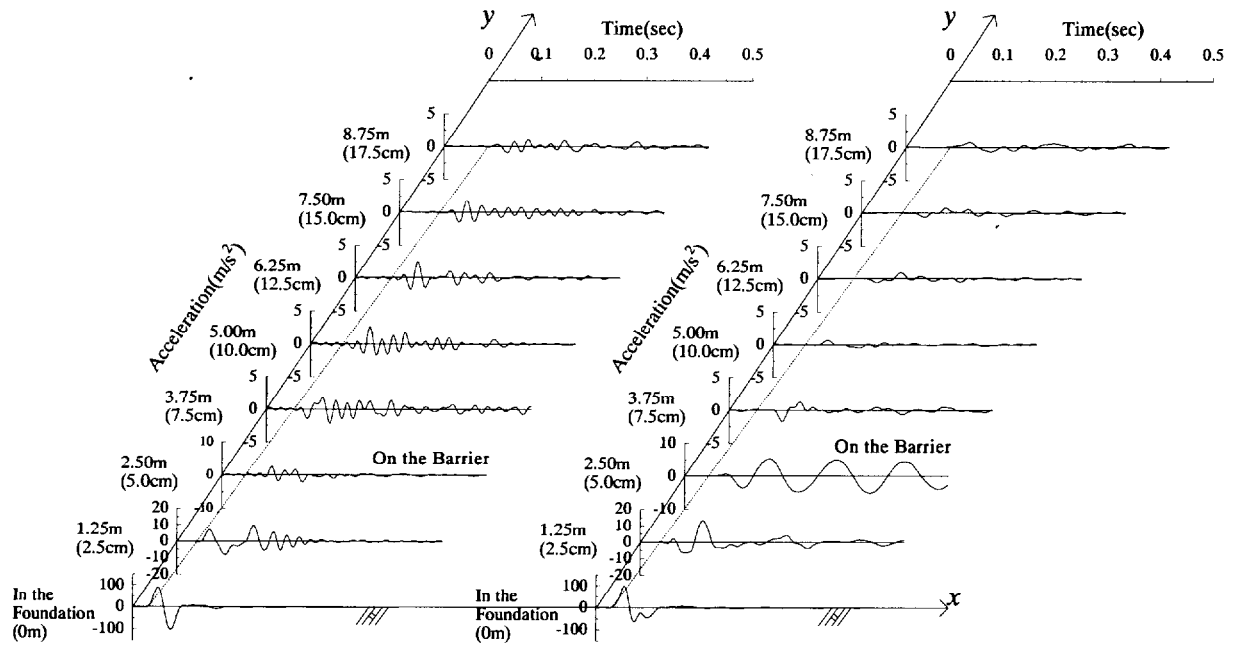
(c) Acryl barrier   (d) EPS barrier

Figure 4.32 Typical examples of wave propagation change with and without cylindrical barrier of various materials (barrier depth D of 17 m)

Figure 4.33 Attenuation of the maximum acceleration with distance from vibration source for various barrier materials with different embedded depths for cases of cylindrical barriers

ers reduce the vertical acceleration on the barrier, whereas the softer barrier amplifies it. Figure 4.33 presents how the maximum acceleration decreases with distance from the vibration source for various barrier materials with different embedded depths, and also includes data for the case without a barrier. In the case of the Aluminium barrier, a marked effect of the barrier becomes evident for the case of embedded depth of 17 m, in which a sharp drop in the maximum acceleration is observed on the barrier and after which the level of the acceleration remains much smaller than the other cases (See Fig. 4.33(a) above). This observation implies that stiffer barriers, with the wave impedance A of about 50, are effective in screening the vibration when these barriers are installed into a deeper depth. This observation does not seem relevant for the case of Acryl barrier, with the wave impedance A of about 7, regardless of embedded depth, as is seen in Fig. 4.33 (b). In the case

(a) Location at 3.75 m from source   (b) Location at 5.00 m from source
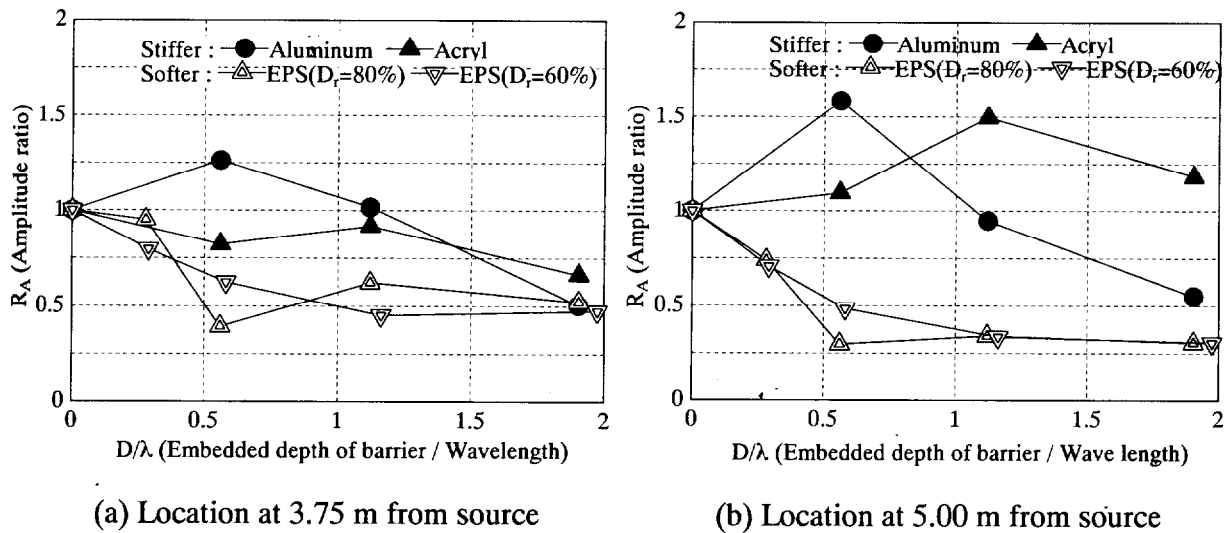
Figure 4.34 Changes in amplitude ration R_A (= (vertical maximum acceleration with the barrier) / (vertical maximum acceleration without the barrier)) to embedded depth of barrier / wavelength D/λ for different barriers

of EPS barrier, with the wave impedance A of about 0.08, the screening effect continues to remain effective beyond the barrier ever for the case of embedded depth of 5 m. The reduction of the maximum acceleration is more marked in comparison with the cases of the Aluminium barrier.

The influence of normalized depth D/λ and various barrier materials on amplitude ratio R_A are presented in Fig. 4.34 (a) and (b) for locations at 3.75 m and 5.00 m from source, respectively. The screening effect is expressed by the parameter R_A (amplitude ratio): R_A = (vertical maximum acceleration with the barrier) / (vertical maximum acceleration without the barrier). $R_A = 0.25$ means 75% reduction in the ground vibration due to the installation of the barrier (Woods, 1968). As Fig. 4.34 clearly indicates, the Acryl barrier has practically no significant effect on screening and the Aluminium barrier (stiffer barrier) becomes effective only when D/λ exceeds more than unity, whereas the EPS barrier (softer barrier) is indeed effective for a wide range of D/λ values. In particular, if the amplitude reduction of about 0.3 is to be achieved, a minimum depth of $D/\lambda = 0.6$ is required. This observation is in good agreement with the active isolation proposed by Woods (1968). More importantly, from the view of the construction cost, softer barriers need lower values of D/λ, compared to those for stiffer barriers.

(2) *Effect of geometry of the barrier on the reduction of vibration*

Selection of the size and shape of barrier influences the cost of the construction of the barrier. The effect of geometry of the barrier on the reduction of vibration is therefore an important issue to examine.

The barriers adopted in this series of the tests are either cylindrical in shape or rectangular, with three different lengths L as are listed in Table 4.5. Other experimental parameters, such as embedded depth D and radius of the barrier R, were fixed to be 10.0 m and 2.50 m, respectively, throughout this series of the tests. The EPS barrier was selected for the tests. The measurement points are the same as for the tests with a cylindrical barrier (Fig. 4.28), as previously reported.

Table 4.5 Experimental program for point load test using a rectangle barrier

	Embedded depth of barrier D (m)			
	10.0			
	Geometry of the barrier			
	Rectangle			Cylinder
	Barrier length L (m)			Cylinder
	15.0	10.5	6.0	
Wave impedance A >0 (EPS) Distance between source and barrier R (m) 2.50	O	O	O	O

During the model preparation, the barrier was set in advance and kept in a vertical position using the guide in the experiment of the rectangular barriers, when the sand was poured.

Figure 4.35 presents how the maximum acceleration decreases with distance from the vibration source for different barrier systems, including the data without a barrier for references. As far as the maximum acceleration inside the barrier is concerned, it appears that there is no significant difference among the barriers with different geometry. This observation is consistent with the results reported by Woods et al. (1974). However, appreciable difference in the maximum acceleration on the barrier is noticed. Beyond the barrier, the cylindrical barrier seems to be slightly more effective than the rectangular. Figure 4.36 shows the time history of acceleration on the barrier for the barriers with different geometry, together with the input acceleration shown in dotted lines. It is clear in the figure that there is a marked difference in the motion of the barrier, not only in terms of the maximum acceleration, but also in terms of the overall behavior. A possible explanation for the difference in the overall behavior of the motion of the barrier might be that propagating waves reach the cylindrical barrier at the same time with the same phase, whereas propagating waves reach the rectangular barrier at different times with different phase lag. This phase lag in the arriving waves would cause amplification for cylindrical shape and attenuation for rectangular shape. Figure 4.37 shows the ratio of the maximum acceleration on the barrier to the input maximum acceleration measured in the model foundation, R_α, plotted against an aspect ratio L/R of the rectangular barrier. As one might expect, there is a sharp decreasing trend of R_α with increasing the aspect ratio.
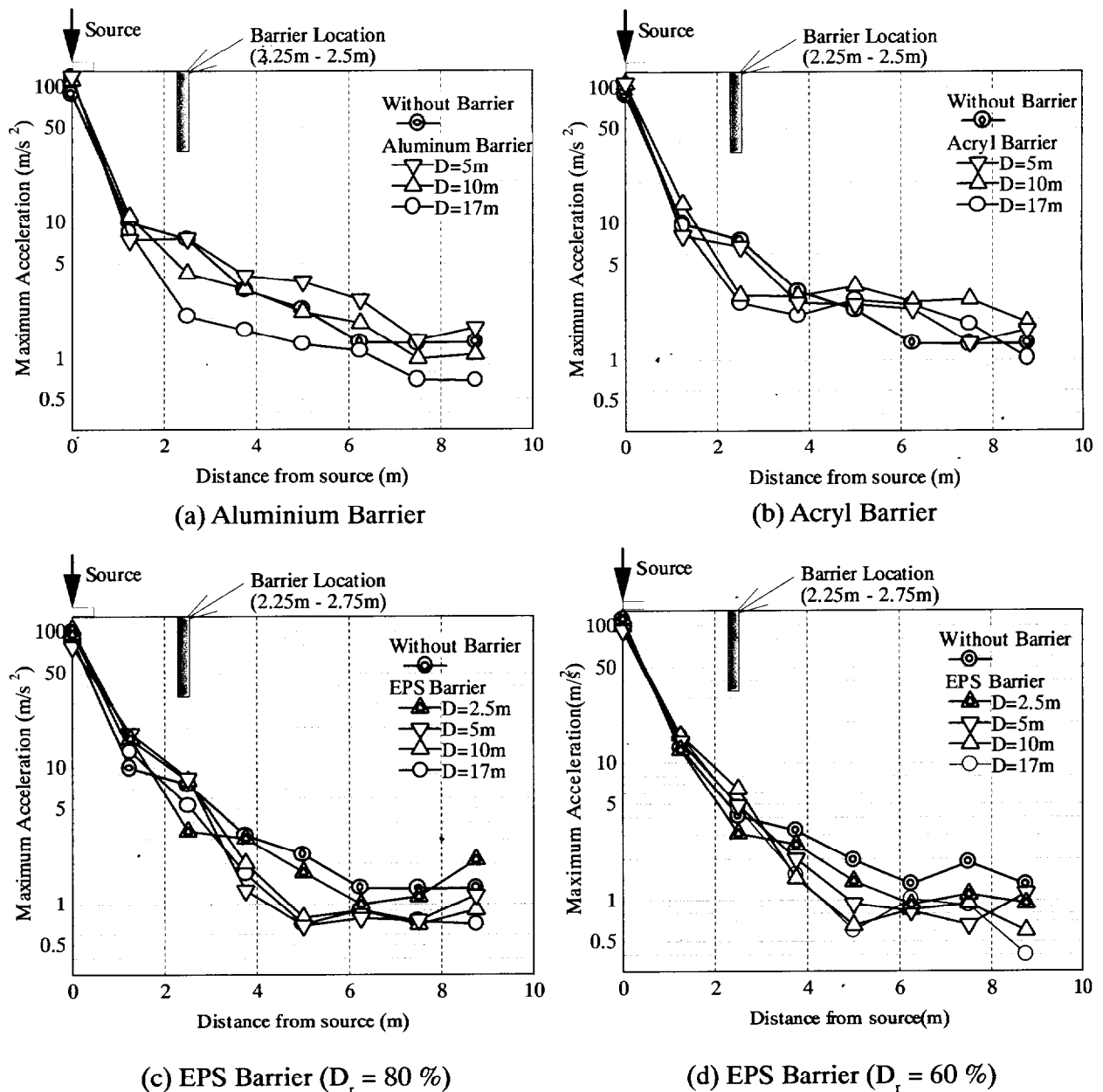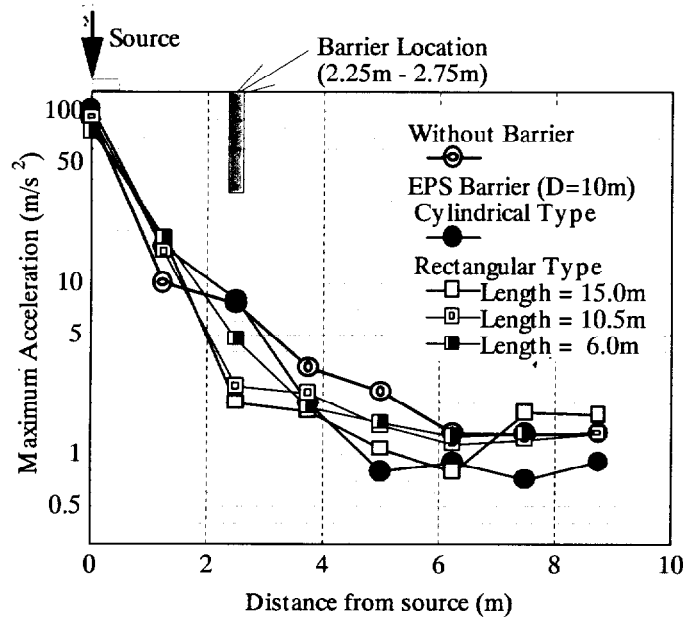
Figure 4.35 Attenuation of the maximum acceleration with distance from vibration source for various barrier forms for the case of the rectangular and cylindrical barrier
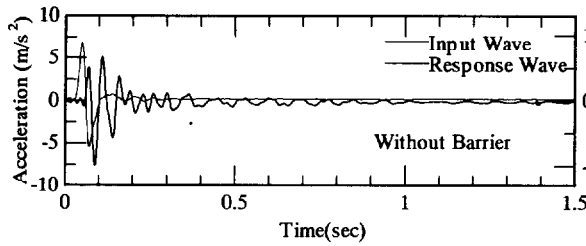
(a) Without barrier
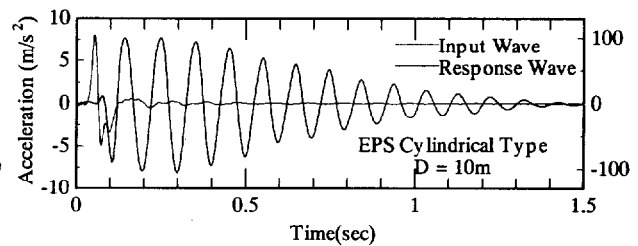
(b) EPS cylindrical barrier (D=10m)
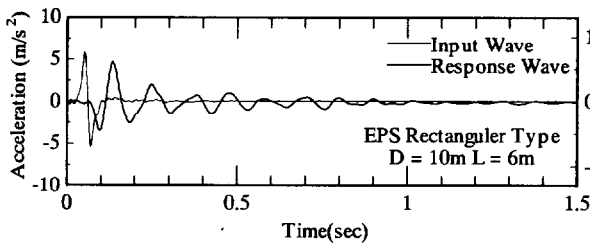
(c) EPS rectangular barrier (D=10m, L=6m)
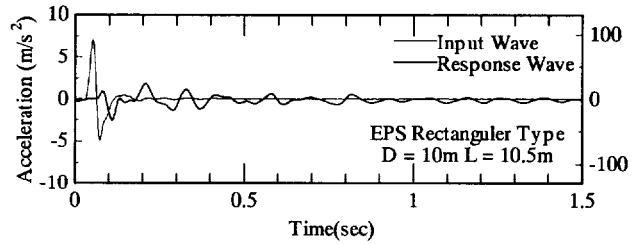
(d) EPS rectangular barrier (D=10m, L=10.5m)
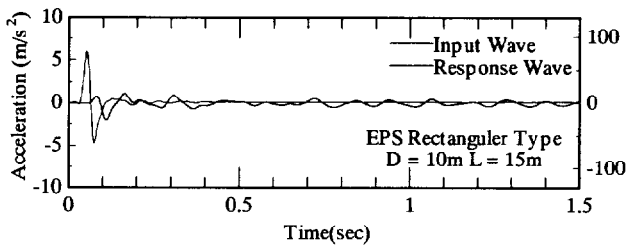
(e) EPS rectangular barrier (D=10m, L=15m)

Figure 4.36 Time histories of vertical acceleration on the barrier with various types of barrier
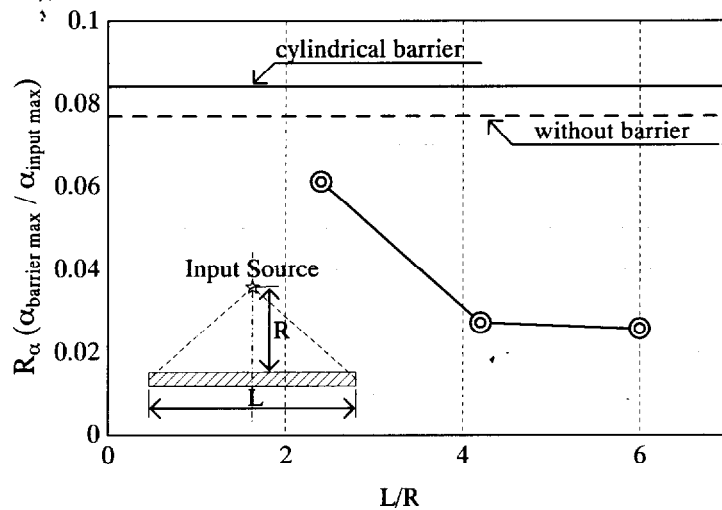
Figure 4.37 Change in R_α with different values of barrier length / distance between source and barrier

4.1 IMPACT POINT LOADING - VIBRATION COUNTERMEASURES AT VIBRATION SOURCE-

4.1.1 General

This section presents the results of a series of centrifuge model tests to investigate the effect of a vibration reduction method which uses a crumb rubber-modified asphalt (CRMA, the details of this material are shown in Chapter 3) layer at the vibration source. In addition, the effect of this method combining with Expanded Poly-Styrol (EPS) barrier, which is a countermeasure method applied at transmitting path, is studied.

4.1.2 Test procedures

Figure 4.38 shows the details of this system (Fig. 4.38(a)) and outer view of model set up (Fig. 4.38(b)). The soil used was air-dried Toyoura sand. The sand was poured from a certain height (150mm) for consistent production of uniform deposit with an average dry unit weight γ_d of 15.4 kN/m^3, which targeted to a relative density of 80%. The ground vibration was recorded by piezo-electric accelerometers (CBC111BW and CBC107S, CBC Materials Co., Ltd.) which provided data on the vertical accelerations at chosen positions on the ground surface, as shown in Fig. 4.39. This study examines the effect of using CRMA at trackbed and EPS wave barrier at transmission path in vibration reduction. In the field, a railway road consists of track beds (including tie) and roadbed, as shown in Fig. 4.40. The high-speed train wheels rolling on the rails create vibration energy transmitted through the track support system into the track bed and roadbed. The experimental concept of vibration source is shown in Fig. 4.41. High-speed train that generates vibration is modeled by an aluminium cylinder hit by a dropping ball. The aluminium cylinder is 30 mm in diameter and 25 mm in height, which houses a built-in piezo-electric accelerometer (CBC107S, CBC Materials Co., Ltd.) so as to measure the input acceleration directly. In this study, the ball used was a steel ball 19.8 mm in diameter and 28.0 g in mass. The ballast was modeled by the aluminium

View of slider

24

20

10

20

230

20

Motor

Crank

Steel ball

Guide

Plan view

Motor

Crank

Hole

Slider

Guide

100

100

20

20

EPS barrier

15

unit : mm

Ground surface
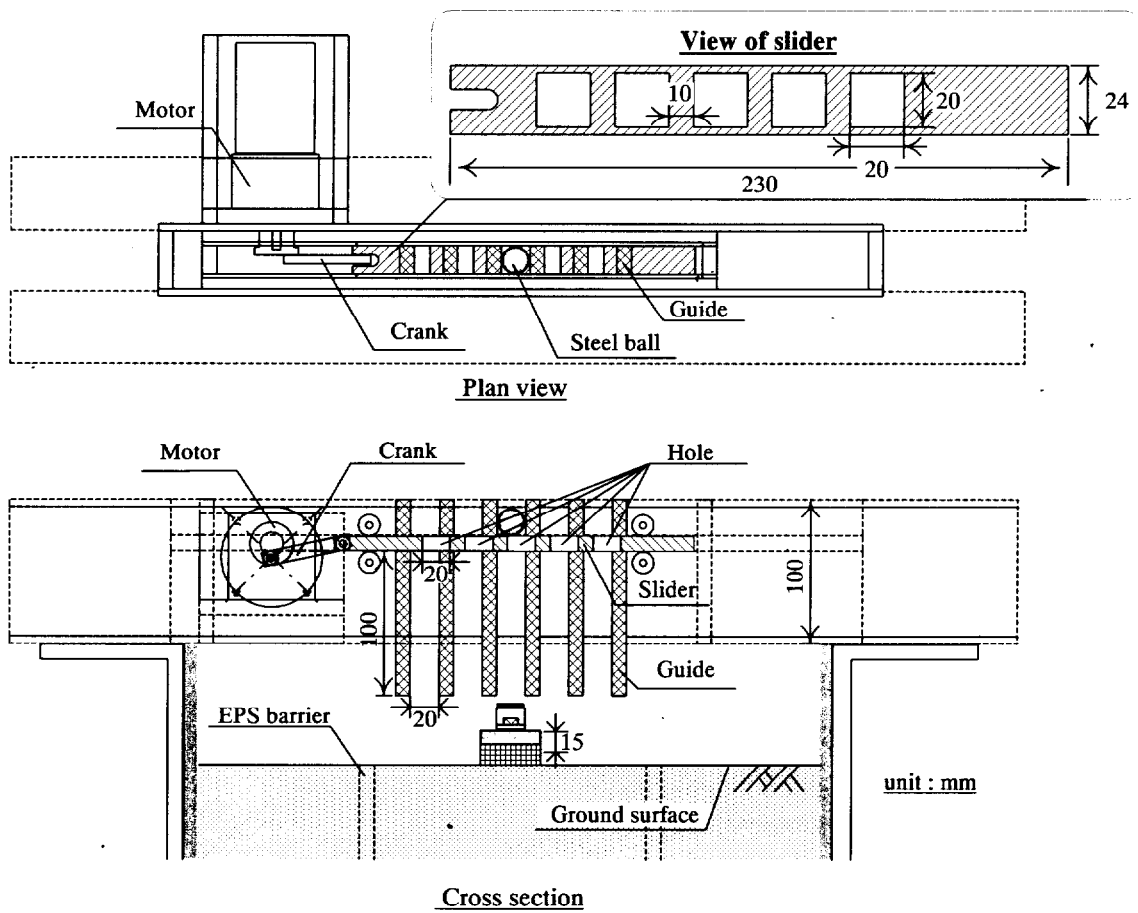
Cross section

(a) Details of test system
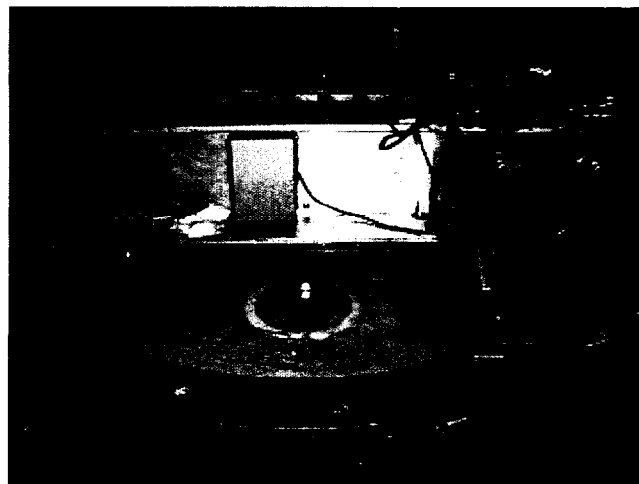
(b) Outer view of model set up

Figure 4.38 Details of ball-dropping system

Input Acceleration
(Location No.1)

Accelerometer of
Location No.

2

3 4 5 6 7 8 9

25mm@7= 175 mm
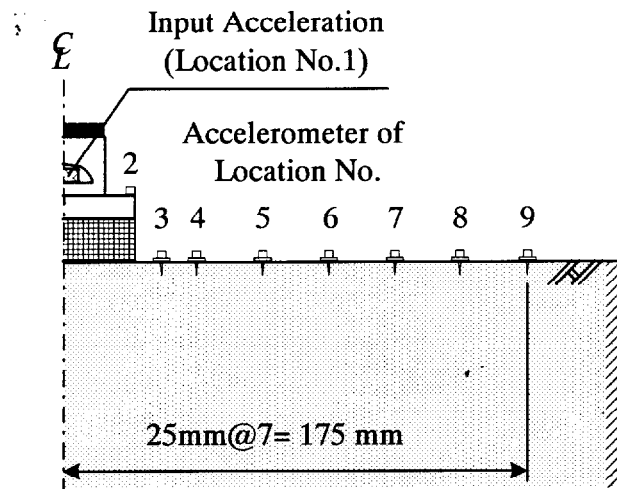
Figure 4.39 Location of accelerometers

High-Speed Train
(Vibration Source)

Ballast

Countermeasure material

Road Bed
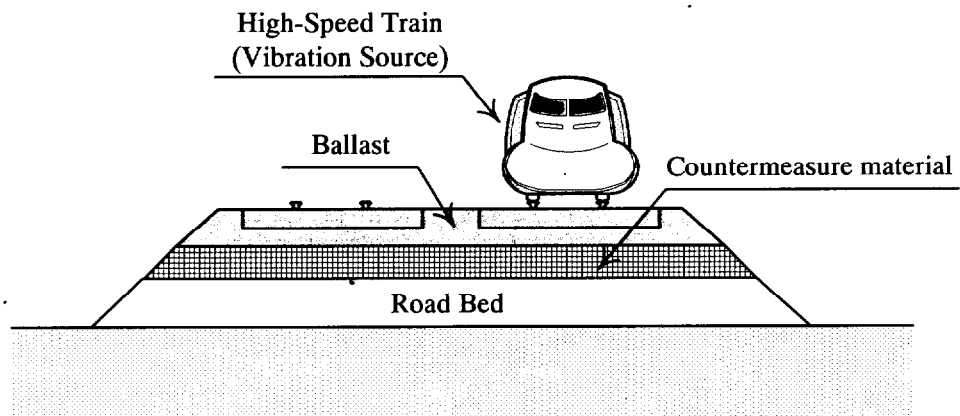
Figure 4.40 Cross section of a typical railway road

Foundation
(modelled vibration source)

Aluminium plate
(modelled trackbed)

Countermeasure material
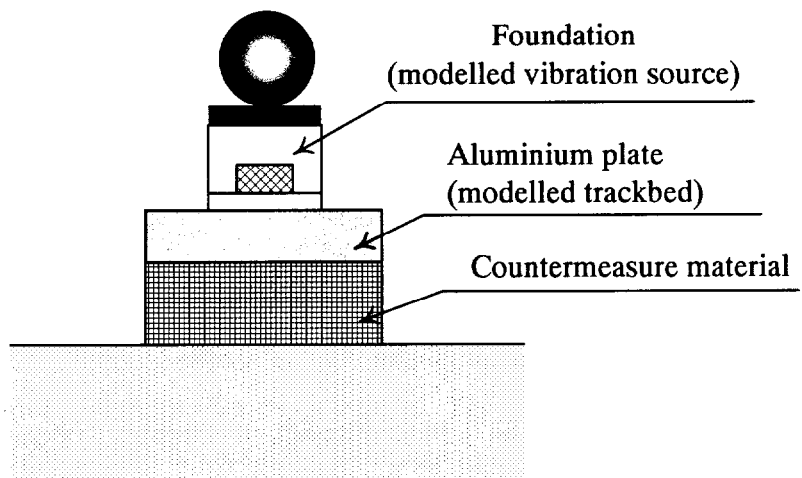
Figure 4.41 Model of a railway track structure

Table 4.6 Experiment program for point load test using the vibration countermeasure materials

		Trackbed materials			
		Aluminium	CRMA Prototype	CRMA 1/5 scale	Rubber
Barrier	Without	O	O	O	O
	EPS φ200×200	O	-	O	O

circular plate of 60 mm in diameter and 15 mm in height. The experimental conditions are listed in Table 4.6. Selected vibration reduction materials under the trackbed were rubber and CRMA, while a stiff foundation was modeled by aluminium. The vibration reduction material under the trackbed was modeled by a ring plate of 60 mm in diameter and 15 mm in height. Regarding boundary condition between the foundation and the aluminium plate, the foundation was only placed on the aluminium plate, rather than glued together. The CRMA modified trackbed was not modeled by a material that would satisfy the scaling law of aggregate size. To simulate the field situation accurately, the aggregate size in the centrifuge model test should be reduced by the model scale (which was 50 for the tests reported here). However, it is not possible to make asphalt with such small grains. Thus the aggregate size was reduced by only about 5. In addition, in order to study the effect of the aggregate size of CRMA, another CRMA sample which used the same aggregate size as in the prototype used in the experiments. In the field, foundation made of pure rubber material is not applicable, because rubber is too soft, very expensive, and would not last long in natural weather conditions. In this study it was used as an extreme example of a soft foundation. Of course the long term performances of CRMA such as true creep, chemical processes, weathering etc...were beyond the scope of this study. These mechanical properties of the materials are listed in Table 4.7. Each test was carried out at least twice to check the repeatability of experimental results.

All tests were carried out under 50 G acceleration. Hereafter all the results of the centrifuge tests are presented in prototype scale.

4.1.3   Test results and discussions

(1)   Accelerations recorded at vibration source

Figure 4.42 shows the time histories of vertical acceleration and the results of Fast Fourier Transform (FFT) in the foundation (accelerometer No. 1) which is modelling the vibration source caused by the dropping ball. In this figure, two pulse waves were observed in the first wave. This response is likely caused by the rebound between the foundation and the aluminium plate since in the experimental setup the foundation was placed on the aluminium plate, rather than glued together. This response affected the results of FFT as the Fourier Spectrums in the range from 40 to 80 Hz had

Table 4.7 Mechanical and material properties of Trackbed materials

	Dry unit weight γ_d (kN/m^3)	Shear modulus G (MN/m^2)	Maximum grain size (mm)	Mean particle diameter D_{50} (mm)
Aluminium	26.5	2.56 × 10^4	---	---
CRMA Prototype	23.1	9.50 × 10^2	15	3.35
CRMA 1/5 scale	23.5	9.60 × 10^2	4.75	0.25
Rubber (Natural rubber)	9.60	1.08 × 10^2	---	---

larger amplitude than accelerations recorded at other locations. Comparing the shape of FFTs, the results of the CRMA foundation and aluminium foundation are similar. On the other hand, the result of using the rubber foundation looks very different. The first dominating frequency in this case was lower than that recorded in other cases and the intensity was much higher. This response is associated with the stiffness and damping of the materials. Figure 4.43 shows the time histories of vertical acceleration and the results of FFT on the aluminium plate (accelerometer No.2), which simulates ballast used in railway trackbed. Compared with the recording of accelerometer No. 1, the influence of rebound between the foundation and the aluminium plate were not observed at this location. The recorded maximum acceleration reduced as the stiffness of the foundation material increases in the sequence of aluminium, CRMA which used prototype aggregates, CRMA which used scaled (1/5) down aggregates, and the rubber. In this experiment, recorded amplitudes on the aluminium plate (accelerometer No. 2) ranged from 31.7 (case of Aluminium) to 71.6 m/s^2 (case of Rubber). In addition, dominating frequencies recorded by accelerometer No. 2 had a wide range from 5 to 40 Hz. These values are compared with typical train load. Degrande and Lombaert (2000) measured time history of the vertical acceleration of the sleeper during the passage of the Thalys High-speed train with a speed of v = 314 km/h. According to their measurement results, the maximum acceleration is about 60 m/s^2. From the point of view of the maximum acceleration, the recorded results on the aluminium plate are similar to the measured results of the sleeper in the field site. Turning now to the vibration form, it describes the differences in behavior between these two results. To be more precise, the results which were measured during the passage of the Thalys High-speed train observed cyclic wave, whereas the results of this experiment observed a pulse wave. However a pulse wave covers the wide range of frequency in the frequency domain. Thus these frequencies are within a typical range of the predominant frequency of traffic vibration caused by high-speed train.
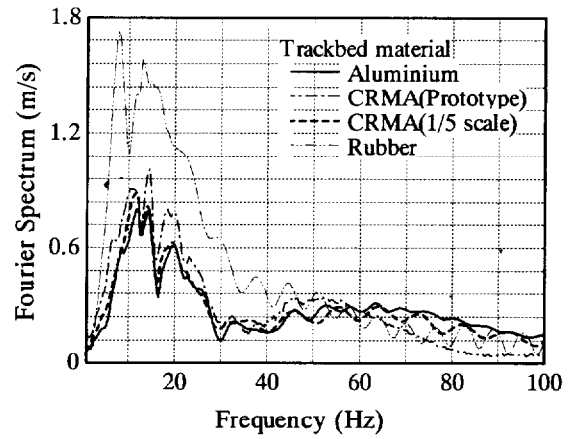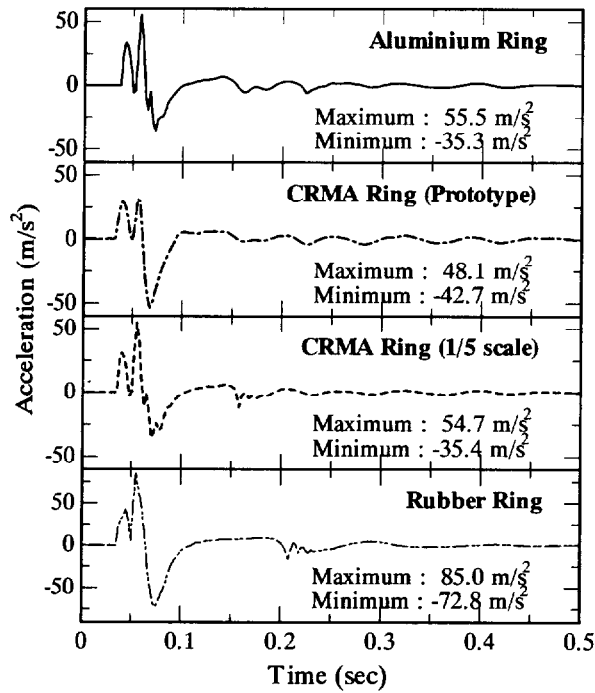
Figure 4.42 Time histories of vertical acceleration and results of FFT recorded by accelerometer No.1
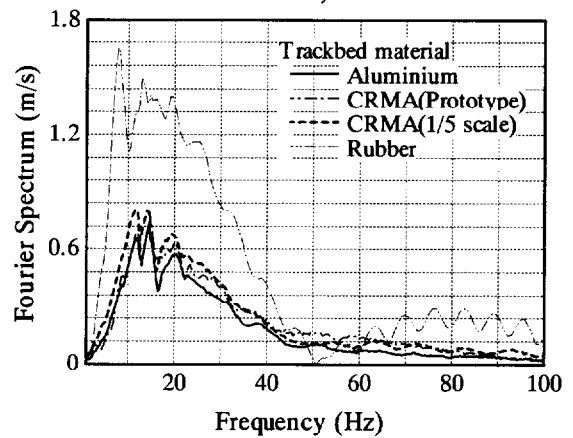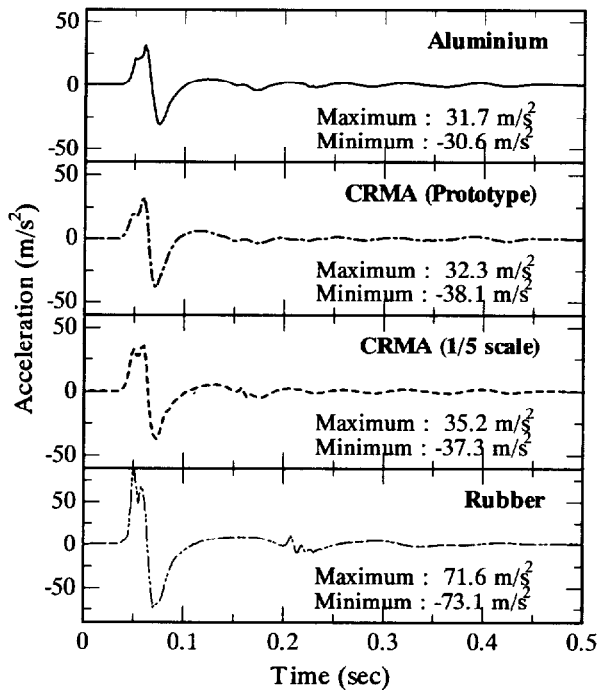
Figure 4.43 Time histories of vertical acceleration and results of FFT recorded by accelerometer No.2

(2) *Effect of modified trackbed on vibration attenuation*

Figure 4.44 shows the attenuation of the maximum acceleration as the distance from the vibration source for various modified trackbed materials. The case of aluminium trackbed is used to model currently used trackbed without countermeasure materials. As shown clearly in the figure, the maximum acceleration decreases gradually with distance from vibration source. A significant effect of vibration reduction becomes evident for the case of the rubber-modified trackbed. The effect of CRMA is between these two with the CRMA which used scaled down aggregates producing vibration attenuation similar to that of rubber foundation. Figure 4.45 shows the time histories of vertical acceleration in the case of various modified trackbed materials (Fig 4.45 (a): CRMAs, Fig 4.45 (b): Aluminium and rubber) at the all measurement points. It can be concluded that the repeatability of the experimental results is very good except for the case of the aluminium track bed at accelerometer No.6 because accelerometer used malfunctioned. In comparison with the time history recorded when using aluminium trackbed, the starting time of vibration has a phase lag at the No.3 location in the case of rubber trackbed. The likely cause for the time delay is the difference in the propagation speed of elastic waves in the two materials. It was observed that the rubber modified trackbed recorded lower vertical acceleration at the ground surface than that when the aluminium trackbed was used. In the case of two CRMAs, the maximum accelerations recorded were between the value
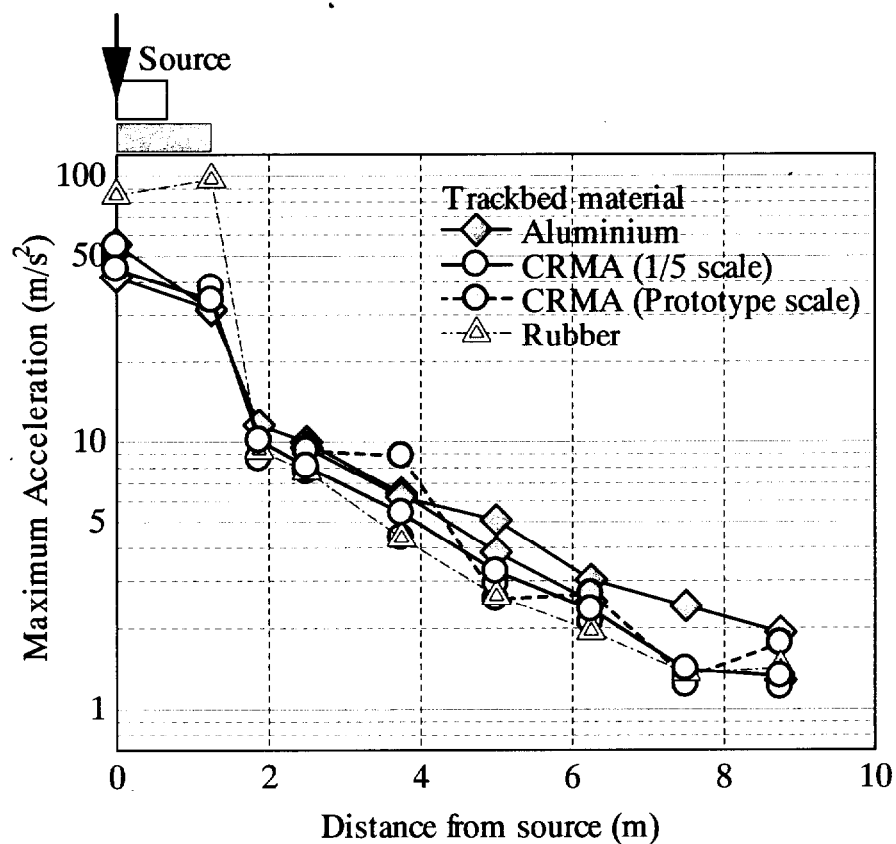
Figure 4.44 Attenuation of the maximum acceleration with distance from vibration source for various trackbed materials

- 90 -
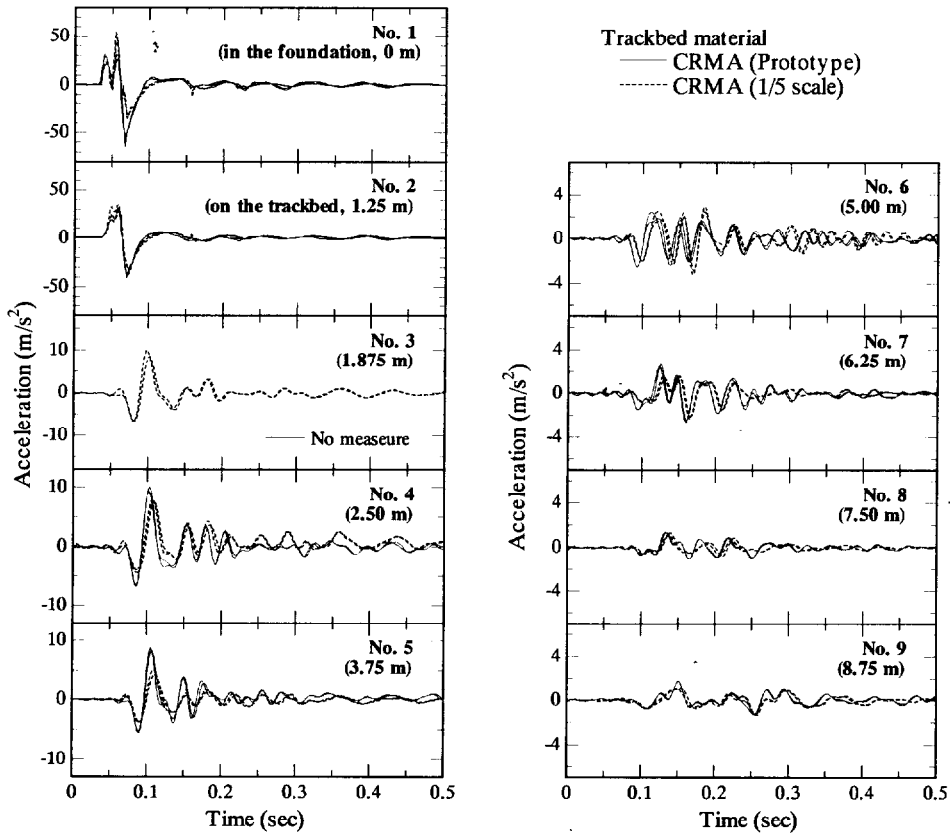
(a) Model trackbed materials using two types of CRMA
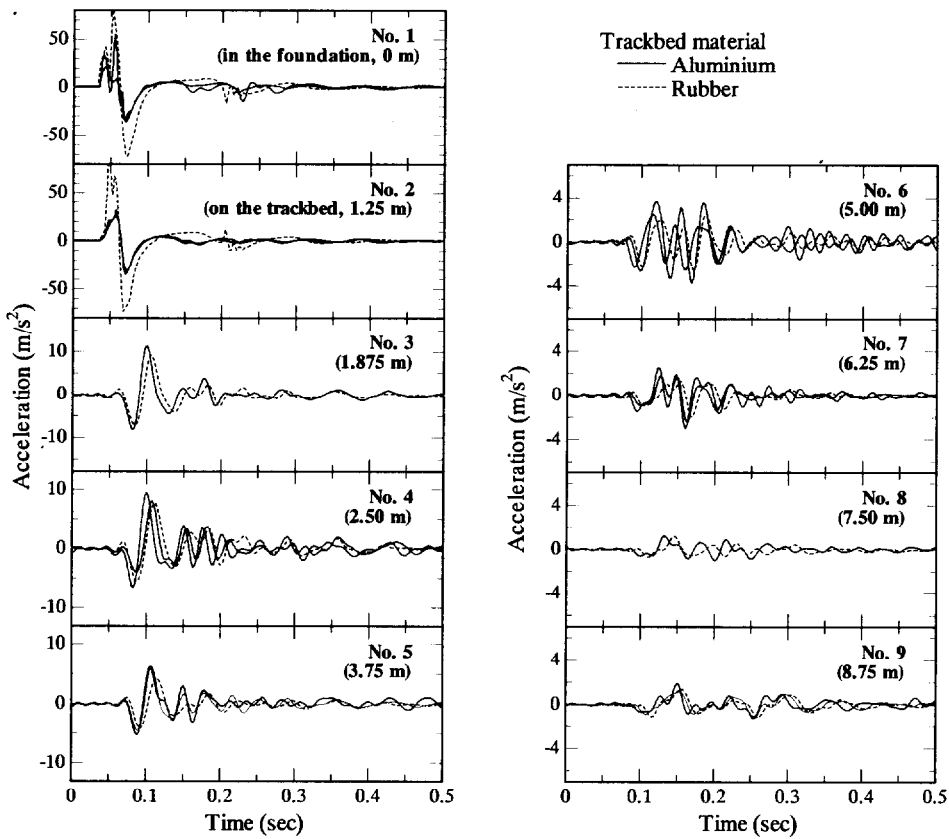
(b) Model trackbed materials using rubber and aluminium

Figure 4.45 Time histories of vertical accelerations at different locations

(a) Location of No. 2 (On the model trackbed)   (b) Location of No.4
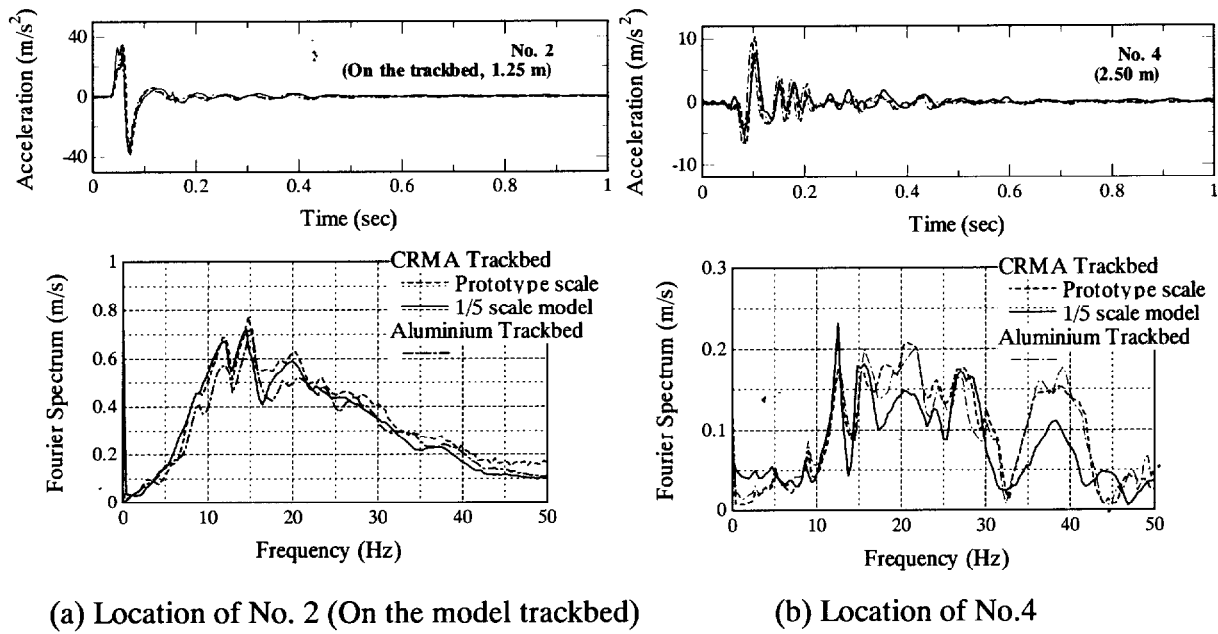
Figure 4.46 Scale effect of aggregate size of CRMA (Time histories of accelerations and results of FFT using various CRMA materials)

(a) 1/5 scale model   (b) Prototype scale model
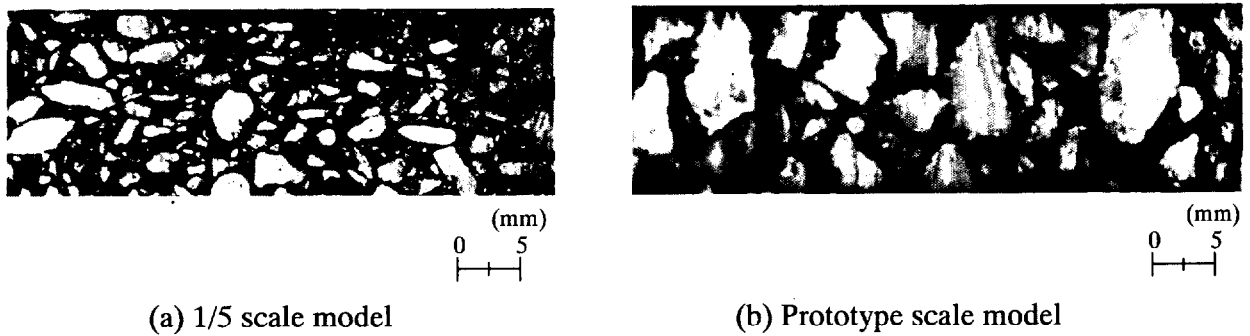
Figure 4.47 Cross section of the two types of CRMA materials

recorded in the aluminium trackbed and that recorded in the rubber trackbed except for accelerometer No. 5 of the CRMA trackbed which had a full scale aggregate, as shown in Fig 4.44. The scale effect of the aggregate size in CRMA was examined. Figure 4.46 shows the time histories of vertical acceleration and the results of FFT for two CRMAs on the ballast (accelerometer No. 2) and at the surface ground (accelerometer No.4), which also includes data for the case of aluminium trackbed. At the vibration source, the overall agreement between two kinds of CRMA and the aluminium is very good, both in magnitude and shape of the Fourier spectrum. On the other hand, the recording data by accelerometer No.4 shows a significant difference. For the CRMA trackbed that used full-scale aggregate size, the shape and magnitude of the time histories and Fourier spectrum are about the same as the aluminium trackbed. However, in the case of CRMA which used aggregates at 1/5 scale of the prototype, the Fourier spectrum in the area around 20 Hz and 38 Hz showed a 30 % reduction compared with the other two. The cross sections of CRMA are shown in Fig 4.47, respectively. In this experiment, the thickness of these materials used is D = 15 mm. The maximum gravel size of 1/5 scale aggregate was 4.75 mm. Thus there are at least several layers of gravel stones bounded by asphalt and rubber in the cross section. On the other hand, there could be only one

gravel layer for the prototype CRMA because the maximum gravel size was 15 mm. CRMA is a bituminous mix, consisting of blended aggregates, recycled crumb rubber, and petroleum asphalt binding agents. The rubber, which influences the damping ratio, adheres around the gravel. It appears that the numbers of gravel layers per trackbed are associated with vibration attenuation. For this reason, full scale CRMA did not reduce vibration as much as the 1/5 scale CRMA. If CRMA which satisfied the scaling law of aggregate size was used in this experiment, more significant vibration reduction would be expected.

Of the three materials used in the experiment, aluminium has the highest stiffness, followed by CRMA and rubber. For damping ratio, the sequence is just the opposite with rubber which has the highest damping ratio. Based on the results obtained in the tests, it shows that the higher the stiffness of the material, the lower the vibration generated at the source. However, for the vibration away from the source, it is controlled by the damping ratio with the rubber foundation recording the lowest vibration away from the trackbed. For the CRMA foundation, the vibration at the source is about the same as that for the aluminium foundation while at the same time for locations away from the source, the vibration is just slightly higher than that for rubber foundation. This can be explained by the material properties of CRMA reported by Zeng et al. (2001). The stiffness of CRMA was quite high while the damping ratio was 3-4 times higher than aluminium or concrete. In our tests, the ability of energy absorption of CRMA was not completely simulated as the size of aggregate is not properly scaled. If its ability is simulated properly, we would expect even lower vibration away from the source. In the field it is unrealistic to use a foundation as soft as rubber because the impact load generated on the trains and the local deformation of the track would be too large. It seems that CRMA can lead to a vibration as low as the stiff foundation at the source while at the same time can reduce the vibration away from the source because of its high damping ratio. Therefore, it is an attractive material for trackbed construction.

(3) *Effect of CRMA foundation with EPS barrier on the reduction of vibration*

In addition to the countermeasure methods adopted at the vibration source, another method that applied at transmission path is commonly used. This is an effective countermeasure method for routes that are already in operation. In this study, a few cases combining the methods at the source and an EPS barrier are investigated. Figure 4.48 shows how the maximum acceleration decreases with distance from the vibration source for various modified trackbed materials with EPS barrier. It also includes data for the case of aluminium trackbed without barrier. As shown in the figure, the maximum acceleration decreases gradually with distance from the vibration source. Comparing the data from tests without a barrier with that with a barrier and various trackbed materials, it can be seen that the barrier is quite effective. The rubber modified trackbed makes a significant effect in reducing vibration both before and after the barrier. As for other modified trackbed materials, it is observed that the maximum acceleration was reduced by about 50% beyond the barrier, but there was no reduction in front of the barrier.

Figure 4.49 shows the time histories and the results of FFT of accelerations recorded at the location for the four tests that include three trackbed materials with EPS barrier and one aluminium

trackbed without barrier. It is clear from the figure that there is a marked difference in the vibration of the barrier. The accéleration on EPS barrier was like a damped free-vibration for about 2 seconds, whereas the vibration without barrier at the same location stopped in about 0.8 seconds. From the results of FFT, the first, the second and the third dominating vibration frequencies are around 8.5 Hz, 17.0 Hz, and 26.0 Hz respectively.

In order to examine the cause of different behavior for cases of aluminium trackbed with and without a barrier, Fig 4.50 presents the time histories and the results of FFT in front of (No. 5 accelerometer) and behind (No. 7 accelerometer) the barrier, together with the case of rubber modified trackbed with EPS barrier which reduced vibration the most. In front of the barrier, the result with EPS barrier was dominated by the frequencies of the vibration of the barrier. In another words, the motion of the barrier has a profound effect on ground vibration in front of barrier. In comparison with the FFT result of acceleration of the aluminium trackbed with EPS barrier, it can be seen that the result of rubber modified trackbed with EPS barrier has a similar shape, but the magnitude of the spectrum is about 70% less. For the results beyond the barrier, it is shown by the FFT data that for vibration over 30 Hz, the reduction is more than that using aluminium trackbed without barrier.
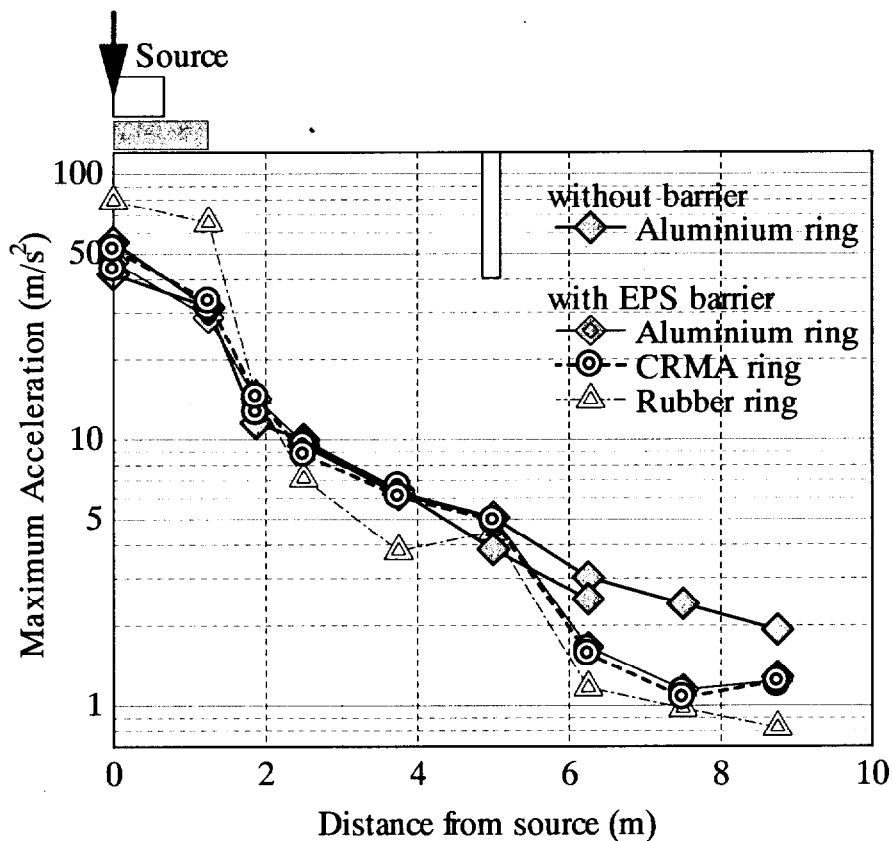
Figure 4.48 Attenuation of the maximum acceleration with distance from vibration source for various trackbed materials with EPS barrier
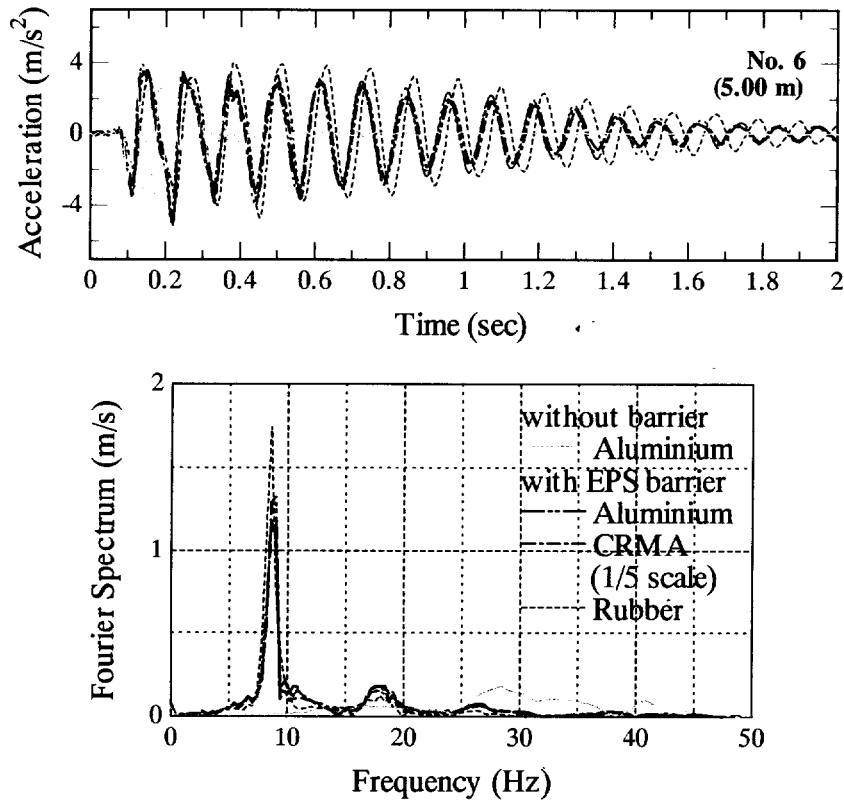
Figure 4.49 Time histories and FFT of accelerations on the EPS barrier
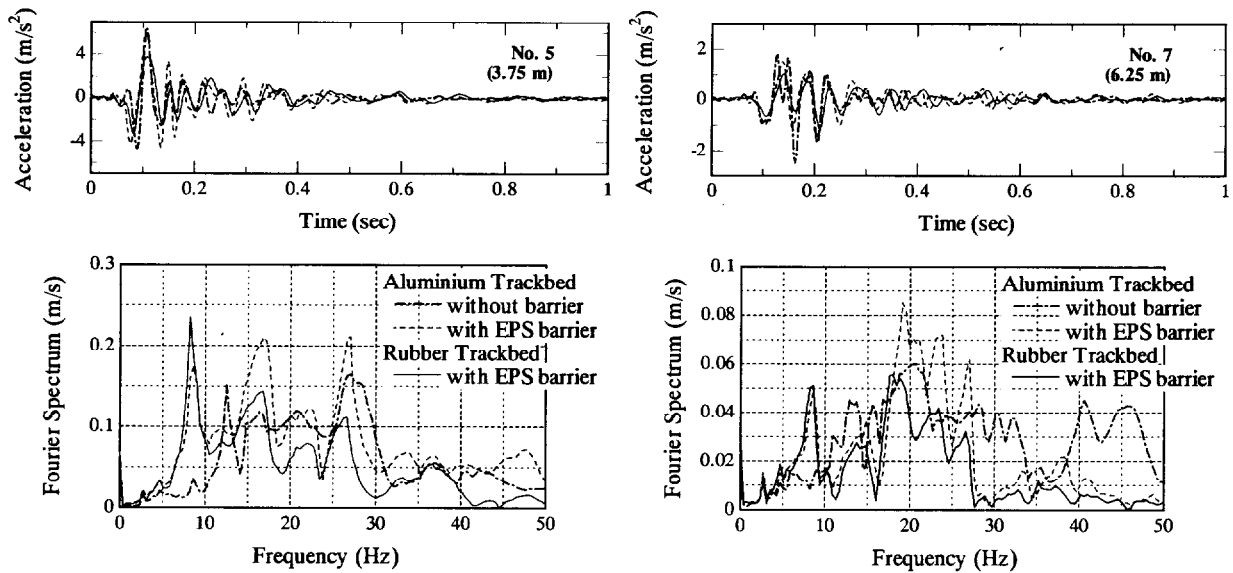
(a) Location of No. 5   (b) Location of No. 7

Figure 4.50 Effect of using EPS barrier on vibration in front and beyond the barrier

4.2 MOVING LOAD

4.2.1 Concept and mechanism of the system

Moving load such as high-speed trains has been recognized as a potential source of ground vibrations. Figure 4.51 schematically illustrates the concept of moving load, where a moving load caused by a running high-speed train through a series of viaducts is modelled. Figure 4.52 gives the experimental system of moving load simulation used in this study. The mechanism of creating a moving load is as follows. Two steel balls are stored at the two extreme sides of this system with three different distances which are 6.0m, 4.5m and 3.0m in prototype scale (Figure 4.52). Two balls drop onto a corresponding foundation. One foundation deliberately has a height slightly higher than the other foundation. The two steel balls drop simultaneously and hit different model foundations. There is a slight difference in height of the model foundations to provide a certain time lag. Consequently, this arrangement leads to slight differences in mass of the foundations and in input maximum acceleration
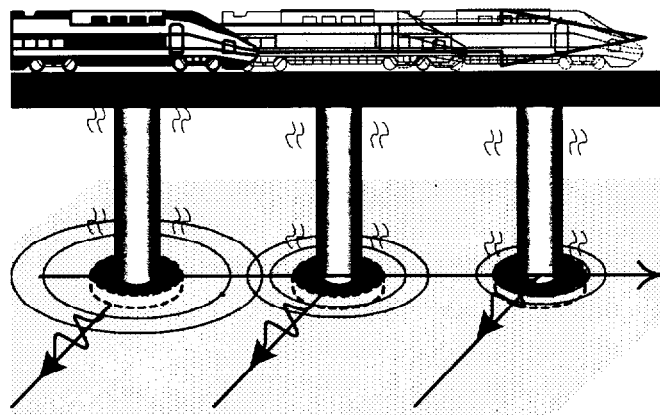
Figure 4.51 Concept of moving load
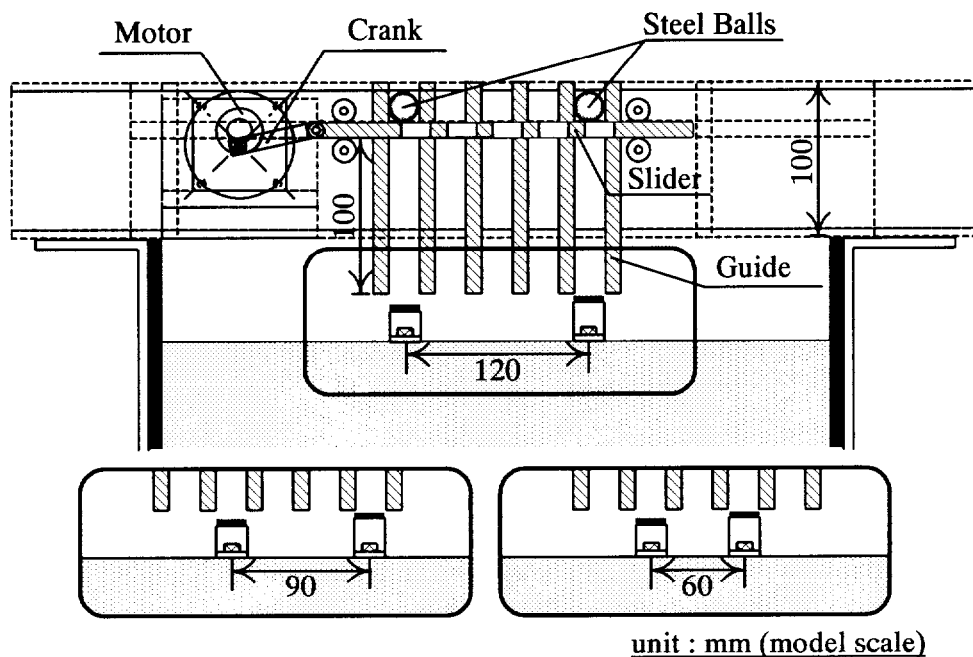
Figure 4.52 Experimental system of moving load simulation

- 96 -

in the foundations. In this particular series of the tests, the foundation hit firstly has a mass of 78.5 g and a height of 41.0 mm, while the mass of the foundation hit later is 62.0 g and a height of 32.0 mm. Another possibility to create the same time lag would be by adjusting distance between the two holes. When a running high-speed train with a velocity of about 500 km/h passes through a series of viaducts with a typical spacing of 6 m, the time lag for the wave head from one foundation to the next is calculated to be 0.0022 sec at the prototype scale. In the multiple ball-dropping system, the moving velocity of slider is 16 mm/s with the motor of a rotation speed of 1250 r/min and a gear ratio of 1/50. If the slider generates the time lag directly by letting the second hole for the ball open a bit later, the required distance between the two holes should be 0.035mm, which poses a mechanical difficulty to achieve. Therefore, changing the height difference between the two foundations can easily alter the time lag in this test.

4.2.2 Test procedures

The experimental conditions are listed in Table 4.8. The effect of the vibration reduction method was examined by using EPS barrier in case 3. The location of accelerometers and barrier is shown in Figure 4.53. There are two cases of experimental setup. One case views the scope of the behavior of the wave propagation from one foundation (Type- I, Fig. 4.53) and another case views the scope of the behavior of an overall area (Type- II, Fig. 4.53). All tests were carried out under the 50 G acceleration. Using the same model ground, three sets of the tests were carried out with a view to examine whether the superimposition can hold or not, except for the case 1 and 2. The first was to conduct a usual moving load test and in the second test only the No. 1 foundation was hit, and finally in the third test only the No. 2 foundation was hit. All the results of the centrifuge tests are presented at prototype scale, hereafter.

4.2.3 Test results and discussions

(1) Characteristics of wave propagation

The difference in foundation height was selected to be 9 mm in model scale, to provide the time lag as shown in Table 4.8. The time lag for the wave head from the one foundation to the next foundation differed on each case. Because all balls did not fall exactly in the same manner due to the limited precision of the slits of the slider. In the case of Type-I, the velocity of the moving load can be readily calculated as about 320 km/h (= 88.89 m/s), thus the source speed is less than the surface wave velocity (=178.6 m/s), which is called 'subtonic condition'.

Figure 4.54 presents typical examples of set of data of vertical acceleration at various points on the ground surface for each interval of viaduct and each train speed. The amplitude of acceleration at the location 2.5 and 7.5 m from the foundation No. 1 (accelerometer No. 3 and 8) and the foundation No. 2 (accelerometer No. 5, 7, 10 and 11) was the same order, independent of the interval of viaduct. However, the accelerometer which was in the center of two viaducts indicates that amplitude of acceleration in viaduct interval of 3 m was larger than that of 6m, because the distances between the source and these positions were different for each case.

The geometrical and material damping of this ground was investigated. Figure 4.55 shows

Table 4.8 Experimental programs for moving load test and the calculated moving load speed

Test case	1	2	3	4	5	6	7	8	9
Interval of viaduct (m)	6.0	6.0	6.0	6.0	6.0	6.0	6.0	4.5	3.0
Barrier (D × L × W)	×	EPS 300 × 200 × 10	×	×	×	EPS 300 × 200 × 10	×	×	×
Type of alignment of accelerometer	Type-I	Type-I	Type-I	Type-II	Type-II	Type-II	Type-I	Type-II	Type-II
Relative density D_r (%)	80	80	80	80	80	80	60	80	80
Superposition	×	×	O	O	O	O	O	O	O
Train speed (km/h)	260	260	350	90	65	65	260	90	43
Test number	ML-09	ML-07	ML-12	ML-18	ML-22	ML-25	ML-17	ML-20	ML-21

unit : mm (model scale)
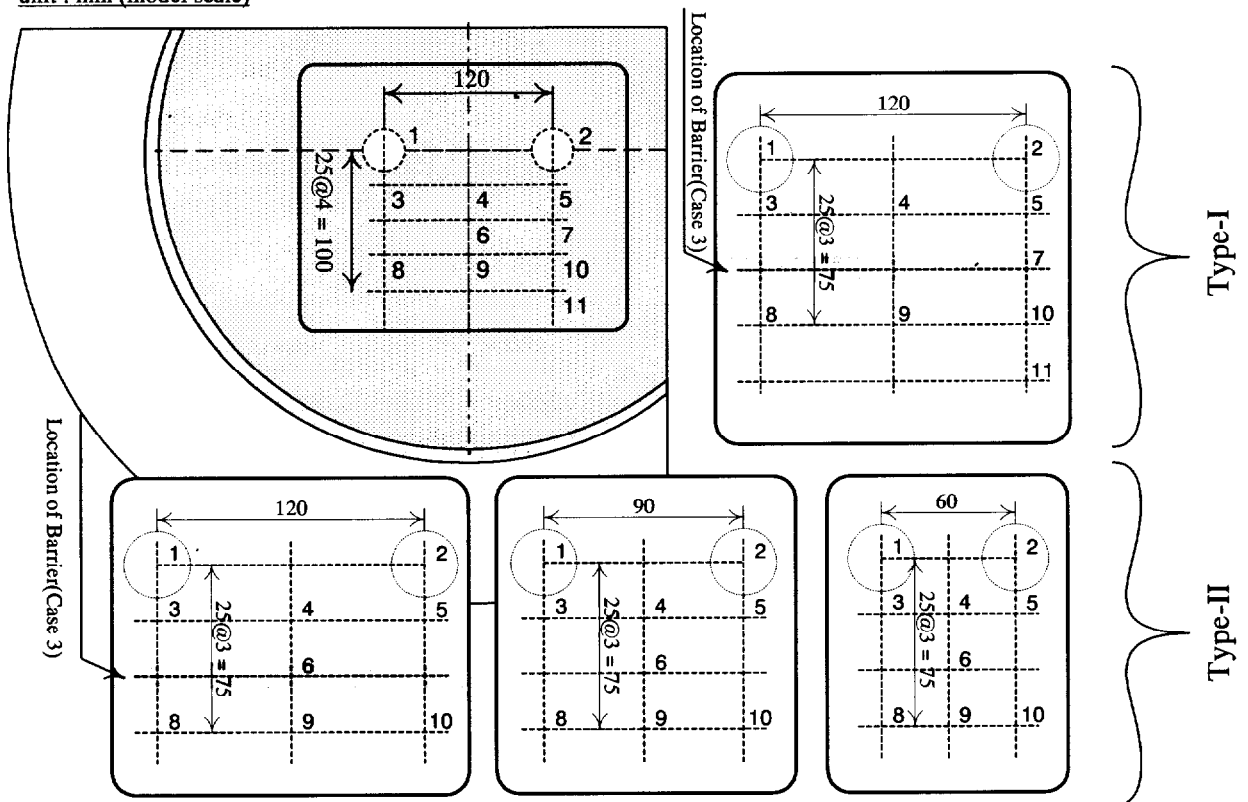
Type-I : 1,2,3,4,5,7,8,9,10,11
Type-II: 1,2,3,4,5,6,8,9,10

Figure 4.53 Location of accelerometers and barrier

the ratio of the maximum acceleration measured on the ground surface to the input maximum acceleration measured in the model foundation, R_α, plotted against distance from source r in this test, in the cases of high-speed (Fig. 4.55(a)) and low-speed (Fig. 4.55(b)), respectively. The closed circles indicate the results by the moving load and the half closed circles indicate the results by the point load represent the measured attenuation of R_α by the result of point load test. And the line represents theoretical attenuation predicted by Bornitz (1931, see above in Chapter 2). The black solid line represents the attenuation of surface wave (n =0.5), the dashed and single gray line represents the attenuation of body wave (n =2). These figures clearly show that the attenuation of surface wave fit each experimental data. It appears that the motion at the ground surface is propagated by surface wave mainly in moving load test also. The amplitude of acceleration is related to the distance from the nearest vibration source, independent of the input condition.

(2) *Effect of EPS barrier on reduction of vibration*

An EPS barrier of rectangular shape (300 × 200 × 10 mm, in model scale) was selected for this test. In order to remove the influence on the reflection wave from edge of barrier, wave barrier
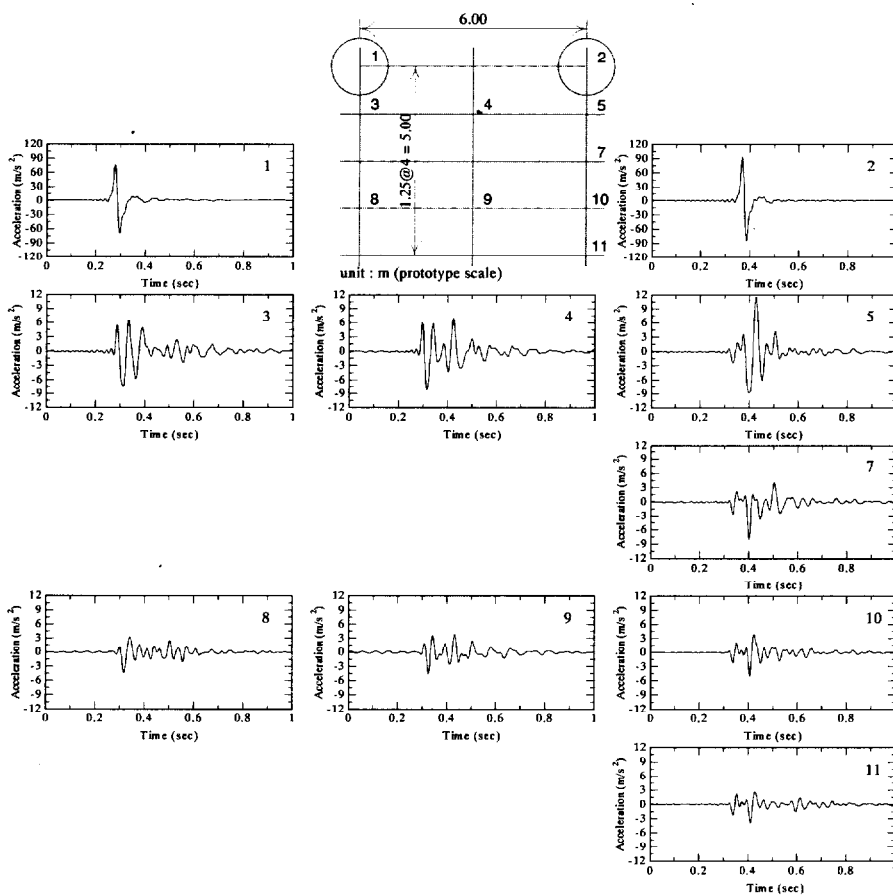
i) Case-1 (Moving load speed of 260 km/h)
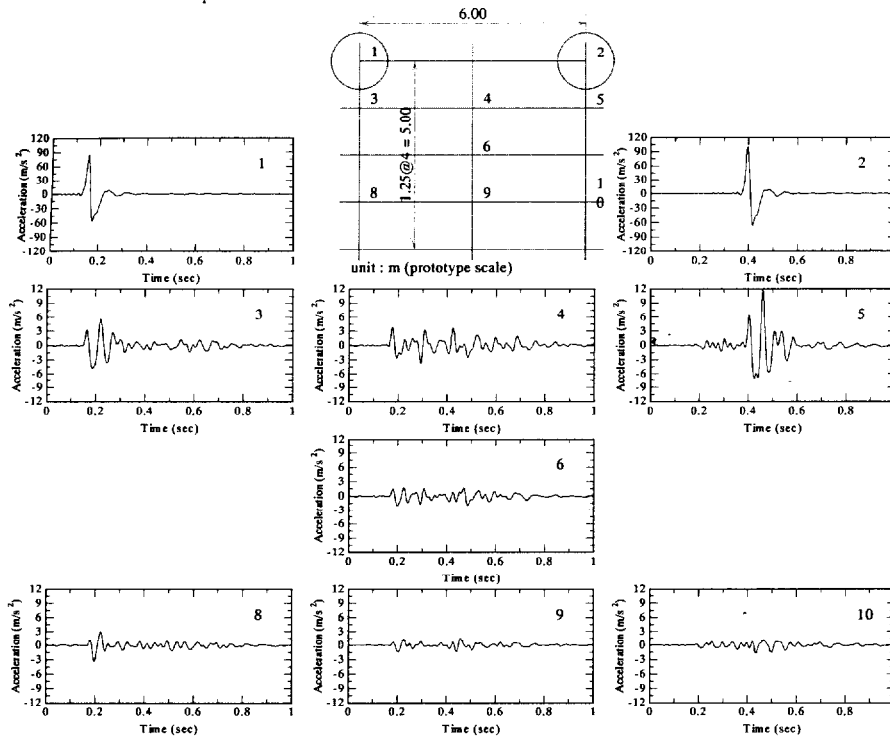
ii) Case 4 (Moving load speed of 90 km/h)

(a) Distance of interval viaduct = 6.0 m
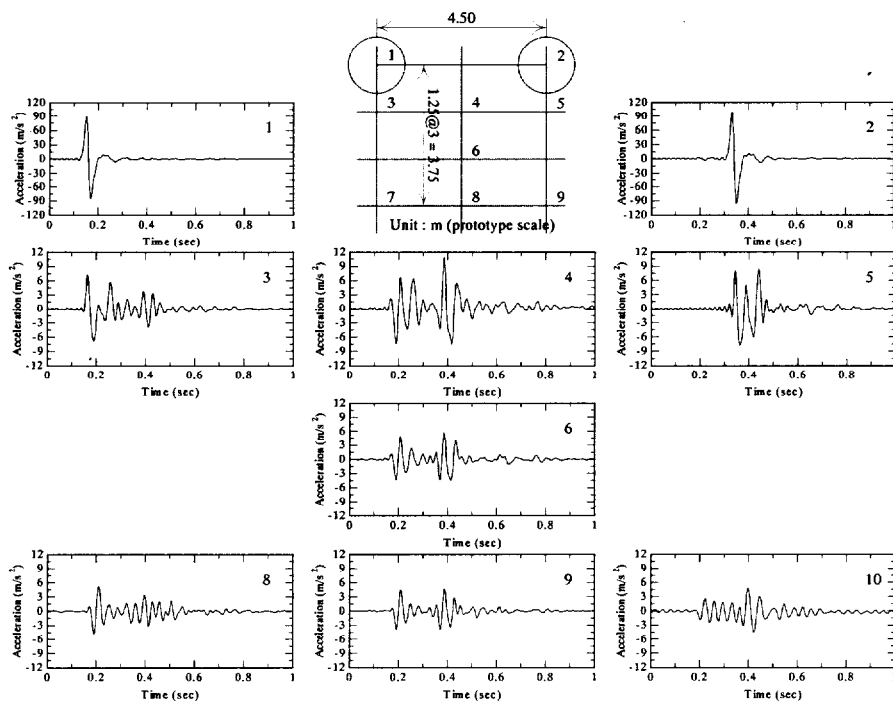
(b) Distance of interval viaduct = 4.5 m (Case 8, Moving load speed of 90 km/h)
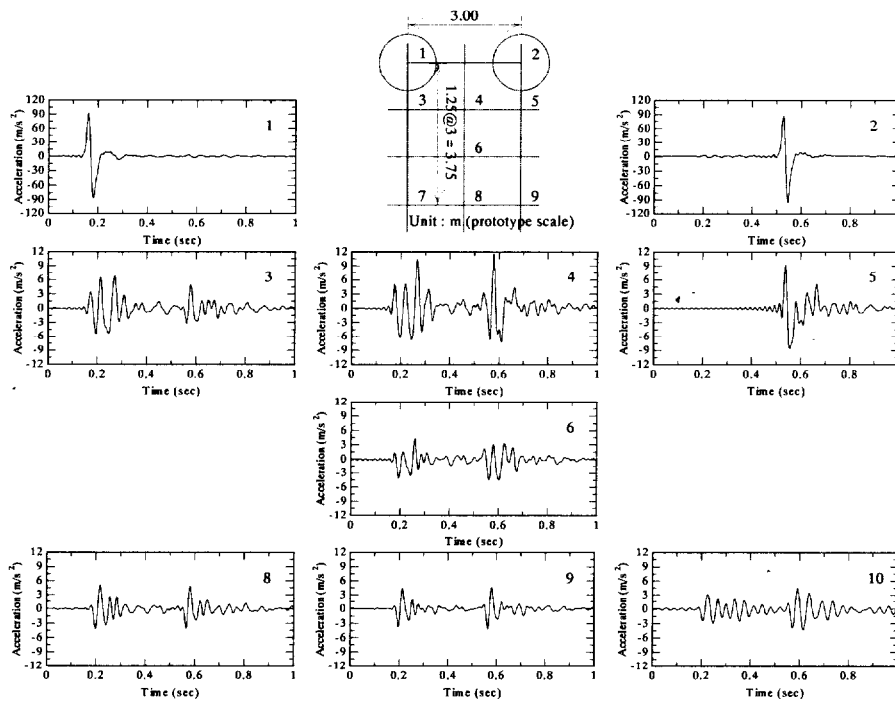
(c) Distance of interval viaduct = 3.0 m (Case 9, Moving load speed of 43 km/h)

Figure 4.54 Time histories in case of various viaduct spaces
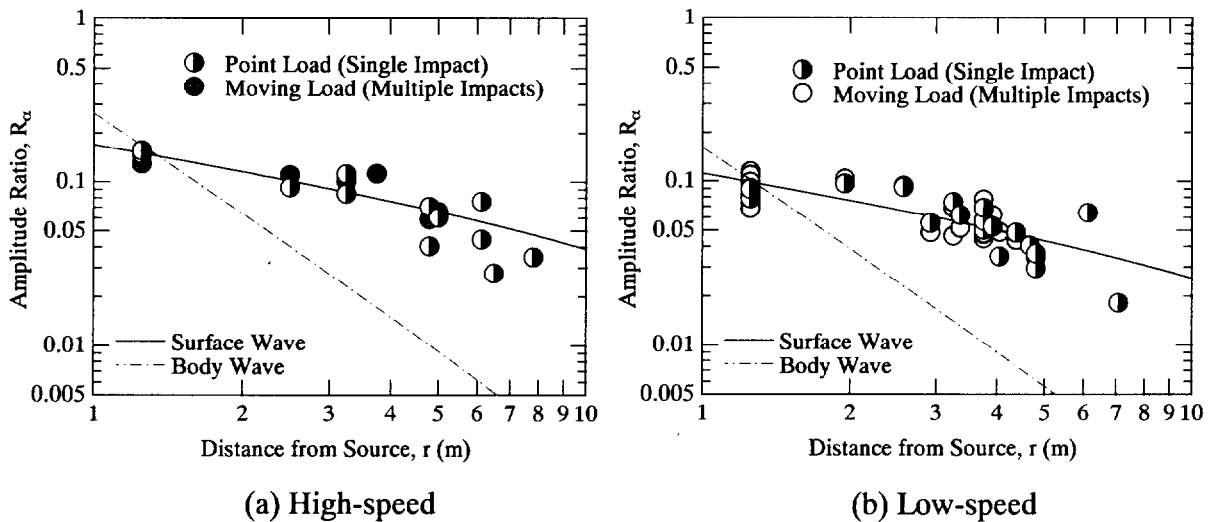
(a) High-speed

(b) Low-speed

Figure 4.55 Attenuation of wave with distance from source

length used was as long as possible in this study. During the model preparation, the barrier was set in advance and kept in a vertical position using the guide in this experiment, when the sand was poured (Figure 4.29). When installing the EPS rectangular barrier of the embedded depth of 10 m and running various velocities of the moving load, the motion of the ground changes as is shown in Fig 4.56, together with the case of without for comparison. The velocities of the moving load can be calculated as about 65 km/h (= 18 m/s, Fig. 4.56(a)) and 260km/h (= 72m/s, Fig. 4.56(b)) at the two loading points 6 m apart. An apparent observation in this figure is the magnification of maximum acceleration in front of the barrier and the reduction on and behind the barrier. To be more precise, the peak amplitude of with EPS barrier was about twice as magnitude as without barrier in front of the barrier. And the EPS barrier reduced amplitude by 30-60 % on and behind the barrier.

(3) Verification of superposition principle of waves

An attempt was made to examine whether the superposition can hold or not, and in what circumstances, if it holes. Figure 4.57 explains what kind of experimental strategy has been taken in this study. The data from the second test which hit only the foundation No. 1 was superposed over the data from the third test which hit only the foundation No. 2, considering the time lag measured at the first test. Thus calculated results are compared with the result of moving load test.

In Fig. 4.58, four cases are presented for the cases of D_r = 80 % (ML-09) and 60 % (ML-17)
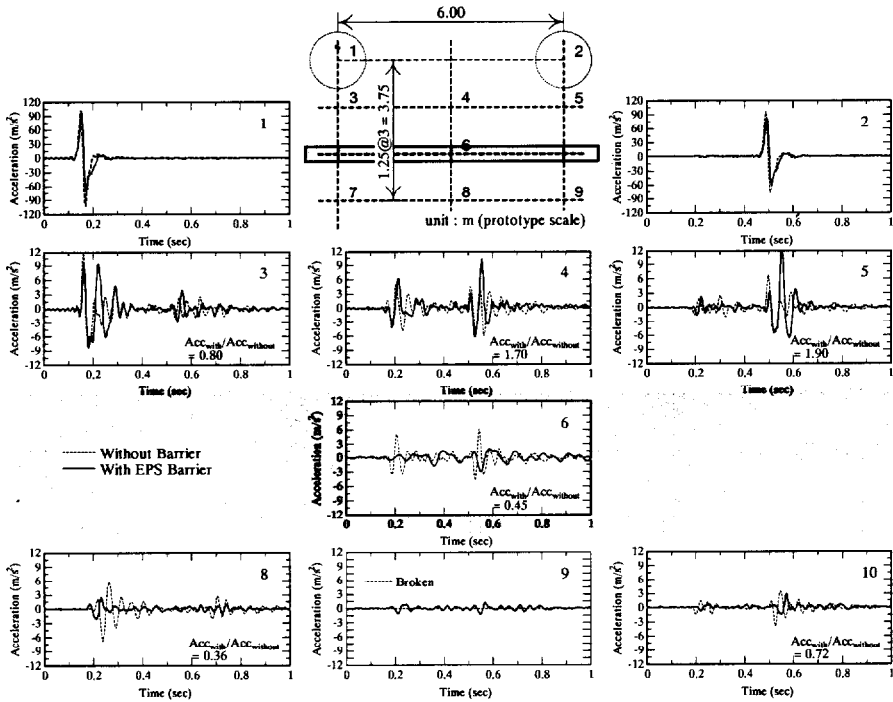
(a) Moving load speed of 65 km/h

at two positions of the accelerometer No. 4 and No.6, together with the input waves. It is observed that among the four figures in Fig. 4.58, the maximum accelerations of the No.2 foundation are always 25% larger than those of the No.1 foundation (Fig. 4.59). It is stemmed from the fact that the falling height of the ball for the No.2 foundation is larger than that of the No.1, resulting in the larger impact force on the No.2 foundation. For the cases of $D_r = 80\%$ (Fig.4.59 (a), (b)), the overall agreement between the moving load data and the superimposed is fairly well, both in magnitude and shape of the wave. Fig. 4.60 shows the different range in relative density, D_r, by the bearing pressure at static loading. It may be said therefore that the superposition of the waves could be applicable, provided that load intensities caused by impact loads are well below the ultimate bearing capacity of the foundation. But it should be noted that the accuracy of the superposition deteriorates, when a factor of safety for bearing failure decreases (Fig. 4.60), as is seen in the cases of the relative density of 60 % of Fig.4.58 (c) and (d).

Fig. 4.61 presents the typical case for comparison between with (ML-25) and without EPS barrier (ML-22) at position of No. 3 and No. 7, together with the input waves. Regarding both cases, it is clear that the overall agreement between the experiment data of moving load and the calculation data of superposition is fairly well, both in magnitude and shape of the wave. It was suggested that the superposition of the waves could be applicable to cases of moving load. Additionally, the superposed result with EPS barrier is similar to its result without barrier.
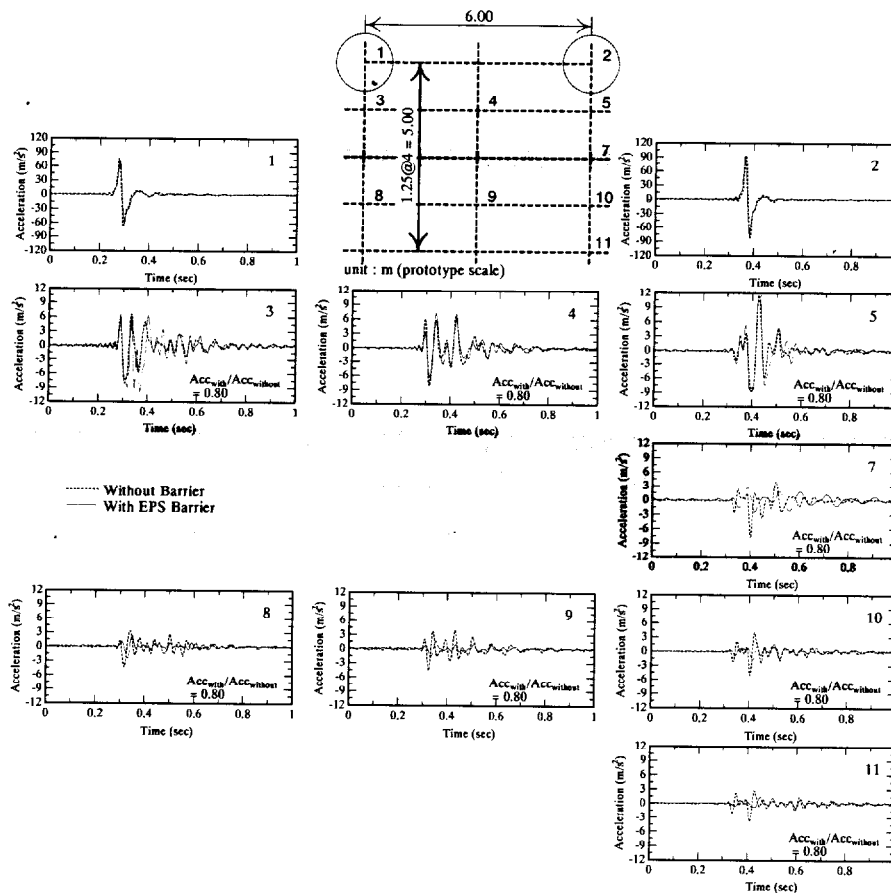
(b) Moving load speed of 260 km/h

Figure 4.56 Comparisons of the wave between with and without EPS barrier
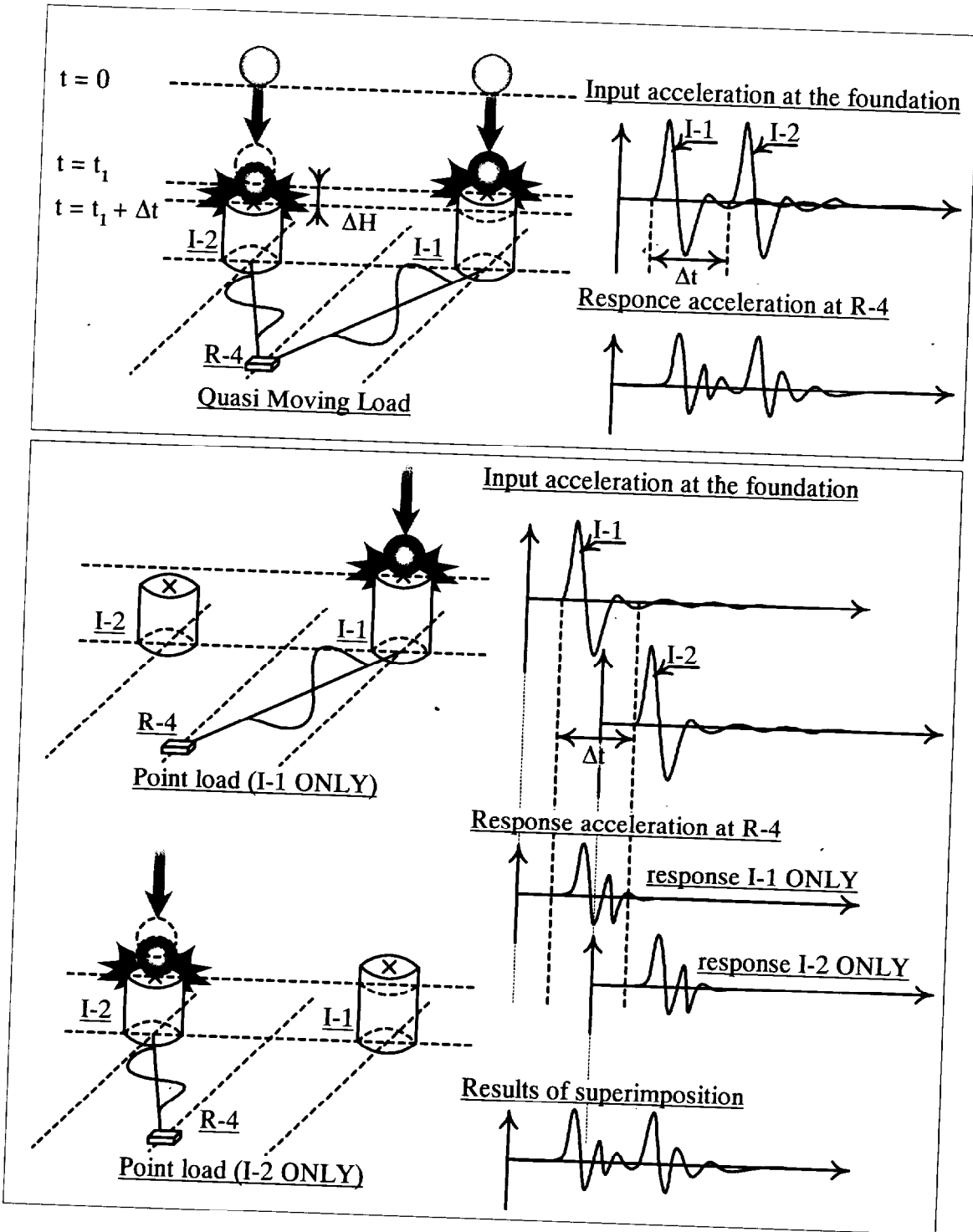
Figure 4.57 Experimental programs for verification of superposition of waves from difference sources

(a) No. 4 (D_r = 80 %)

(b) No. 6 (D_r = 80 %)

(c) No. 4 (D_r = 60 %)

(d) No. 6 (D_r = 60 %)
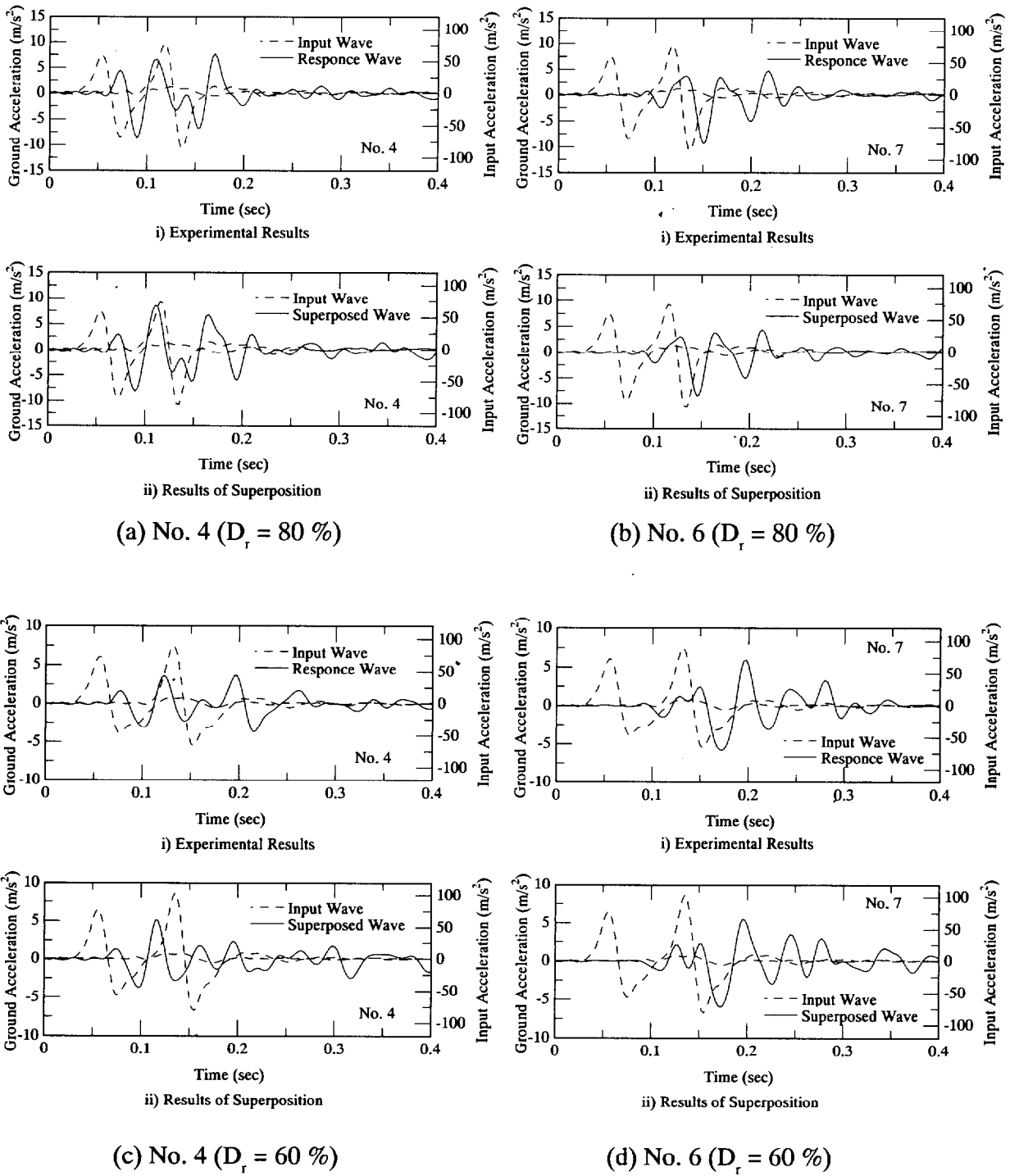
Figure 4.58 Comparisons of the waves between calculated results of superposition and experimental results
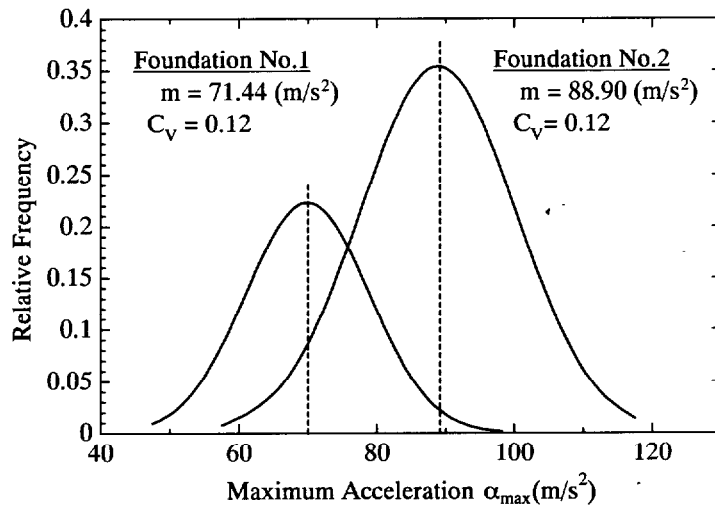
Figure 4.59 Distribution of relative frequency and maximum acceleration at Foundation No. 1 and No. 2
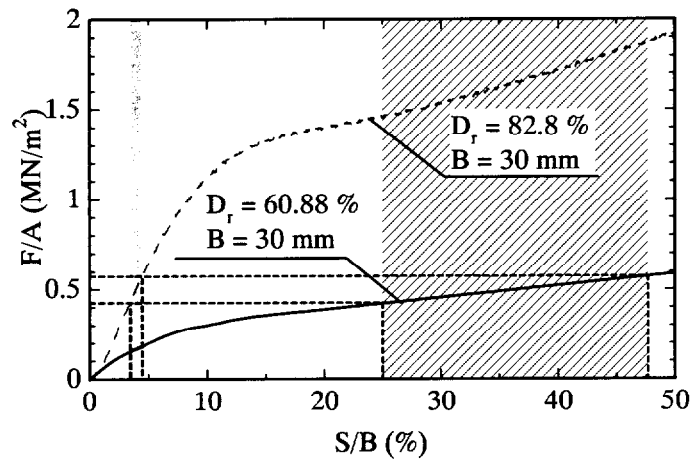
Figure 4.60 Range of bearing pressure at the model foundation in the cases of D_r = 80% and 60%

(a) No. 3 (without barrier)

(b) No. 6 (without barrier)

(c) No. 3 (with EPS barrier)

(d) No. 6 (with EPS barrier)
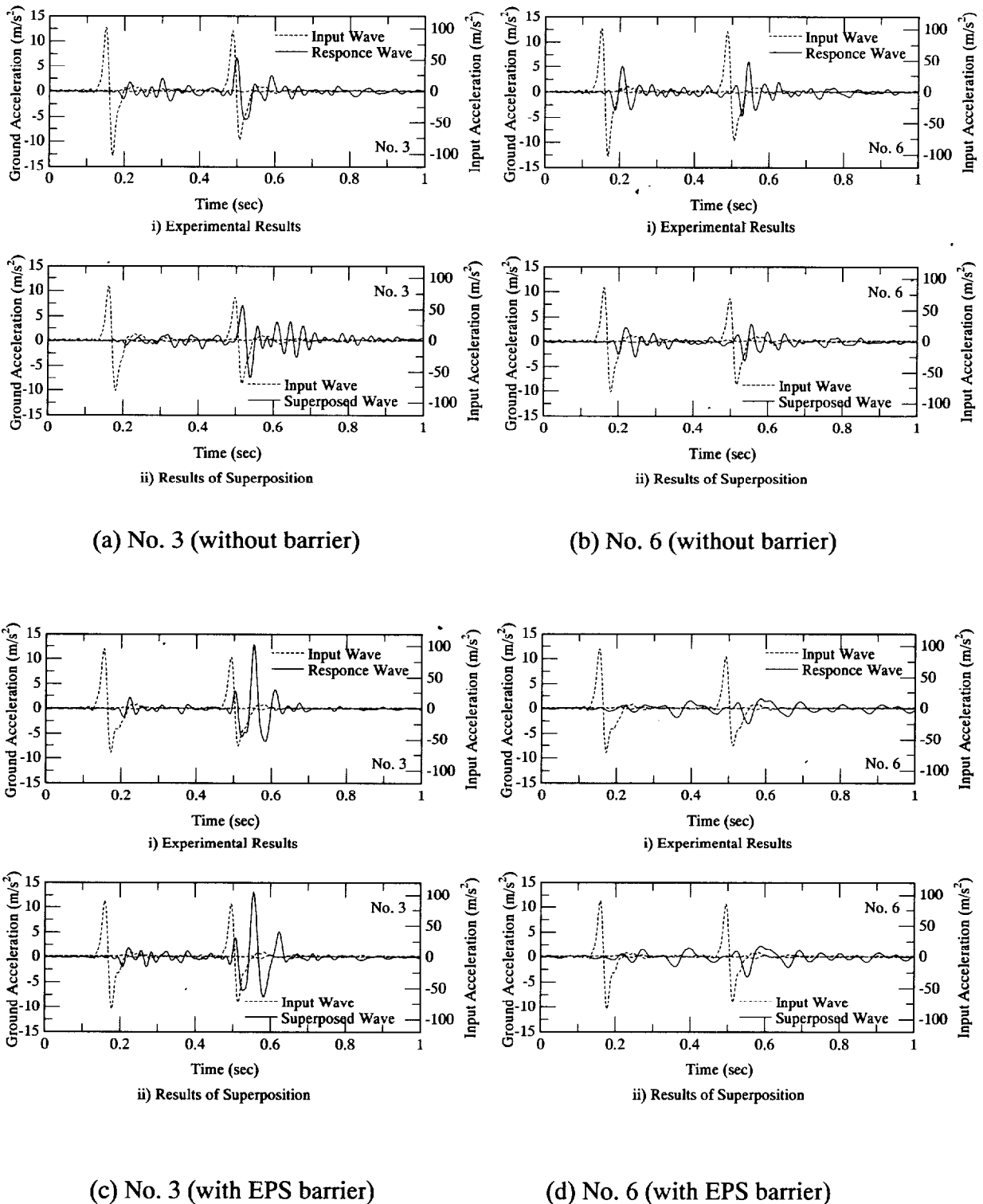
Figure 4.61 Comparisons of the waves between calculated results of superimposition and experimental results
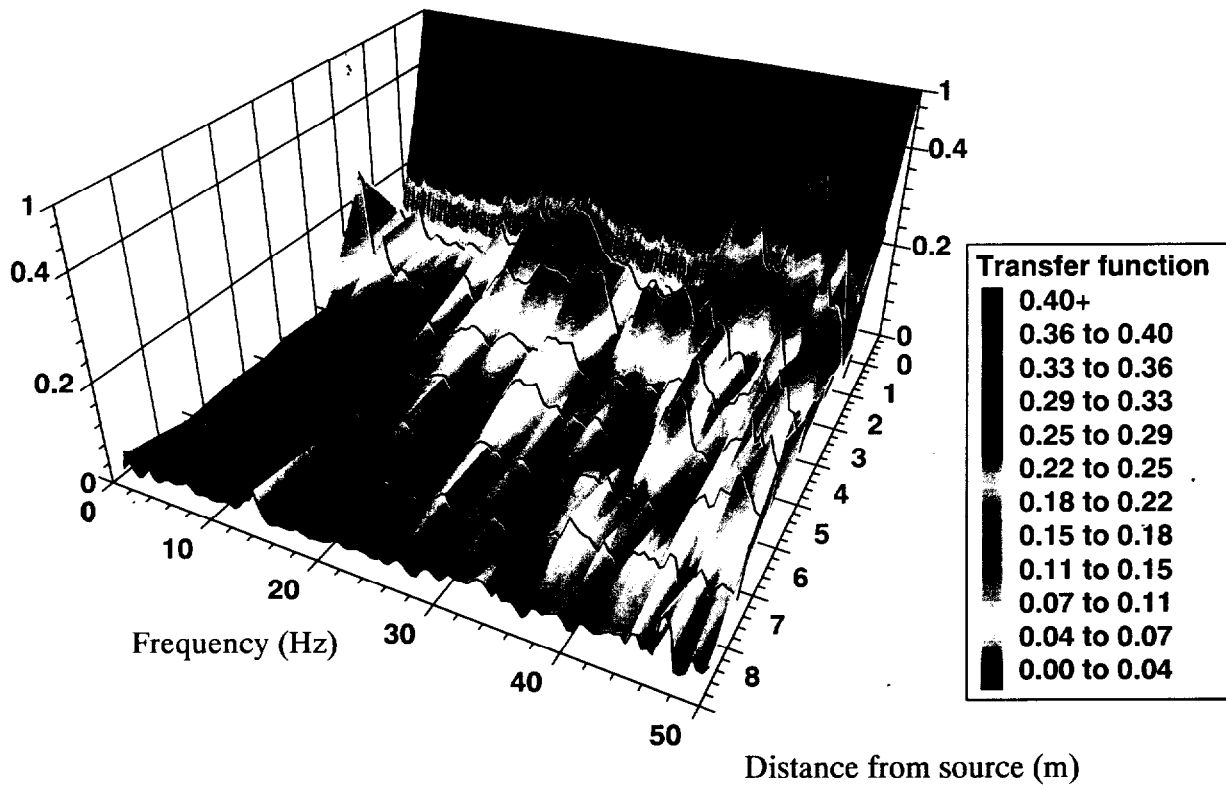
Figure 4.62 Transfer function H at multi-distance

(4) Prediction of the wave propagation

In this section the prediction of the wave propagation to construct a simplified but reasonable model for predicting the responses based on some empirical and theoretical results is described. Most of the prediction models are composed of several separable independent formulas, each of which serves as a control parameter and can affect, to a certain extent, the final response. A simple prediction model such as this can be used to provide tentative estimations when one cannot afford to conduct extensive individual measurements immediately. Yoshioka et al. (1980) originated a simple prediction method by a weight dropping experiment as follows;

$$O(\omega, P, j) \sim H(\omega, P, j) \cdot I(\omega, j) \qquad (4.10)$$

where,

$O(\omega, P, j)$ = the response acceleration spectra only by a j-th pier at the P point, $I(\omega, j)$ = the input acceleration spectra only by a j-th pier, $H(\omega, P, j)$ = the transfer function only by a j-th pier at the P point.

Time domain records of input and response acceleration are already known from this experiment. Our experiment can arrive at $H(\omega, P, j)$ by calculating the results of $O(\omega, P, j)$ and $I(\omega, j)$, as is seen in Figure 4.62. If the information of transfer function $H(\omega, P, j)$ at many positions is known, it is possible to extrapolate at the request distance from the source.

- 108 -

i) Experimental Results

ii) Results of Prediction
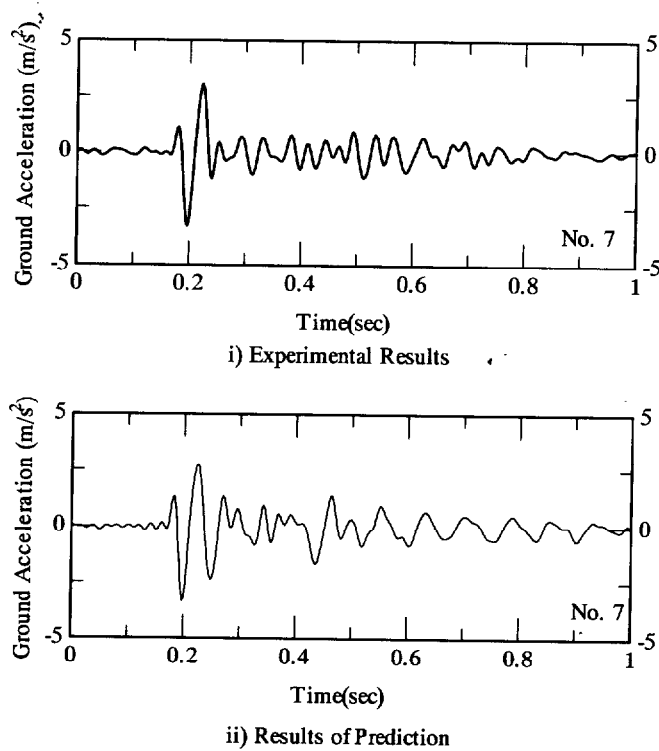
Figure 4.63 Comparison of ground acceleration between the results by the prediction method and the experiment results

As typical example, this study attempted predicting the response acceleration at the No. 7 location of the interval of viaduct of 6m (Case 2). The distances from two vibration sources to No. 7 location are 3.75 m and 7.08 m respectively. Assuming that the relationship between the transfer function value before and after the objective position shows the linear tendency, the transfer functions at these distances were obtained. Figure 4.63 shows the comparison between the results by the prediction method and the experiment results. The overall agreement between the experiment results and the prediction results is good, both in magnitude and shape of the wave. More sophisticated prediction methods than this method were proposed by many researchers (i. e. Lai et al. (2000) and Svinkin (2001) etc. Details of their researches have been reviewed above Chapter 2, already.). The information derived from this experiment is seen to be of use to verify the methods that many researchers have proposed.

4.3 Conclusions

In this chapter, the newly developed Multiple Ball Dropping System in the centrifuge was introduced for the purpose of investigating the simulation of wave propagation in various input point loads and effective countermeasure method to reduce the vibration at various locations. Details of the system were described. Performance of this system and centrifuge model test results on wave propagation in various input point load and some cases of its reduction method were described. The following conclusions are derived:

1. The Multiple Ball-Dropping System developed in this study provides a consistent and repeatable source of surface ground vibration. The system could simulate a moving load of velocity as fast as 350 km/h.

2. It was found that softer barriers are generally superior to stiffer barriers and the geometry of the barrier significantly affects the motion of the barrier. Softer hollow cylindrical barriers were effective when the embedded depth of barriers is more than 60 % of the wavelength.

3. For the CRMA foundation, the vibration as the source is as low as stiff foundation while at the same time, the vibration away from the source is just slightly higher than that for the very soft rubber foundation. If the aggregate of the CRMA is properly scaled, it is expected that the effect in vibration attenuation will be even better.

4. It was suggested that the superposition of the waves could be applicable to cases of moving load not only without barrier but also with EPS barrier, provided that the factor of safety for bearing capacity of foundation is sufficiently high. In addition, a comparison between experiment results with the simple prediction method proposed by Yoshioka et al. (1980) showed good agreement. The information presented in this paper is of use to verify similar prediction methods.

CHAPTER 5

WAVE PROPAGATION AND
ITS ISOLATION METHOD USING
CENTRIFUGAL VIBRATION TESTING SYSTEM

5.1 INTRODUCTION

This chapter describes the development of the Centrifugal Vibration Testing System, which can measure the input acceleration directly and generate cyclic loading for various frequencies on the ground surface. Details of the Centrifugal Vibration Testing System are described, and centrifuge model test results on wave propagation by various input frequencies are presented. In addition, various vibration countermeasures which apply at transmitting path and vibration source are examined.

5.2 DEVELOPMENT OF THE VIBRATION TESTING SYSTEM

5.2.1 System description

The Centrifugal Vibration Testing System was designed with the aims of

    1) Controlling the input frequency,

    2) Working loads are below an allowable level of bearing capacity,

    3) Measuring input acceleration, and

    4) The vertical amplification is dominate vibration over the horizontal one.

A general arrangement of the model is presented in Fig. 5.1, and details of this system are shown in Fig. 5.2. The source of the exciting supply was an electronic vibration testing machine (MEE15, Akashi, Co., Ltd., Fig. 5.3) in this study. Table 5.1 shows the specifications of MEE15. The mass of the machine is 1.0 kg, which is the lightest among other machines available. This exciter can supply frequency in the range from DC to 12000 Hz. When this system operates under 50 G acceleration, it is possible to generate the frequency of 240 Hz at prototype scale. In order to generate vertical vibration mainly, this exciter was supported by two linear bearings (M3318 (SUS), Nippon Thompson Co., Ltd) and one bearing. And the stiffness girders which supported two linear bearings were connected by the model container, as shown in Fig. 5.2. Figure 5.4 shows the view of the model foundation. The model foundation was made of an aluminium cylinder of 30 mm in diameter, 25 mm in height, and 41.42 g in mass, housing a built-in piezo-electric accelerometer (CBC107S, CBC Materials Co., Ltd.) in order to measure the input acceleration of vertical direction directly. Figure 5.5 shows the flowchart of how to generate the vibration in this system. At first, a function synthesizer (Multifunction Synthesizer 1940S, NF electronic instruments) modulated the input frequency. After that, the amplifier (AME50, Akashi, Co., Ltd, Fig. 5.6) controlled the
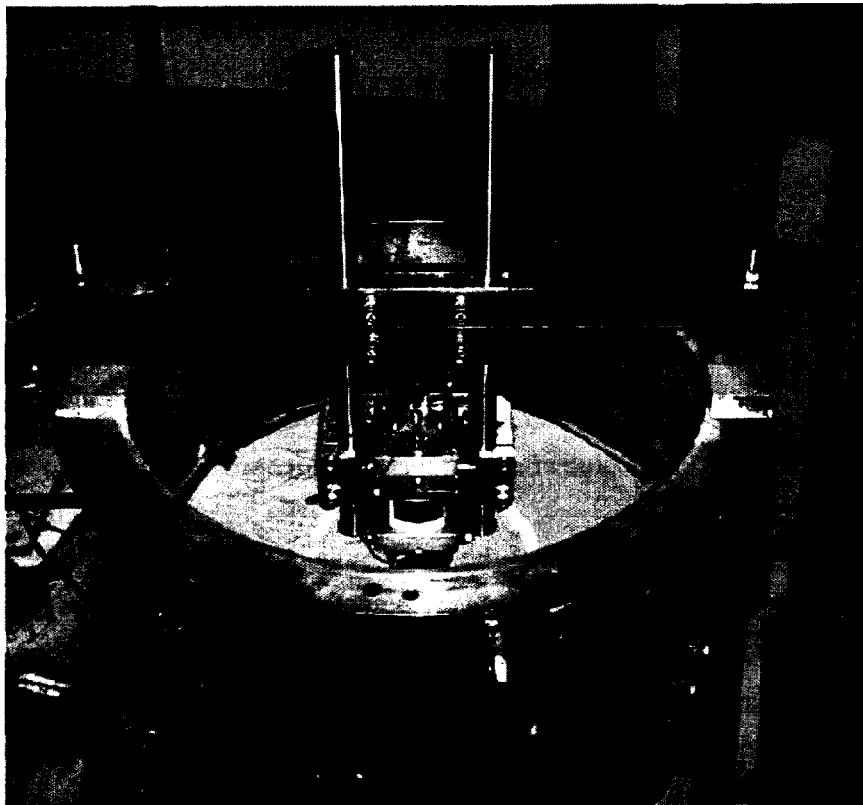
Figure 5.1 View of the Centrifugal Vibration Testing System
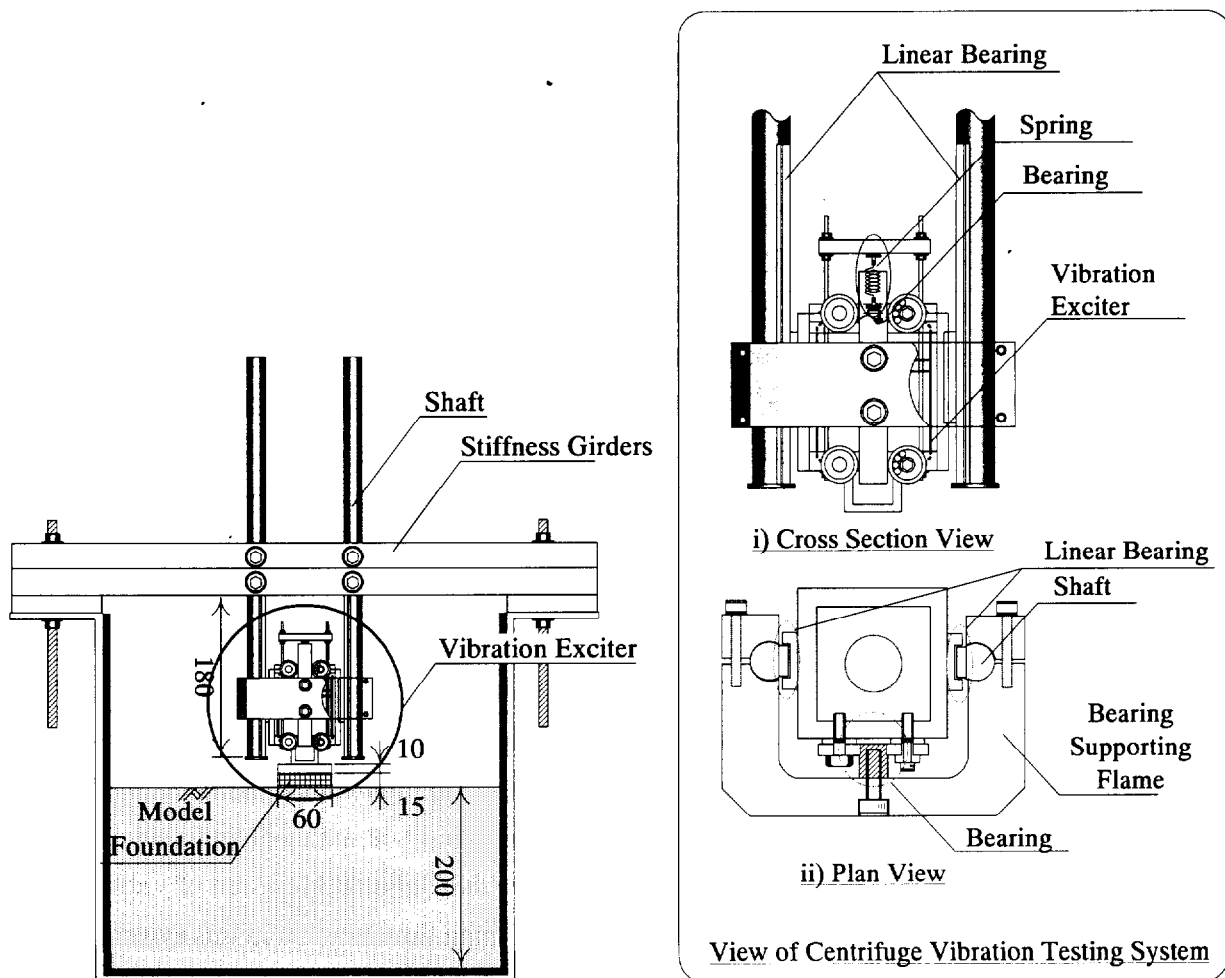

Figure 5.2 System of Centrifugal Vibration Testing System
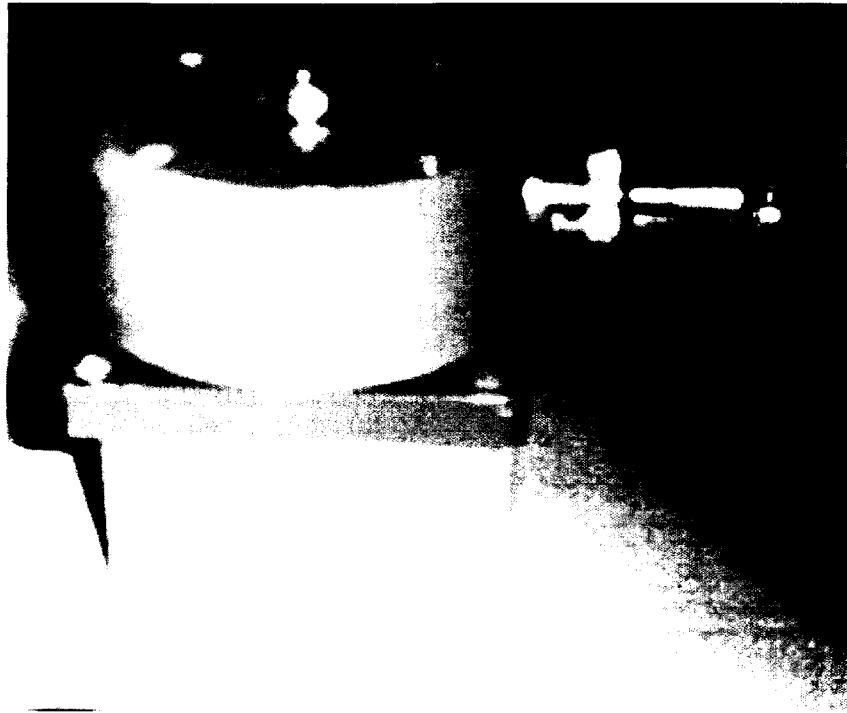
Figure 5.3 Vibration exciter MME15 (Akashi Co., Ltd)

Piezo-electronic
accelerometers

▨ : Vertical
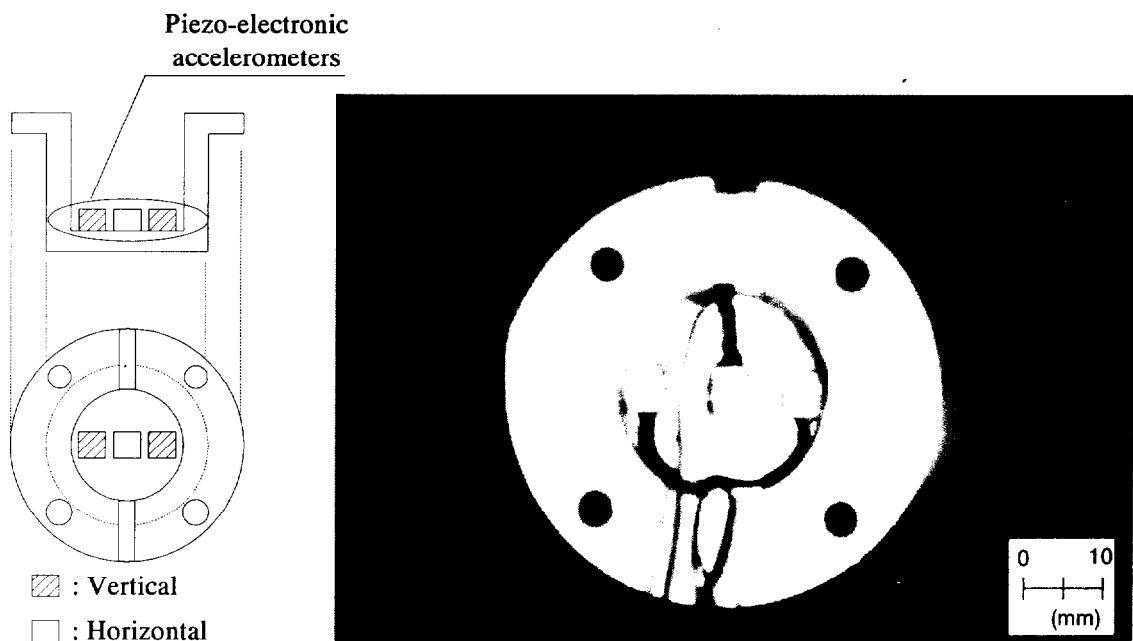☐ : Horizontal

0   10
(mm)

Figure 5.4 Model foundation (Establishment at the performance confirmation of Vibration
Testing System.)
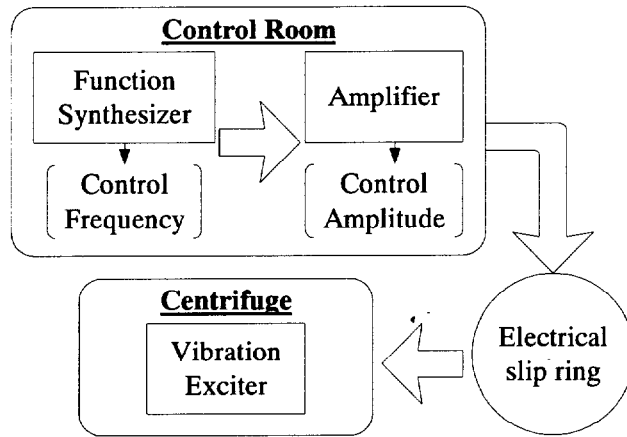
Figure 5.5 Vibration exciting system
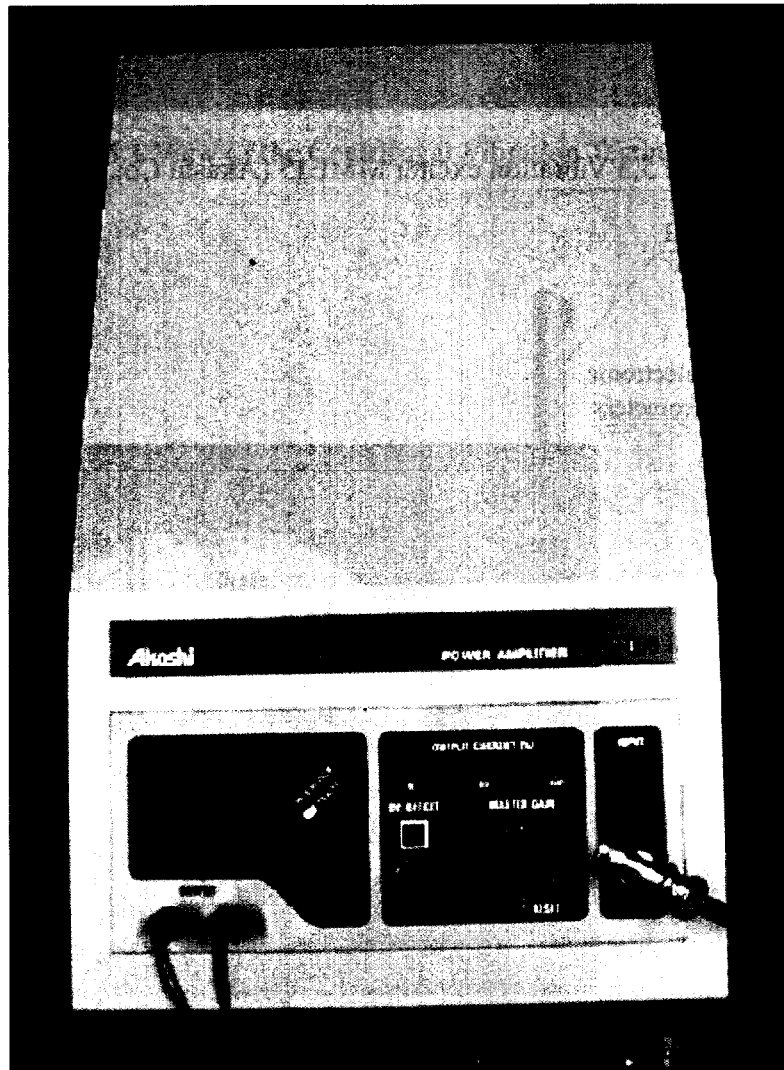
Figure 5.6 Amplifier (AME-050, Akashi Co., Ltd)

Table 5.1 Specifications of MEE15 and AME50

	Serial No.	MEE15
Vibration Testing	Rating vibration power (N_{peak})	9.8
	Maximum frequency (Hz)	12000
	Maximum acceleration (m/s^2)	653
	Maximum velocity (m/s)	1.27
	Rating displacement (mm_{p-p})	5
	Movable part equivalent mass (kg)	0.015
	Movable part supporting spring constant (N/mm)	1.47
	Dimensions (mm)	φ 60 × 80H
	Mass (kg)	1
Amplifier	Serial No.	AEE50
	Maximum voltage output (VA)	50
	Range of frequency (Hz)	DC to 15000
	Dimensions (mm)	230W × 400D × 87H
	Mass (kg)	3
	External power supply (VA)	83

magnitude of output voltage. These amplitude and frequency excited the vibration machine through the slip ring. The performance of this system was confirmed by some proof tests described in the next section.

5.2.2 Performance of the Vibration Testing System

In order to confirm the performance of this system, some proof tests were carried out under the 50 G acceleration. Input frequencies were 5, 10, 15, 20, 25, 30 and 40 Hz at prototype scale, respectively. In the proof test, three piezo-electric accelerometers were housed into the model foundation to measure horizontal and vertical accelerations as shown in Fig. 5.4. Figure 5.7 shows the frequency content of the horizontal and vertical accelerations in each input frequency. It is observed that the dominating frequency of response acceleration has a close relation to the input frequency. FFT result in the case of input frequencies of 5, 15 and 25 Hz tended to amplify not only input frequency but also the multiple of input frequency. Especially, in the case of 15 Hz, the result of spectrum at 75Hz which is three times input frequency, 15 Hz, amplified more than the result of 15Hz. As for the Fourier spectrum in the input frequency, vertical spectrum was compared with horizontal one. Figure 5.8 shows the comparisons of the maximum Fourier spectrum between horizontal and vertical amplitude in each input frequency. Except for the case of 25 Hz, Fourier spectrum in the vertical direction is larger than that of horizontal direction by over three times. From the result of this test, the performance of this system, which was intended to dominate the vertical movement over the horizontal movement, became clear.
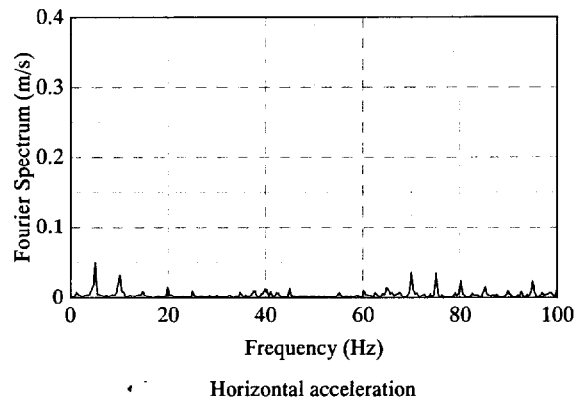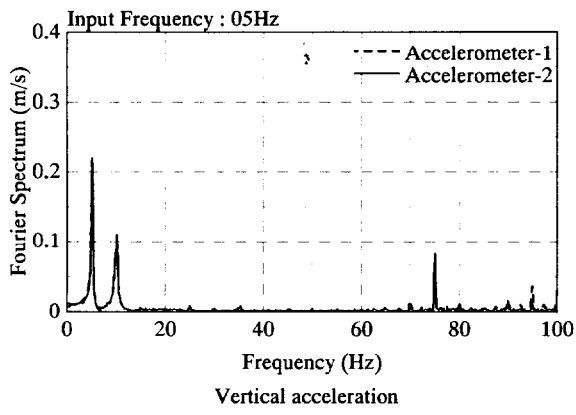
(i) 5Hz
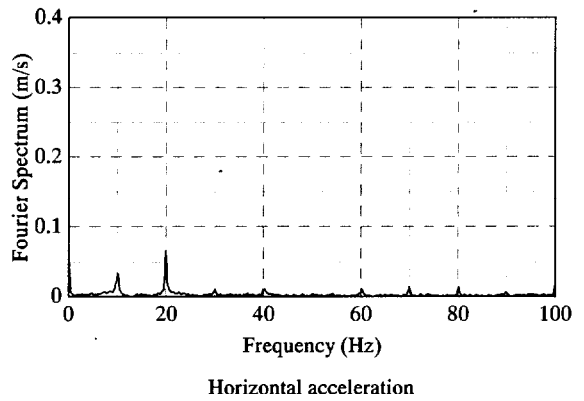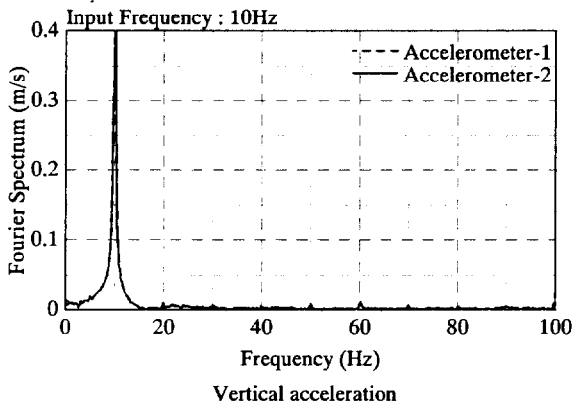
(ii) 10Hz
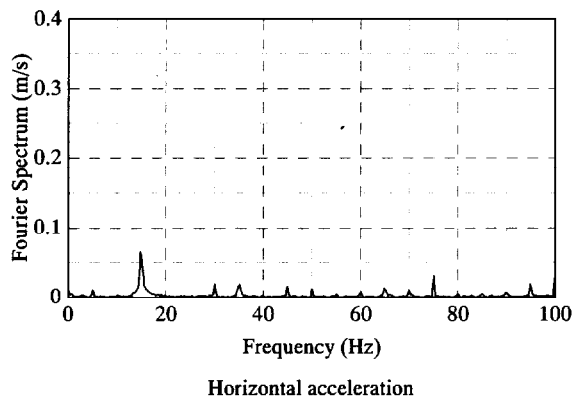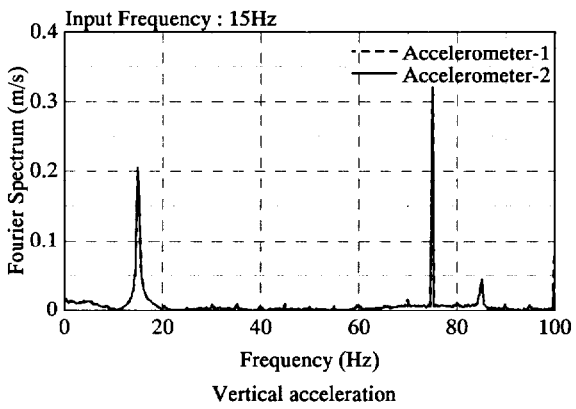
(iii) 15Hz
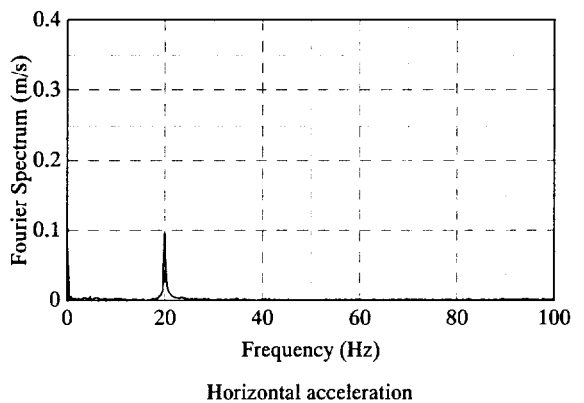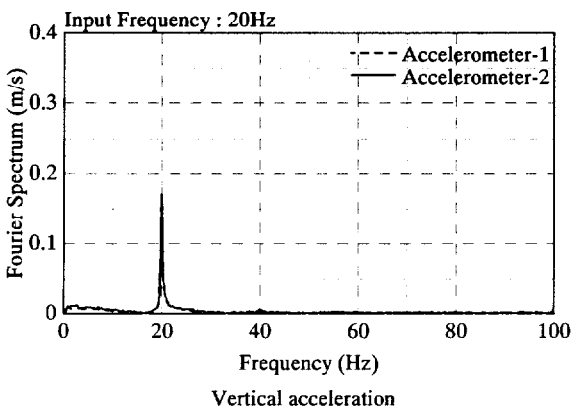
(iv) 20Hz
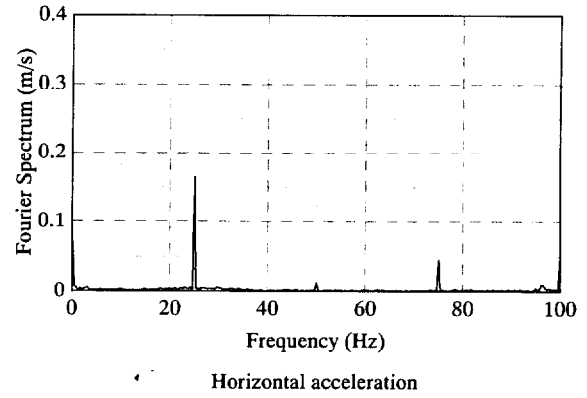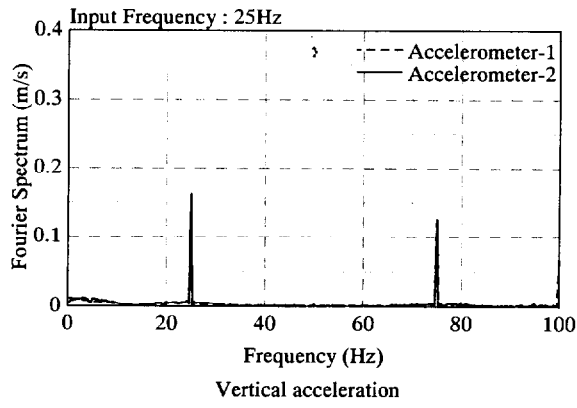
(v) 25Hz
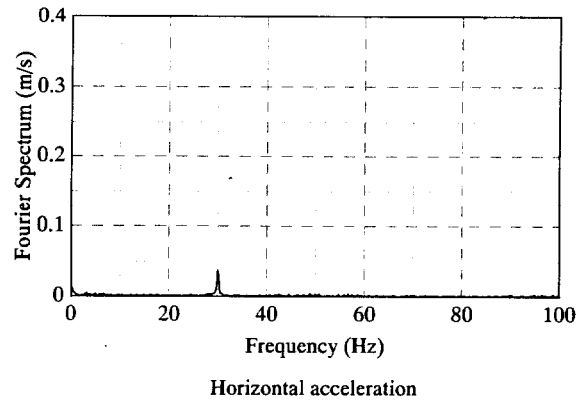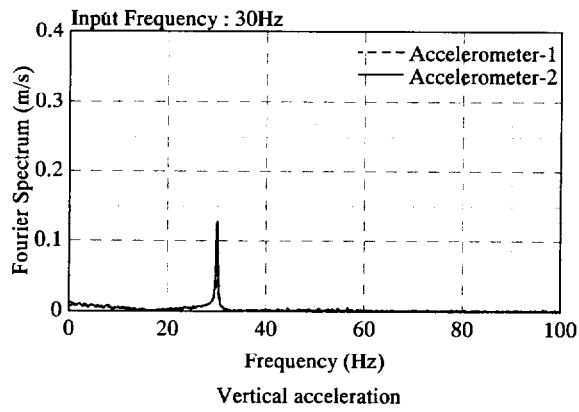
(vi) 30Hz
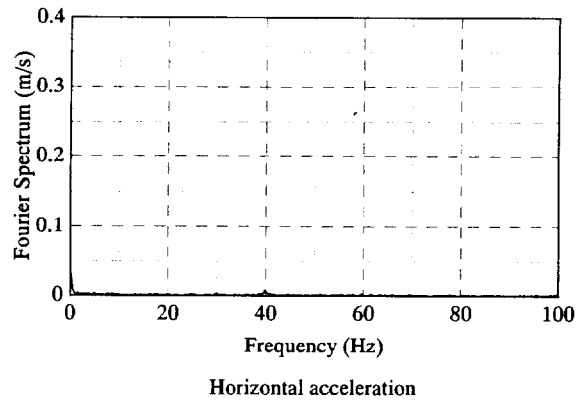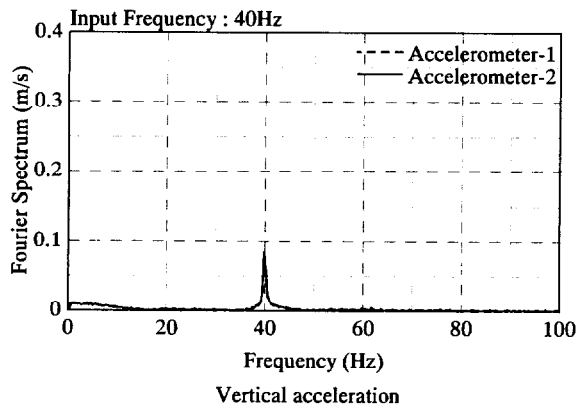
(vii) 40Hz

Figure 5.7 Frequency contents of the inputted vertical and horizontal acceleration
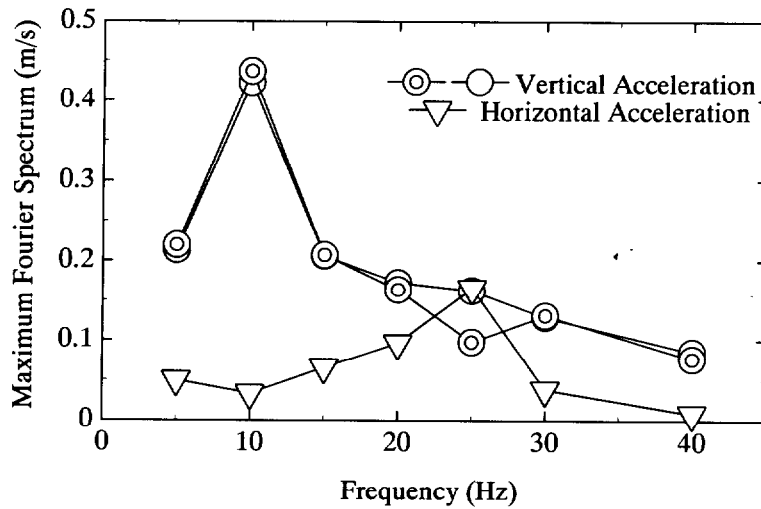
Figure 5.8 Comparisons of the maximum Fourier spectrum between horizontal and vertical movement

5.3 TEST PROCEDURES

The soil used was air-dried Toyoura sand. The sand was poured from a certain height for consistent production of uniform deposit with an average dry unit weight γ_d of 15.4 kN/m³, and a targeted relative density of 80%. In this series of the test, thickness of layer was 200mm in model scale (10m in prototype scale). Thus this experiment setup takes a different thickness of layer compared to the experiment setup using the multiple ball-dropping system, of which depth of the sand layer is 17 m in prototype scale. The ground surface was leveled by vacuuming. This study examined the effect of CRMA at trackbed and EPS wave barrier at transmission path on the reduction of vibration. In the field, a railway road consists of track beds (including tie) and roadbed, as shown in Fig. 5.9 (the same as Figure 4.36). The high-speed train wheels rolling on the rails create vibration energy transmitted through the track support system into the track bed and roadbed. The experimental concept of vibration source is shown in Fig. 5.10(a). All the experimental programs in this chapter are listed in Table 5.2.

The motions of the ground were recorded by the piezo-electric accelerometers (CBC111BW, CBC Material Co., Ltd.) which provided data on the vertical accelerations at the ground surface, as shown in Fig. 5.10(b). In addition, the vertical movement of the foundation exciter was recorded by the piezo-electric accelerometers (CBC107S, CBC Material Co., Ltd.). Input frequencies are 5, 10, 15, 20, 25, 30, 35, and 40 Hz at prototype scale (250, 500, 750, 1000, 1250, 1500, 1750, 2000 Hz at model scale), respectively.

All the tests were carried out under the 50 G acceleration. All the results are presented at prototype scale, hereafter.
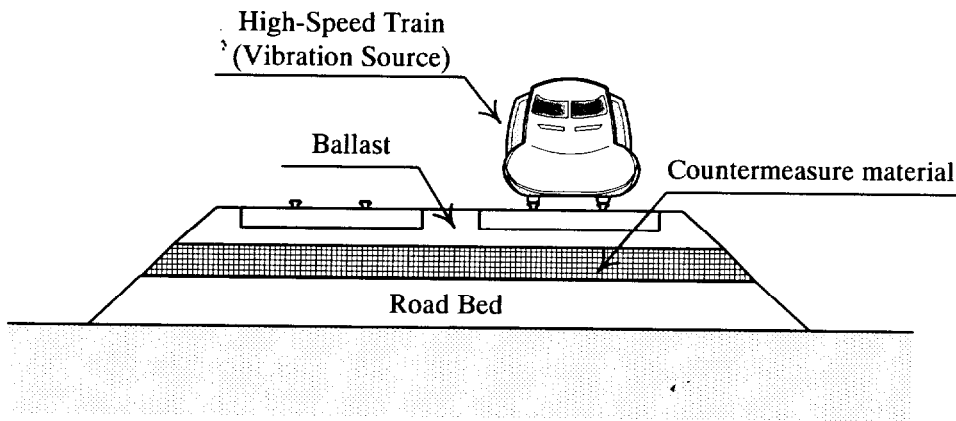
Figure 5.9 Cross section of a typical railway road (the same as Fig. 4.36)
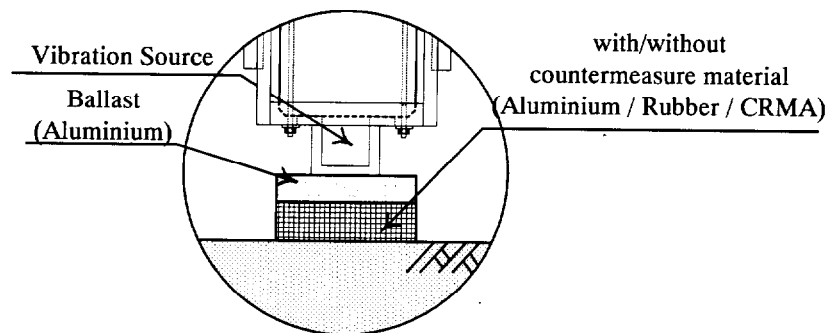
(a) Model of a railway track structure
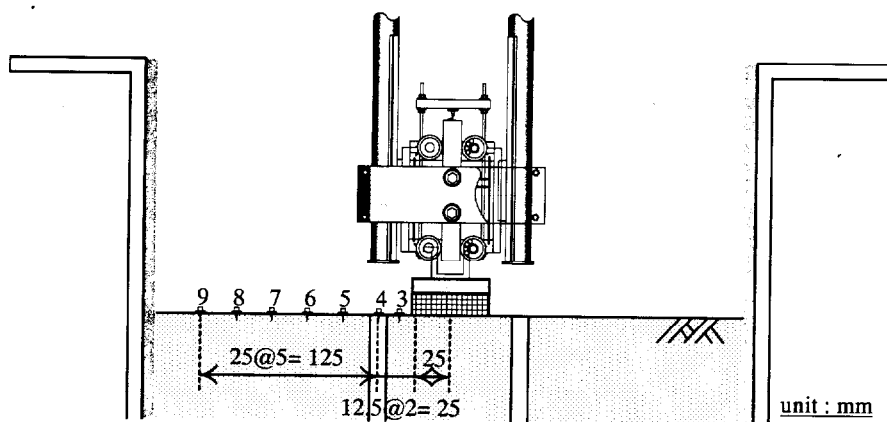
(b) Location of accelerometers

Figure 5.10 Layout of measurement system and detail of this model

5.4 TEST RESULTS AND DISCUSSIONS

5.4.1 Effect of the sponge rubber gluing the sidewalls and the bottom of the container on the reduction of the reflection waves

As for the effect of the sponge rubber gluing the sidewalls and the bottom of the container on the reduction of the refection waves, Fig. 5.11 shows the time histories and FFT results in the case with (SH-35) and without (SH-33) a sheet of sponge rubber which is glued to the sidewalls and the bottom of the container for location No. 2, 4, and 8 in each input frequency. No. 2, 4 and 8 are the locations on the vibration source, near the vibration source and near the sidewalls, respectively. As

-119-

Table 5.2 Experimental programs in this chapter

Test case	Countermeasures at transmitting path			Countermeasures at vibration source	With / without sponge rubber gluing the sidewalls and bottom of the container	comment
	Material	Embedded depth D (m)	Radius of cylindrical barrier R (m)			
SH-1~9	-	-	-	Aluminium	O	Preliminary test
SH-10~16	-	-	-	Aluminium	O	Proof test
SH-31	-	-	-	Aluminium	O	
SH-35	-	-	-	Aluminium	O	
SH-33	-	-	-	Aluminium	X	
SH-18	Aluminium	5.0	2.5	Aluminium	O	
SH-17	Aluminium	10.0	2.5	Aluminium	O	
SH-24	EPS	2.5	2.5	Aluminium	O	
SH-19	EPS	5.0	2.5	Aluminium	O	
SH-20	EPS	10.0	2.5	Aluminium	O	
SH-30	EPS	2.5	2.5	Aluminium	O	
SH-29	EPS	5.0	5.0	Aluminium	O	
SH-26	EPS	10.0	5.0	Aluminium	O	
SH-36	-	-	-	CRMA-(1/5)	O	
SH-37	-	-	-	Rubber	O	
SH-38	EPS	10.0	5.0	Aluminium	O	
SH-39	EPS	10.0	5.0	CRMA-(1/5)	O	
SH-40	EPS	10.0	5.0	Rubber	O	

far as the behavior at vibration source (Location No. 2) is concerned, both cases with and without a sheet of sponge rubber are satisfied with the request of this research, which means that input frequency is dominated, except for the case of input frequency of 5 Hz. On the other hand, each ground motion essentially shows that the response acceleration with a sheet of sponge rubber is different from that without it. From the standpoint of ground movement, the result without a sheet of sponge rubber reveals that there is larger amplitude (spectrum) than the result with sponge rubber and there are dominating frequencies which generate not only input frequency but also higher frequencies than input frequencies. In contrast, as to the case with a sheet of sponge rubber, the spectrum has a tendency to dominate the only input frequency, with a single exception of input frequency of 20Hz. Figure 5.12 shows how the Fourier spectrum in the input frequency decreases with distance from vibration source with and without a sheet of rubber sponge. The case without a sheet of sponge rubber gluing the side walls and the bottom of the container seems to be complicated unevenness decay line because of the refection wave from the side walls. In spite of qualitative judgment, it is clear from the reason mentioned earlier that a sheet of sponge rubber reduces the reflection wave from the sidewalls and the bottom of container.
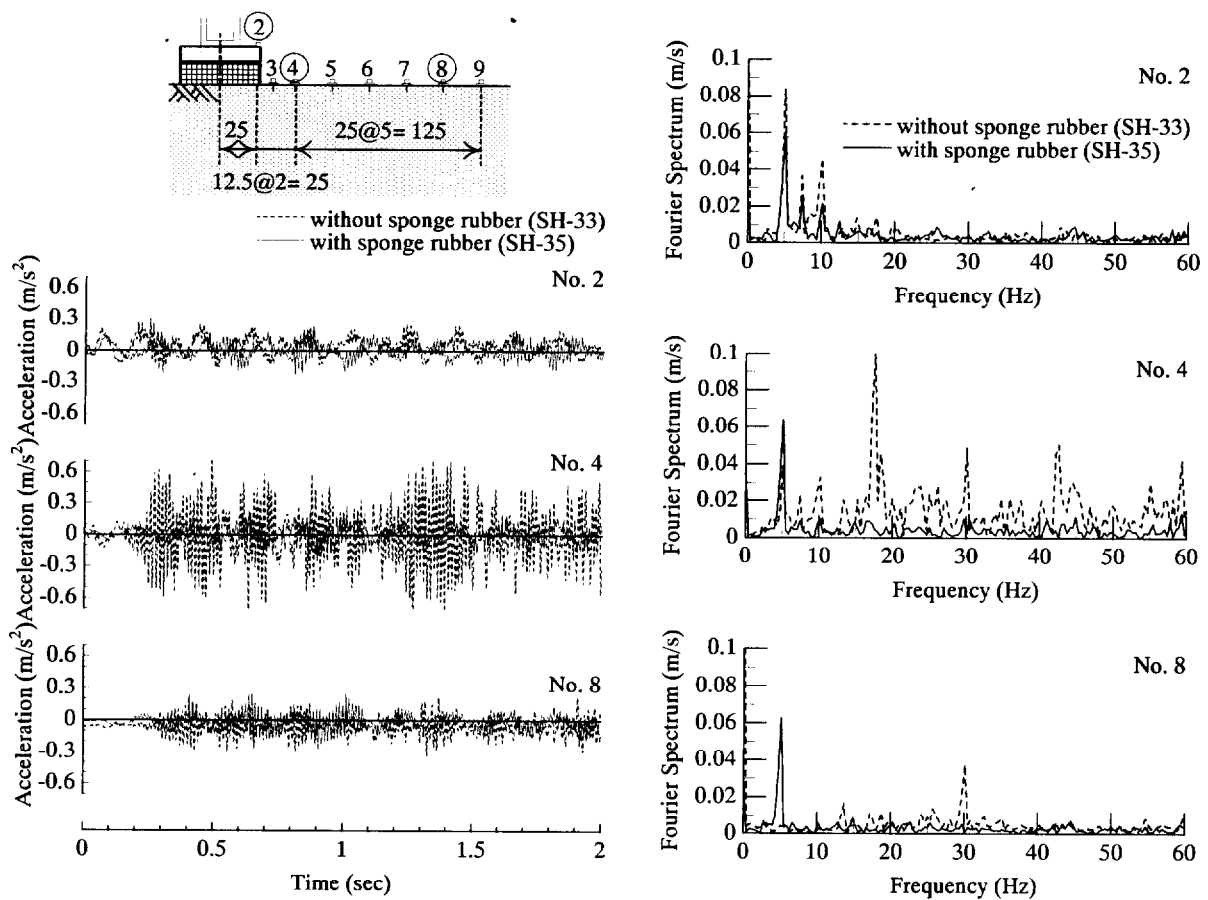
(i) 5 Hz
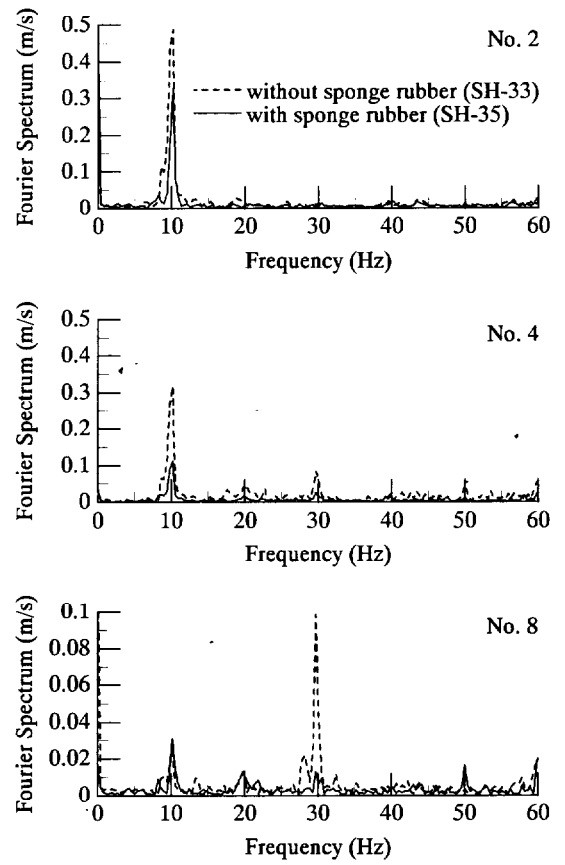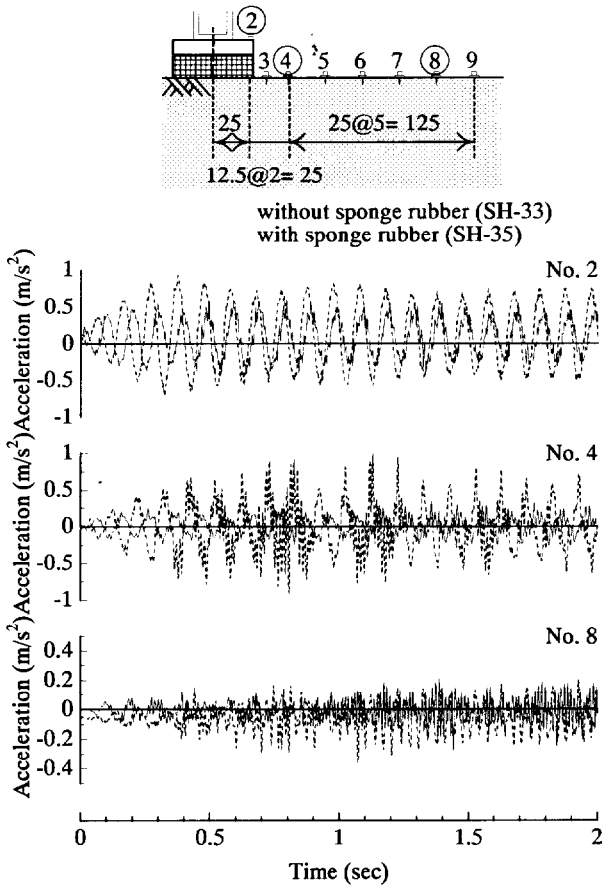
(ii) 10 Hz
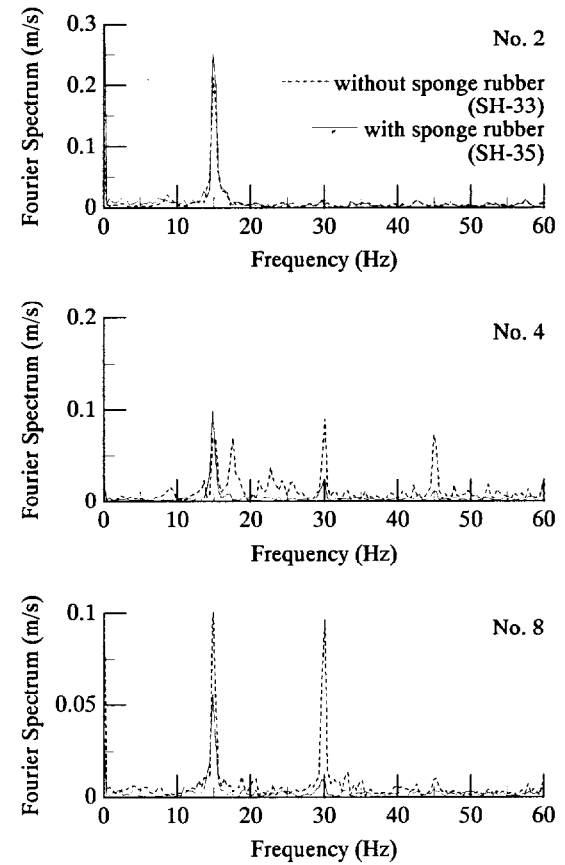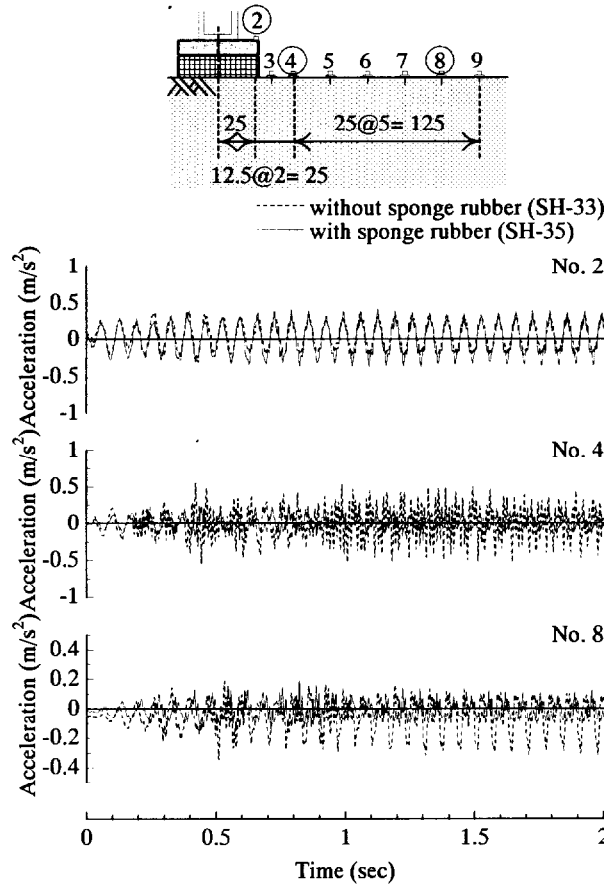
(iii) 15 Hz
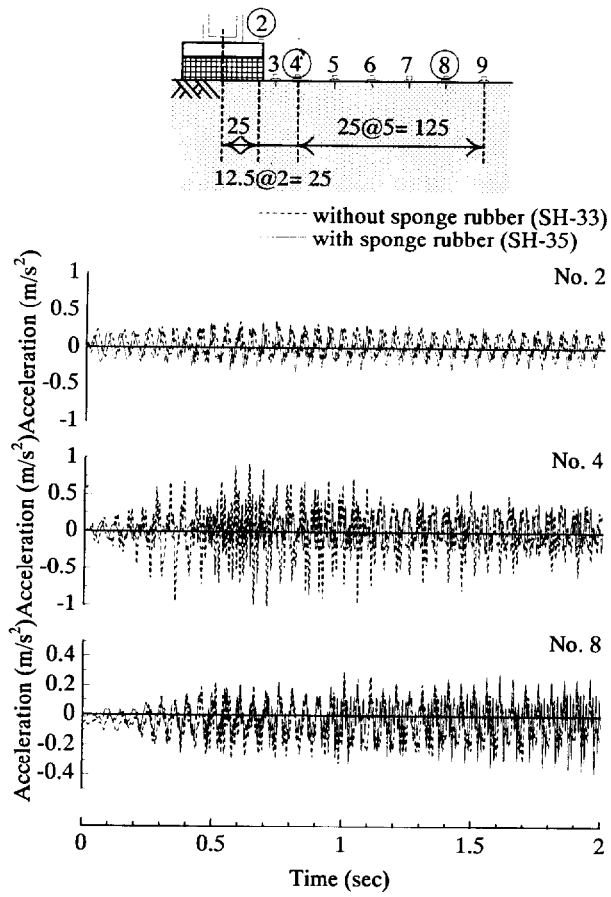
(iv) 20 Hz
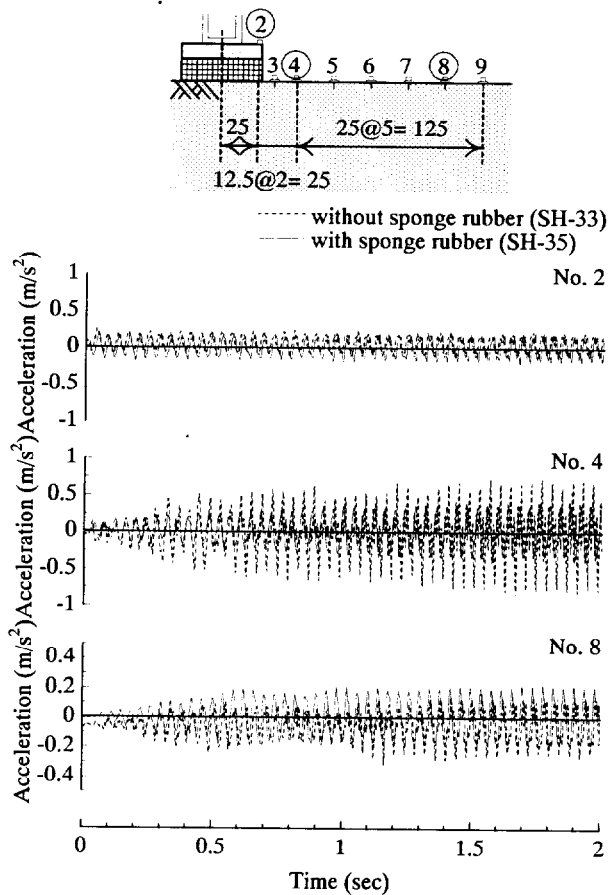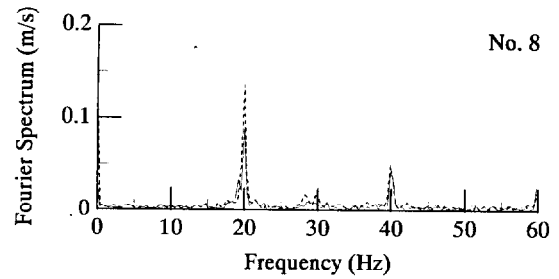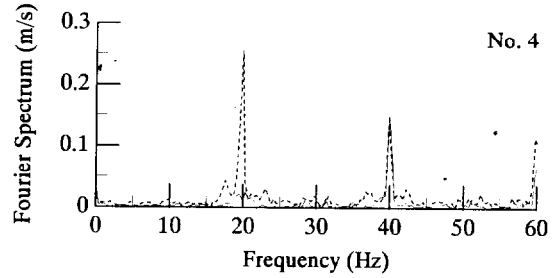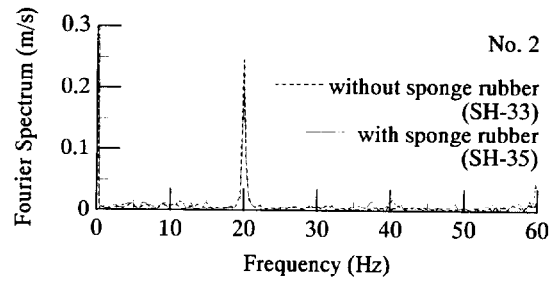
(v) 25 Hz
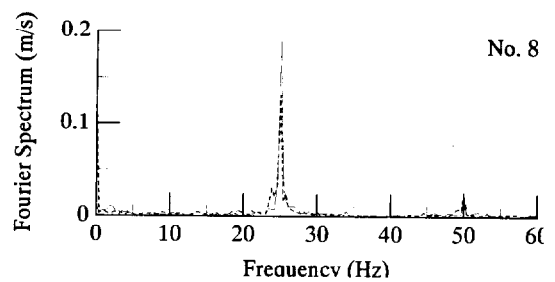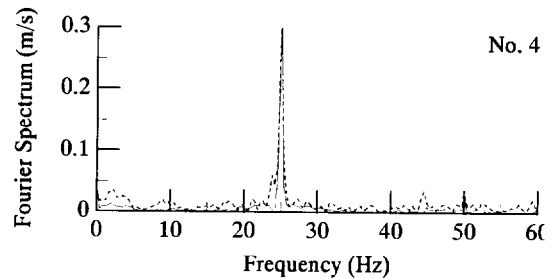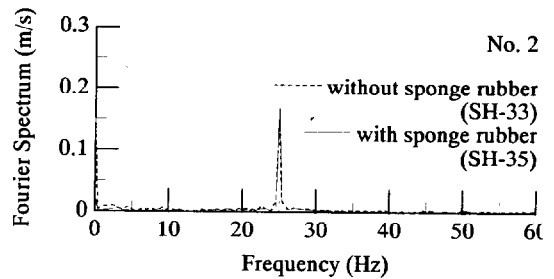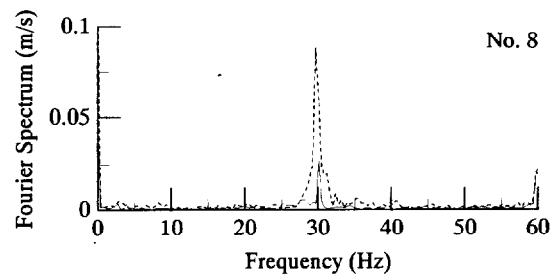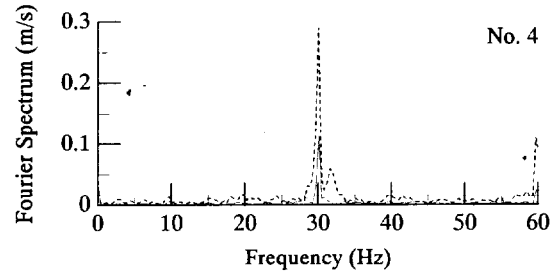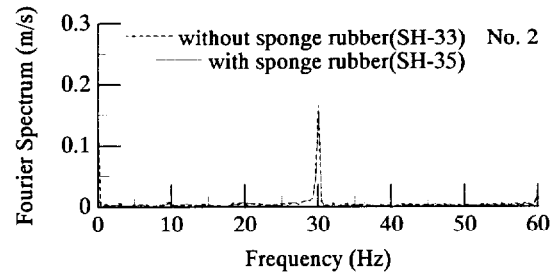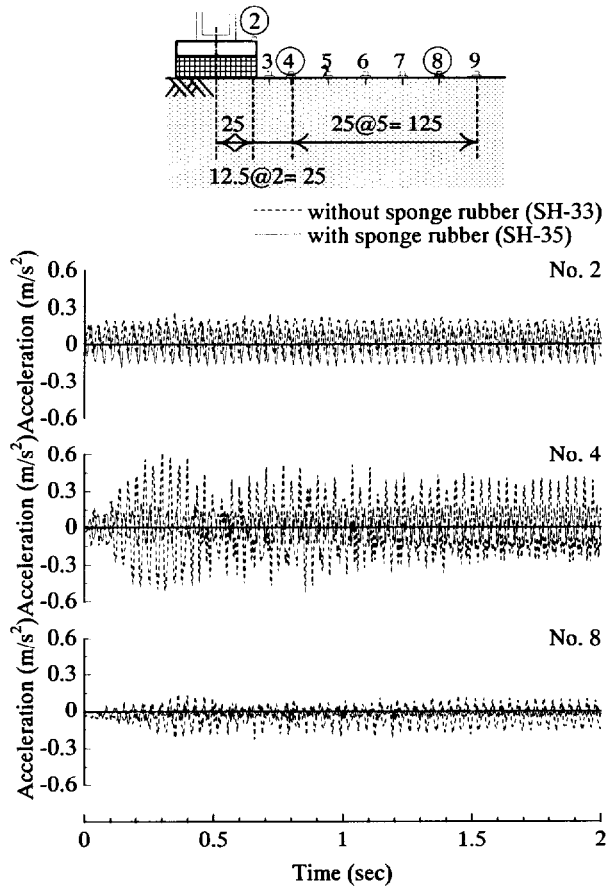
(vi) 30 Hz
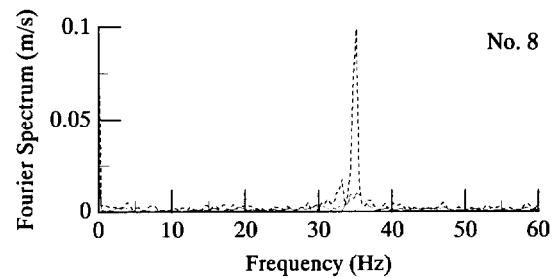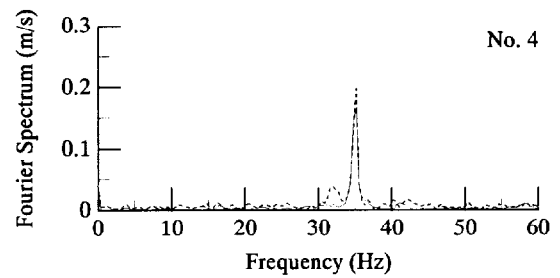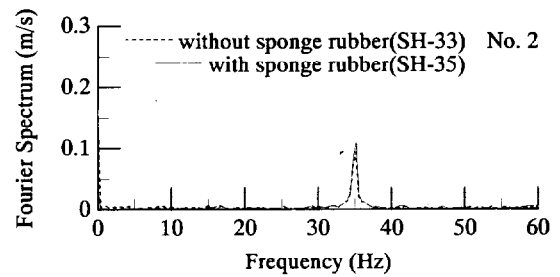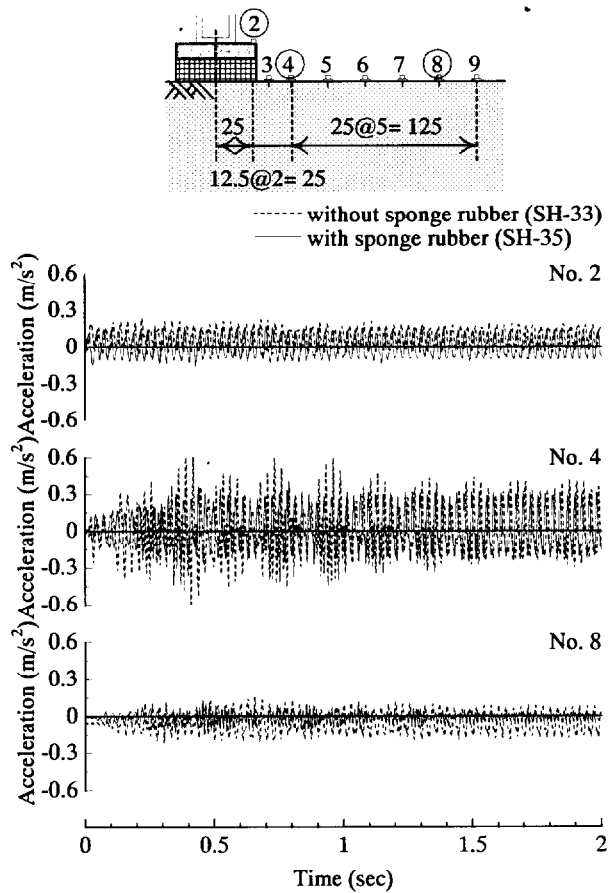
(vii) 35 Hz
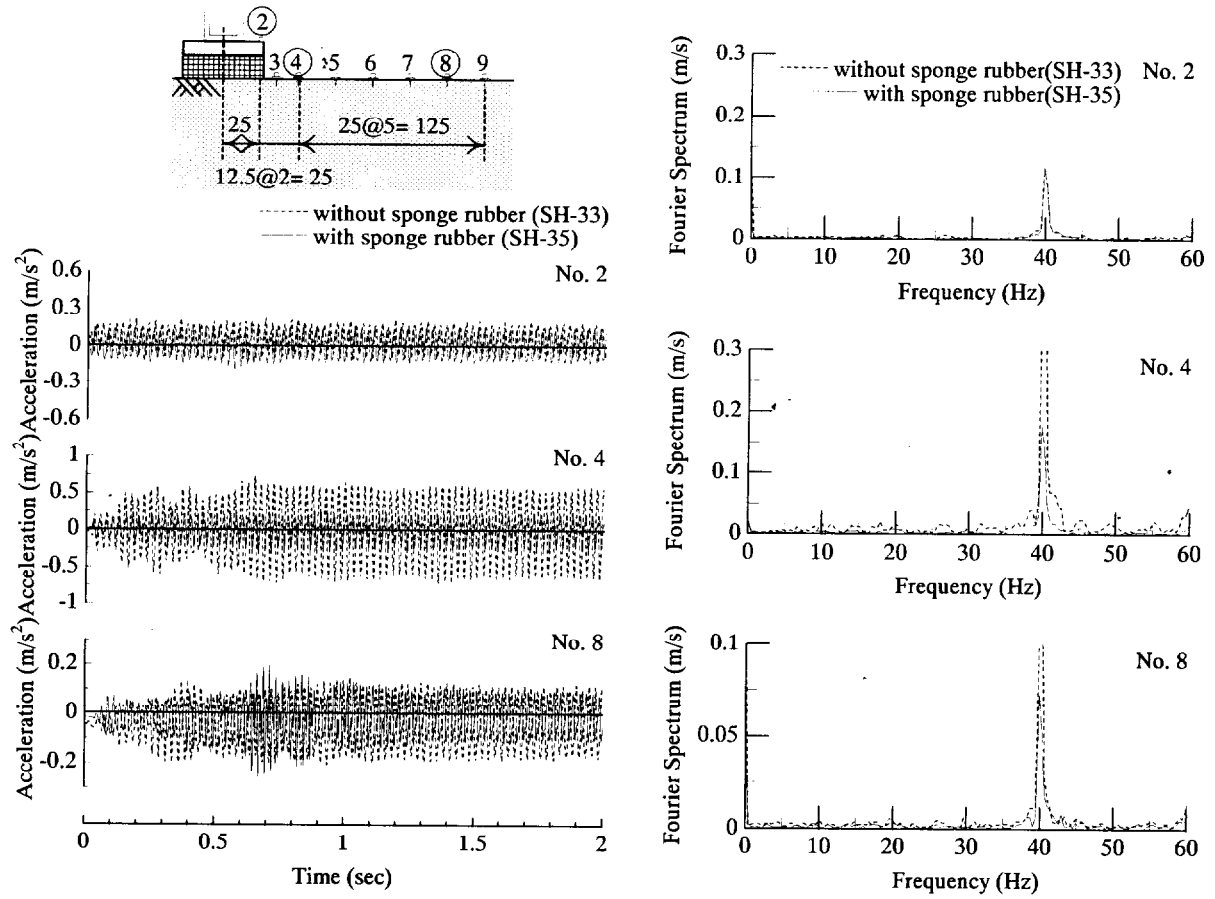
(iix) 40 Hz

Figure 5.11 Time histories and FFT results in the case with and without a sheet of sponge rubber which was glued to the sidewalls and the bottom of the container
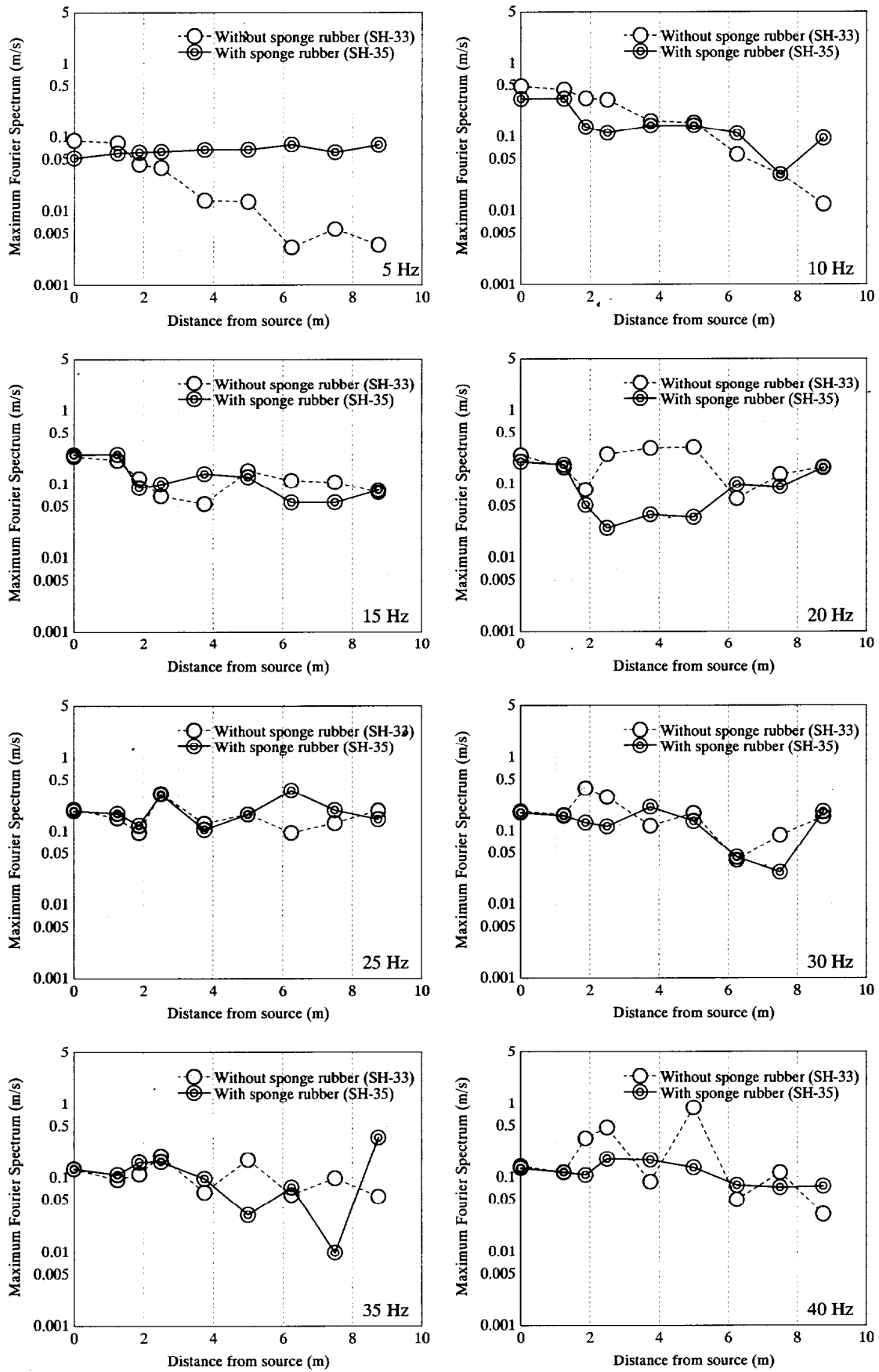
Figure 5.12 Attenuation of the maximum Fourier spectrum in the inputted frequency with distance from source with and without sponge rubber gluing the bottom and the sidewalls of container

5.4.2 Characteristics of wave propagation

Figure 5.13 shows the time histories and FFT results at all the locations in the case of each input frequency, respectively. The tests under the same condition test were repeated twice to check the repeatability (SH-31 and SH-35). The wave forms in both cases seem to noisy due to inclusion the action of high frequencies. Most FFT results show the same amplitude and frequency, while the case of SH-31 at No.6 and the case of SH-35 at No. 9 observe the dominating frequencies not only at input frequency but also at 45 Hz. The cause of generated dominating frequency of 45 Hz is a piezo-electronic accelerometer breakdown. The identical accelerometer (Serial No. 2028) set up on No. 6 in the case of SH-31 and on No. 9 in the case of SH-35, respectively. Figure 5.14 shows attenuation of the root-mean-square acceleration with distance from vibration source observed in the case of SH-31 and of SH-35, except the result of the malfunctioned accelerometer. The root-mean-square acceleration, A_{RMS}, is given by

$$A_{RMS} = \sqrt{\frac{1}{T}\int_0^T a^2(t)\,dt} \qquad\qquad\qquad\qquad\qquad\qquad\qquad (5.1)$$

where $a(t)$ = acceleration time history at time t, T = the number of data. The root-mean-square refers to the most common mathematical method of defining the effective magnitude. For a sine curve, the root-mean-square value is 0.707 times the peak value, or 0.354 times the peak-to-peak value.

These figures show the theoretical attenuation line predicted by Eq. (2.2) (Bornitz, 1931) alongside the experimental data. The solid black line represented attenuation of surface wave (n = 0.5), and the dashed and single-dotted gray line represented attenuation of body wave (n = 2). These figures show some interesting associations that the theoretical attenuation line represented of surface wave fit each experimental data. It appears that the major tremor at the ground surface is the type of surface wave

Travel time is calculated by the phase angle, which can be obtained by transforming acceleration into the frequency domain by using FFT. Figure 5.15 shows the calculated results, together with the theoretical travel curve which is shown in the black thick solid line. Plotted results by travel time curve from the experiment vary widely, because the precision of phase angle is rough. However, their results exist around the theoretical curve.

5.4.3 Effect of cylindrical barrier on the reduction of vibration

This section examines the effect of cylindrical barrier on the reduction of vibration using various barrier conditions. The experimental conditions in this section are listed in Table 5.3. Embedded depth of barrier D and wave impedance A are considered. The stiffer material (A>1; stiffer barrier) used was aluminium. And the softer material (A<1; softer barrier) used was Expanded Poly-Styrol (EPS). As for material of barrier, Acryl was not selected in this chapter because inefficient results in
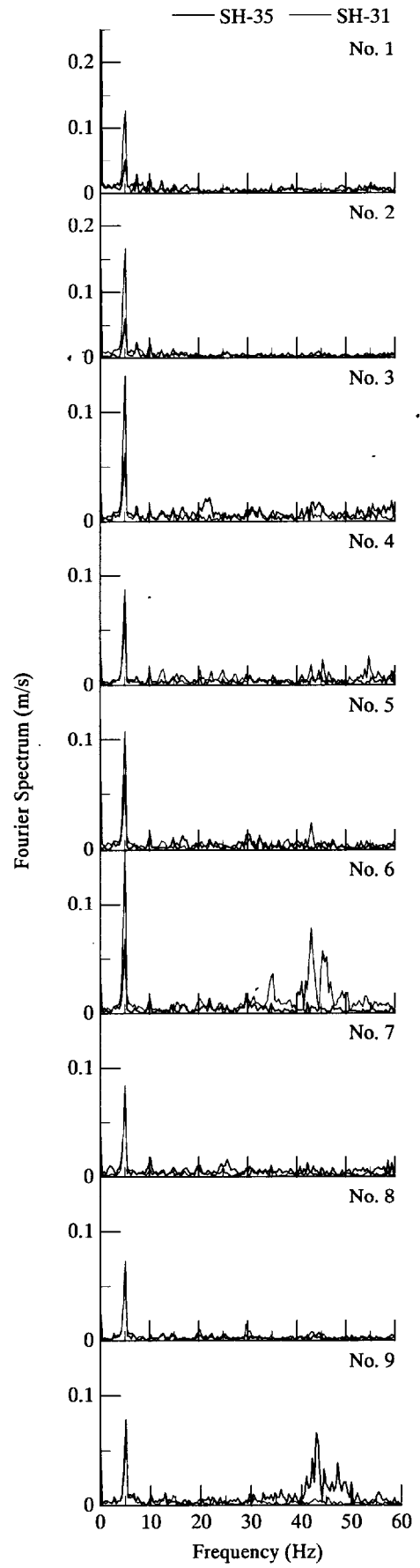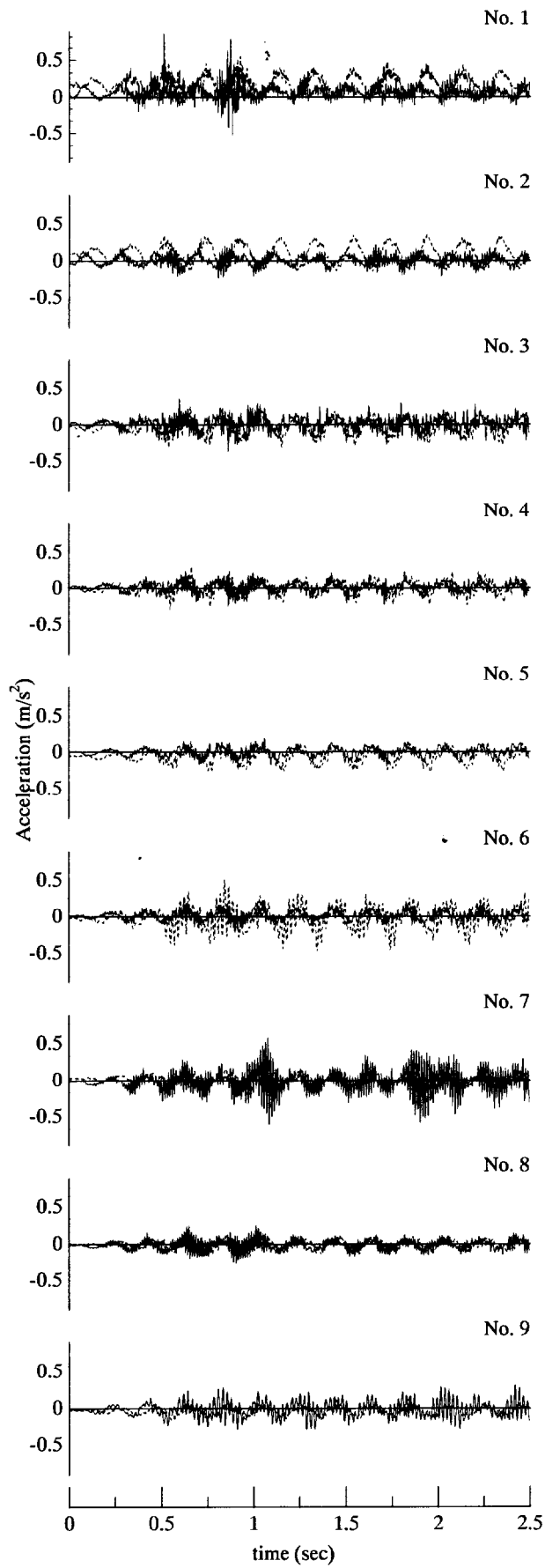
(i) 5Hz
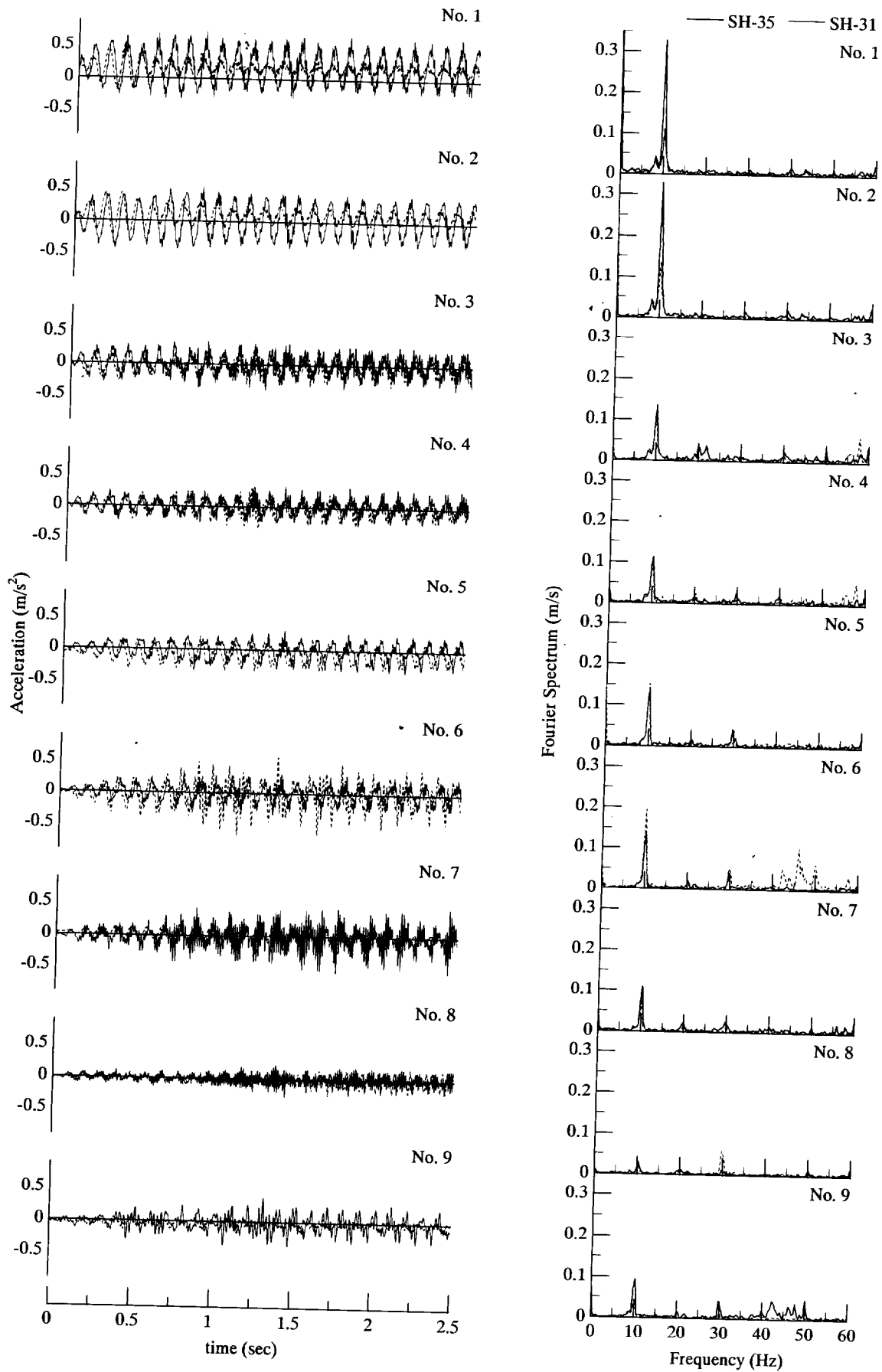
(ii) 10Hz
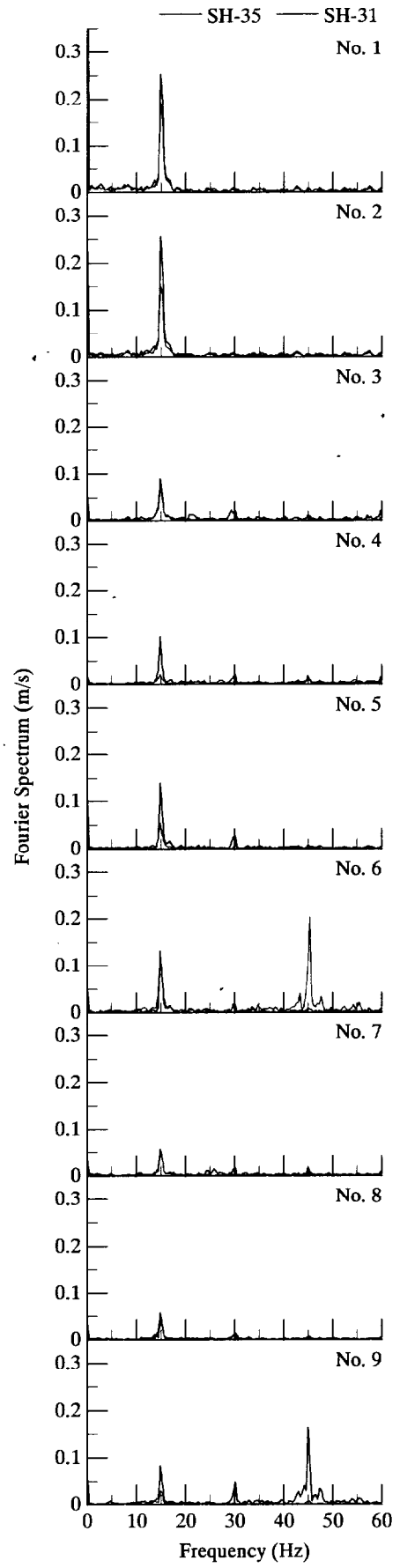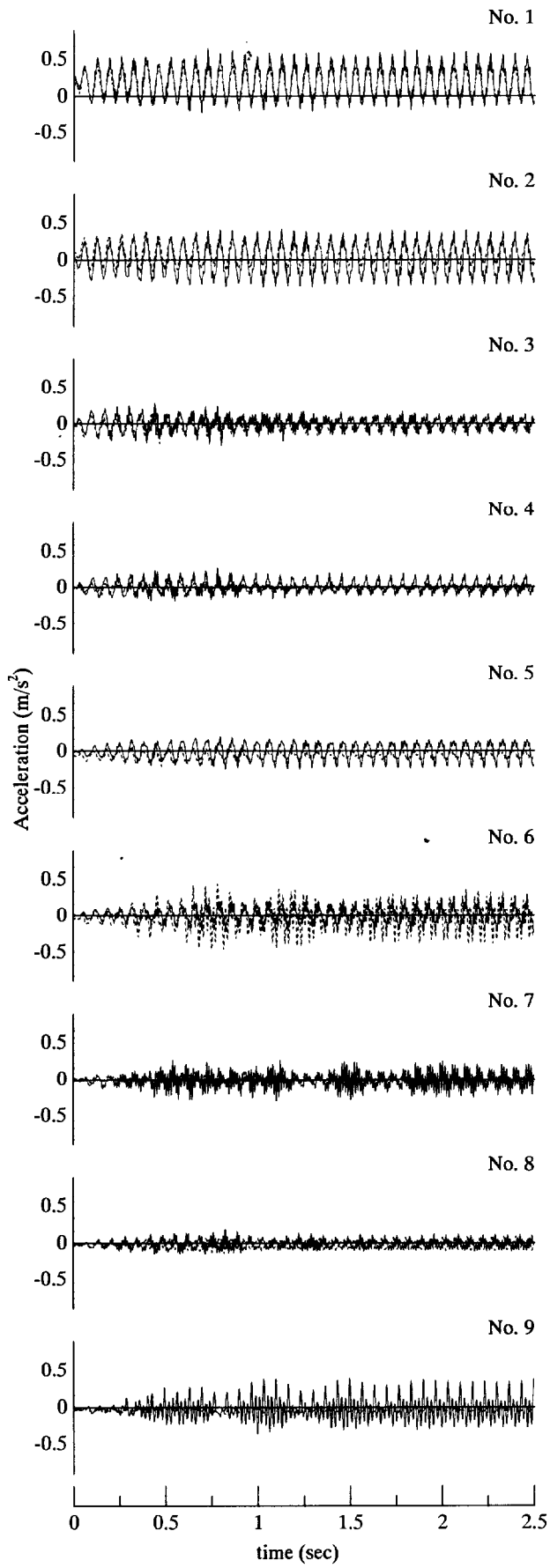
(iii) 15Hz
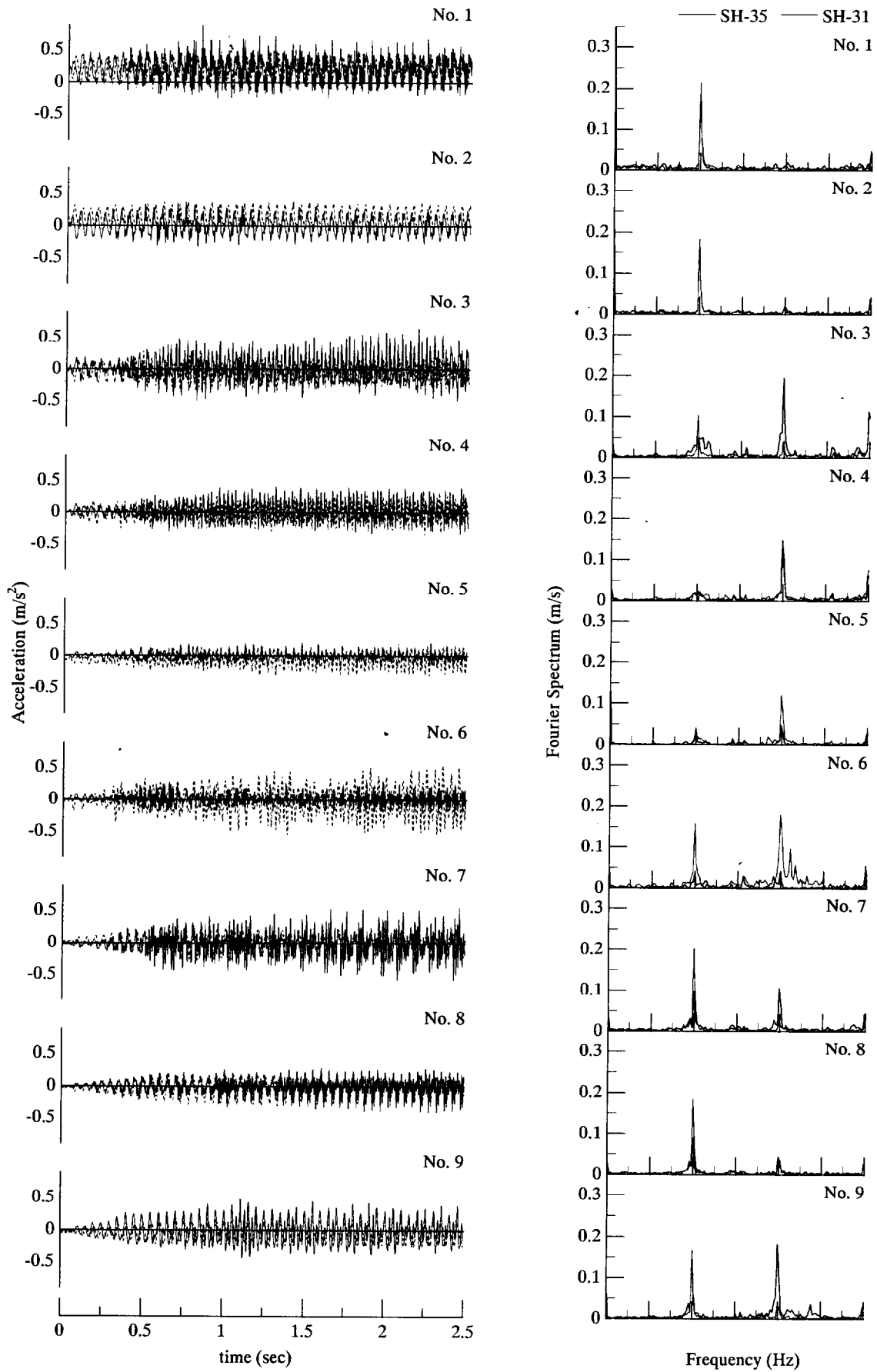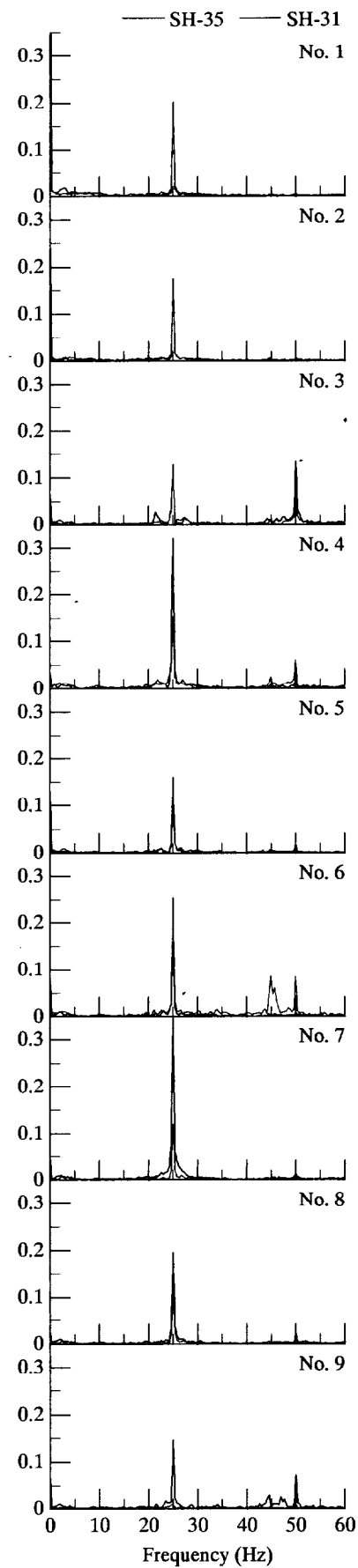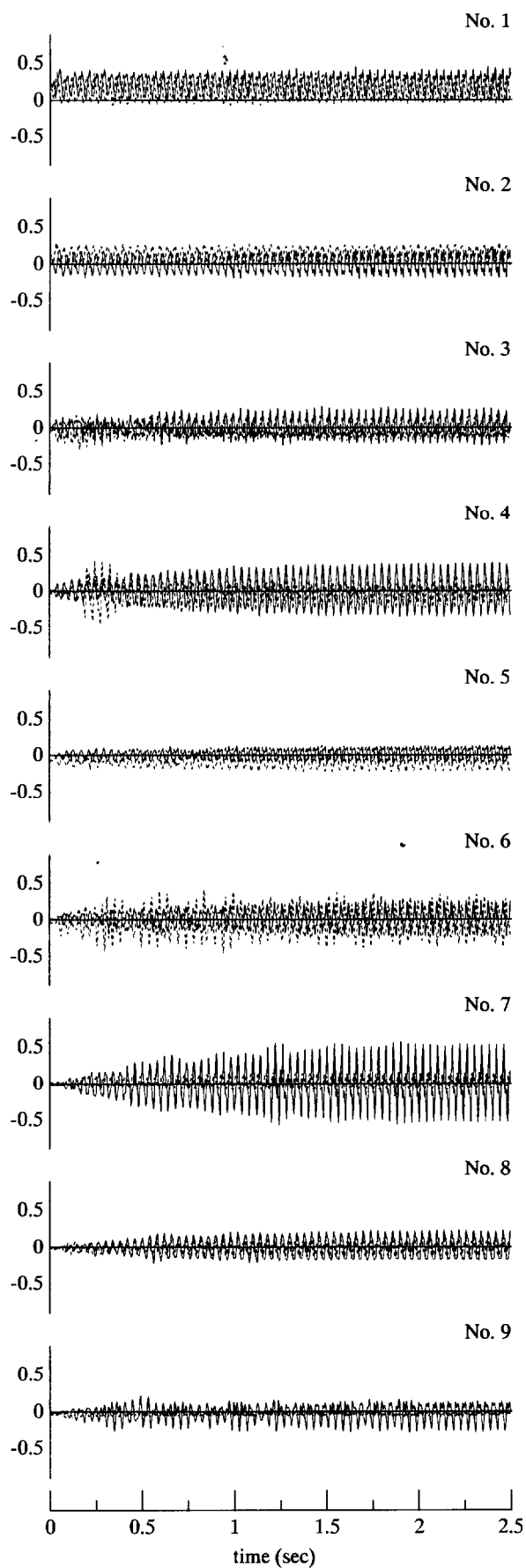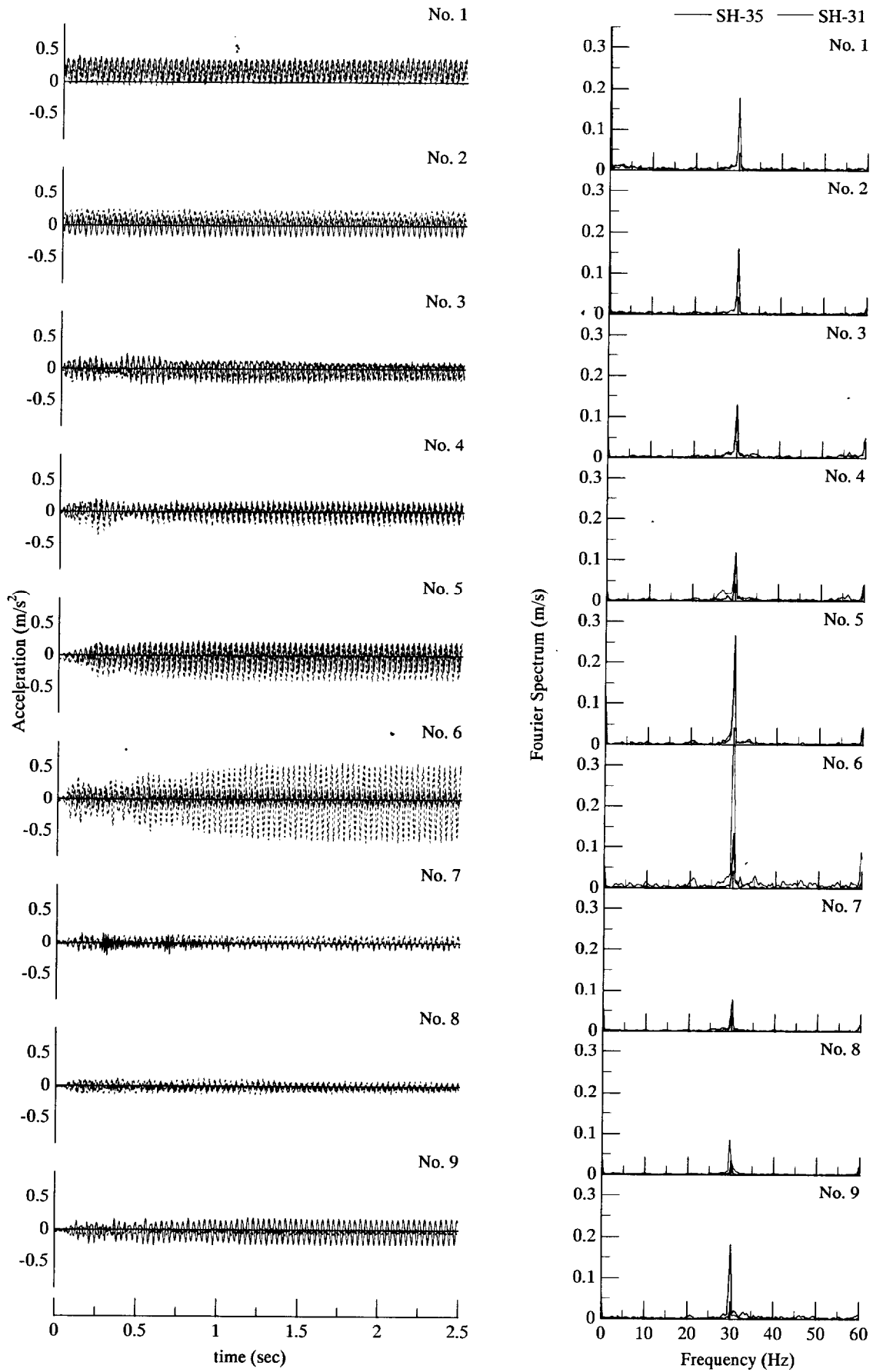
(iv) 20Hz
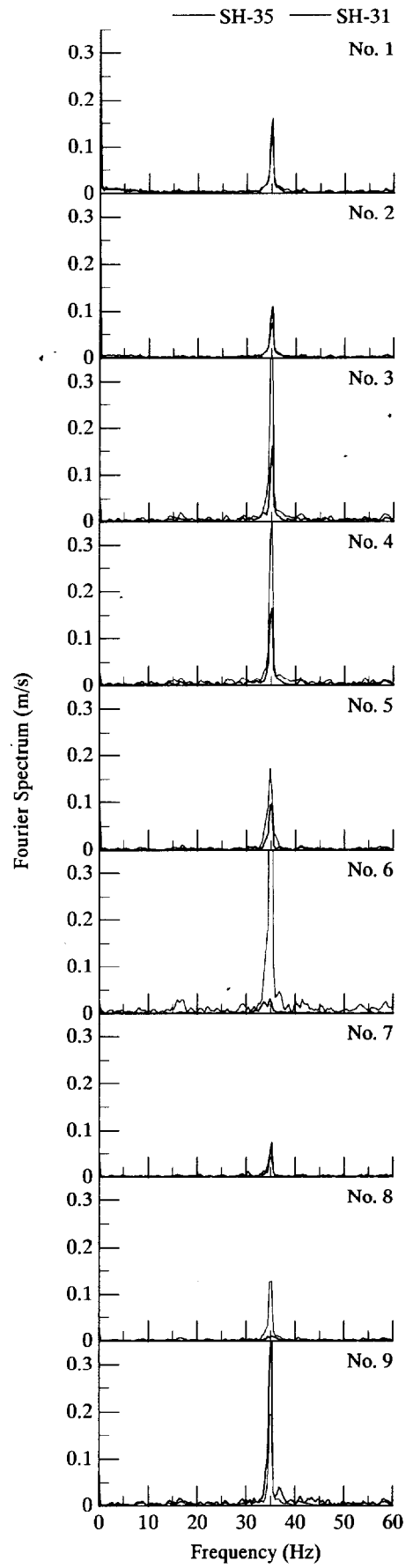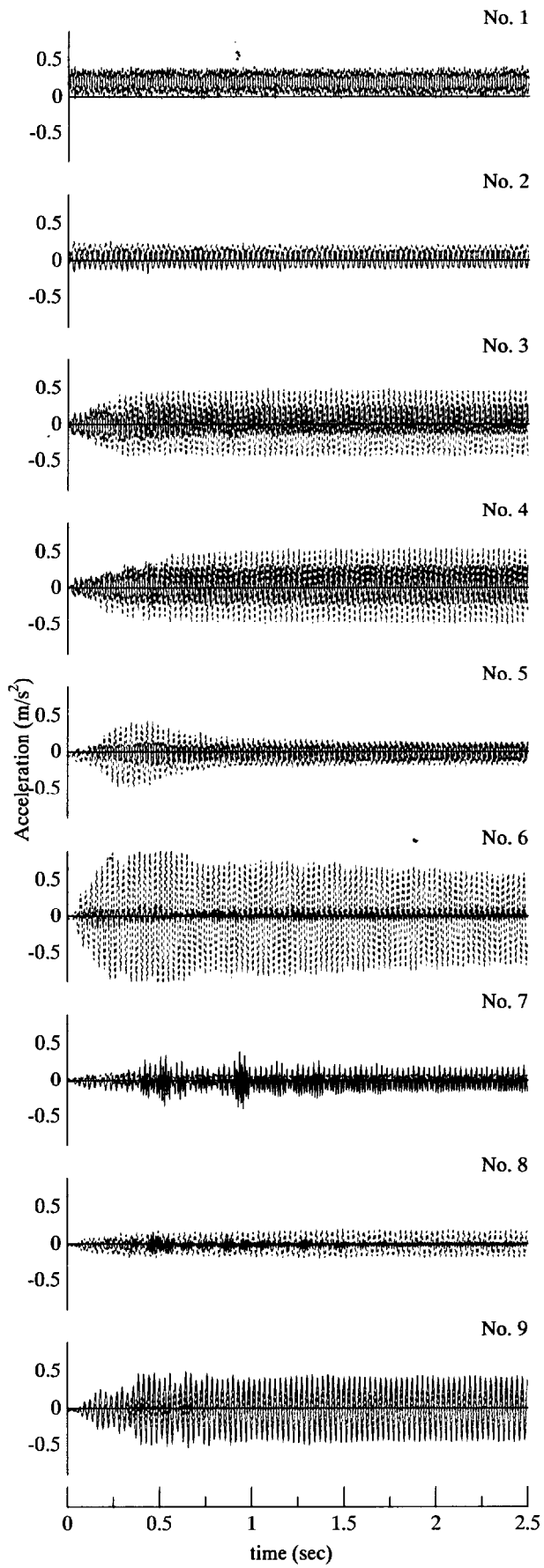
(v) 25Hz

(vi) 30Hz

(vii) 35Hz
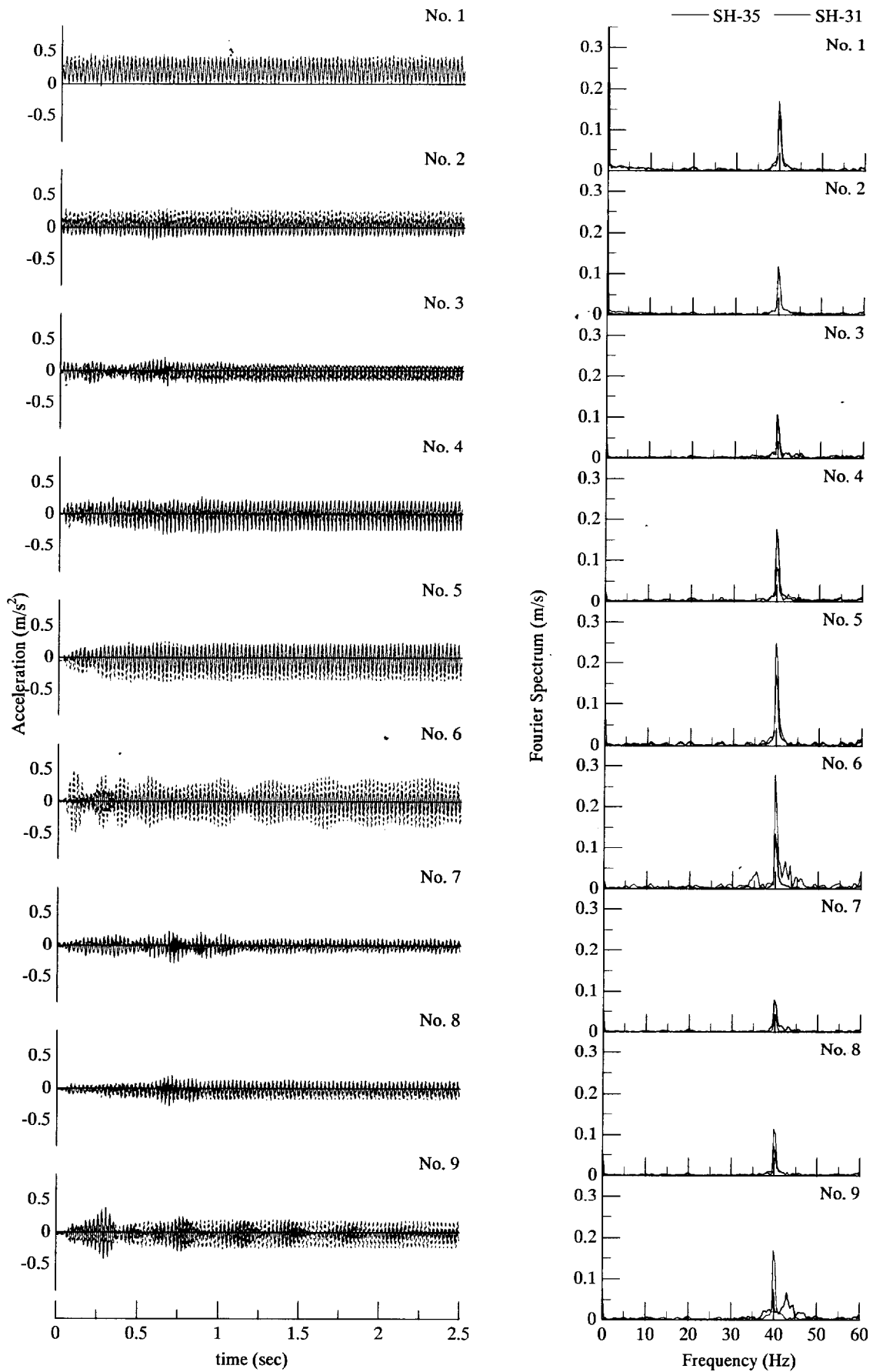
(iix) 40Hz

Figure 5.13 Time histories and results of FFT for the all locations
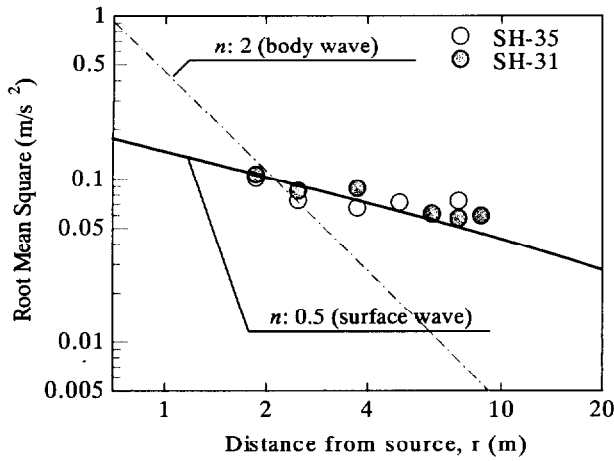
(i) 5Hz
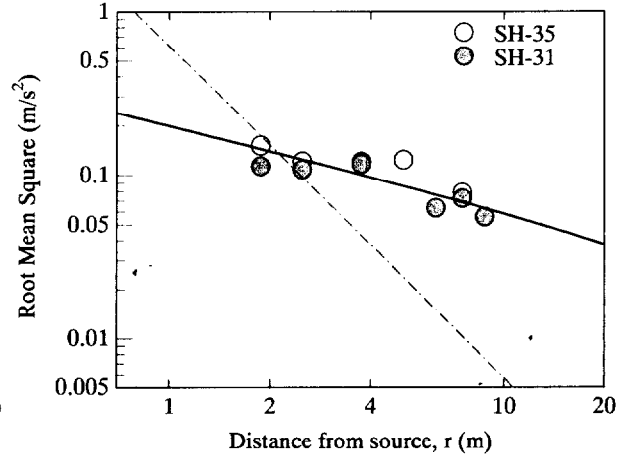
(ii) 10Hz
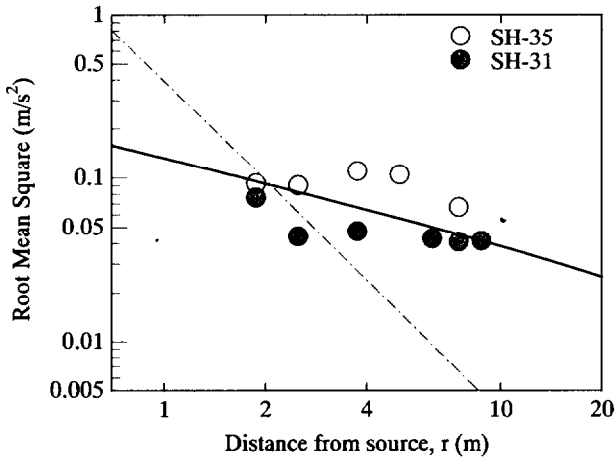
(iii)15Hz
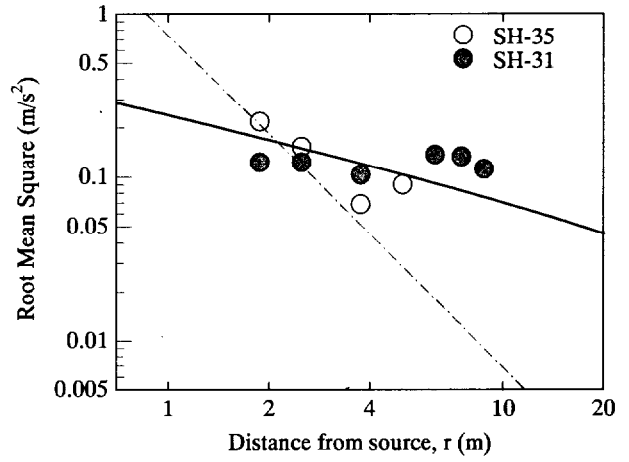
(iv) 20Hz
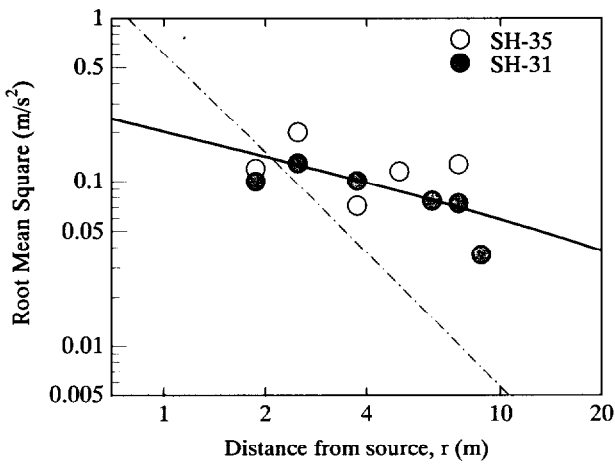
(v) 25Hz
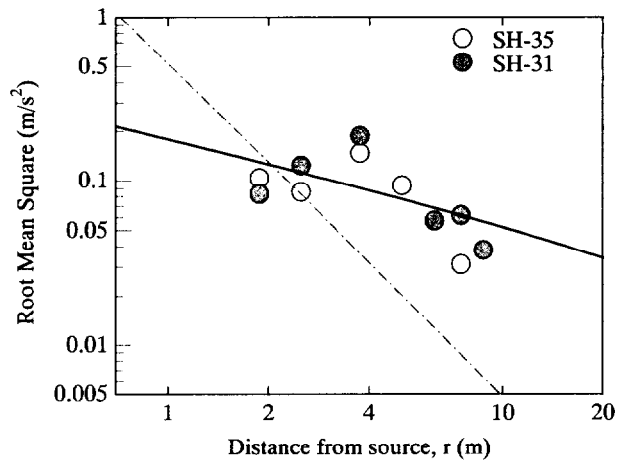
(vi) 30Hz

(vii) 35Hz   (iix) 40Hz
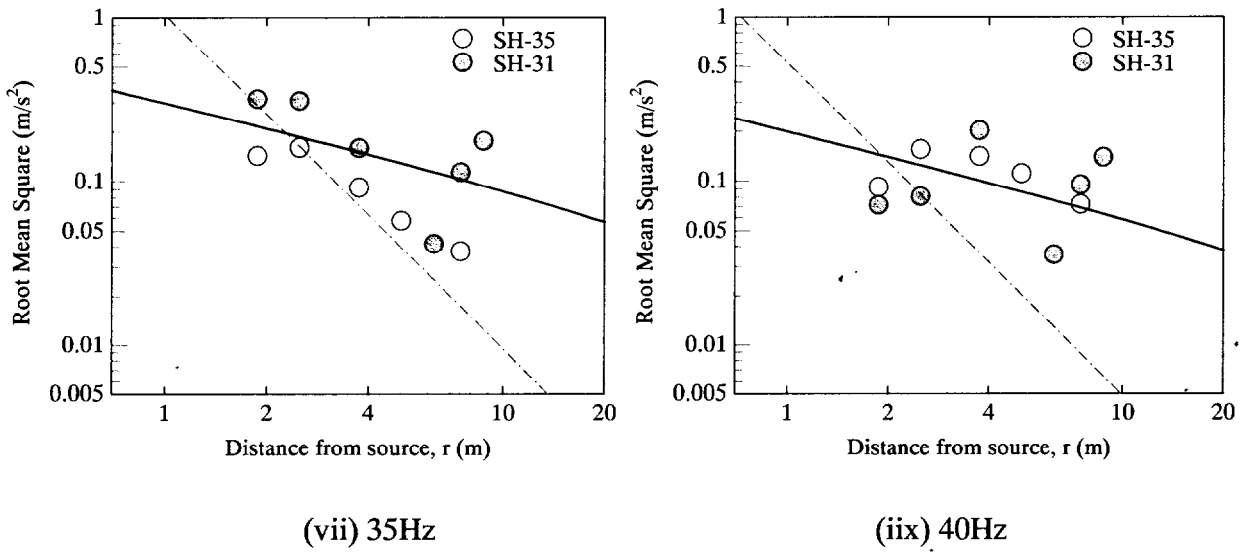
Figure 5.14 Attenuation of the root-mean-square acceleration with distance from vibration source
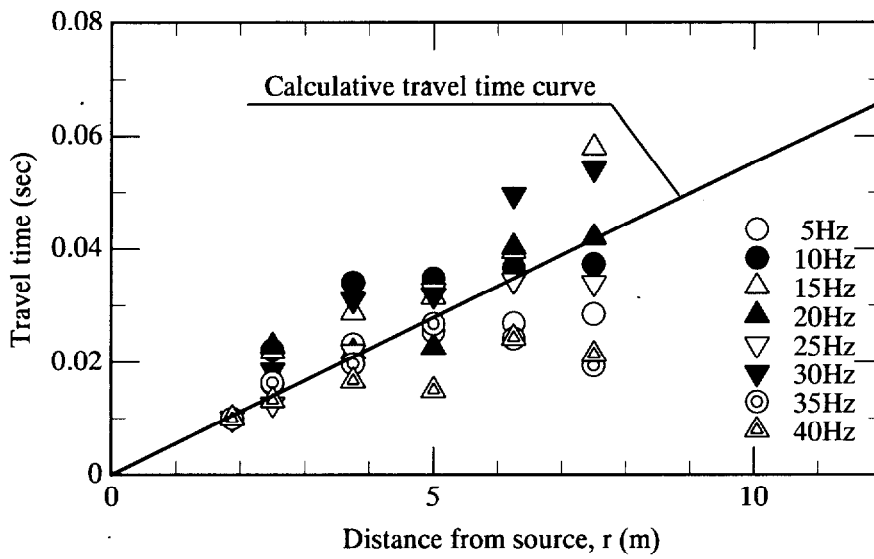
Figure 5.15 Calculative travel time curves

Table 5.3 Experimental program for vibration exciting test using cylindrical barrier

		Material of wave barrier		
		Aluminium	EPS	
		Radius of cylindrical barrier R (m)		
		2.5		5.0
Embedded depth of barrier D (m)	2.5	-	'O	O
	5.0	O	O	O
	10.0	O	O	O

Table 5.4 Mechanical properties of cylindrical barrier and Toyoura sand (same as Table 4.4)

	Dry unit weight γ_d (kN/m^3)	Shear modulus G (MN/m^2)	Wave impedance A	Relative shear modulus between barrier and soil β
Aluminium	26.5	25.6×10^3	49.6	about 1400
EPS	0.12	11.1×10^{-1}	0.007	about 0.10
Toyoura sand (D_r=80%) on ground surface	15.4	17.9	1	-

reducing the vibration were observed in Chapter 4. In addition, this chapter examines the effect of radius of cylindrical barrier R on the reduction of vibration in the case of EPS barrier. These mechanical properties are listed in Table 5.4 (the same as Table 4.4).

(1) Comparisons of the reduction of vibration between various barrier materials

Figures 5.16 and 5.17 presents how the root-mean-square acceleration decreases with distance from the vibration source for two barrier materials, which are aluminium (Fig. 5.16) and EPS (Fig. 5.17), with different embedded depths and with various input frequencies, and also includes data for the case without barrier. In the case of the Aluminium barrier, a marked effect of the barrier becomes evident for the case of embedded depth of 10 m, in which a sharp drop in the root-mean-square acceleration is observed on the barrier and after which the level of the acceleration remains much smaller than the case of embedded depth of 5 m. In previous study using the multiple ball-
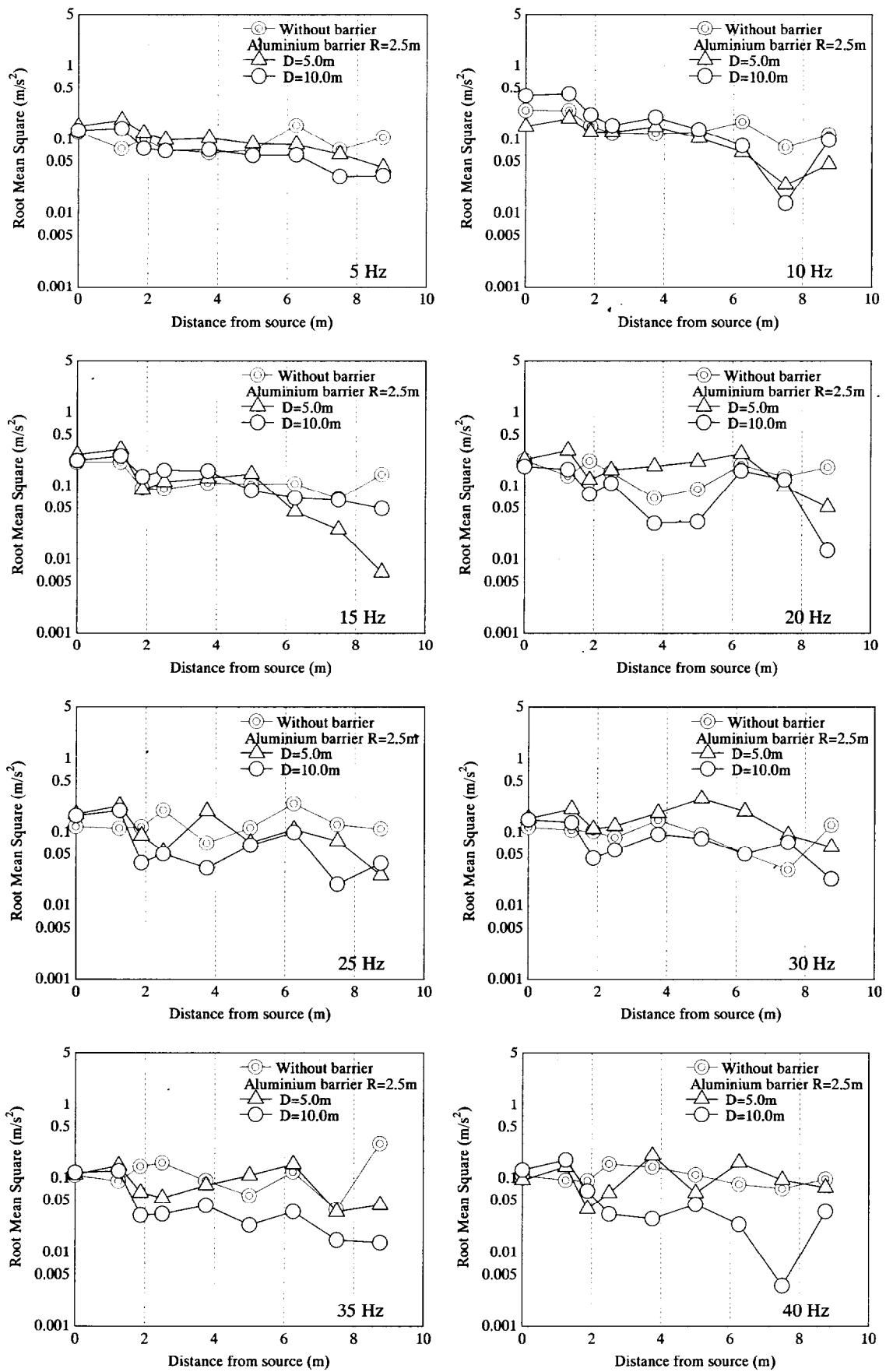
Figure 5.16 Attenuation of the root-mean-square acceleration with distance from vibration source for various embedded depths for the case of Aluminium barrier
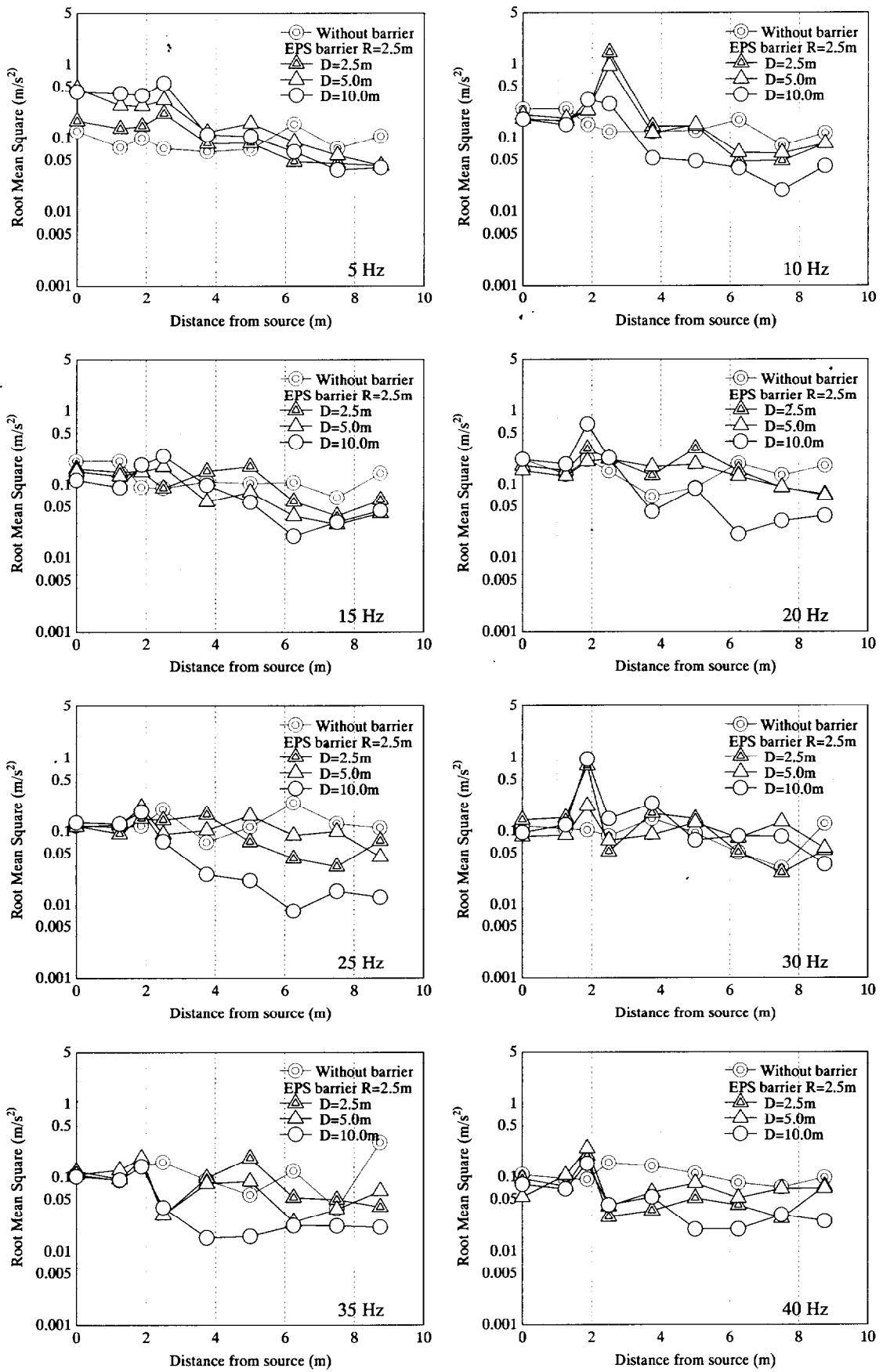
Figure 5.17 Attenuation of the root-mean-square acceleration with distance from vibration source for various embedded depths for the case of EPS barrier (R=2.5m)

dropping system, as to the case of embedded depth of 10 m and aluminum barrier, this observation seems to be contradictory, because embedded depth of 10 m was inefficient in Chapter 4. However, from the viewpoint of the relationship between embedded depth D and layer thickness H, both cases are the same conditions like installing wave barrier at the bottom of container (D/H = 1). To be more precise, these conditions do not take influence of diffraction wave, which propagates from the end of wave barrier, to the amplification of vibration. Hence the case of embedded depth of 10 m becomes effective in screening vibration in this experimental setup. The case of aluminium barrier has a tendency to be the reduction of vibration in front of and on the barrier (See above Fig. 5.16). In the case of EPS barrier (Fig. 5.17), the screening effect continues to remain effective behind the barrier ever for the case of embedded depth of 10 m, the same as the case of Aluminium barrier. However some cases such as input frequency of 15, 35 and 40 Hz have an effect of wave barrier on reduction of vibration in the case of embedded depth of 5 m. In the case of EPS barrier, it appears that the behavior of vibration around the barrier has a close relation to input frequency. In the case of input frequency from 5 to 15 Hz, the magnification of vibration on the barrier is observed. On the other hand, in the case of which input frequency over 20 Hz the magnification of vibration in front of the barrier and the reduction of vibration on the barrier are observed. According-ing to the results using multiple ball-dropping system in Chapter 4, the first dominating frequency of EPS barrier material is around 8.5 Hz. The different behavior caused by input frequency appears to have a profound effect on the dominating frequency of wave barrier materials.

The influence of normalized depth D/λ and various barrier materials on relative reduction vibration level, L_{rv}, are presented in Fig 5.18 (a), (b), and (c) for location at 3.75 m, 5.00m, and 6.25 m from source, respectively. The reduction effect is expressed by the parameter L_{rv} (relative reduction vibration level):

$$L_{rv} = 20 \times \log \left(\frac{\text{Normalize Amplitude with barrier}}{\text{Normalize Amplitude without barrier}} \right) \quad (dB) \quad \dots\dots\dots\dots\dots\dots \quad (5.2)$$

As Fig. 5.18 clearly indicates the Aluminium barrier becomes effective only when D/λ exceeds more than unity, whereas the EPS barrier tends toward effectiveness for a wide range of D/λ values. However, this vibration reduction level in the case of EPS barrier is not clearly effective in comparison with the decay line which shows the influence of D/λ on the reduction of vibration in Chapter 4. Especially, L_{rv} value in the range under 1 wave length (D/λ = 1) depth varies widely. It is likely that these results have something to do with some factors, such as input frequency, distance from source to wave barrier, dynamic interaction between ground and wave barrier. In order to begin addressing these factors, the effect of the relationship between radii of cylindrical barrier R and radii of foundation B on the reduction of vibration in the case of EPS barrier is examined in the next section.

(2) Influence of radius of cylindrical barrier on the reduction of vibration

As to EPS barrier, influences of radius of cylindrical barrier R on the reduction of vibration are shown by comparing at radii of cylindrical barrier R = 5.0 m and 2.5 m. Figure 5.19 presents how
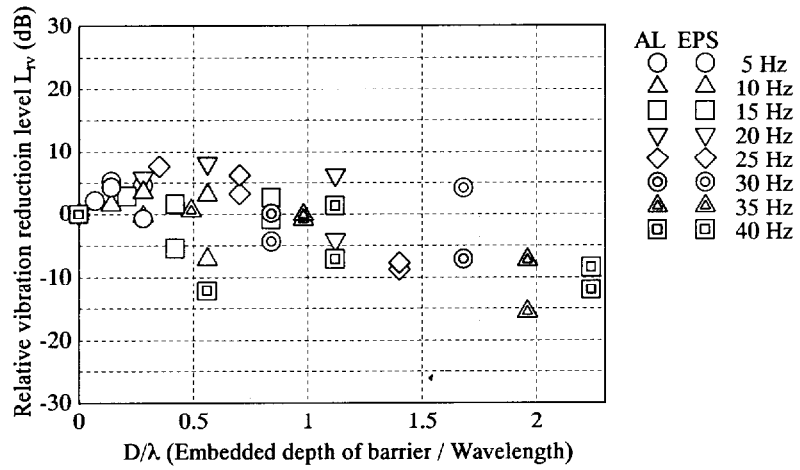
(a) Location at 3.75 m (=1.5R) from source
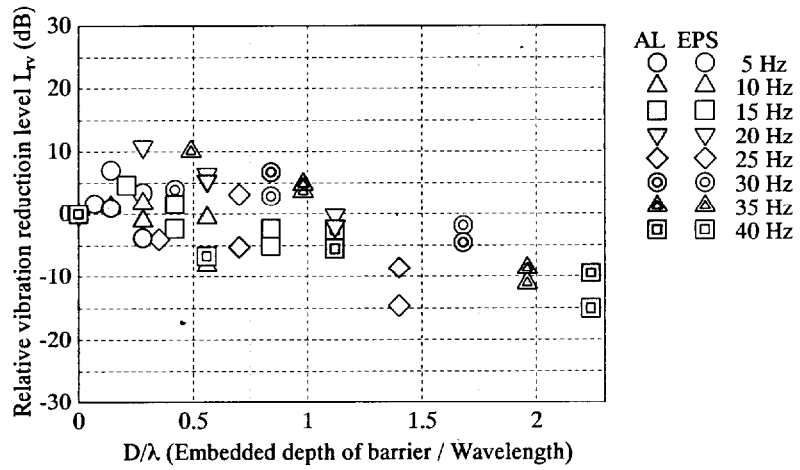
(b) Location at 5.00 m (=2.0R) from source
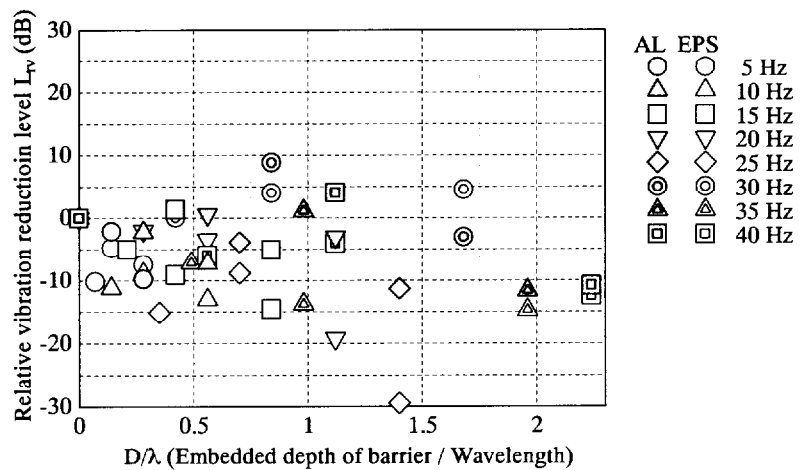
(c) Location at 6.25 m (=2.5R) from source

Figure 5.18 Changes in relative vibration reduction level L_{rv} to embedded depth of barrier / wavelength D/λ for different barriers

the root-mean-square acceleration decreases with distance from the vibration source for EPS barrier materials, with different embedded depths and with various input frequencies, and also includes data for the case without barrier. In the case of R = 5.0m, the behavior around the barrier tended to be similar to the result of R = 2.5m. In other words, it is observed that the magnification of vibration amplifies on the barrier in the case of input frequencies of less than 15 Hz. In the cases over 20 Hz, it is similarly shown that the magnification of vibration amplifies in front of the barrier and reduces on the barrier.

On the basis of the distance from wave barrier, it examines the effect of various radii of cylindrical EPS barrier on the reduction of vibration, as shown in Fig. 5.20. From the point of view of the distance from wave barrier, it is clear that the relative vibration reduction level far from the source decreases more than that level near the source. To be more precise, the case of R = 2.5 m has a magnificent area in the range under 1 wave length (D/λ = 1) depth at 1.25 m and 2.50 m from barrier, while the case of R = 5.0 m does not have that area. Furthermore, this tendency to reduce vibration in the case of R = 5.0m is similar to the impact point loading result in Chapter 4. In order to compare this cyclic loading result and the impact point loading result, the distance between source and barrier, R, is normalized with radius of foundation, B, to give R/B (Fig. 5.21). This condition in the case of R=5 equals the condition in Chapter 4 in normalized clear distance between source and barrier. In contrast with two different test systems, Fig. 5.22 shows that the change in amplitude ratio R_A to normalize depth D/λ at L=2.253(R/B). As far as input frequencies of 5- 25 Hz are concerned, the tendencies of cyclic loading results are similar to that of impact point loading test. According to FFT results using multiple ball-dropping system, Fourier spectrum exists in a wide range of from 0 to 50 Hz (Fig. 4.15). However, dominating frequency at surface ground is within a range from 10 to 25 Hz. This range is consistent with the result in Fig. 5.22. Accordingly it appears that not only input frequency but also response frequency at ground surface has a close relation to the vibration reduction by wave barrier used.

For practical countermeasures, there are many cases where the locating position of the wave barrier is fixed already. Consider now the implication of distance from source to target position, L. The influence of normalized depth D/λ and two different radiuses of barrier on relative reduction vibration level, L_{rv}, are presented in Fig 5.23 (a), (b), and (c) for location at 6.25 m, 7.50m, and 8.75 m from source, respectively. Although the positioning conditions of barrier are different, both results seem the same tendency of reduction of vibration. If this observation is correct, distance from target position to source rather than the distance from barrier to source influences vibration reduction wherever location of barrier is installed within target position. However, twice radius of wave barrier increases the construction area by a factor of four. From the point of view of construction cost, wave barrier which is far from source is unacceptable. In addition, the barrier which has a finite extension shows the effect on reduction of the vibration near distance from source rather than far from distance from source.
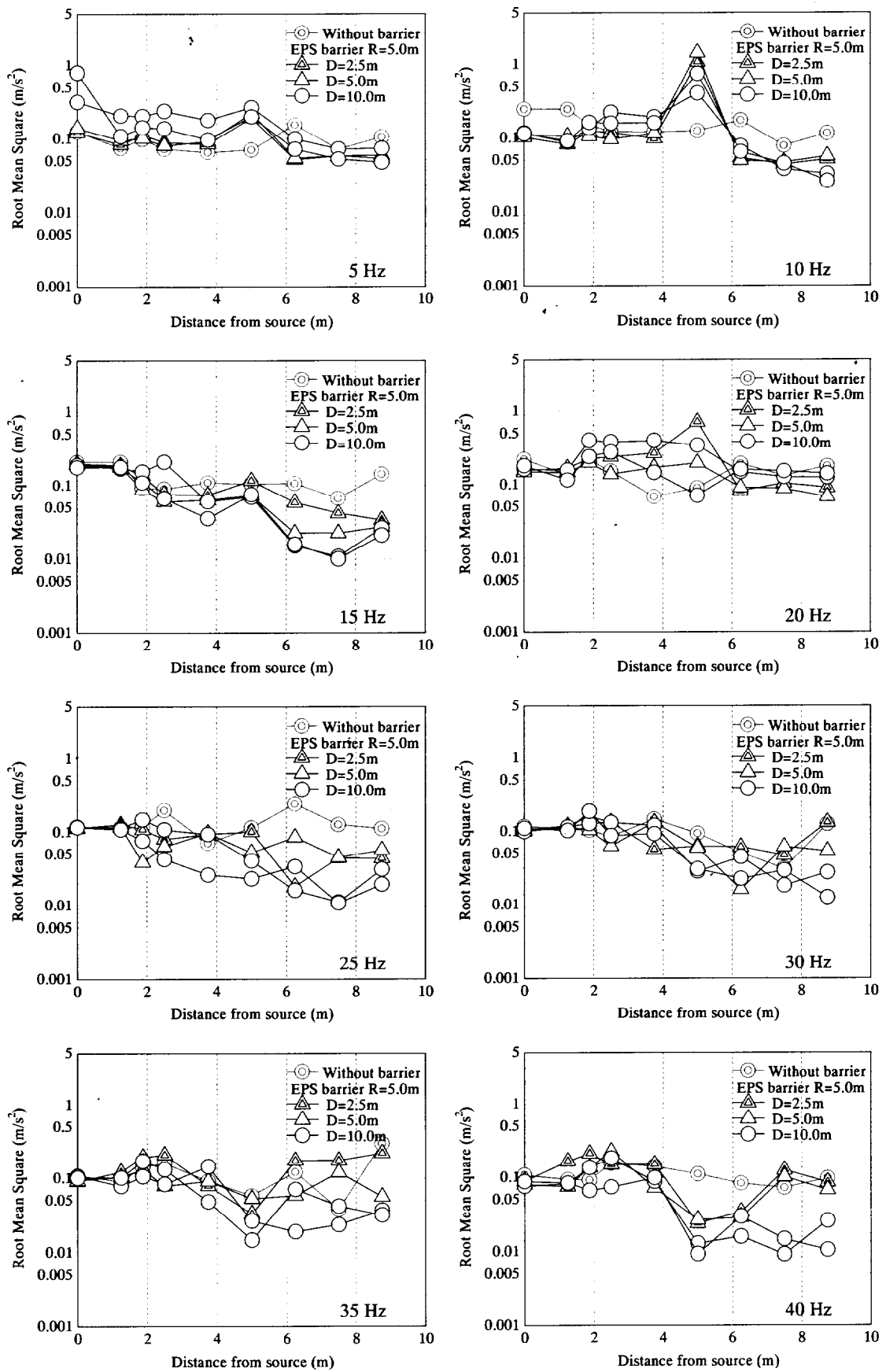
Figure 5.19 Attenuation of the root-mean-square acceleration with distance from vibration source for various embedded depths for case of EPS barrier (R=5.0m)
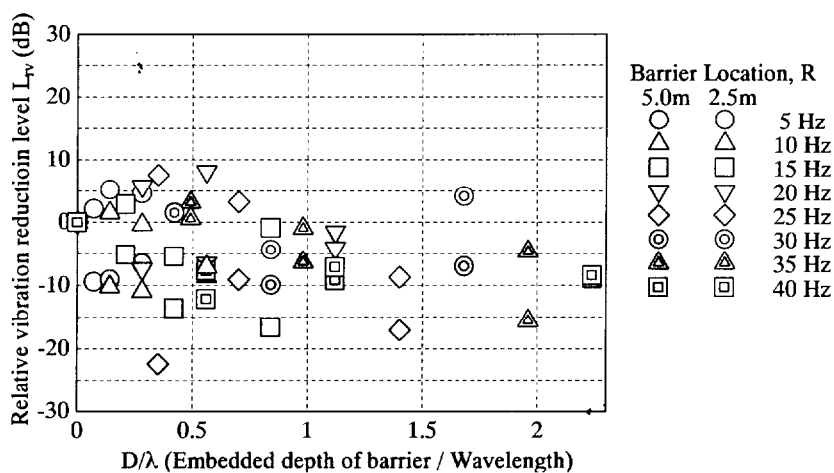
(a) Location at 1.25 m from barrier (3.75 m from source)
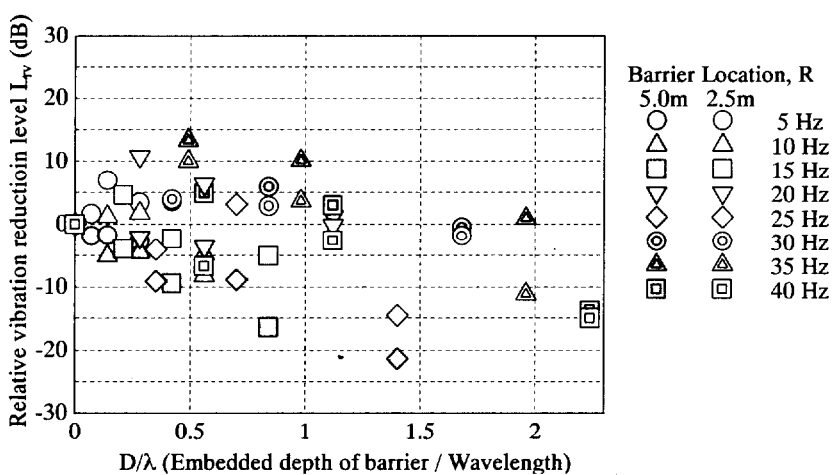
(b) Location at 2.50 m from barrier (5.00 m from source)
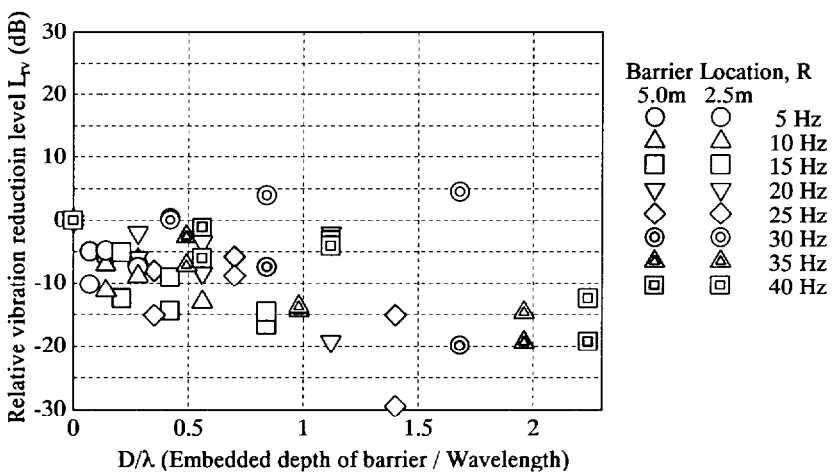
(c) Location at 3.75 m from barrier (6.25 m from source)

Figure 5.20 Variations of relative vibration reduction levels to normalized depth D/λ for two kind of radius of barrier at the same distance from barrier
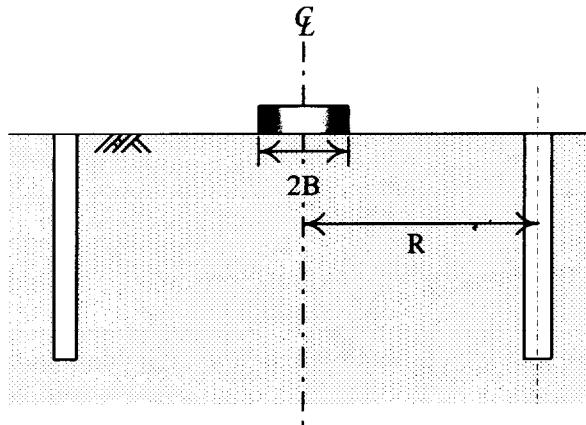
Figure 5.21 The relationship between radius of foundation and radius of wave barrier
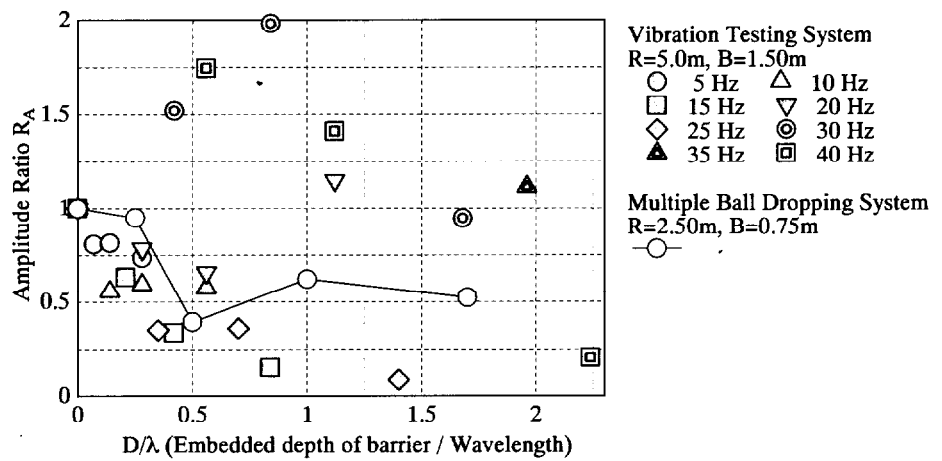
Figure 5.22 Change in amplitude ratio R_A to normalized depth D/λ for different test systems at L
= 2.25 × (R/B)
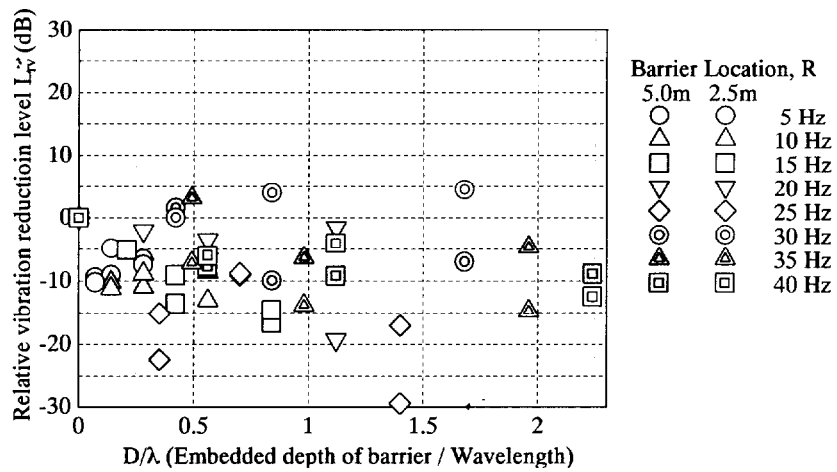
(a) Location at 6.25 m from source
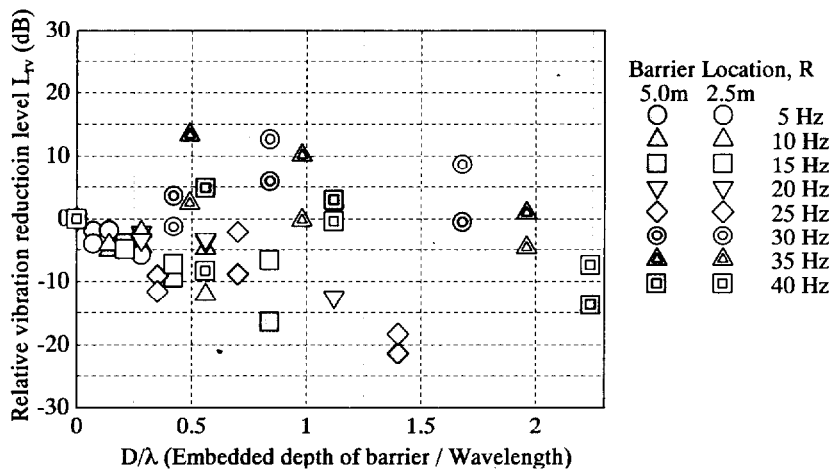
(b) Location at 7.50 m from source
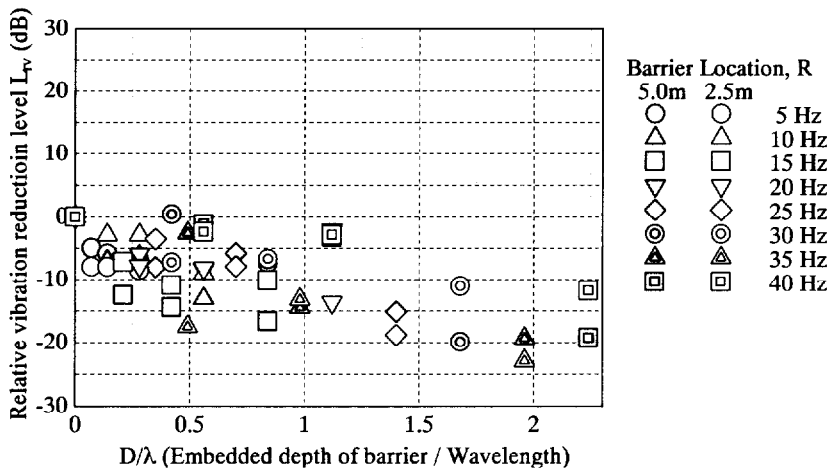
(c) Location at 8.75 m from source

Figure 5.23 Variations of relative vibration reduction levels to normalized depth D/λ for two kind of radius of barrier at the same distance from source

5.4.4 Vibration countermeasures at vibration source

The experimental conditions in countermeasures at vibration source are listed in Table 5.5. Selected vibration reduction materials under trackbed were rubber and CRMA, while a stiff foundation was modeled by aluminum. The vibration reduction material under trackbed was modeled by a ring plate of 60 mm in diameter and 15 mm in height. The CRMA modified trackbed was not modeled by a material that would satisfy the scaling law of aggregate size. CRMA with scaled 1/5 down aggregates was used in this study. These mechanical properties of the materials are listed in Table 5.6 (the same as Table 4.7).

Figure 5.24 shows the attenuation of the root-mean-square acceleration as the distance from the vibration source increases for various modified trackbed materials. The case of aluminium trackbed is used to model currently used trackbed without countermeasure materials. As shown clearly in the figure, a significant effect of vibration reduction becomes evident for the case of rubber-modified trackbed. The attenuation curve of CRMA is more similar to that of aluminium trackbed because the aggregate size in CRMA is not perfectly satisfied with scaling law. Essentially, the effect of CRMA is between these two with the CRMA which used scaled down aggregates producing vibration attenuation similar to that of rubber foundation. These behaviors in each frequency are good agreement with that of impact point loading test in Chapter 4. However, the

Table 5.5 Experiment program for cyclic load using the various countermeasure materials

	Aluminium	Rubber	CRMA (1/5 scale)
Without barrier	O (SH-35)	O (SH-37)	O (SH-36)
With EPS barrier (R= 5 m, D= 10 m)	O (SH-38)	O (SH-40)	O (SH-39)

Table 5.6 Mechanical and material properties of Trackbed materials

	Dry unit weight γ_d (kN/m^3)	Shear modulus G (MN/m^2)	Maximum grain size (mm)	Mean particle diameter D$_{50}$ (mm)
Aluminium	26.5	2.56×10^4	---	---
CRMA 1/5 scale	23.5	9.60×10^2	4.75	0.25
Rubber (Natural rubber)	9.60	1.08×10^2	---	---
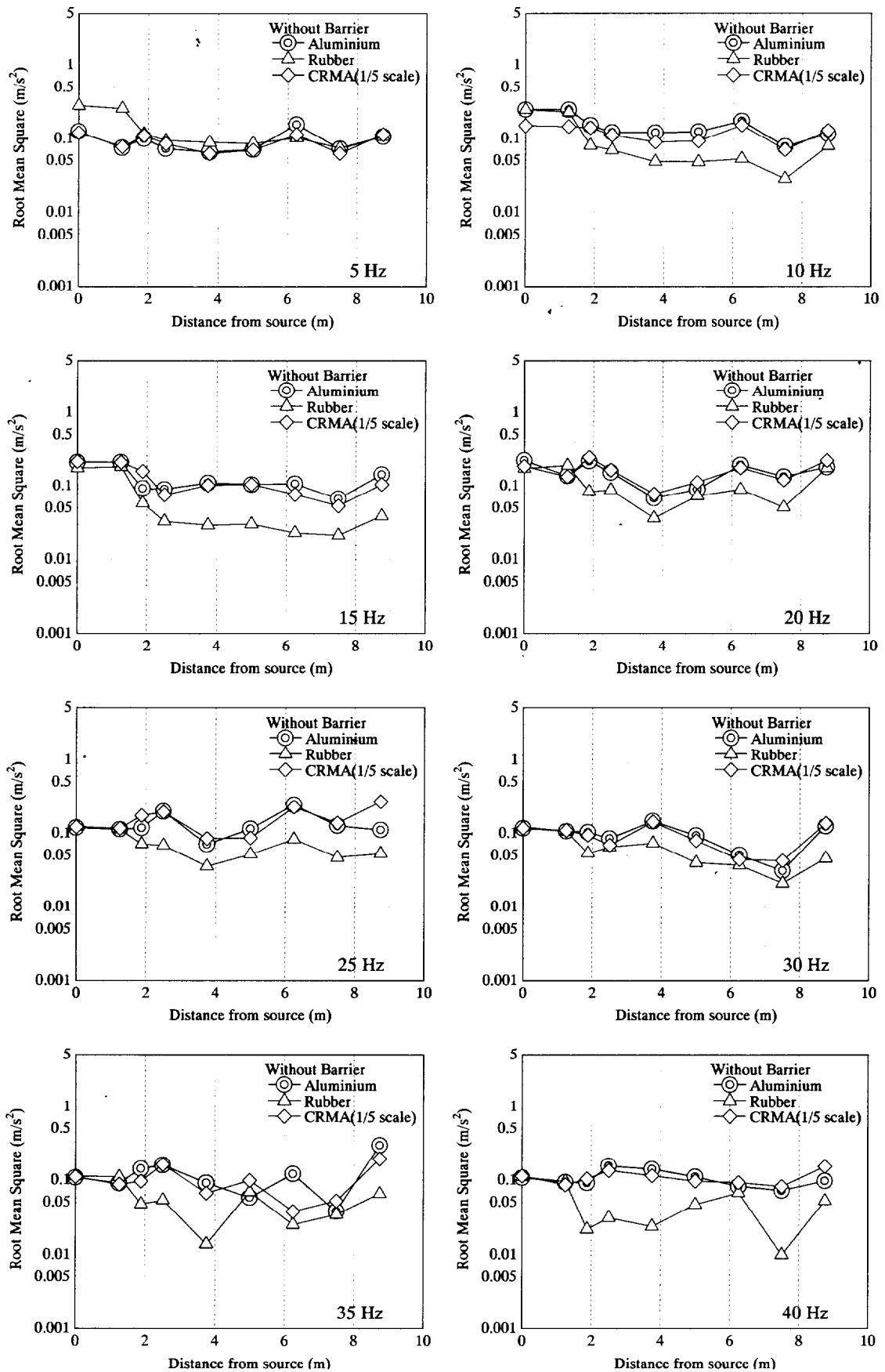
Figure 5.24 Attenuation of the root-mean-square acceleration with distance from vibration source for various trackbed materials
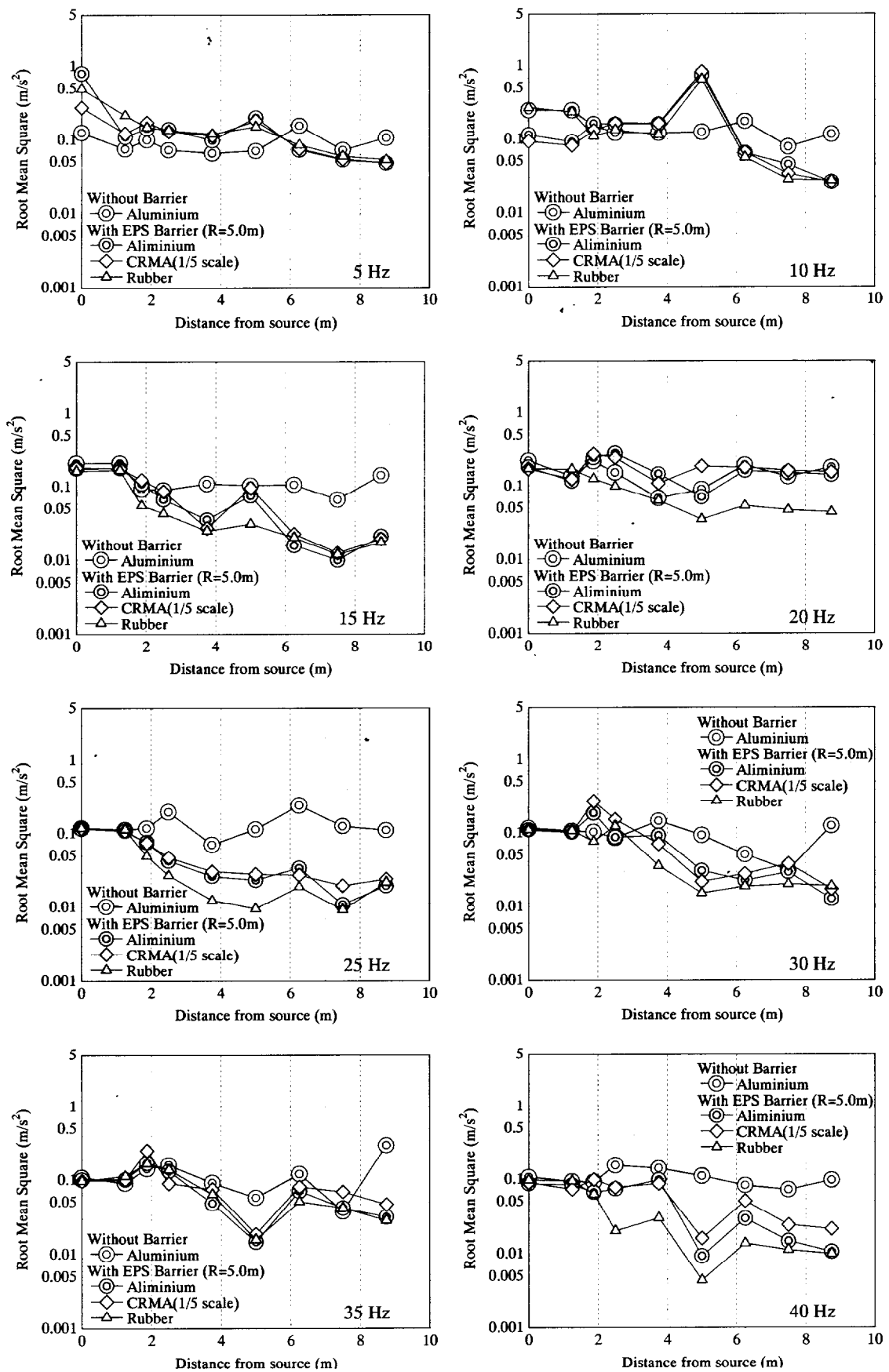
Figure 5.25 Attenuation of the root-mean-square acceleration with distance from vibration source for various trackbed materials with EPS barrier

amplification of rubber trackbed is different from the same cases in Chapter 4. In other words, the amplification using this system is weak in comparison with that of impact point loading test, as same as the amplification of other materials. It appears that not only the different system of exciting but also the foundation weight influences that behavior.

In addition to the countermeasure methods adopted at the vibration source, another method that applied at transmission path is commonly used. Figure 5.25 shows how the root-mean-square acceleration attenuates with distance from the vibration source for various modified trackbed materials with EPS barrier. It also includes data for the case of aluminium trackbed without barrier. Comparing the data from tests without barrier with that with barrier and various trackbed materials, it is observed that vibration clearly reduces behind the barrier except for the case of 20 Hz and 30 Hz. The rubber modified trackbed makes a significant effect in reducing vibration both in front of and behind barrier. The attenuation curve of CRMA is more similar to that of aluminium trackbed, such as the case of the result without barrier.

5.5 CONCLUSIONS

In this chapter, the newly developed Centrifugal Vibration Testing System was introduced for the purpose of investigating the simulation of wave propagation in various input frequencies and effective countermeasures various locations. Details of the system were described. Performance of this system and centrifuge model test results on wave propagation by various frequencies and some cases of its reduction method were described. The following conclusions are derived:

1. The Centrifugal Vibration Testing System developed in this study provides a consistent and repeatable source of surface ground vibration. From the point of the measurement of wave propagation on the surface ground, it was found that this system can supply mainly surface wave.

2. For influence of stiffer and softer wave barriers and different embedded depths of wave barrier on the reduction of ground vibration, it was found that when D/λ is larger than one, the effect of the barriers in vibration reduction is obvious with EPS barrier slightly more effective. When D/λ is less than one, data were quite scattering.

3. In order to compare this cyclic loading test and the impact point loading test in Chapter 4, the experiment were carried out by the same relationship between radius of foundation and the distance from source. As far as input frequencies, which are the area of dominating frequencies by the impact point loading test, are concerned, the results of the cyclic loading test are similar to that of the impact point loading test.

4. It was found through tests that CRMA, which is a material with high shear stiffness and damping ratio, can reduce the vibration away from the source especially when working together with EPS barrier.

CHAPTER 6

FIELD TEST OF ISOLATION OF
GROUND VIBRATION BY EPS BEADS MODIFIED
CEMENT-IMPROVED COLUMN

6.1 INTRODUCTION

As described in the previous Chapters 4 and 5, the series of centrifuge model tests had been carried out on vibration screening by wave barrier. From these results, the softer barrier of which the wave impedance was less than the soil, was effective in reducing vibration. In order to reflect these results, the field test has been performed on vibration screening by softer wave barrier which will be described in this chapter. Railway Technical Research Institute (RTRI), Tenox Corporation and Tokyo Institute of Technology (Tokyo Tech) have proposed a newly constructed method for the wave barrier using EPS beads and cement-improved column (Hirayama et al.; 2002, Koda et al.; 2002, Itoh et al.; 2002). To investigate the effect of produced wave barrier on the countermeasures with EPS beads modified cement-improved column, the measurements of ground vibration were carried out before and after the countermeasures.

Incidentally, RTRI and Tenox Co. have already obtained a patent for construction method and for material used from the Japan Patent Office (Patent Application No. 2002-193036).

6.2 SITE CONDITION AND SOIL PROFILE

The test site is located in Kunitachi city, in the middle of the Tokyo metropolitan area. Since 1986 this site has been let to the RTRI as a test site for geotechnical investigations and experimental installations. In past years, Yoshioka and Ashiya (1990) and Haya et al. (1996) conducted the field test regarding ground vibration screening technique at the field. Since then, it has been open for research projects aimed at improving knowledge of ground vibration screening technique. The test field is under the administration of RTRI. Figure 6.1 shows the site map and the plan view. Figure 6.2 presents the construction area of wave barrier. Most of the site is open grass-covered land. In this field, standard penetration test, sampling, and PS logging were already carried out by Yoshioka and Ashiya (1990). Figure 6.3 shows the soil condition and measured S and P wave velocities at the test site reported by them. In addition, a trial boring test was carried out at four places with an interval of 10 m in this study. The site conditions and profiles in this site are shown in Fig. 6.4. There is a thin cover of filling material on top of the Kanto loam. Soil profiles are composed of filling material, Kanto loam, and gravel from the surface ground. The bedrock at this site consists of gravel. Their material properties are as follows;

TOP VIEW

Shaker (EX-1000DC)

3,750   8,000   8,000   3,750

KEY PLAN

place for machinery material

Embankment

N

* ● :Trial Test Point

No. 1   No. 2   No. 3   No. 4

EPS60   EPS40   EPS20
15@500 = 7,500   500   15@500 =7,500   500   15@500 =7,500   15,600

Wave Barrier 47@500 =23,500 (φ600, n=48)

PLAN VIEW

EPS60   EPS40   EPS20

No. 1   No. 2   No. 3   ▽ Ground surface

Filling material

Kanto Loam   ▽ Gravel layer

Gravel

View direction of
Figure 6.2
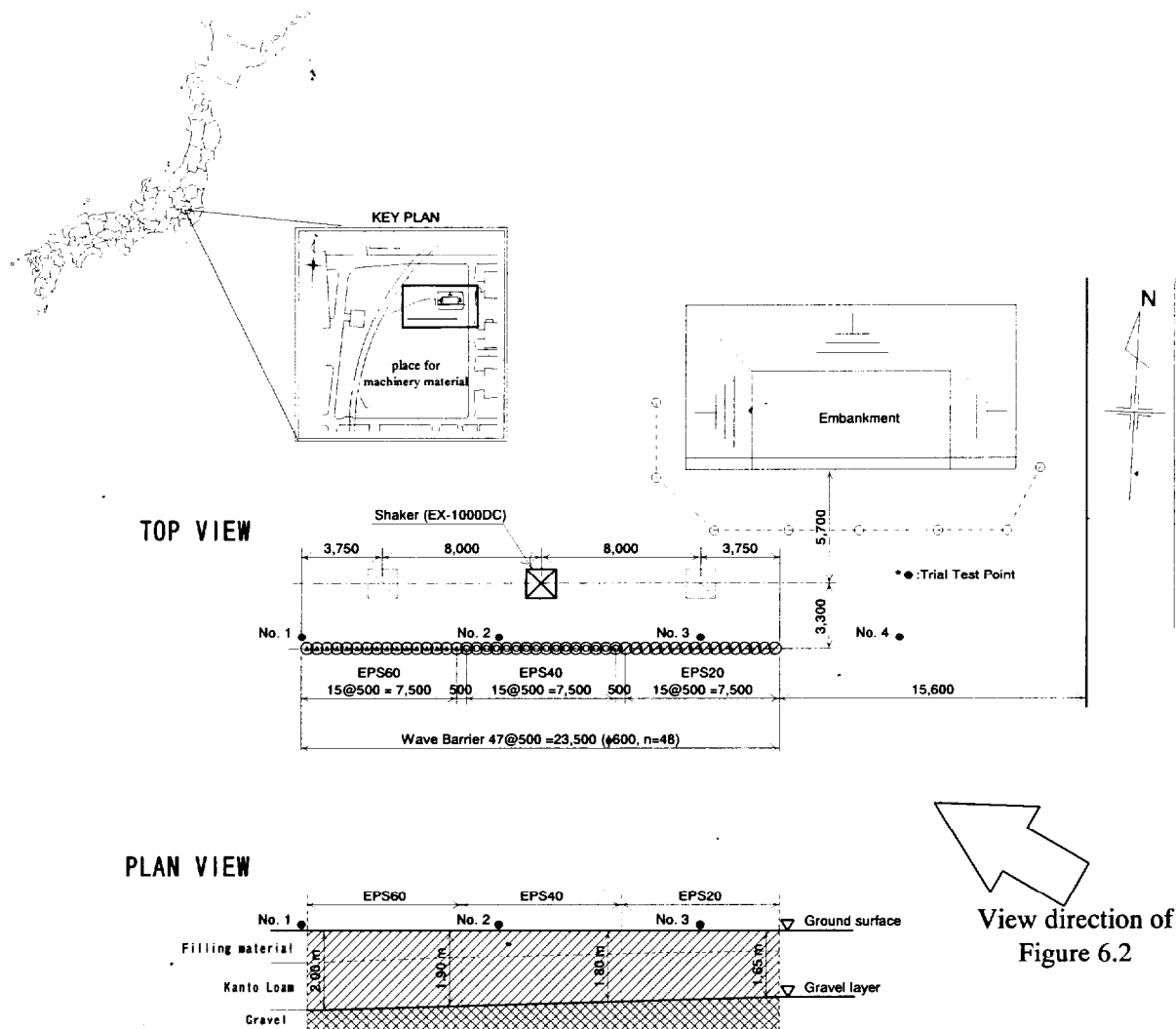
Figure 6.1 Test site map (Railway Technical Research Institute, Kokubunji, Tokyo)

(1)   Filling material: The material of the upper layer is composed of sandy loam mainly, containing some crushed rock (macadam) and concrete pieces. At the No. 1 location, the thickness of the filling material is about 0.8 m. The thickness of the filling material and the depth to the bedrock varies. This layer has a mild downward slope towards the west to east, according to the research results collected by the trial boring test. In the part of the test site where the current investigation was carried out, the thickness of filling material layer at No.1 was 0.8m and the filling material at No.4 was 0.5 m thick.

(2)   Kanto loam: Kanto loam which prevails over the Kanto area is a volcanic cohesive soil which was supplied by Mt. Fuji, Mt. Hakone, Mt. Akagi, and Mt. Nantai during the latter part of the Pleistocene epoch, as shown in Fig. 6.5. The thickness contours of the Kanto loam elongate and thin eastward from these volcanoes over the Kanto area. The thickness of loam beds changes regionally, thicker in volcanic areas and thinner in non-volcanic areas. Kanto loam mainly consists of allophane clay mineral. Geologically, Kanto loam is distributed in the order of Tachikawa loam and Musashino loam from the surface. Tachikawa loam is the newest stratum and its allophane content exceeds 50%. Whereas, the allophane content of Musashino loam is less than 40%. Kanto loam has very high water content and high sensitiv-

Figure 6.2 The location of wave barriers
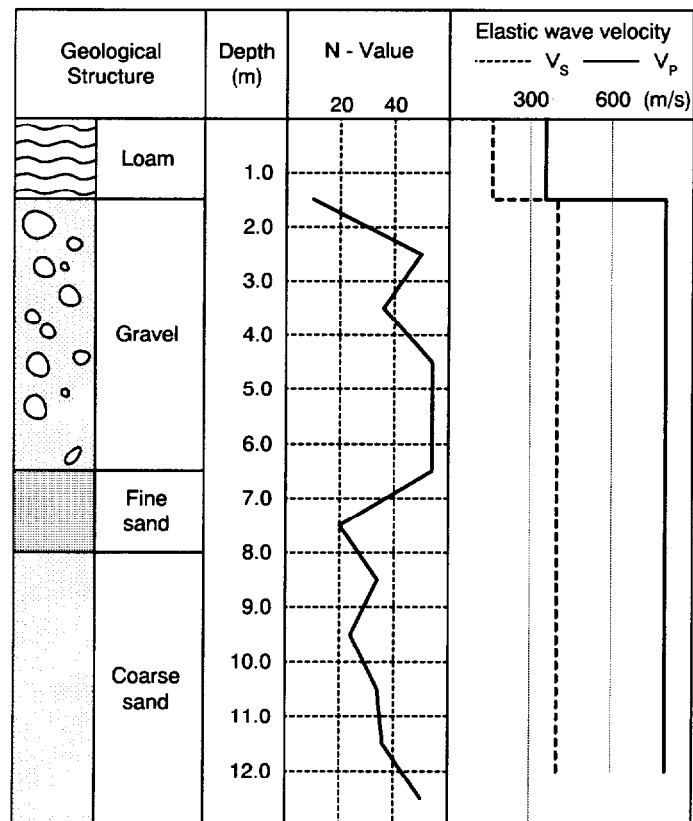
Figure 6.3 Soil conditions and elastic wave velocities at test site (after Yoshioka and Ashiya, 1990)
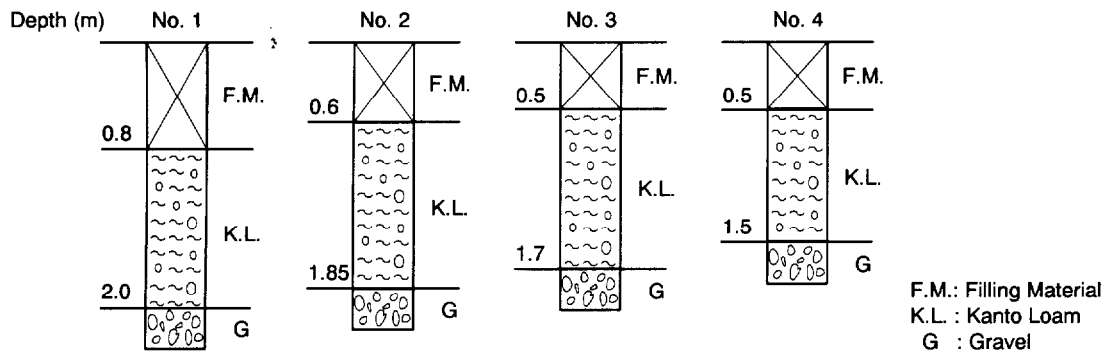
Figure 6.4 Soil profiles at test site

F.M.: Filling Material
K.L. : Kanto Loam
G : Gravel
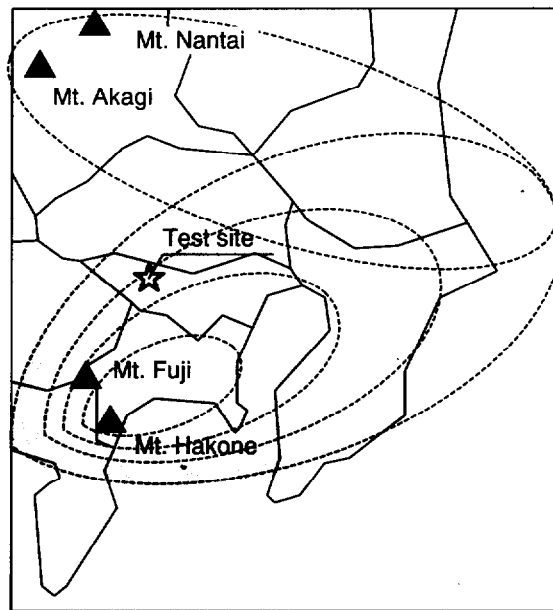
Figure 6.5 The relationship between test site and the volcanoes which supply Kanto loam

ity caused by containing allophane clay mineral. These facts suggest Kanto loam have strong local characteristics due to local precipitation and the properties of the soil itself.

This layer, which is called Tachikawa loam, exists under the filling material layer. This layer also had a mild downward slope towards the west to east. The thickness of this layer varies between about 1.2 and 1.0 m. Furthermore the cobbles of about 200 mm diameter were occasionally found in this layer. The ground water condition was investigated in open holes at four locations in this field. The bottom of the trial boring was 2.0 m depth from ground surface. However it did not observe the ground water because the ground water table was located under this layer. Hence the condition of Kanto loam is unsaturated.

Some soil tests were carried out newly as for Kanto loam. The mechanical and material properties of Kanto loam are summarized in Table 6.1.

(3) Gravel: The material of bedrock is composed of circular gravel which is approximately 300 mm diameter. Grain size is comparatively narrow distribution within this layer. In the trial boring at the west side, the depth to bedrock had been found to be 1.5 m and on the east side of the test field it had been found to be 2.0 m.

Table 6.1 Mechanical and material properties of Kanto loam

		Kanto loam (G.L. -1.0m)		
General	Wet density ρ_t (g/cm^3)	1.157		
	Dry density ρ_d (g/cm^3)	0.518		
	Soil particle density ρ_s (g/cm^3)	2.564		
	Natural water content w_n (%)	123.4		
	Void ratio e	3.964		
	Degree of saturation S_r (%)	80.2		
Characteristic of consistency	Liquid limit w_L (%)	158.3		
	Plastic limit w_P (%)	112.6		
	Plasticity index I_P	45.7		
Unconfined compression test	Unconfined compressive strength q_u (kN/m^2)	34.1	43.7	57.9
		35.0	44.9	57.5
		(Average)	45.5	
	Strain at failure ε_f (%)	2.1	3.4	6.0
		4.2	2.9	2.6
		(Average)	3.53	
	Modulus of deformation E_{50} (MN/m^2)	2.3	1.8	1.7
		1.5	1.9	2.4
		(Average)	1.93	

Grain size distribution curve

6.3 DESIGN OF WAVE BARRIER

6.3.1 Background

Vibration countermeasures using wave barrier have been studied by a number of researchers (see above Chapter 2). In their methods, it is necessary to construct the processes as follows (e.g. Fig. 6.6, Massarsch, 1991);

1) Excavation of trenches
2) Scaffold and construction equipment
3) Air trench
4) Construct wave barrier materials (ex. concrete, steel and EPS block, gas cushion etc...)

   The past researchers who presented some of construction methods could not establish the way of vibration countermeasures which satisfied the low cost and reliability requirement. Thus there was no special machine which was able to satisfy all processes mentioned above so far. When there is a construction site adjacent to existing public transportation structures such as high-speed
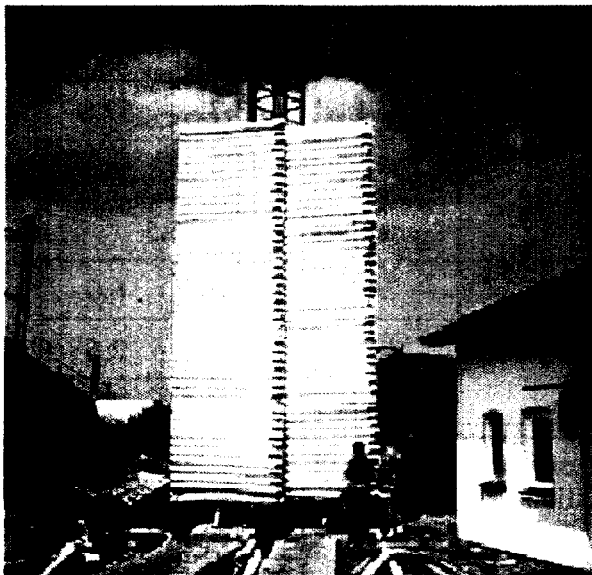
(a) Mounting of the gas-inflated screen prior to installation
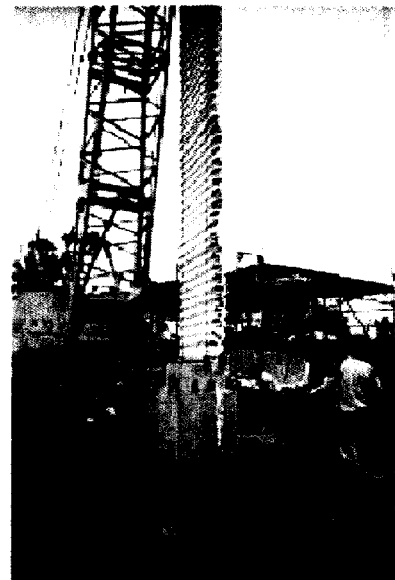
(b) Placement of the screen in trench using a heavy weight

(c) Covering of hardened cement-bentonite filled trench with Styrofoam

(d) Surface above isolation screen with asphalt cover

Figure 6.6 The general process to construct wave barrier (after Massarsch and Erson, 1985)

train lines, some problems were indicated by Ejima (1979) and Murata et al. (2001). One of problems is the influence of the deformation of the air trench caused by the running train. Besides, it is necessary to restrict the height of construction machine because construction site adjoins railway line. To satisfy these requirements, the soil improvement machine for improving soft terrains by mixing cement slurry with the soil in place is applied in this study. To be more precise, using soil improvement machine, an automatic construction method, which can excavate the ground and construct wave barrier at the same time, has been proposed. By virtue of this method, some problems such as the influence of the deformation caused by the air trench could be minimized. The design of wave barrier materials which is effective in reducing vibration is described in the next section.

6.3.2 Design of mix proportion for EPS Beads Modified Cement-improved column

RTRI, Tenox Co. and Tokyo Tech have proposed a newly constructed method for the wave barrier using "EPS beads modified cement-improved column". Figure 6.6 presents the configuration of equipment for the construction method on site. After positioning, the mixing blade of the soil improvement machine penetrates to the target depth with the rotation. When the tip of the mixing blade arrives at the target depth, the mixing blade is rotated and withdrawn while injecting the EPS beads modified cement-improved slurry which was conveyed and pressurized from the plant. And a stabilized column is finally formed in the ground. The material of wave barrier needs to be satisfied with the performance requirements as follows;
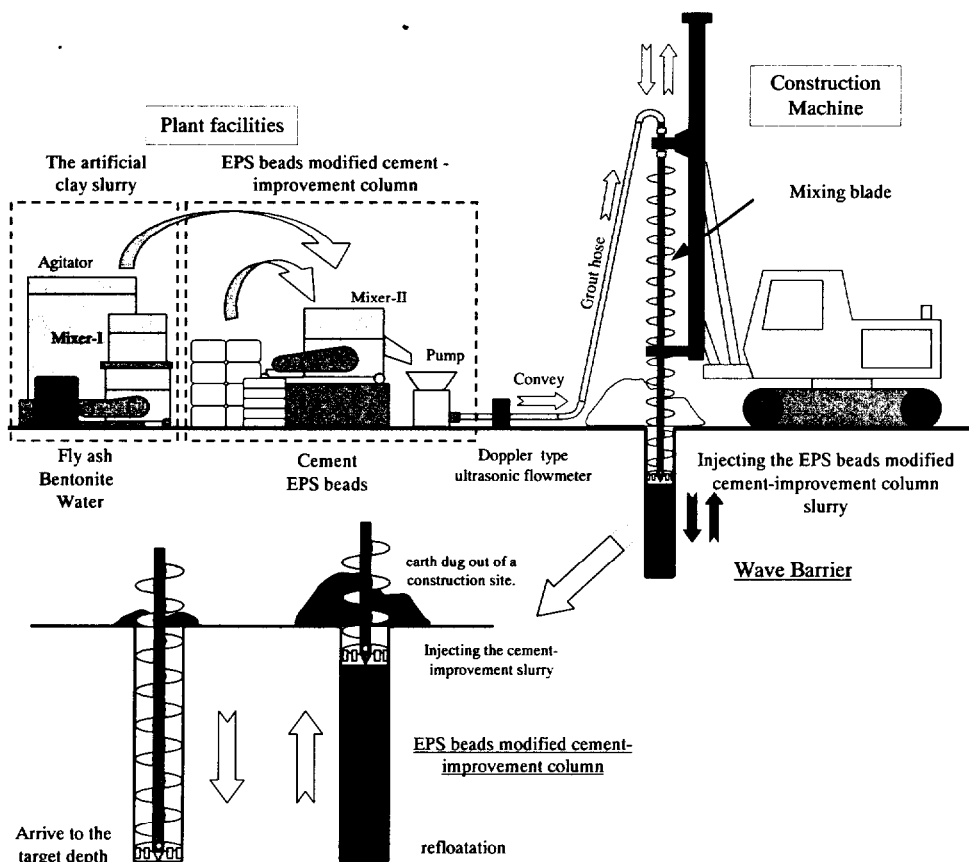
Figure 6.7 The configuration of equipment for construction method

1)Engineering condition (effect of wave barrier on the reduction of vibration)

- Effectiveness in reducing vibration at the target position.
- Evident information of mechanical and material properties of wave barrier (characteristics of stiffness and damping ratio)
- Reliability of wave barrier on the reduction of vibration

2)Execution

- Anti-separation of material
- pump-ability

3)Economical condition

- Low cost

In order to satisfy the above requests, the materials used in this study were cement, the artificial clay which has evident information of material property, and EPS beads such as light weight. The artificial clay used is composed of the fly ash and the bentonite because the consistency can be changed by the mixture proportion of them. The artificial clay can cling to EPS beads which float by buoyancy on account of its viscosity. In this study, the ratio of bentonite to fly ash (mass ratio) =

Table 6.2 Mixing proportion of improved soil

F:B	w_L (F+B) (%)	w (F+B) (%)	C (kg/m^3)	W/C (%)	ΣW (kg/m^3)	ρ_t (g/cm^3)
7:3	65	100	100	400	755	1.355

Table 6.3 Mixing proportion of EPS beads modified cement-improved column (per 1m^3)

φ600mm, @ 500mm		F	B	C	W	S-c	E	total	ρ_{ESC}
EPS20	m(kg)	273	117	56	613	1059	4.6	1064	1.064
L=1.65~1.80m	v(l)	124	45	18	613	800	200	1000	
EPS40	m(kg)	205	88	42	460	795	9.2	804	0.803
L=1.80~1.90m	v(l)	93	34	13	460	600	400	1000	
EPS60	m(kg)	137	58	28	307	530	13.8	544	0.544
L=1.90~2.00m	v(l)	62	22	9	307	400	600	1000	
	ρ(g/cm^3)	2.20	2.60	3.15	1.00	1.33	0.023		—

Symbol) F: Fly ash, B: Bentonite, C: Portland blast-furnace slag cement (B), W: Water,

S-c: Soil cement, E: EPS beads, ρ_{ESC}: Density of EPS beads modified cement-improved column

S-c: See Table 6.2

EPS beads: True specific gravity ρ_E = 0.023 g/cm^3, Bulk specific gravity ρ_E = 0.015 g/cm^3,

Average particle size: 3.8 mm

- 160 -

(a) EPS 20

(b) EPS40

(c) EPS60
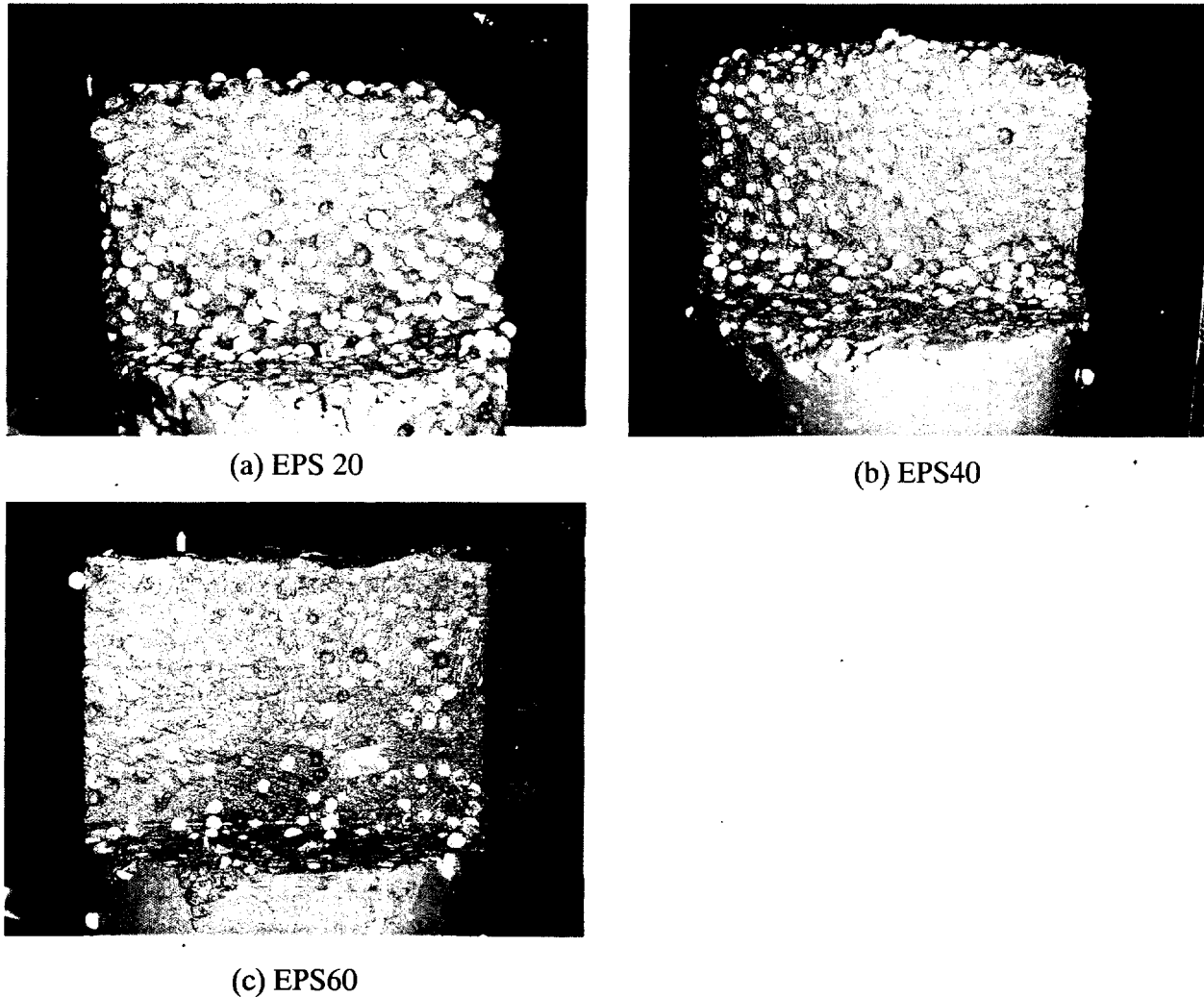
Figure 6.8 Cross section of test piece

7:3 was selected. In order to make the low strength material, the low volumes of cement added to the artificial clay. Owing to add high volumes of fly ash to the cement as a stabilizing agent, it is possible to perform uniform agitation and mixing in the low strength range (Asano et al., 1996). On the basis of the above conditions, the mixture ratio of the soil improvement slurry is listed in Table 6.2 and the mixing proportions of EPS beads modified cement-improved column slurry is listed in Table 6.3. The mixed percentages of EPS beads were 3 types, 20%, 40% and 60% in mass. The cross sections of test piece in laboratory test are showed in Figure 6.8. To estimate the properties of EPS beads modified cement-improved column sample, laboratory tests on samples of improved soil were carried out. The stiffness, together with the undrained shear strength, was determined through a series of unconfined compression tests. And cyclic triaxial tests were performed to measure the stiffness and the damping ratio of EPS beads modified cement-improved column.

(1) Unconfined compression test

Of prime importance in the design of the EPS beads modified cement-improvement is the stiffness of the improved soil. The test results in a stress-strain curve from which the undrained compressive strength and the modulus of deformation (E_{50}) can be deduced. An example of the results is presented in Fig. 6.9 and Table 6.4.
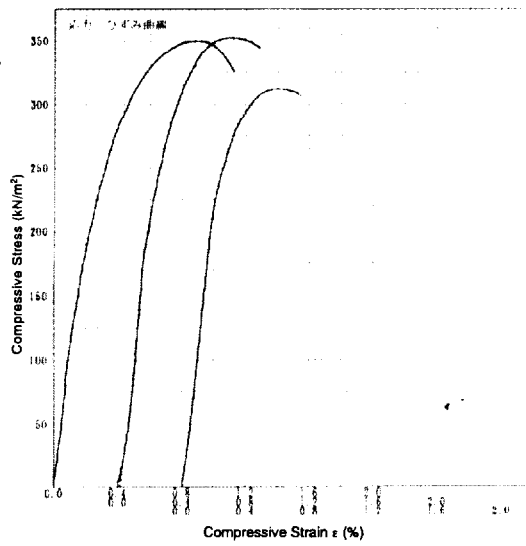
(a) EPS20
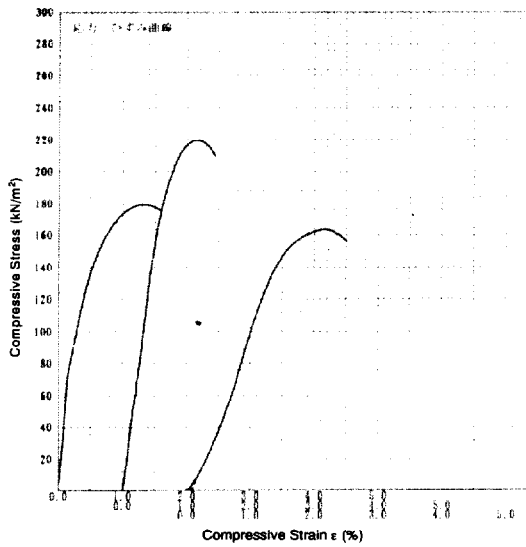
(b) EPS40
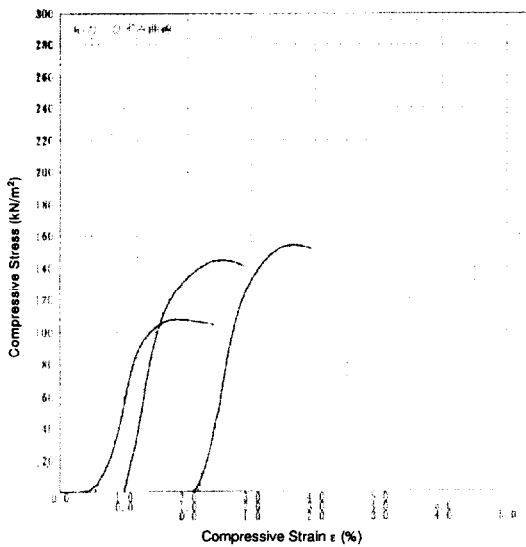
(c) EPS60

Figure 6.9 Typical examples of unconfined compression test on improvement sample

Table 6.4 Results of unconfined compression test on improvement sample

		Test Number			Average
		No. 1	No. 2	No.3	
EPS20	Height h (mm)	100	100	100	
	Interval diameter d (mm)	50	50	50	
	Mass m (g)	178.6	182.9	186.4	
	Wet density ρ_t (g/cm^3)	0.910	0.932	0.949	0.930
	Unconfined compressive strength q_u (kN/m^2)	350.12	352.61	312.08	338.27
	Failure strain ε_f(%)	0.89	0.68	0.61	0.73
	Modulus of deformation E_{50} (MN/m^2)	95.34	124.41	113.01	110.92
EPS40	Height h (mm)	100	100	100	
	Interval diameter d (mm)	50	50	50	
	Mass m (g)	135.5	114.3	135.7	
	Wet density ρ_t (g/cm^3)	0.690	0.582	0.691	0.654
	Unconfined compressive strength q_u (kN/m^2)	179.45	219.74	163.36	187.52
	Failure strain ε_f(%)	1.35	1.14	2.07	1.52
	Modulus of deformation E_{50} (MN/m^2)	36.76	31.46	10.52	26.25
EPS60	Height h (mm)	100	100	100	
	Interval diameter d (mm)	50	50	50	
	Mass m (g)	98.5	79.9	91.3	
	Wet density ρ_t (g/cm^3)	0.502	0.407	0.465	0.458
	Unconfined compressive strength q_u (kN/m^2)	107.91	144.74	153.87	135.50
	Failure strain ε_f(%)	1.25	1.57	1.55	1.46
	Modulus of deformation E_{50} (MN/m^2)	12.13	20.04	17.55	16.57

(2) Cyclic triaxial test to measure deformation properties

The cyclic triaxial test has been commonly used for the measurement of dynamic soil properties. The EPS beads modified cement-improvement column specimens were tested without saturation, and the confining pressure was set at 49 kN/m^2 during the tests to simulate the soil condition in the field. The cylindrical specimen size is 75 mm (diameter) $\times$ 150 mm (height). Specific properties of the improvement soil are shown in Table 6.5. All the tests were carried out on isotropically-consolidated specimens. The difference between the axial stress and the radial stress, i.e., the deviator stress, is applied cyclically under stress controlled conditions for this automated triaxial testing system. The axial displacement gauge is LDT. For one stage, a sinusoidal wave of about 0.1 Hz is applied about 6 times, and data processing is with the hysteresis loop of the 6th waves.

About eight different amplitudes of cyclic stress were used in multi-stage cyclic loading tests for on test series to obtain the stress-dependent shear modulus and damping in the wide range of strain amplitude between 10^{-5} to 10^{-2}. Figure 6.10 shows the relationship between shearing strain, g, and equivalent shearing modulus, G, and hysteresis damping constant, h. The wave number used for arranging is 6th wave. And Figure 6.11 shows a typical example of deviator stress versus axial strain for all cases at cyclic stress of approximately 15.0 kN/m^2 (the 7th step) and 0.5 kN/m^2 (the 2nd step), respectively. As for shown in these figures, the results of EPS20 have a high damping ratio and low shearing modulus in comparison with the result of EPS40. According to the observation in advance of test, EPS20 sample was already cracking because of insufficient filling material. It is likely that EPS20 sample used has a profound effect on the value of these parameters. Thus it is discussed by using these results except for the result of EPS20, hereafter. From this figure, it is confirmed that equivalent shearing modulus, G, and hysteresis damping constant, h, depend on shearing strain, and the dynamic characteristics of the EPS beads modified cement-improvement column showed the same non-linear tendency as soil improvement EPS0.

Table 6.5 Properties of the improvement soil using cyclic triaxial test

	EPS0	EPS20	EPS40	EPS60
Height h (mm)	150.00	172.00	173.45	170.00
Interval diameter d (mm)	77.00	77.03	76.93	77.40
Mass m (g)	936.40	770.50	580.34	380.32
Wet density ρ_t (g/cm^3)	1.341	0.961	0.720	0.475
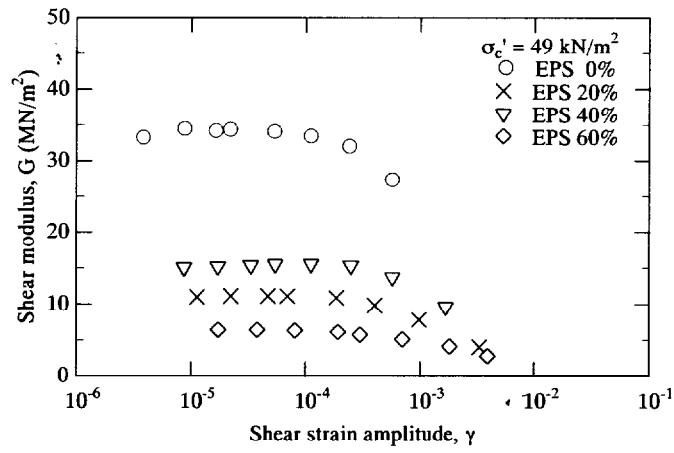
(a) Shear modulus, G, versus shear strain amplitude
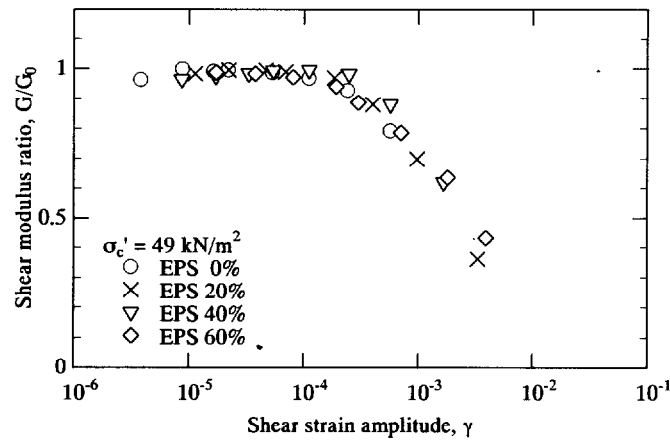
(b) Shear modulus ratio, G/G_0, versus shear strain amplitude
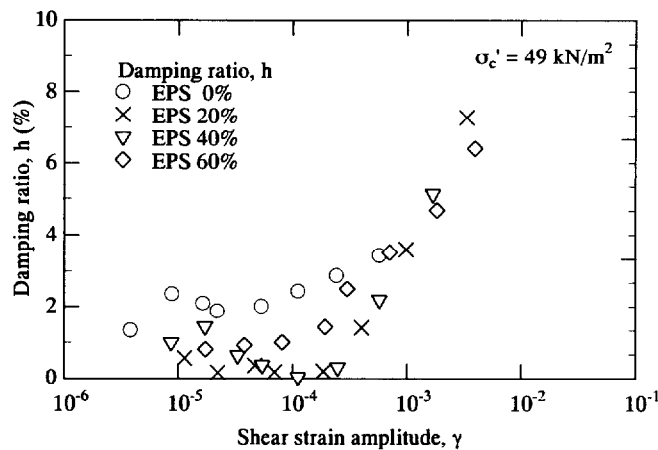
(c) Damping ratio, h, versus shear strain amplitude

Figure 6.10 The relationship between shearing strain, γ, and equivalent shearing modulus, G, and hysteresis damping constant, h.
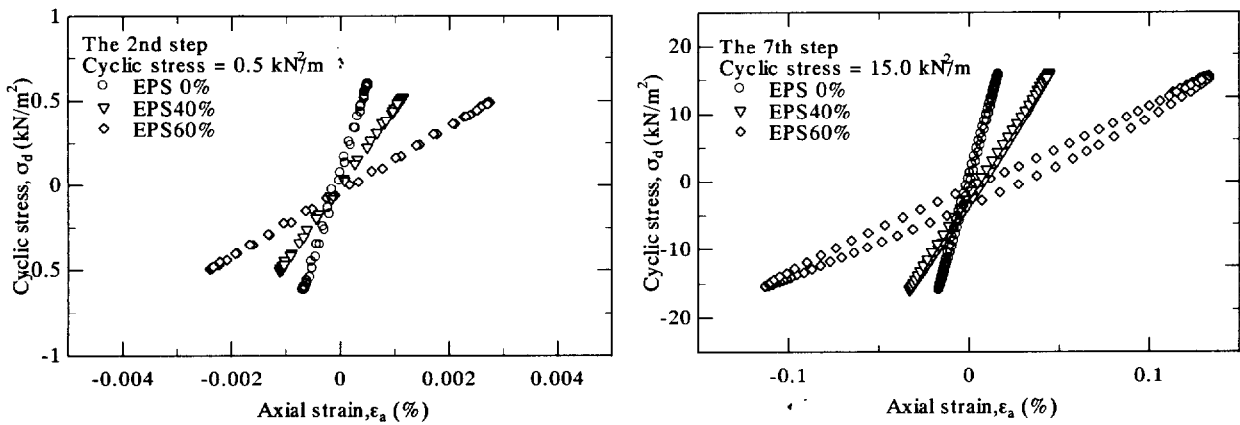
(a) The 2nd step loop (cyclic stress 0.5 kN/m^2)   (b) The 7th step loop (cyclic stress 15.0 kN/m^2)

Figure 6.11 Stress-strain loops of the 2nd and 7th step

6.4 EXECUTION

Three kinds of wave barrier, which were different mixed percentages of EPS beads as was described in section 6.3, were constructed at the field site. This section outlines instrumentation and procedures for constructing the wave barrier.

6.4.1 Instrumentation

(1) Soil improvement machine (Wave barrier construction machine)

The wave barrier construction machine used was a soil stabilizing rigs, NISSHA DHJ-12 manufactured by NIPPON SHARYO, Ltd. The general arrangement and major dimensions of this machine is shown in Figure 6.12. The specifications of this machine is listed in Table 6.6.

Table 6.6 Specification of the wave barrier construction machine

Dimensions	(unit : mm)
Overall width	2415
Crawler center to center distance	1870
Shoe width(steel made)	450
Tumblers center to center distance	2234
Ground clearance	380
Rear end radius	1980
Overall length in transportation	8567
Overall height in transportation	2714
Performance	
1) Rotary drive	
Torque	9.1 ~ 27.4 kN-m
Speed	18 ~ 110 rpm
Drive/extraction force	59.8 kN
Elevation speed	0.5 ~ 8.6 m/min
2) Mixing rod	
Length	6.6m + 2 ~ 5m
Hexagon	132 mm
Rod	ϕ 130

- 166 -
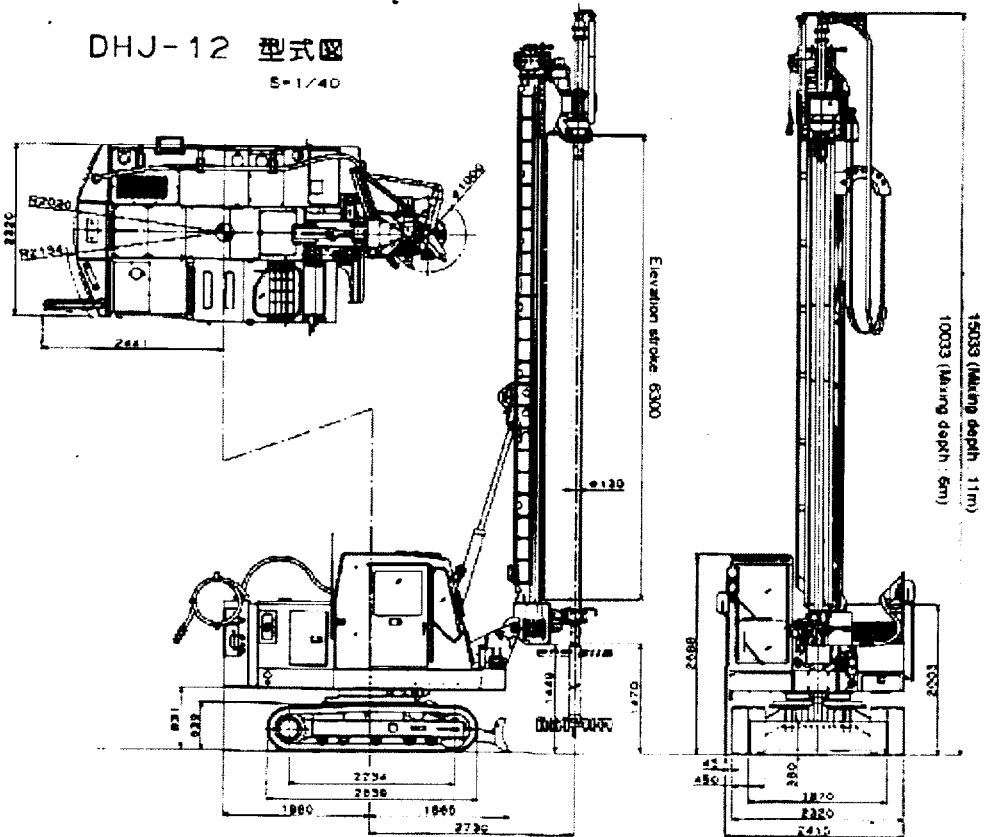
Figure 6.12 The soil improvement machine (wave barrier construction machine) DHJ-12

Figure 6.13 Mixer-I
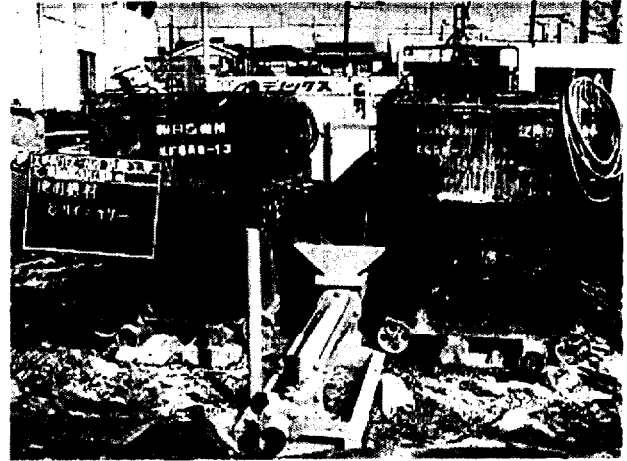
Figure 6.14 Mixer-II
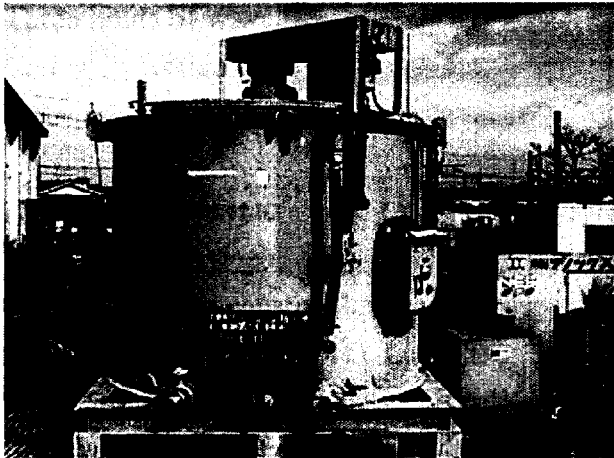
Figure 6.15 Agitator
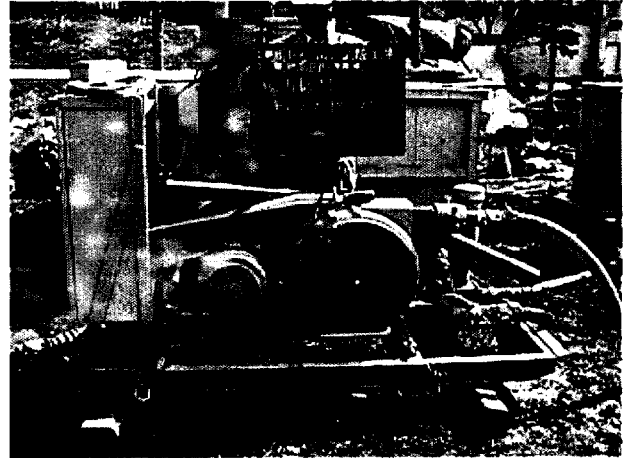
Figure 6.16 Tube pump
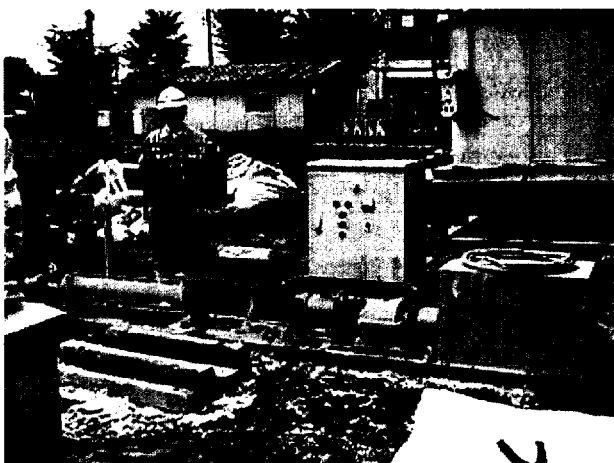
Figure 6.17 Nemo pump
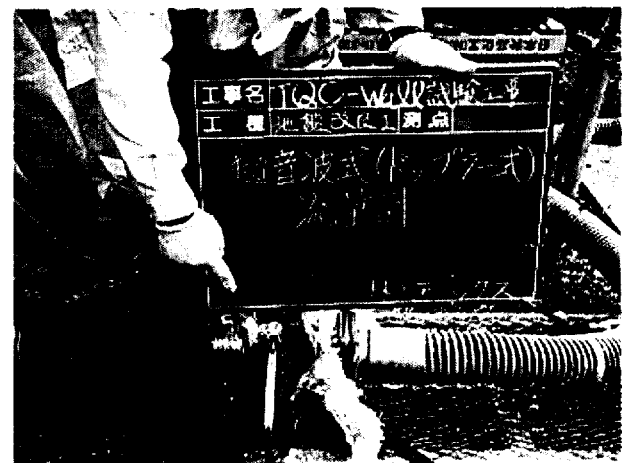
Figure 6.18 Flowmeter-II
(Doppler type ultrasonic flowmeter)

- 168 -
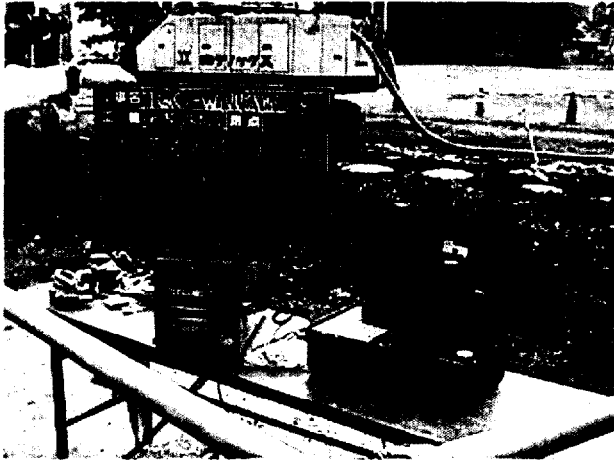
Figure 6.19 Flowmeter-II
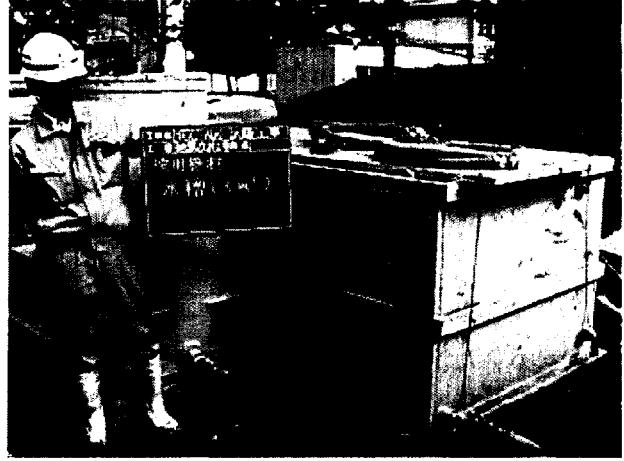
Figure 6.20 Tank
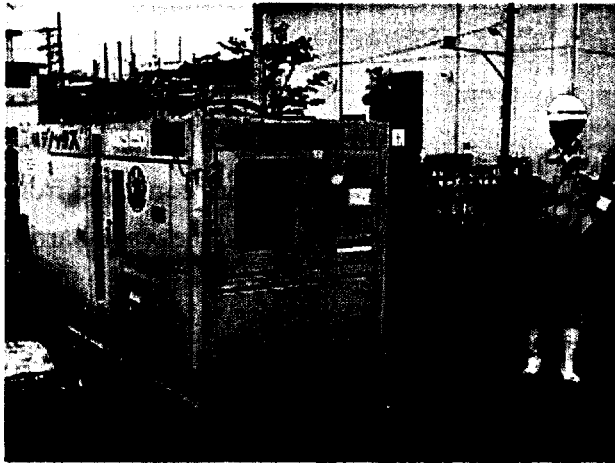
Figure 6.21 Generator

(2) Plant facilities

The plant facilities were used to mix the slurry of wave barrier material and to supply it to the wave barrier construction machine. The plant facilities used are shown as follows;

Mixer-I (Fig. 6.13): is the slurry mixer which mixes fly ash and bentonite with water.

Mixer-II (Fig. 6.14): is the moltal mixer which mixes EPS beads and cement with the slurry which was made by Mixer-1. In this study, two mixers of which capacity was 400 l were used.

Agitator (Fig. 6.15): is the storage which stores and agitates the slurry which was made by Mixer-I. Its volume capacity is 4 m³.

Pump-I (Fig. 6.16): is the tube pump used in this study.

Pump-II (Fig. 6.17): In order to be applied to a wide range of products from watery slurry to high viscosity, the NEMO pump (NM-50, HEISHIN NETZSCH Co., Ltd) was used in this study.

Flowmeter-I: In order to measure the flowing volume of the artificial clay slurry, the electric flow-meter was used.

Flowmeter-II (Fig. 6.18 and 19): The flowmeter, which can measure the flowing volume of EPS

beads modified cement-improved column slurry, used the Doppler type ultrasonic flow-

meter because the electric flowmeter could not measure the volume of flowing EPS

beads.

Tank (Fig. 6.20): This is the storage to store water. This volume capacity is 3 m^3.

Generator (Fig. 6.21): 150 kVA generator used.

6.1.1 Procedure

Figure 6.22 shows the flow chart of the composition of the field test plant. The procedure can be divided into three processes, as follows;

1) The process for making the artificial clay slurry (Fig. 6.23): In this process, Mixer-I and Agitator were used. The artificial clay slurry, which mixed fly ash and bentonite with water, was made by Mixer-I. After that, this slurry was stored and agitated by Agitator. Lastly, this slurry was conveyed from Agitator to Mixer-II through the flowmeter by pump. Flowmeter was measuring the flowing volume of slurry to verify a good stabilizing result.

2) The process for making the EPS beads modified cement-improved column (Fig. 6.24): In order to make the EPS beads modified cement-improvement slurry, Mixer-II was used in this process. Mixer-II mixed EPS beads and cement with the artificial clay slurry which was conveyed from agitator. After that, this slurry was conveyed and pressurized from Mixer-II to the wave barrier construction machine through the ultrasound transducer type flowmeter by the pump.
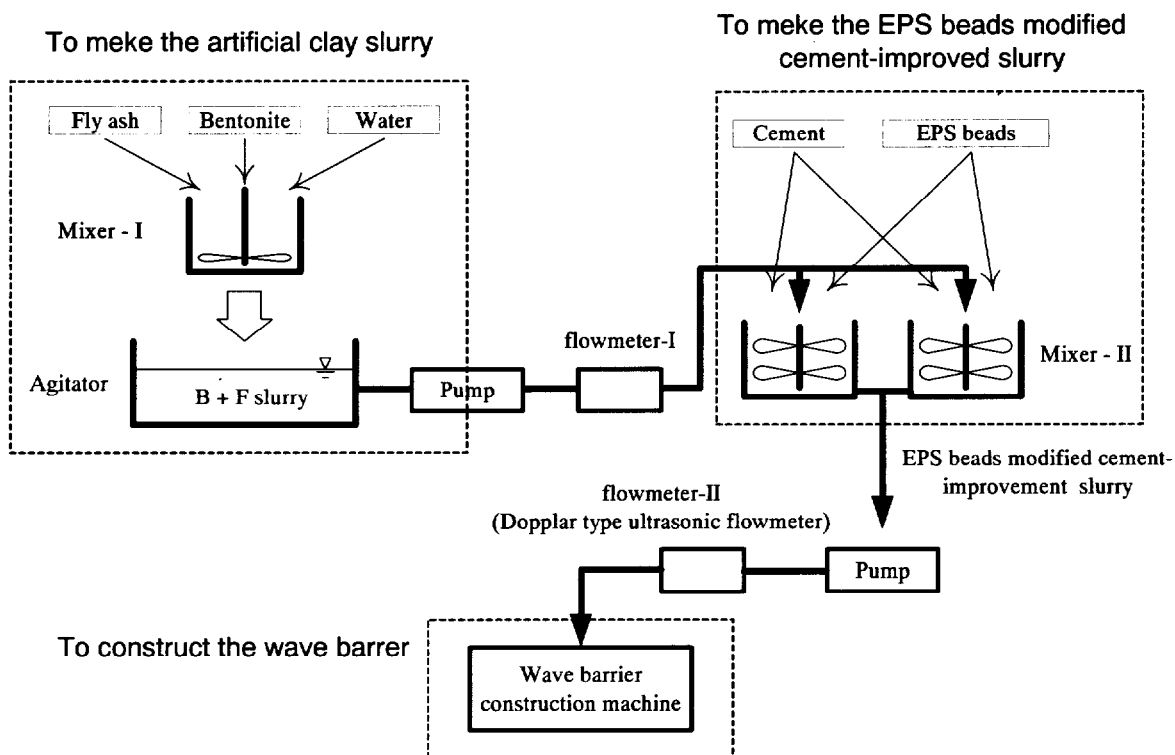
Figure 6.22 Flow chart of the composition on the field test

Figure 6.23 Mixed fly ash and bentonite with water

Figure 6.24 Mixed EPS beads and cement with the artificial clay slurry

Figure 6.25 Mixing blade penetrates to the target depth

3) The process for constructing the wave barrier: In this process, the wave barrier construction machine was used. The mixing blade is drilled down to the target depth and EPS beads modified cement-improvement slurry is added through an inner tube with an injecting at the mixing tool (Fig. 6.26). Overlapping of the columns is particularly important when the columns are installed for the reduction of vibration homogeneously. Installation sequence in overlapping columns to create interlocking column is given in Fig. 6.27 installing the columns in some formed.

The plan view of the constructing wave barrier is shown in Fig 6.28. The time schedule for the total works was approximately two weeks starting from October, 2001 (Table 6.7).

6.4.3 Control of column quality

Figure 6.29 shows the cross section of wave barrier in the case of EPS20. As a result of the observations, it was confirmed that the artificial clay did not segregate EPS beads and the quality of the wave barrier was good.

Figure 6.26 Injection of the EPS beads modified cement improvement slurry (completion)

(a) Condition before overlapping of the column   (b) Overlap each improvement column

Figure 6.27 Construction condition

Table 6.7 Time schedule

	October, 2001																
	15	16	17	18	19	20	21	22	23	24	25	26	27	28	29	30	31
	Mon	Tue	Wed	Thu	Fri	Sat	Sun	Mon	Tue	Wed	Thu	Fri	Sat	Sun	Mon	Tue	Wed
Constitution	■																
Construct EPS20			■					■									
Construct EPS40				■					■								
Construct EPS60					■					■							
Another test											■	■					
Dismantle															■		
Level the land																	■

Figure 6.28 Completion condition of constructed wave barrier
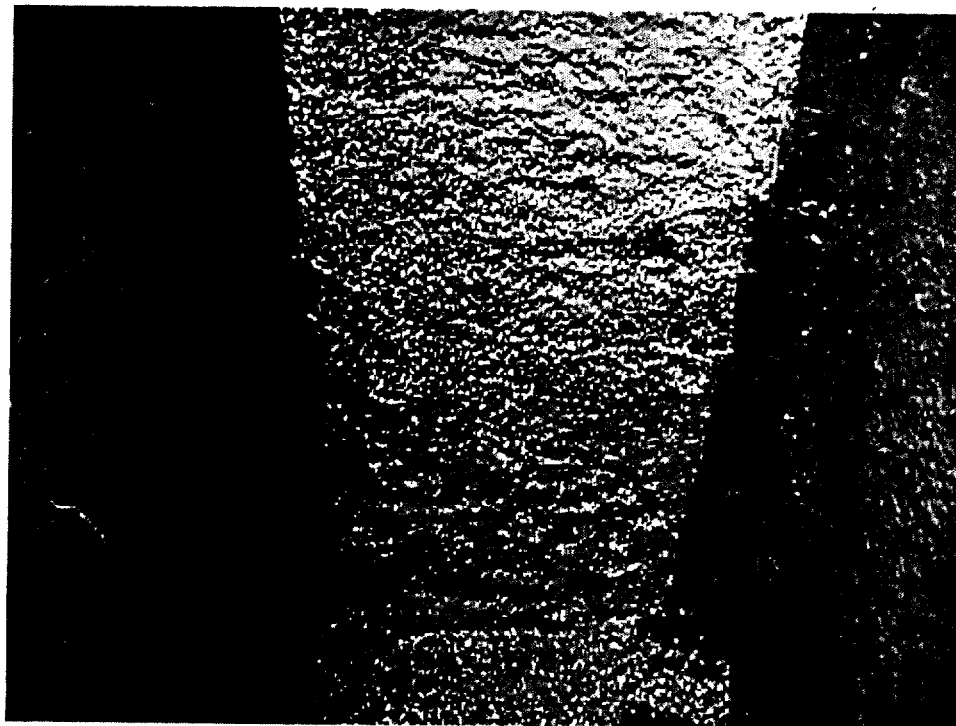
Figure 6.29 Quality of wave barrier (Cross section of EPS20 barrier)

6.5 VIBRATION TESTING

6.5.1 General

The prime results of measurement which was recorded in the surrounding ground before and after the countermeasures are described in this section. Some information such as the influence of the countermeasures on the reduction of vibration is also presented. This section focuses on the explanation about the instrumentation of the vibration testing and discusses the experiment results.

6.5.2 Instrumentation

(1) Vibration exciter

A vibration exciter generates steady sinusoidal force, the frequency of which is changed in a step-by-step manner. In the vibration exciter, the mechanism of a generating vibration is "synchronous reverse rotation mass" or "slide mass", generally. In this study, "synchronous reverse rotation mass" type was used (EX-1000DC, Itoh precision Co., Ltd.). The general arrangement and principal di-

Figure 6.30 Vibration exciter (EX-1000DC, Itoh precision Co., Ltd.)

Table 6.8 Specifications of the vibration exciter

Designation	EX-1000DC (Itoh precision Co., Ltd.)
Mass (kg)	3000
Dimension (mm)	1524 (L) × 1524(D) × 1200(H)
Excitation direction	Vertical
Frequency range (Hz)	2 ~ 30
Excitation mechanism	Reverse-rotation-mass

mensions of the machine is shown in Fig. 6.30. The specification of the machine is listed in Table 6.8. In addition, in order to be modeled by the spread foundation, this vibration exciter was set up on the concrete foundation, of which dimension is 1.5 m in wide, 1.5 m in breadth, 0.4 m in height, and 22.05 kN in weight.

(2) Measurement sensor

Velocity meter (Fig 6.31): In order to measure the vertical and horizontal vibration at ground, the velocity meter was used in this study. The velocity meter used is VSE-15 servo seismometers (Tokyo Sokushin Co., Ltd.). The VSE-15 servo seismometers have been developed to provide accurate measurement of velocity. Characteristics of this velocity meter are high sensitivity, wide dynamic range, and able to measure both velocity and acceleration signal outputs. The specifications are listed in Table 6.9.

Accelerometer (Fig. 6.32): The motion of the vibration exciter was detected by the piezo-electronic accelerometer PV-85 (Rion Co., Ltd) which provided data on the vertical and horizontal accelerations. This specification is listed in Table 6.10.
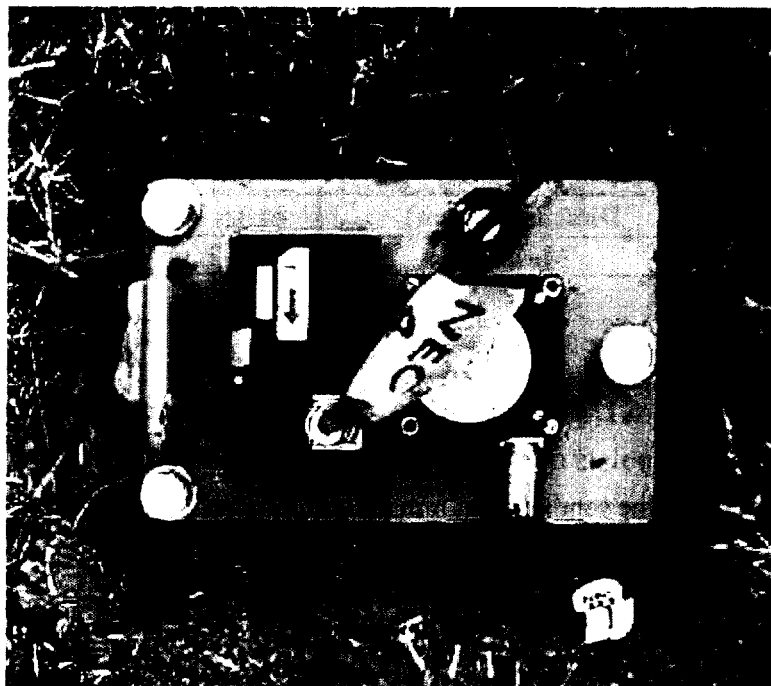
Figure 6.31 Velocity meter (VSE-15, Tokyo Sokushin Co., Ltd.)

Table 6.9 Specifications of the velocity meter

Model	VSE-15 (Tokyo Sokushin Co., Ltd.)
Dimension (mm)	ϕ 49 × 57
Frequency range (Hz)	0.07 ~ 100
Maximum Measurement (kine)	100
Sensitivity (mV / kine)	100

Figure 6.32 Accelerometer (PV-85, Rion Co., Ltd.)

Table 6.10 Specifications of the accelerometer

Model	PV-85 Rion Co., Ltd.
Electrical charge sensitivity $(pC/m \cdot s^{-2})$	6.4
Frequency range (Hz)	1 ~ 7000
Resonance frequency (kHz)	Over 24
Dimension (mm)	$\phi 18.5 \times 17.0$
Mass (g)	2.3

6.5.3   Test procedures

The test site is shown in Fig. 6.1. The layout consists of the vibration exciter, concrete foundation, wave barrier, and 14 pickup points of each wave barrier. The concrete foundation under the vibration exciter was installed on the sand of 20mm in height to represent a rough condition. The motion of the vibration exciter was detected by the piezo-electronic accelerometer (PV-85, Rion Co., Ltd, in section 6.5.2 (2)). And the motion of the ground vibration was detected by servo velocity meters (VSE-15, Tokyo Sokushin Co., Ltd., in section 6.5.2 (1)) which provided data on the vertical and horizontal velocities at different locations on the ground surface, as shown in Fig. 6.33. The dynamic load, harmonically varying with time and operational frequency of 5 Hz, 10 Hz, 15 Hz, 20 Hz, 25Hz, and 30Hz, are applied on the foundation. The motion was recorded for 4 second after vibration keeps its equilibrium. The vibration tests in the case without barrier were carried out at October 9- 11, 2001, before constructing a wave barrier. The wave barrier was constructed between October 17 -24. After the construction of the wave barrier, which cures over 28 days, the vibration tests in the case with barrier were carried out at November 26 -28, 2001. The weather conditions from October 2001 to November 2001 are shown in Fig. 6.34. From the observation of the trial boring test, it is found that ground water table was located under Kanto loam layer. It is likely that the condition of Kanto loam was unsaturated.
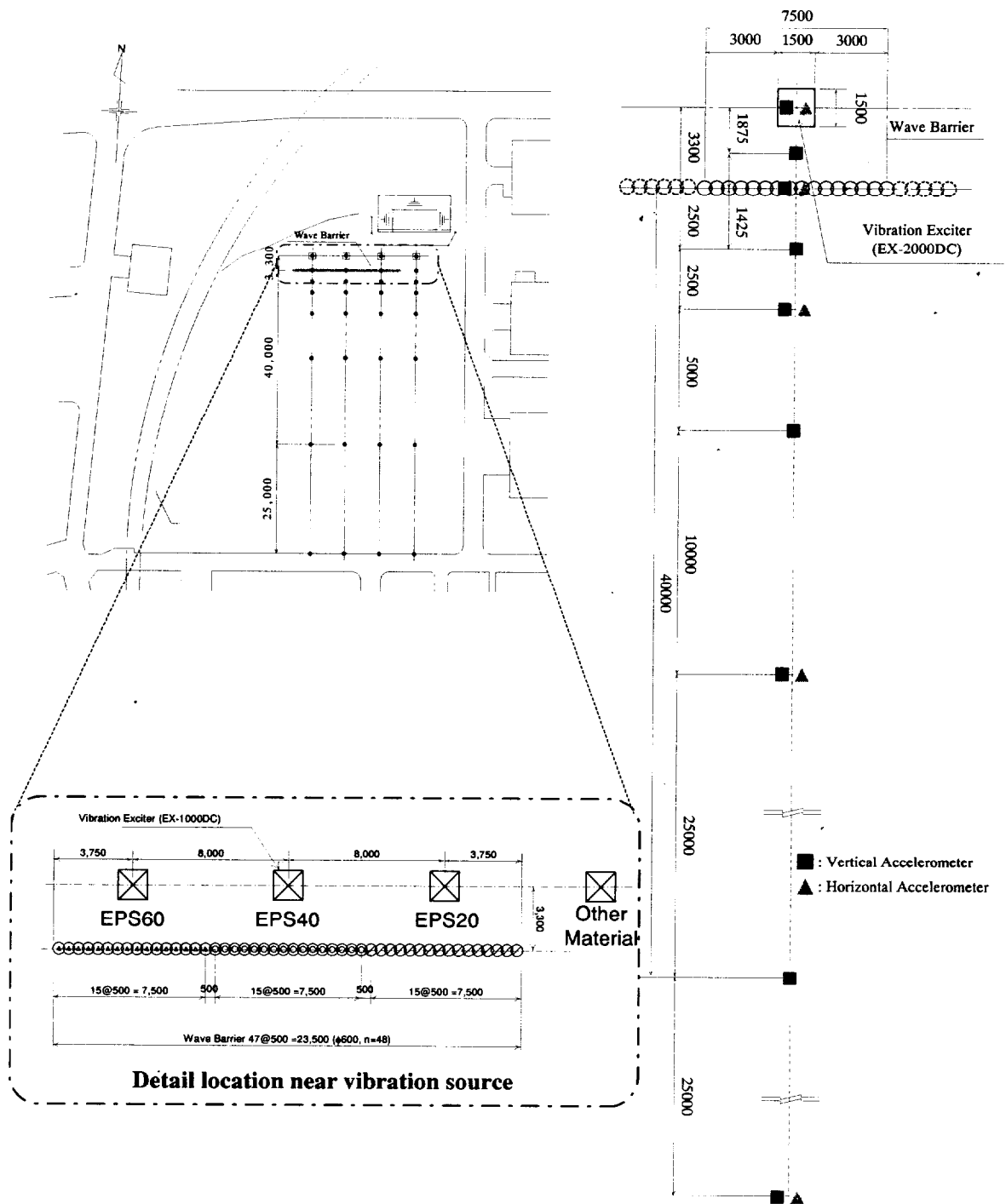
Figure 6.33 Measurement location

October, 2001

SUN	MON	TUE	WED	THU	FRI		
	1	2	3	4	5		
	8				12		
15	16	17	18	19			
22	23	24	25	26			
29	30	31					

November, 2001

SUN	MON	TUE	WED	THU	FRI		
				1	2		
5	6	7	8	9			
12	13	14	15	16			
19	20	21	22	23			
29	30						

■ : measure ground vibration before constructing wave barrier   ■ : measure ground vibration after constructing wave barrier

: Constructing wave barrier
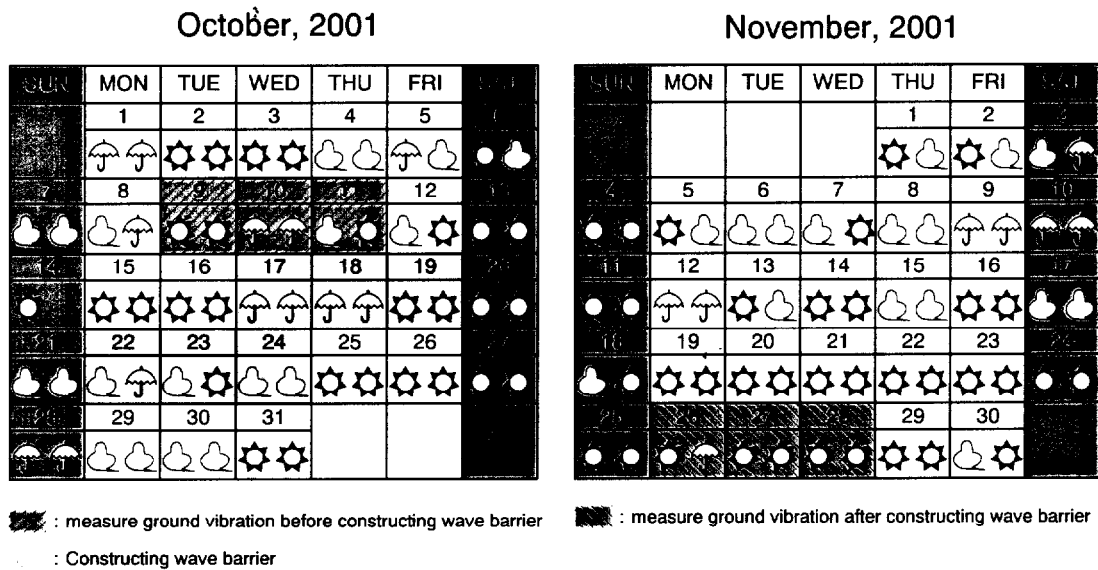
Figure 6.34 Weather conditions from October, 2001 to November, 2001 (CRC Solutions Co.)

6.5.4 Test results and discussions

First of all, the accelerometers before constructing wave barrier could not record some data which located over 13.3m from source, with the exception of other constructing wave barrier location as shown in Fig. 6.33. Hence the effect of wave barrier on the reduction of vibration can be shown only from under 8.3 m.

(1) Characteristics of wave propagation at test site

The motion of the ground vibration was recorded by the velocity-meter. As for the recording data on the ground surface, time history of velocity is transformed into the velocity amplitude of ground motion by FFT. Moreover, the velocity amplitude is transformed into the acceleration amplitude of ground motion as the following equation;

$$A_{amp} = V_{amp} \cdot 2\pi \cdot f_{input} \quad\quad\quad\quad\quad\quad\quad\quad\quad\quad\quad (6.1)$$

in which

A_{amp}: acceleration amplitude (m/s^2), V_{amp}: velocity amplitude (m/s), f_{input}: input frequency (Hz). Figure 6.35 shows typical examples of acceleration time histories and FFT results in the case of EPS60. Figure 6.36 shows amplitude-decay curves observed in the field at the four locations, together with the theoretical attenuation line predicted by Eq. (2.2) (Bornitz, 1931)

The black curve represents attenuation of surface wave (n = 2), and the gray curve represents attenuation of body wave (n = 0.5). Additionally solid lines mean including both geometrical and material damping (h = 0.05), and dotted lines mean only geometrical damping (h =0). It is important to note the difference between the condition given by Eq (2.2) and test conditions. To more precise, this equation does not take into account the wave propagation in layered media which becomes extremely complicated because the reflected and refracted waves are generated at the
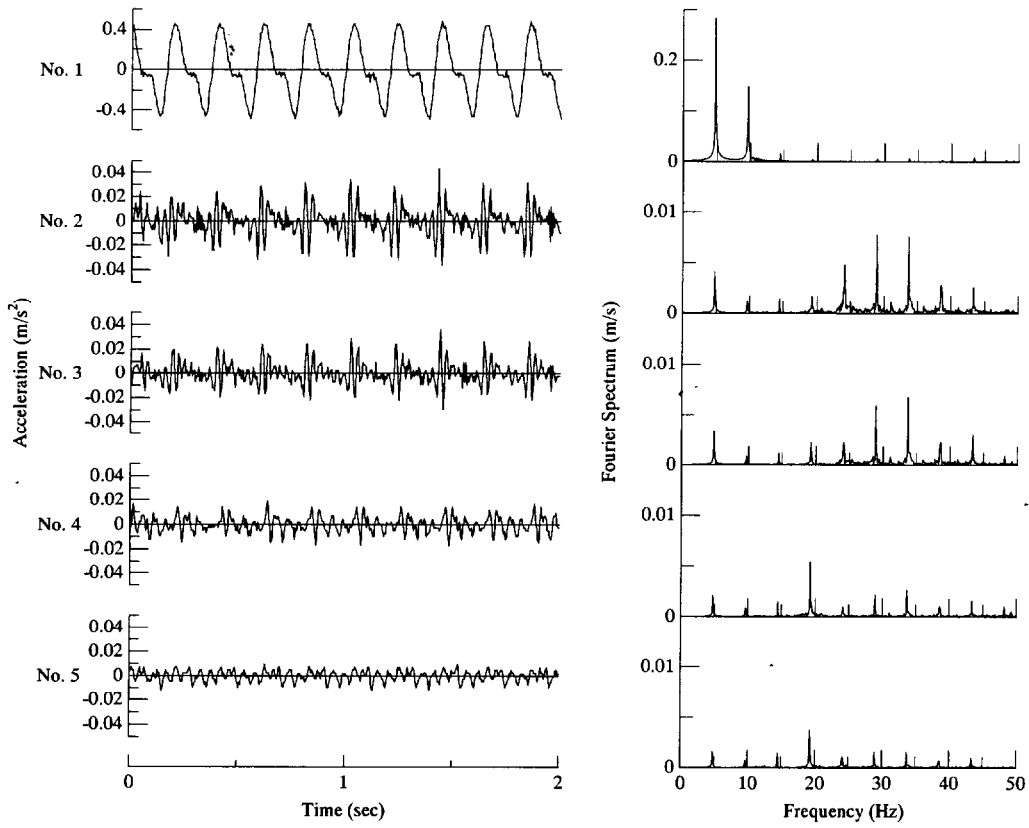
(i) Inputted frequency of 5 Hz
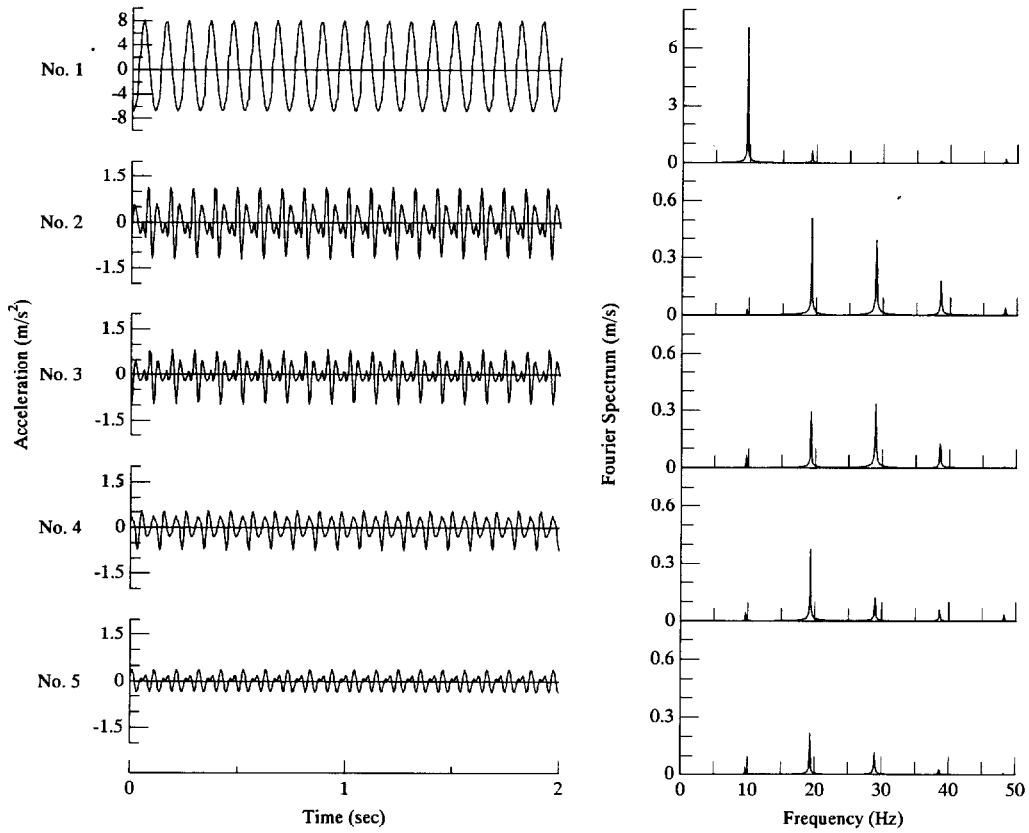
(ii) Inputted frequency of 10 Hz
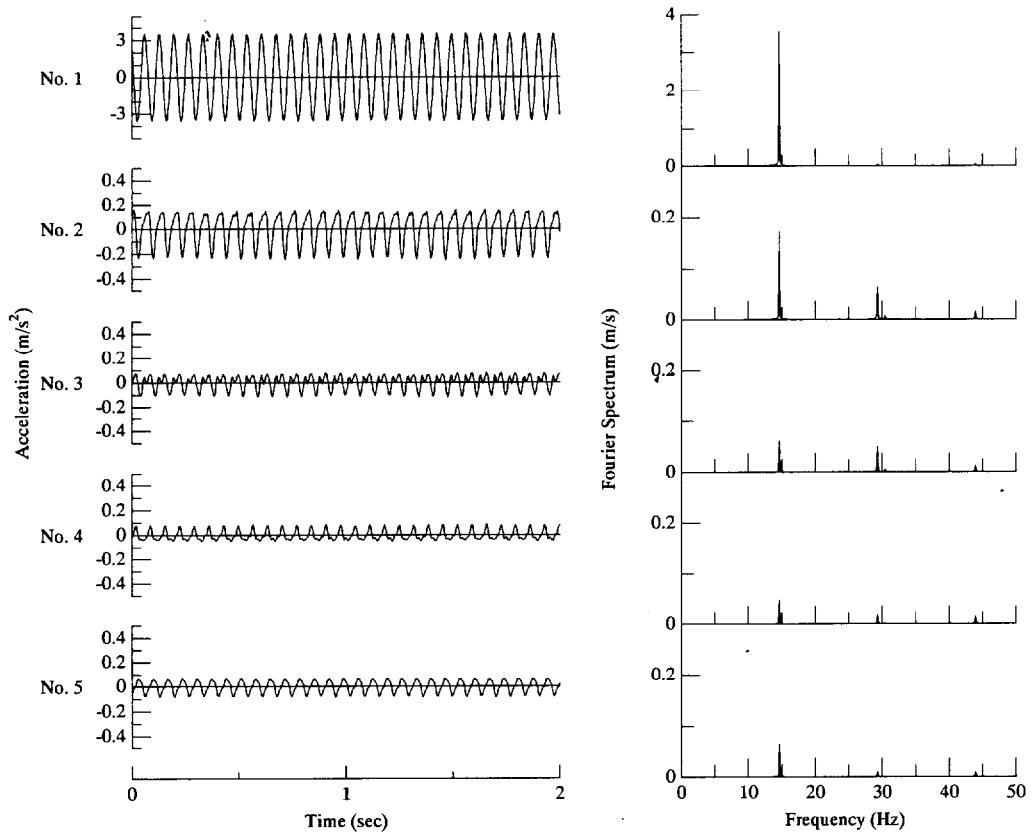
(iii) Inputted frequency of 15 Hz

(iv) Inputted frequency of 20 Hz

- 180 -
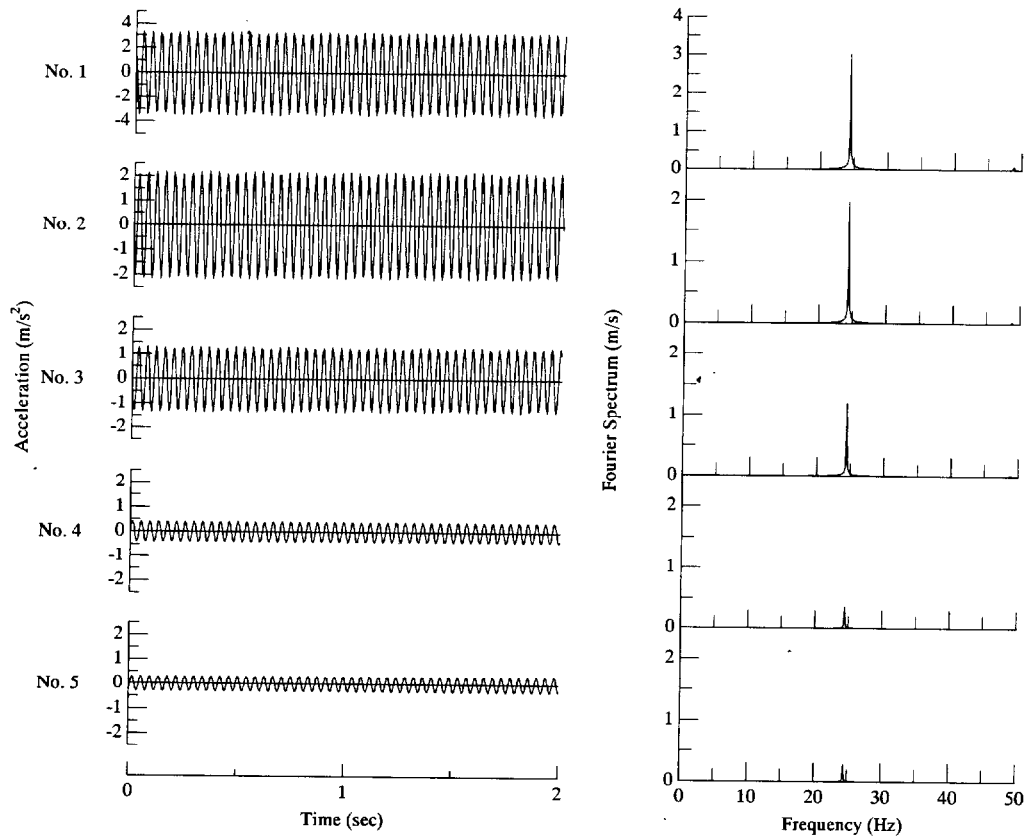
(v) Inputted frequency of 25 Hz

(vi) Inputted frequency of 30 Hz

Figure 6.35 Typical examples of acceleration time histories and FFT results
(Location of H = 1.9m, before constructing wave barrier of EPS60)

$$A(r) = A(r_1)\left\{\frac{r_1}{r}\right\}^n \times \exp[-\alpha(r-r_1)]$$

with $\alpha = \dfrac{2\pi f h}{V}$

$h = 0$

$\left\{\begin{array}{l} \text{------} : n = 2 \text{ (body wave)} \\ \text{------} : n = 1/2 \text{ (surface wave)} \end{array}\right.$

$h = 0.05$

$\left\{\begin{array}{l} \text{------} : n = 2 \text{ (body wave)} \\ \text{------} : n = 1/2 \text{ (surface wave)} \end{array}\right.$

5 Hz
- ◇ H=1.6m
- ○ H=1.7m (EPS20)
- △ H=1.8m (EPS40)
- □ H=1.9m (EPS60)

(i) Inputted frequency of 5Hz

10 Hz
- ◇ H=1.6m
- ○ H=1.7m (EPS20)
- △ H=1.8m (EPS40)
- □ H=1.9m (EPS60)

(ii) Inputted frequency of 10Hz

15 Hz
- ◇ H=1.6m
- ○ H=1.7m (EPS20)
- △ H=1.8m (EPS40)
- □ H=1.9m (EPS60)

(iii) Inputted frequency of 15Hz

20 Hz
- ◇ H=1.6m
- ○ H=1.7m (EPS20)
- △ H=1.8m (EPS40)
- □ H=1.9m (EPS60)

(iv) Inputted frequency of 20Hz

(v) Inputted frequency of 25Hz

(vi) Inputted frequency of 30Hz

Figure 6.36 Amplitude-decay curves together with theoretical curves in condition of half-space ground

interfaces. Thus it is clear that test result does not fit the equation because of a shallow layer, which is 1.5 m ~ 2.0 m thick at the upper layer. Nevertheless, almost results exist within the range from the attenuation curve of surface wave (n = 1/2) to attenuation curve of body wave (n = 2).

If the upper layer of a horizontally layered half-space has wave velocities lower than those of the second layer, a critical angle of incidence can be found for a wave which originates at the surface and intersects the interface. The refracted wave which is generated by the critically incident wave travels parallel to the interface in the lower medium, as shown in Fig. 6.37(a). From the ray theory, it would not be expected that this critically refracted wave could be detected at the surface. However, it can be shown by elasticity theory that the refracted wave causes a disturbance along the interface and that this disturbance generates a wave in the upper medium (Fig. 6.37(b)).Travel time equations can be written for the direct wave and the refracted (head) wave. The travel-time equation of direct wave can be written as,

$$T_1 = \frac{x}{V_1} \quad \text{.. (6.4)}$$

in which T_1 is the travel time of the direct wave, V_1 is the velocity of the upper layer, and x is the

- 183 -
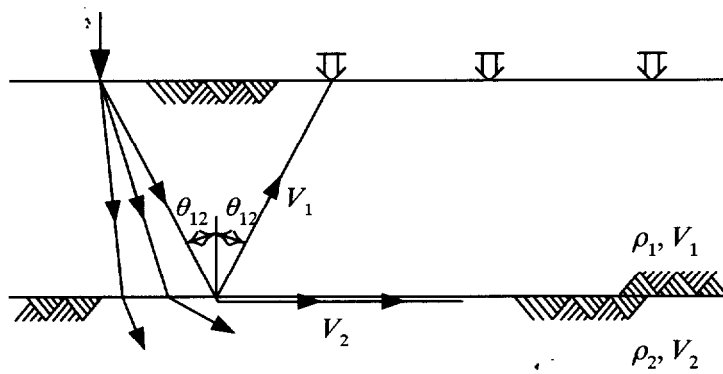
(a)
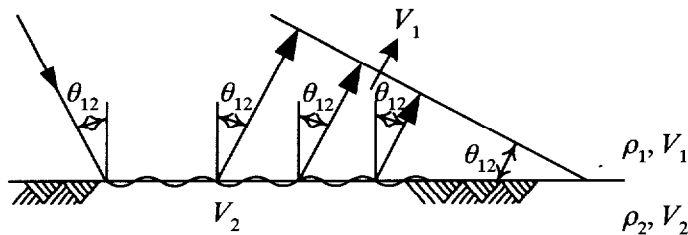
(b)

Figure 6.37 Head wave generated by critically refracted wave.
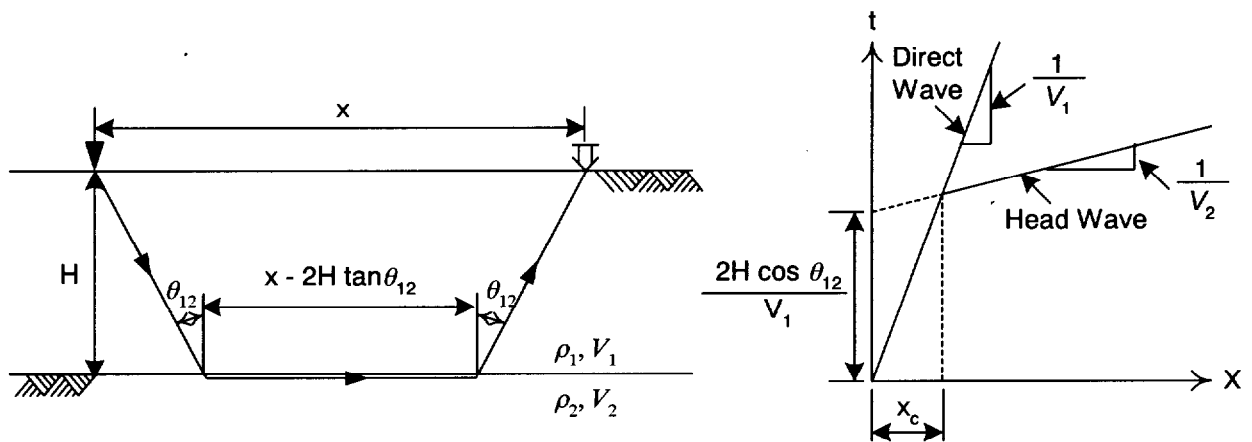
Figure 6.38 Ray paths and travel time curve for direct wave and head wave

$H =$
$1.5 \sim 2.0$ (m)

$\rho_1 = 1.8$ (g/cm^3)
$V_1 = 160$ (m/s)

$\rho_2 = 1.9$ (g/cm^3)
$V_2 = 400$ (m/s)
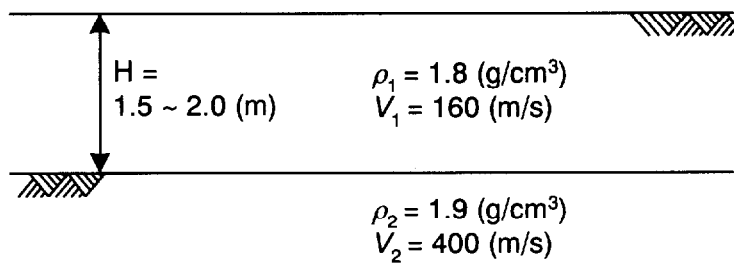
Figure 6.39 The information of field site (Yoshioka and Ashiya, 1990)
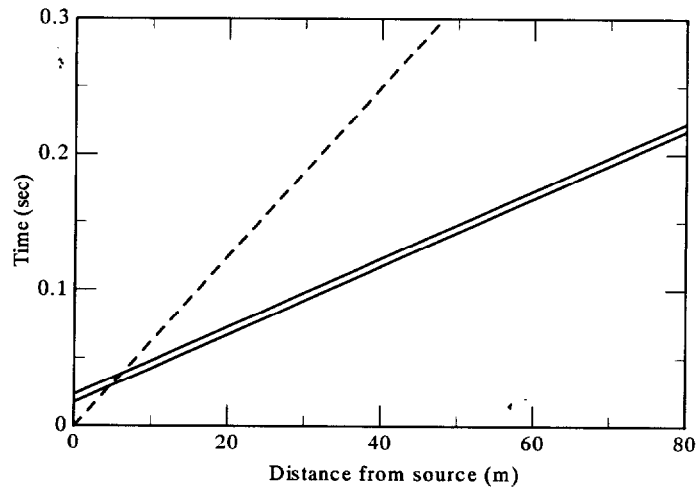
Figure 6.40 The travel time curve at this site
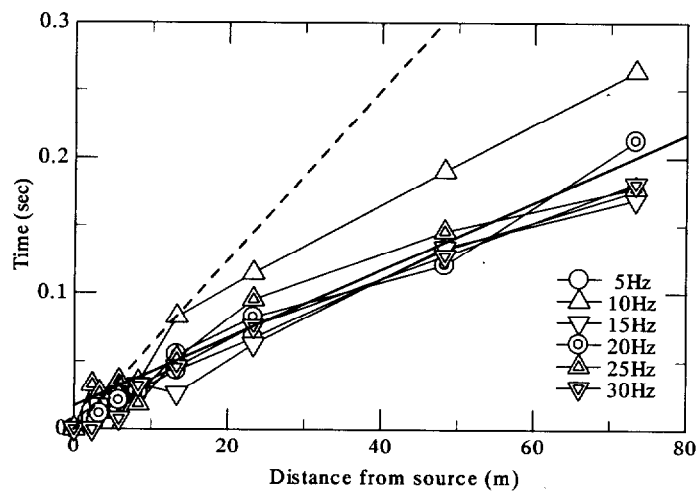
Figure 6.41 Travel time curve making phase angle of FFT, together with theoretical travel time curve

distance from source. For the travel time of head wave T_2,

$$T_2 = \frac{2H \cos\theta_{12}}{V_1} + \frac{x}{V_2} \quad\quad\quad\quad\quad\quad\quad\quad\quad\quad\quad\quad\quad\quad\quad (6.5)$$

where,

$$\theta_{12} = \sin^{-1}\left(\frac{V_1}{V_2}\right)$$

in which H is the thickness of upper layer, Literature Cited$_{12}$ is the critical angle of incidence, and V_2 is the second layer (Fig. 6.38). In this case, V_1, V_2, and H are already known by Yoshioka and Ashiya (1990); $V_1 = 160$ m/s, $V_2 = 400$ m/s, and $H = 1.5 \sim 2.0$ m as shown in Fig. 6.39. Thus the travel time of direct wave T_1 can be written;

$$T_1 = \frac{x}{160}$$

and travel time of head wave T_2 can be written;

$$T_2 = \frac{2 \times (1.5 \sim 2.0) \times 0.917}{160} + \frac{x}{400}$$

The travel time curves for both direct and head waves are plotted in Fig. 6.40. The distance from the source to the point at which the direct wave and the head wave arrive at the same time is called crossover distance. In this case, the crossover distance is from 4.59m (at $H = 1.5$m) to 6.11m (at $H = 2.0$m). It is found that head wave is recorded from almost measuring locations. The travel time at field site is determined from the phase angle which can be obtained by transforming acceleration into the frequency domain by using FFT. Figure 6.41 shows the calculated results, together with the theoretical travel curves shown in the gray thick solid line. Because the precision of phase angle is rough, plotted results by travel time curve from test have a wide range. However, it appears that the trend of travel time curve for head waves is good agreement with theoretical prediction.

(2) *Effect of wave barrier on the reduction of vibration*

Figures 6.42, 6.43, and 6.44 show the measured vibration amplitudes with and without wave barrier, for various input frequencies and various wave barriers (EPS20, EPS40, and EPS60), respectively. In order to facilitate the comparison of the test data, the vibration amplitudes are normalized by the value which measured input accelerometer. In spite of some scatter of the test data, the reduction efficiency of the wave barrier is apparent. Figure 6.45 shows the effect of wave barrier on the reduction of vibration. The reduction efficiency is expressed in term of the relative vibration

(a) Without barrier   (b) With barrier
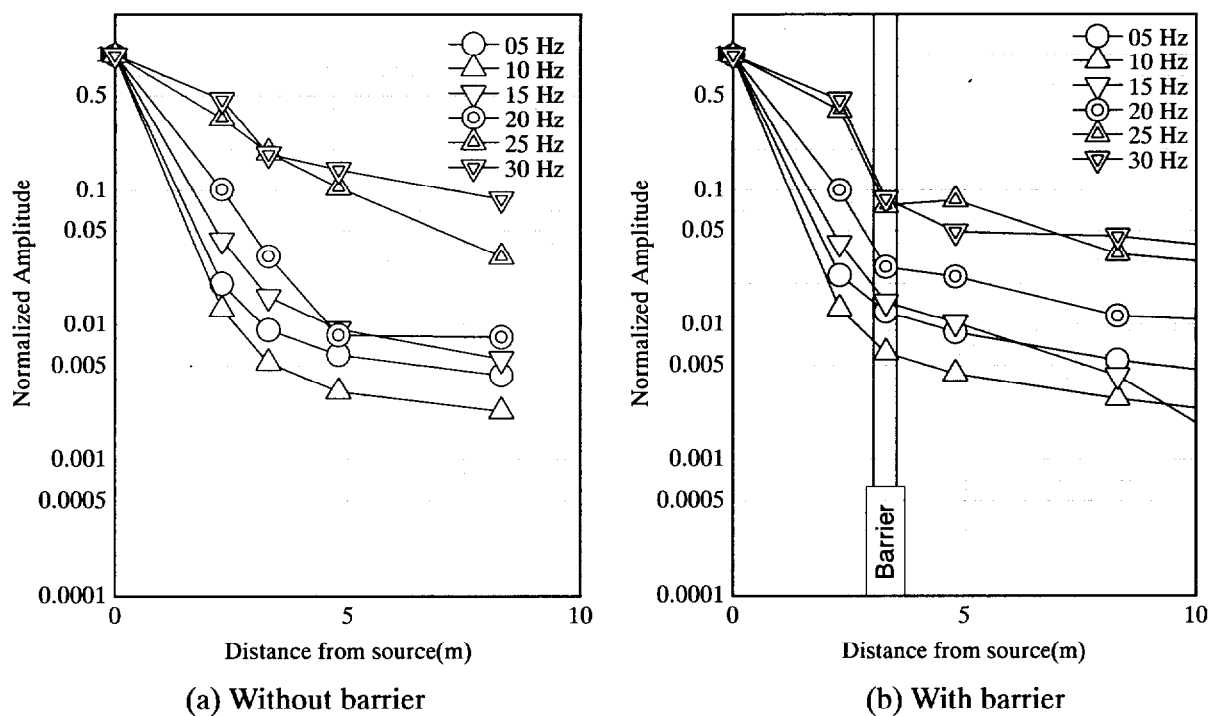
Figure 6.42 Normalized vertical vibration amplitudes (logarithmic scale) as a function of the distance from the vibrator, with and without barrier, in the case of EPS20

(a) Without barrier   (b) With barrier
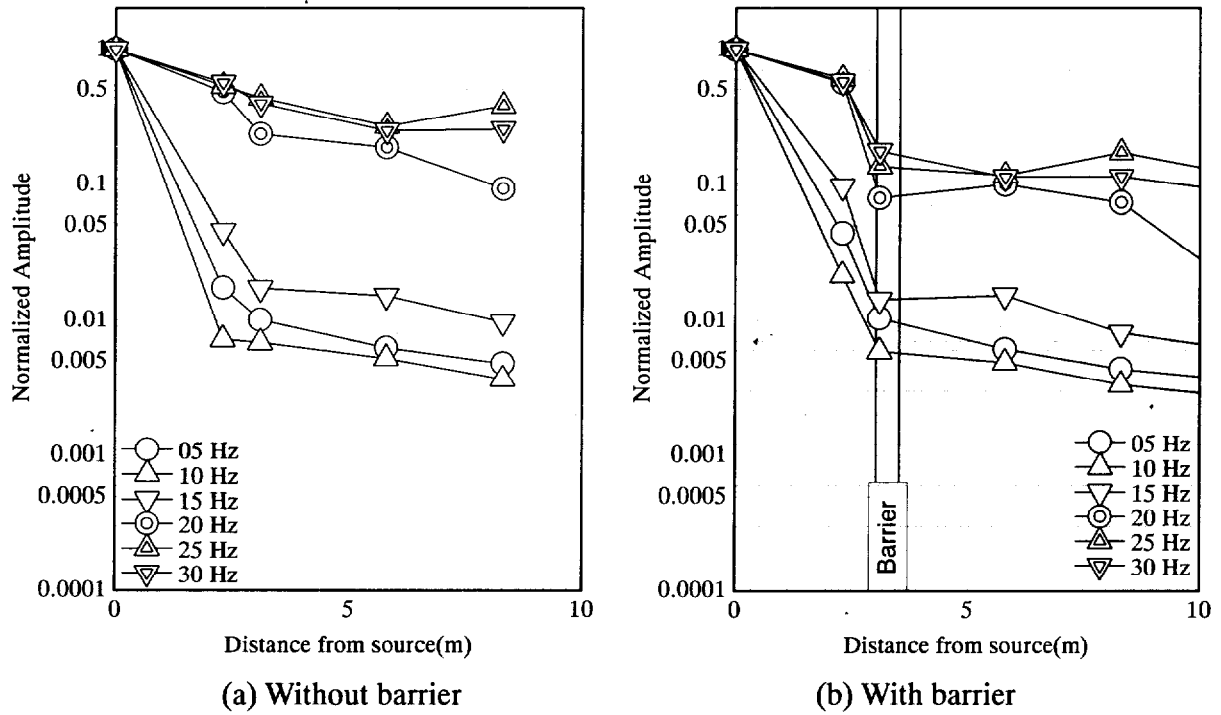
Figure 6.43 Normalized vertical vibration amplitudes (logarithmic scale) as a function of the distance from the vibrator, with and without barrier, in the case of EPS40

(a) Without barrier   (b) With barrier
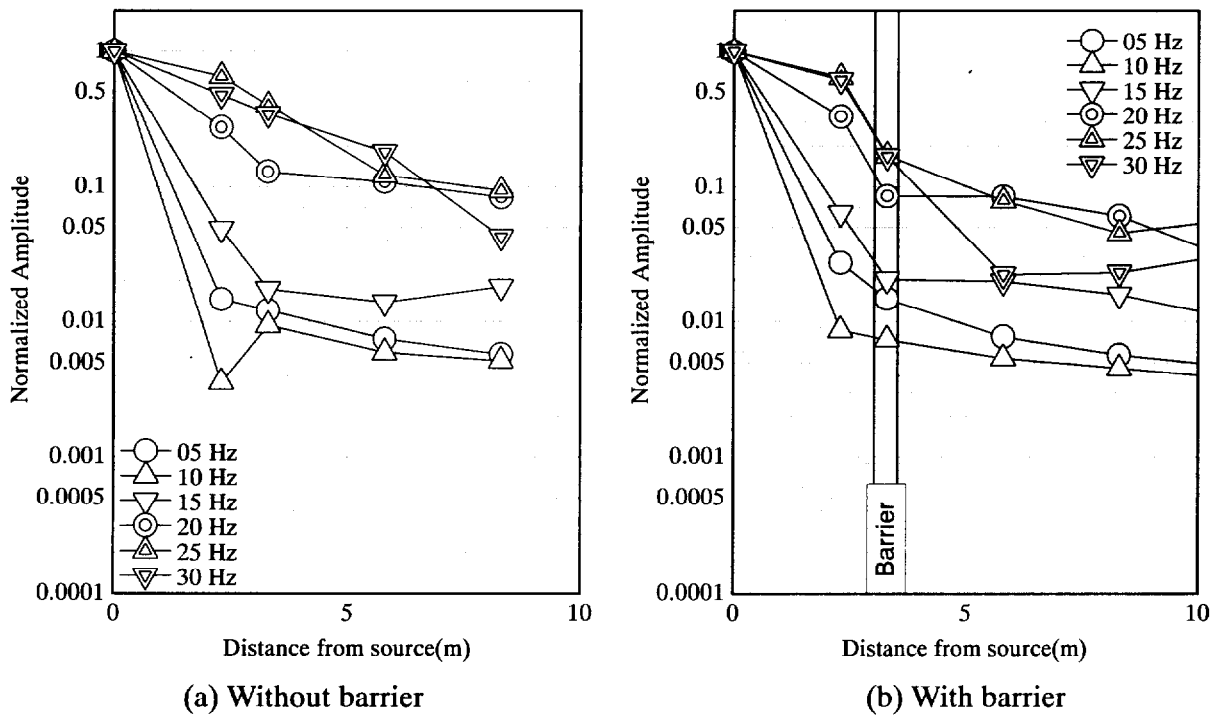
Figure 6.44 Normalized vertical vibration amplitudes (logarithmic scale) as a function of the distance from the vibrator, with and without barrier, in the case of EPS60

reduction level L_{rv}, as a distance from the source. The relative vibration reduction level (L_{rv}) is defined as,

$$L_{rv} = 20 \times \log\left(\frac{\text{Normalize Amplitude with Barrier}}{\text{Normalize Amplitude without Barrier}}\right) \quad (dB) \quad \text{..........................} (6.6)$$

It is clear from these figures that the vibration reduces behind barrier in some input frequencies. In the cases of EPS40 and EPS 60, some cases such as the input frequencies of 20, 25, and 30 Hz have the effects of wave barrier on the reduction of vibration. There is the vibration reduction value from 5 to 10 dB. On the other hand, three other cases such as the input frequencies of 5, 10, and 15 Hz obtained the reduction of vibration range from -3 dB (which mean vibration amplification) to 3dB. The influences of input frequency and various wave barriers on relative vibration reduction level, L_{rv}, are presented in Fig. 6.46 (a), (b), (c), and (d) for locations at 1.85 m, 3.30 m, 5.80 m, and 8.30m from source, respectively. For the presented result in front of the barrier as shown in Fig. 6.46 (a), the cases of EPS40 and EPS60 have an amplification of L_{rv} value in some cases such as the input frequencies of 5, 10, and 15 Hz. On the other hand, in the case of EPS20, there is not the effect of wave barrier on the reduction of vibration. For the presented result on the barrier as shown in Fig. 6.46 (b), it is observed that all barriers reduce vibration in cases of high frequencies such as 20, 25, and 30 Hz. Finally, Figs. 6.46 (c) and (d) show the relationship between input frequency and L_{rv} value in the cases of beyond barrier. In the cases such as the input frequency of 20, 25, 30 Hz, the case of EPS40 and EPS60 have a reduction of L_{rv} value, whereas the case of EPS20 has an amplification of L_{rv} value. It was found through the field test that some cases such as input frequency of high frequency have a tendency to reduce ground vibration in the cases of EPS40 and EPS60. The decrease of L_{rv} value between with and without barrier is in the order of 5-20 dB.
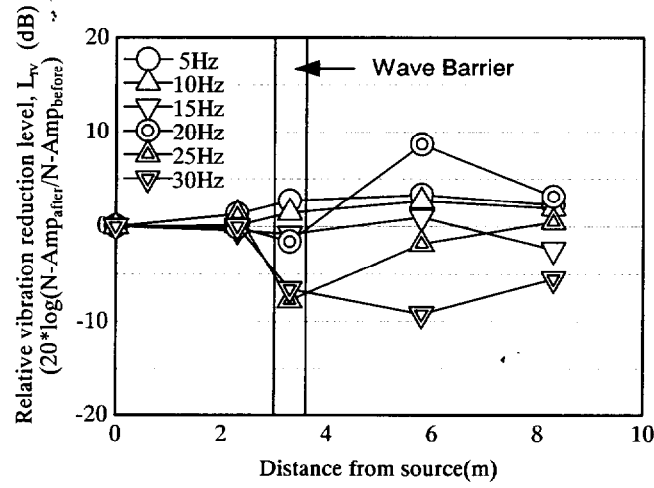
(a) EPS20
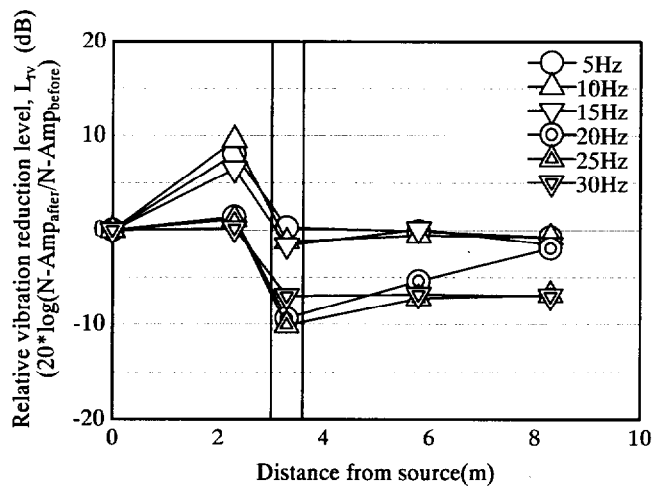
(b) EPS40
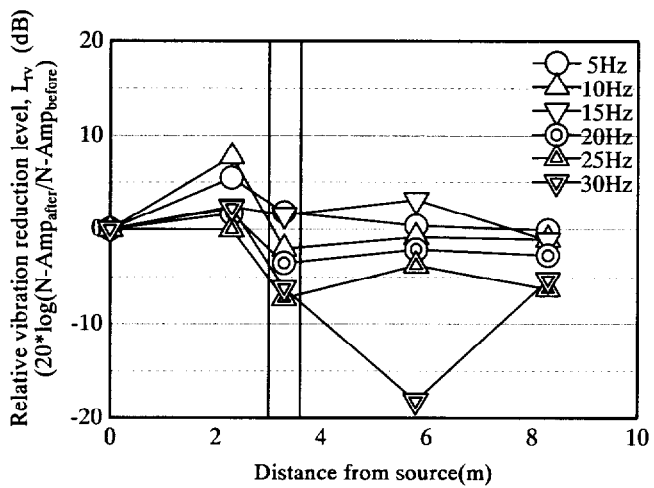
(c) EPS60

Figure 6.45 Attenuation of the relative vibration reduction level with distance from vibration source for various barriers

(a) Location at 1.85 m from source
(in front of the barrier)

(b) Location on the barrier
(3.3 m from source)

(c) Location at 5.8 m from source
(behind the barrier)

(d) Location at 8.3 m from source
(behind the barrier)
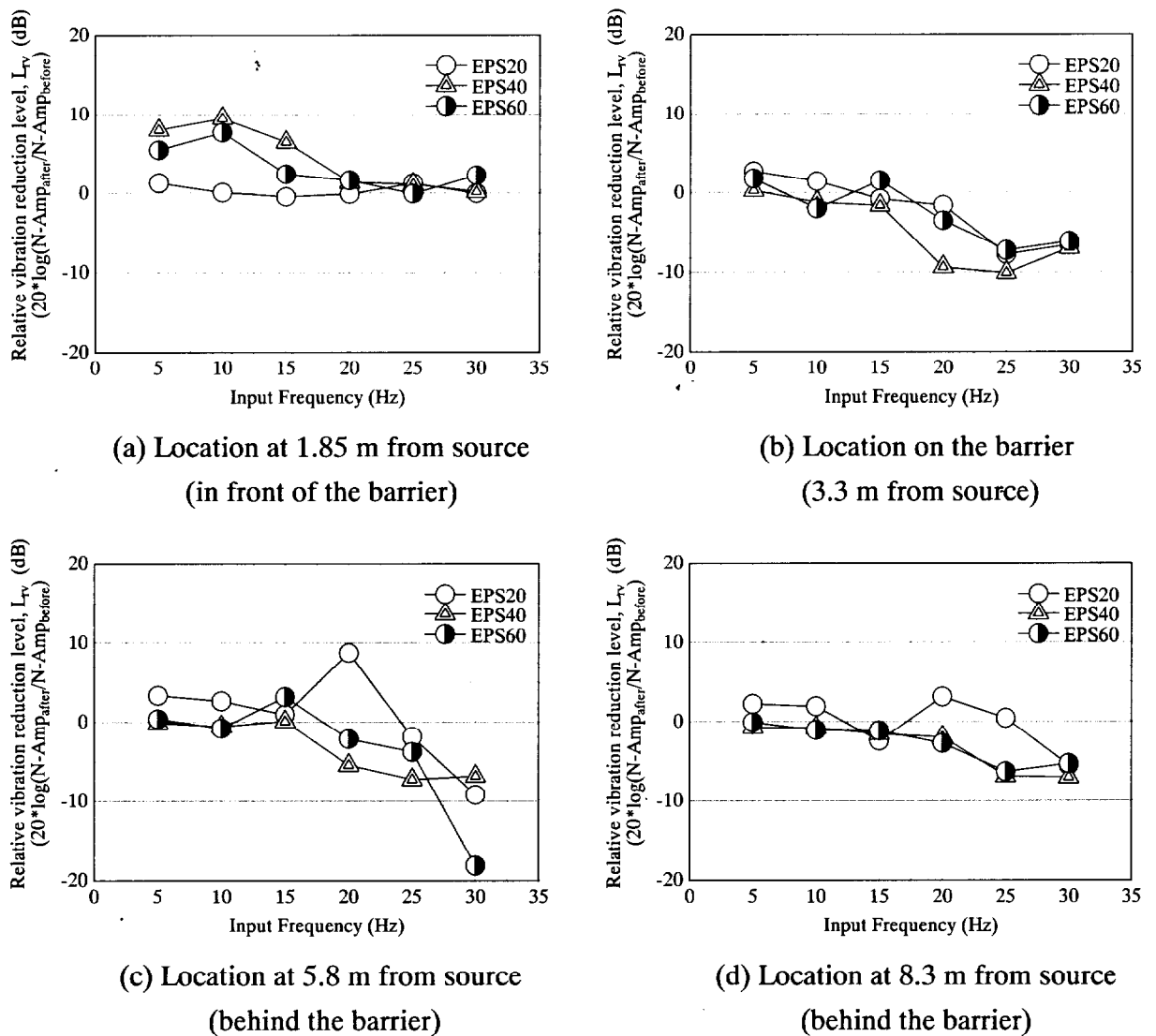
Figure 6.46 Change in relative vibration reduction level to input frequency for different barriers

6.6 CONCLUSIONS

In this chapter, a newly developed wave barrier material, new process for making wave barrier, and an effect of wave barrier on the reduction of vibration were described. The following conclusions are derived:

1. In order to reflect the results of effective parameter of wave barrier described from the result of centrifuge model test, a newly developed wave barrier, of which wave impedance is less than the soil, was proposed in this chapter. In addition, the newly constructed method for the wave barrier using "EPS beads modified cement-improved column" was developed in order to satisfy some requirements such as reliability of reducing vibration, pump-ability, economically etc.

2. As for the effect of wave barrier on the reduction of vibration, the vibration test were carried out using vibration exciter supplied the various input frequencies. It was concluded that the vibration reduced behind wave barrier in some input frequencies. Especially, it was found through the field test that some cases such as input frequency of high frequency have a tendency to reduce the ground vibration.

CHAPTER 7

CONCLUSIONS

In this dissertation, physical modelling of wave propagation from ground vibration and vibration countermeasures has been investigated. Using the centrifuge model test, the behavior of wave propagation and its vibration countermeasures were investigated in this study. It uses small-scale models subjected to a centrifugal acceleration of many times the gravitational acceleration to simulate prototype problems that are difficult to test at full scale. Two kinds of systems, which can generate various types of vibration on the ground-surface, were developed newly. In addition, to investigate the effect of produced wave barrier on the reduction of vibration, the measurements of ground vibration were carried out before and after the measures.

The conclusions obtained from the present study are as follows;

Chapter 2 shows the literature review of studies on the ground vibration problems. The initial part of this chapter presents wave propagation studies to various approaches, numerically, theoretically, and experimentally. The review of vibration regulations and vibration countermeasures at the transmitting path and at the vibration source is also described in this chapter.

• Compared with the numerical and theoretical approaches, there were few researchers who took experimental approaches in ground vibration problem. Because while full-scale tests are practically too expensive to be carried out, small-scale model test results obtained in 1 G environments often pose a question of how to interpret their data and to deduce the implications under prototype situations. In past researchers, the technique of centrifuge modelling test which the scaling relationship agrees with the relevant effect of self weight induced stresses appropriate to the prototype earth structures and satisfied scaling laws for the behavior of wave propagation has been used previously in investigations of blast loading and seismic. However their research did not provide systematic results and data, yet. There was not systematic research as for vibration reduction method used centrifuge. Hence the information derived from such investigation using centrifuge is seen to be of value to the vibration countermeasures.

The Multiple Ball-Dropping System in a centrifuge is developed to investigate the behavior of wave generation and propagation from surface ground vibration sources in *Chapter 4*. This system can simulate not only point load, but also quasi-moving loads caused by high-speed trains running through a viaduct. The experimental study in this chapter particularly focuses on the investigation of wave propagation and its vibration countermeasure using this system.

- In order to investigate the effect of the various materials and depths of wave barrier on the reduction of vibration, point loading test which focuses the simulation of wave propagation with various wave barriers were carried out. The experimental results reveal that softer barriers were generally superior to stiffer barriers.

- As for the effect of the geometry of the wave barrier on the reduction of vibration, point loading tests using EPS barrier of varied forms were carried out. The barriers adopted in this series of the tests are either cylindrical in shape or rectangular with three different lengths. It was found that the geometry of the barrier significantly affects the motion of the barrier.

- The results of a series of centrifuge model tests to investigate the effect of a vibration reduction method which used a crumb rubber-modified asphalt (CRMA) layer at the vibration source and an EPS barrier at the transmitting path were described. It was found through centrifuge tests that CRMA, which was a material with high shear stiffness and damping ratio, could reduce the vibration away from the source especially when working together with EPS barrier.

- Moving load such as high-speed trains had been recognized as a potential source of ground vibrations using this system. The system could simulate a moving load of velocity as fast as 350 km/h. It was also suggested that the superimposition of the waves could be applicable to cases of moving load, provided that the factor of safety for bearing capacity of foundation is sufficiently high.

Chapter 5 described new development of the Centrifugal Vibration Testing System to investigate wave propagation from shallow foundation in a centrifuge. Centrifuge model test results on wave propagation in various inputted frequencies and vibration countermeasures at the transmitting path and the vibration source were presented.

- The effectiveness of a range of wave barriers was investigated using two materials and two radii of cylindrical barrier, and it was found that softer barriers are generally superior to stiffer barriers. In order to compare this cyclic loading test and the impact point loading test, the experiment were carried out by same relationship between radius of foundation and the distance from source. As far as inputted frequencies, which were the area of dominating frequencies by the impact point loading test, were concerned, the results of the cyclic loading test were similar to that of the impact point loading test.

- This chapter describes the results of a series of centrifuge model tests to investigate the effect of a vibration reduction method which used a crumb rubber-modified asphalt (CRMA) layer at the vibration source and an EPS barrier at the transmitting path. It was found through centrifuge tests that CRMA, which was a material with high shear stiffness and damping ratio, could reduce the vibration away from the source especially when working together with EPS barrier.

In *Chapter 6*, new development of wave barrier material to be satisfied with requirements such as reliability of the reducing vibration, pump-ability, and economically, etc. and a newly developed method for making wave barrier, which can excavate the ground and construct wave barrier at the same time, were presented.

- In advance of the field test, the series of centrifuge model test had been carried out vibration countermeasures by wave barrier. The softer barrier, of which the wave impedance was less than the soil, was effective in reducing vibration. In order to reflect these results, the soil improvement slurry mixed the artificial clay and cement slurry with EPS beads. It is called "EPS beads modified cement-improved column". From the laboratory test, the performance of this material was verified. As a result of the test, it was found that there are low strength and light weight.

- The field vibration test particularly focuses on the effect of wave barrier on the reduction of vibration. The vibration test were carried out using vibration exciter supplied the various inputted frequencies. It was concluded that the vibration reduced behind wave barrier in some inputted frequencies. Especially, it was found that the effect in reducing vibration with inputted frequency of high frequencies such as 20, 25 and 30 Hz.

LITERATURE CITED

Aboudi, J. (1973): "Elastic waves in half-space with thin barrier," *Journal of Engineering Mechanics*, ASCE, 99(1), pp. 69-83.

Ahmad, S. and Al-Hussaini, T. M. (1991): "Simplified design for vibration screening by open and in-filled trenches," *Journal of the Geotechnical Engineering*, ASCE, Vol. 117(1), pp. 67-88.

Ahmad, S., Al-Hussaini, T. M. and Fishman, K.L. (1996): "Investigation on active isolation of machine foundations by open trenches," *Journal of the Geotechnical Engineering*, ASCE 122(6), pp. 454-461.

Al-Hussaini, T. M. and Ahmad, S. (1996): "Active isolation of machine foundations by in-filled trench barries," *Journal of Geotechnical Engineering*, ASCE 122(4), pp. 288-294.

Ando, K., Horike, T., Kubomura, K., Hansaka, M. and Nagafuji, T. (1996): "Present status on slab track and environmental," *Quarterly Report of RTRI*, Vol. 37, No. 4, pp. 204-209.

Asano, J., Ban, K., Azuma, K., and Takahashi, K. (1996): "Deep mixing method of soil stabilization using coal ash," *Proceedings of the Second International Conference on Ground Improvement Geosystems (IS-Tokyo'96)*, Tokyo, Vol. 1, pp. 393-398.

Ashiya, K. (2001): "Estimation method for efficiency of vibration reduction wall," *Railway Technical Research Institute Report (RTRI Report)*, Vol. 15, No. 10, pp. 33-38.

Barkan, D. D. (1962): "Dynamics of bases and foundations (translated from the Russian by L. Drashevska, and translation edited by G. P. Tschebotarioff," McGraw-Hill Book Co., New York, 434pp.

Biot, M. A. (1956): "Theory of propagation of elastic waves in a fluid saturated porous solid," *Journal of Acoustical Society of America*, Vol. 28, pp. 168-178.

Bornitz, G. (1931): Uber die Ausbreitung der von Grozklolbenmaschinen erzeugten Bodenschwingungen in die Tiefe, J. Springer (in German).

Cauchy, A. L. (1830): "Memoire sur la Theorie de la Lumiere, " De Bure Bros., Paris.

Chaudhary, S. K., and Kuwano, J. (2001): "Anisotropic yielding behavior of dense Toyoura sand in p' constant plane," *Proceeding of 3rd International Summer Symposium*, Tokyo, pp. 197-200.

Cheney, J. A., Hor, O. Y. Z., Brown, R. K. and Dhat, N.R. (1988): "Foundation vibration in centrifuge models," *Proceeding of International Conference on Centrifuge Modelling-Centrifuge 88*, Balkema, Paris, pp. 481-486.

Cheney, J. A., Brown, R. K., Dhat, N.R. and Hor, O. Y. Z. (1990): "Modeling free-field conditions in centrifuge models," *Journal of the Geotechnical Engineering*, ASCE, Vol.

116(9), pp. 1347-1367.

Chouw, N., Le, R., and Schmid, G. (1991): "Propagation of vibration in a soil layer over bed-rock," *Proceedings of Engineering Analysis with Boundary Elements*, Vol. 8, No. 3, pp. 125-131.

Chouw, N. and Schmid, G. (1993): "Verfahren und vorrichtung zur reduzierung von fremderregten Schwingungen und Bodenwellen," Patentschrigft DE 4026111 C2, Deutsches Patentamt.

Chouw, N. and Pflanz, G. (2000): "Reduction of structural vibrations due to moving load," *Proceeding of International Workshop WAVE2000*, Balkema, Bochum, pp. 251-268.

Craig, W. H., James, R. G. and Schofield, A. N. (eds) (1988): "Centrifuges in soil mechanics," Ashgate Published Co. Ltd., 274p.

Davies, M. C. R. (1991): "Modelling of dynamic soil structure interaction resulting from impulsive surface loading," *Proceeding of International Conference on Centrifuge Modelling-Centrifuge 91*, Balkema, Colorado, pp. 487-493.

Davies, M. C. R. (1994): "Dynamic soil structure interaction resulting from blast loading," *Proceeding of International Conference on Centrifuge Modelling-Centrifuge 94*, Balkema, Singapore, pp. 319-324.

Degrande, G. and Lombaert, G. (2000): "High-speed train induced free field vibrations: In situ measurements and numerical modelling," *Proceeding of International Workshop WAVE2000*, Balkema, Bochum, pp. 29-42.

deHoop, A. T. (1959): "A modification of Cagniard's method for solving seismic pulse problems," *Applied Scientific Research*, Section B, Vol. 8, pp. 349-356.

Dolling, H. J. (1965):"Schwingungsisolierung von Bauwerken durch tiefe auf geeignete Weise stabilisierte Schlitze, " *VDI-Berichte 88*, S.3741 (in German).

Eason, G. (1965): "The stresses produced in a semi-infinite solid by a moving surface force," *International Journal of Engineering Science*, Vol. 2, pp. 581-609.

Ejima, A. (1979): "Ground vibration and countermeasures," Shubunsya Co., Ltd., 287p (in Japanese).

Environmental Dispute Coordination Commission (2000): http://www.soumu.go.jp/

EPS construction method Development Organization (2002): "Expanded Poly-Styrol construction method," Expanded Polystyrol Construction Method Development Organization (EDO), 147p (in Japanese).

Fryba, L. (1972): "Vibration of solids and structures under moving loads," Noordhoff International Publishing, Groningen, The Netherlands.

Furumura, T., Kennett, B. L. N., and Takenaka, H. (1998): "Parallel 3-D pseudospectral simulation of seismic wave propagation," *Geophysics*, Vol. 63, pp. 279-288.

Gakenheimer, D. C. and Miklowitz, J. (1969): "Transient excitation of an elastic half space by a point load traveling on the surface," *Journal of Applied Mechanics*, ASTM, Vol. 36, pp. 505-515.

Gutowski, T. G. and Dym, C. L. (1976): "Propagation of ground vibration: a review," *Journal of*

Sound and Vibration, Vol. 49, No. 2, pp. 179-193.

Hapern, M. R. and Christiano, P. (1986): "Steady state harmonic response of a rigid plate bearing on a liquid-saturated poroelastic halfspace," *Earthquake Engineering and Structural Dynamics*, Vol. 14, pp. 439-454.

Hatayama, K. and Fujikawa, H. (1998): "Excitation of secondary Love and Rayleigh waves in a three-dimensional sedimentary basin evaluated by the direct boundary element method with normal modes," *Geophysics Journal International*, Vol. 133, pp. 260-278.

Haupt, W. A. (1978): "Surface wave in nonhomogeneous half-space," *Dynamical methods in soil and rock mechanics*, B. Prange ed., Balkema, Rotterdam, pp. 335-367.

Haupt, W. A. (1981): "Model tests on screening of surface waves," *Proceeding of the 10th International Conference on Soil Mechanics and Foundation Engineering*, Stockholm, 3, pp. 215-222.

Haya, H., Murono Y., and Nishimura A. (1996) : "Development of method for reduction of wayside train vibration," *Proceedings of the Second International Congress on Environmental Geotechnics (IS-Osaka)*, Osaka, Vol. 1, pp. 55-60.

Hayano, Y. (1999): "Effects of initial structure on cyclic deformation of Toyoura sand," Bachelor Engineering Thesis, Tokyo Institute of Technology.

Hirayama, Y., Koda, M., Ohta, K., Fukuda, A., Murata, O., Tanamura, S., Itoh, K., and Kusakabe, O. (2002): "Development of wave barrier construction method using EPS beads modified cement-improved column reducing ground vibration," *Proceeding of the 57th JSCE National Conference*, Vol. 1, pp. 207-208 (in Japanese).

Hirose, S. and Hoshi, E. (2001): "Ground motion due to a moving load," *Proceeding of the Fourteenth KKNN seminar on Civil Engineering*, pp. 273-278.

Hirose, S. (2002): "Efficient numerical approach for the analysis of vibrations due to moving load," *Proceeding of International Workshop WAVE2002*, Balkema, Okayama, pp. 113-120.

Holm, G., Andereasson, B., Bengtsson, P., Bodare, A., and Eriksson, H. (2002): "Mitigation of track and ground vibration by high speed trains at Ledsgars, Sweden," *Swedish Deep Stabilization Research Centre*, Report 10, 58pp.

Hung, H. H. and Yang, Y. B. (2001): "A review of researches on ground-bone vibrations with emphasis on those induced by trains," *Proceedings of the National Science Council, Republic of China (A)*, Vol. 25, No. 1, pp. 1-16.

Iai, S. (1989): "Similitude for shaking table test on soil-structure-fluid model in 1 g gravitational field," *Soils and Foundations*, Vol. 29, No. 1, pp. 105-118.

Itoh, K., Koda, M., Lee, K. I., Murata, O., and Kusakabe, O. (2002a): "Centrifugal simulation of wave propagation using a multiple ball dropping system," *International Journal of Physical Modelling in Geotechnics*, Vol. 2, No. 2, pp. 33-51.

Itoh, K., Koda, M., Takahashi, A., Lee, K. I., Murata, O., and Kusakabe, O. (2002b): "Centrifuge simulations of wave propagation using a moving load system," *Proceeding of Inter-*

national Workshop WAVE2002, Balkema, Okayama, pp. 193-200.

Itoh, K., O-hashi, M., Kusakabe, O., Koda, M., Nishioka, H., and Murata, O. (2002c): "The effect of EPS beads modified wave barrier on the reduction of ground vibration, - investigation of 2D-FE analysis -," *Proceeding of the 57th JSCE National Conference*, Vol. 1, pp. 209-210 (in Japanese).

Itoh, K., Takahashi, A., Koda, M., Lee, K. I., Murata, O., and Kusakabe, O. (2002d): "Centrifugal simulations of wave propagation in dry sand," *Proceeding of the 1st International Conference for Physical Modelling in Geotechnics (IS-Canada'02)*, pp. 421-426.

Itoh, K., Zeng, X., Murata, O., and Kusakabe, O. (2002e): "Centrifugal simulations of rubber-modified asphalt foundation and EPS barrier to reduction of vibration generated by high-speed trains," *International Journal of Physical Modelling in Geotechnics*, Vol. 3, No. 2, pp. 1-10.

Iwasaki, T., and Tatsuoka, F. (1977): "Effects of grain size and grading on dynamic shear module of sands," *Soils and Foundations*, Vol. 17, No. 3, pp. 19-35.

Jung, J. B. (1998): "Study on Consolidation Behavior of Clay Ground Improved by the partly Penetrated Sand Compaction Piles," A Dissertation for the Degree of Doctor of Engineering, Hiroshima University, p166.

Kimura, T., Nakase, A., Kusakabe, O., Saitoh, K., and Ohta, A. (1982): "Geotechnical centrifuge model tests at the Tokyo Institute of Technology," *Technical Report*, No. 30, Tokyo Institute of Technology, pp. 7-33.

Kobayashi, Y. (1975): "Influence of ground vibration cause by construction and its isolation methods," Kajima Institute Publishing, pp. 65-68 (in Japanese).

Koda, M., Hirayama, Y., Ohta, K., Yoshida, S., Murata, O., Tanamura, S., Itoh, K., and Kusakabe, O. (2002): "The effect of EPS beads modified wave barrier on the reduction of ground vibration, - vibration test using vibration exciter -," *Proceeding of the 57th JSCE National Conference*, Vol. 1, pp. 211-212 (in Japanese).

Kosloff, D., Reshef, M., and Loewenthal, D. (1984): "Elastic wave calculations by the Fourier method," *The Bulletin of Seismological Society of America*, Vol. 74, pp. 875-891.

Kushida, H. (1997): "Engineering of environmental vibration," Rikohtosyo Co., Tokyo, p169.

Kutter, B. L., O'Leary, L. M., Thompson, P. Y., and Lather, R. (1988): "Gravity-scaled tests on blast-induced soil-structure interaction," *Journal of the Geotechnical Engineering*, ASCE, Vol. 114, No. 4, pp. 431-447.

Lai, C. G., Callerio, A., Faccioli, E. and Martino, A. (2000): "Mathematical modelling of railway-induced ground vibrations," *Proceedings of International Workshop WAVE2000*, Balkema, Bochum, pp. 99-110.

Lamb, H. (1904): "On the propagation of tremors over the surface elastic solids," *Philosophical Transactions of the Royal Society of London. Series A*, Physical Sciences and Engineering, Vol.203, pp. 1-42.

Love, A. E. H. (1911): "Some problems of geodynamics," Cambridge University Press.

Luong, M. P. (1994): "Efficiency of a stress wave mitigation barrier," *Proceeding of Interna-*

tional Conference on Centrifuge Modelling-Centrifuge 94, Balkema, Singapore, pp. 283-288.

Madshus, C., Bessason, B., and Harvik, L. (1996): "Prediction model for low frequency vibration from high speed railway on soft ground," *Journal of Sound and Vibration*, Vol. 193, No. 1, pp. 195-203.

Maeda, K., and Miura, K. (1999): "Confining stress dependency of mechanical properties of sands," *Soils and Foundations*, Vol. 39, No. 1, pp. 53-67.

Massarsch, K. R. (1991): "Ground vibration isolation using gas cushions," *Proceedings 2nd International Conference on Recent Advances in Geotechnical Earthquake Engineering and Soil Dynamics*, St. Louis, Missouri, Vol. 2, pp. 1461-1470.

McNeill, R. L., Margason, B. E., and Babcock, F. M. (1965): "The role of soil dynamics in the design of stable test pads," *Proceeding of Guidance and Control Conference*, pp. 366-375.

Morichi, S. and Tamura, C. (1974): "An experimental study on propagation of elastic wave due to a wave source moving on the surface," *Seisan Kenkyu*, Vol. 26, No. 7.

Murata, O., Itoh, K., Koda, M., Kusakabe, O., and Tanamura, S. (2001): "Parameter studies on effect of reducing ground vibration by in-filled trench barriers," *Railway Technical Research Institute Report (RTRI Report)*, Vol. 15, No. 10, pp. 39-44.

Neumeuer, H. (1963): "Untersuchungen uber die Abschimung eines besehenden Gebaudes gegen Erschutterungen beim Bau und Betrieb einer U-Bahnstrcke, Baumaschrne and Bautechnik," *Jahrgang*, (10), Heft 1,pp. 23-29 (in German).

Ohbo, N. (1985): "A numerical method for analysis of wave propagation in ground and its experimental verification," Thesis presented to the University of Tokyo, in partial fulfillment of the requirements for the degree of Doctor of Philosophy.

Okamura, M. (1993): "Bearing capacity and deformation characteristics of shallow foundations on sand," thesis presented to the Tokyo Institute of Technology, in partial fulfilment of the requirements for the degree of Doctor of Philosophy (in Japanese).

Okamura, Y. and Kuno, K. (1991): "Statistical analysis of field data of railway noise and vibration collected in an urban area," *Applied Acoustics*, Vol. 33, pp. 263-280.

Oprsal, I., and Zahradnik, J. (2002): "3D finite difference method and hybrid modeling of earthquake ground motion," *Journal of Geophysical Research*, Solid Earth, Vol. 8, DOI: 10.1029.

Prevost, J. H., and Scanlan, R.H. (1983): "Dynamic soil-structure interaction: Centrifuge modeling," *Soil Dynamics and Earthquake Engineering*, 2(4), pp. 212-221.

Reshef, M., Kosloff, D., Edwards, M., and Hsiung, C. (1988): "Three-dimensional elastic modeling by the Fourier method," *Geophysics*, Vol. 53, pp. 1184-1193.

Roschen, T. (2000): "Report on the status of rubberized asphalt traffic noise reduction in Sacrament Country," Report Prepared for Sacramento Country Public Works Agency.

Sassa, K., Ashida, Y., and Sugano, T. (1993): "Geophysical exploration," Morikita Shuppan Co., Ltd, Tokyo, 219pp (in Japanese).

Schofield, A. N., and Steedman, R. S. (1988): "State-of-the-art report: Recent developments on dynamic modèl testing in geotechnical engineering," *Proceeding 9th World Conference on Earthquake Engineering*, Tokyo/Kyoto, Vol. 8, pp. 813-824.

Semblat, J.F. and Luong, M. P. (1998): "Wave propagation through soils in centrifuge testing," *Journal of Earthquake Engineering*, Vol. 2, No. 1, pp. 147-171.

Siemer, Th. and Jessberger, H.L. (1994): "Wave propagation and active vibration control in sand," *Proceeding of International Conference on Centrifuge Modelling-Centrifuge 94*, Balkema, Singapore, pp. 307-312.

Svinkin, M. R. (1996): "Overcoming soil uncertainty in prediction of construction and industrial vibrations," *Proceedings of Uncertainty in the Geologic Environment: From theory to Practice*, ASCE, Geotechnical Special publications No. 58, Vol. 2, pp. 663-670.

Svinkin, M. R. (2001): "An impulse response function approach for predicting ground and structure vibration," *Proceedings of the fifteenth international conference on soil mechanics and geotechnical engineering*, Balkema, Istanbul, pp. 785-787.

Syo, K., and Kitamura, Y. (1988): "Dynamic compliance of foundations in half-space porous elastic solid," *Journal of Structural Engineering*, Vol. 34A, pp. 855-864 (in Japanese).

Takenaka, H., Wang, Y., and Furmura, T. (1999): "An efficient approach of the pseudospectral method for modelling of geometrically symmetric seismic wavefield,"☐ @*Earth Planets Space*, The Society of Geomagnetism and Earth, Planetary and Space Sciences (SGEPSS), Vol. 51, pp. 73-79.

Takemiya, H., Goda, K. (1997): "FEM-BEM analysis of vibration of an embankment track on layered soils for harmonic moving loads," *Journal of Structural Mechanics and Earthquake Engineering (Division1)*, JSCE, No. 605/I-45, pp. 143-152 (in Japanese).

Takemura, J., Kondoh, M., Esaki, T., Kouda, M. and Kusakabe, O. (1999): "Centrifuge model tests on double propped wall excavation in soft clay," *Soils and Foundations*, Vol. 39, No. 3, pp. 75-87.

Takibuchi, K., Ejima, A., Okada, H., and Mukai, G. (1977): "Basic tests of Shinkansen-induced ground vibration and its countermeasures," *Journal of the Japan Society of Civil Engineers*, Vol. 62, No. 5, pp. 10-16 (in Japanese).

Telford, W. M., Geldart, L. P., Sheriff, R. E. and Keys, D. A. (1985): "Applied Geophysics," Cambridge University Press, University of Cambridge, p790.

Verhas, H. P. (1979): "Prediction of the propagation of train0induced ground vibration," *Journal of Sound and Vibration*, Vol. 66, No. 3, pp. 371-376.

Watanabe, T. (1953): "Analysis of time-distance curves of mirage form," *Butsuri-Tanko (Geophysical exploration, Japan)*, Vol. 7, No. 2, pp. 1-11(in Japanese).

Wilson, G. P., Saurenman, H. J., and Nelson, J. T. (1983): "Control of ground-borne noise and vibration," *Journal of Sound and Vibration*, Vol. 87, No. 2, pp. 339-350.

Wood, D. M., Crewa, A., and Taylor, C. (2002): "Shaking table testing of geotechnical models," *International Journal of Physical Modelling in Geotechnics*, Vol. 2, No. 1, pp. 1-13.

Woods, R. D. (1968): "Screening of surface waves in soils," *Journal of the Soil Mechanics and Foundations*, ASCE, Vol. 94, No. SM4, pp. 951-979.

Woods, R. D., Barnett, N. E. and Sagesser, R. (1974): "Holography-A new tool for soil dynamics," *Journal of the Geotechnical Engineering*, ASCE, Vol. 100, No. GT11, pp. 1231-1247.

Yoshioka, O., Nagai, M., Kanema, T., and Mitsuzuka, T. (1980): "On prediction method of train-induced ground vibration by a weight dropping experiment and a microbus running test," *Butsuri-Tanko (Geophysical exploration, Japan)*, Vol. 33, No. 6, pp. 333-351(in Japanese).

Yoshioka, O., and Ashiya, K. (1990): "Attenuation properties of vibrator-induced ground vibrations passing through sheet pile in earth," *Railway Technical Research Institute Report (RTRI Report)*, Vol. 4, No. 8, pp. 51-58 (in Japanese).

Yoshioka, O. and Ashiya, K. (1991): "Isolation effect of train-induced ground vibrations by a concrete core wall in earth," *Railway Technical Research Institute Report (RTRI Report)*, Vol. 5, No. 11, pp. 37-46.

Yoshioka, O. (2000): "Basic characteristics of Shinkansen-induced ground vibration and its reduction measures," *Proceeding of International Workshop WAVE2000*, Balkema, Bochum, pp. 219-240.

Zeng, X., Rose, J. G., and Rice, J. S. (2001): "Stiffness and damping ratio of rubber-modified asphalt mixes: Potential vibration attenuation for high-speed railway trackbeds," *Journal of Vibration Control*, 7 (4), pp. 527-538.

Zhang, B., Papageorgiou, A., S., Tassoulas, J., L. (1998): "A hybrid numerical technique, combining the finite-element and boundary-element methods, for modeling the 3D response of 2D scatterers," *Bulletin of the Seismological Society of America*, Vol. 88, pp. 1036-1050.

Zhong, X. G., Zeng, X., Rose, J. G. (2002): "Shear modulus and damping ratio of rubber-modified asphalt mixes and unsaturated subgrade soils," *Journal of Materials in Civil Engineering*, ASCE, pp. 496-502.

APPENDIX A

FINITE ELEMENT METHOD OF WAVE PROPAGATION IN GROUND AND ITS EXPERIMENTAL VERIFICATION

A.1 INTRODUCTION

As for ground vibration problems, most of the previous studies were concentrated either on numerical analysis or field measurement only. Thus, the results of field measurement could not take advantage of numerical analysis as complex boundary conditions and very local soil parameters are needed to contain. In order to estimate vibration reduction by installing the wave barrier by numerical analysis, it is necessary to get the physical data which has clear boundary conditions and soil parameters. For this purpose the centrifuge model test was carried out in this study. It uses small-scale models subjected to a centrifugal acceleration which is many times the gravitational acceleration to simulate prototype problems which are difficult to test at full scale. In this study, two kinds of newly developed systems which can simulate wave propagation from the surface ground vibration and its countermeasures are described. In addition, to investigate the effect of produced wave barrier on the reduction of vibration, the measurements of ground vibration were carried out before and after the placement of wave barrier.

In this appendix, the consistency between the results of the physical modelling and the results of numerical analysis was investigated.

A.2 FINITE ELEMENT MODELLING

In this study, the numerical modelling of wave propagation is performed using DINAS, which is a commercially available finite element program. Within DINAS program, solution of wave propagation equation is performed in the frequency domain. An iterative scheme is required to arrive at a converged solution. This solution of wave propagation approach has provided good results compared with field measurements and is widely used in engineering practice (e. g. FLUSH, Lysmer et. al., 1975). DINAS which is used in this study has similar performance as FLUSH. In wave propagation problems where finite element program is used, element dimensions are chosen with respect to frequency, taking the highest frequency (f_{max}) for the lowest velocity wave (V_R). Element dimensions which are too large will filter high frequencies, whereas very small element dimensions will produce numerical instability. In addition, very small dimensions require considerable computational resources. An approximate element dimension (g) is calculated by using

$$g \leq \chi\lambda_{min}$$

where

$$\lambda_{min} = \frac{V_R}{f_{max}}$$

where λ_{min} = minimum wavelength. The constant χ must be less than 0.5 because of the Nyquist limit. In order to meet this condition, element dimensions have to be decided.

A.3 OUTLINE OF NUMERICAL MODEL TESTS

A.3.1 Numerical model regarding centrifuge model test

The way of modelling different conditions in centrifuge tests is described in this section. In regard to the form of input vibration, two kinds of centrifuge model tests were conducted. In the first set, waves induced by the point load which is generated by the Multiple Ball-Dropping System described in Chapter 4 are propagated through the ground surface. And in the second set, waves generated by cyclic loading for various frequencies were propagated on the ground-surface using Centrifugal Vibration Testing System described in Chapter 5. In this appendix, details of these experiments are not described. See above Chapters 4 and 5 to get more information on those matters. The conditions of these experiments are modeled by using FE analysis, as follows.

In order to simulate the centrifuge model test numerically, two dimensional finite element analyses were conducted under the axisymmetric condition. The finite element mesh with boundary condition regarding above experiments are shown in Fig. A.1. The size of an element considered was 0.25×0.25mm. In general, waves should be allowed to pass easily from/to the analysis domain to/from the outside of the analysis domain in-situ. For this purpose appropriate boundary conditions other than the fixed boundary conditions should be considered. However, experimental data includes the arrival of P or S waves, which are assumed to be reflected from the boundaries of steel cylindrical tub. In order to model this situation, the ends (side and bottom) of the container were structured by shell element. Geomaterial parameters used in the analysis are listed in Table A. 1. The applied vibration motion in the analysis was similar to the wave generated used in the centrifuge test.

A.3.2 Numerical model regarding field test

The way of modelling different conditions on field test is described in this section. In the field considered here, standard penetration test, sampling, and PS logging were already carried out by Yoshioka and Ashiya (1990). This site is composed of filling material, Kanto loam, and gravel which are in the order downward from the ground surface. Layered media becomes extremely complicated because the reflected and refracted waves are generated at the interface. In order to simulate and investigate such behavior in the field test, it is suggested to use three-dimensional finite element analysis. However, the numerical method that is applicable to full scale three-dimensional problems still requires huge capacity and time for computation. In addition, soil profile given by Yoshioka and Ashiya (1990) is the only one position. Soil profile of other position, which is within the scope of this analysis, is not yet known. In order to tackle these problems at the begin-
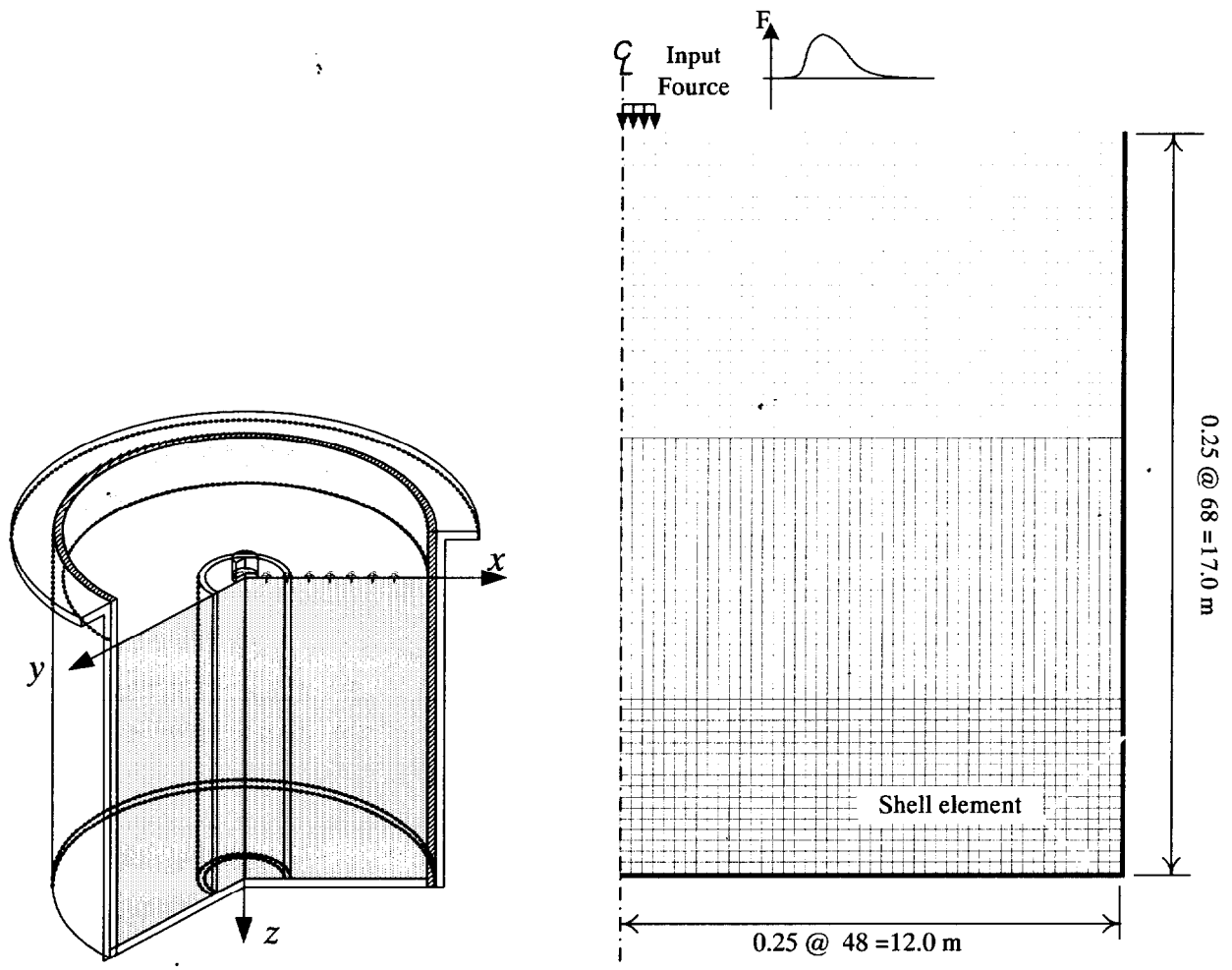
(a) Multiple Ball-Dropping System
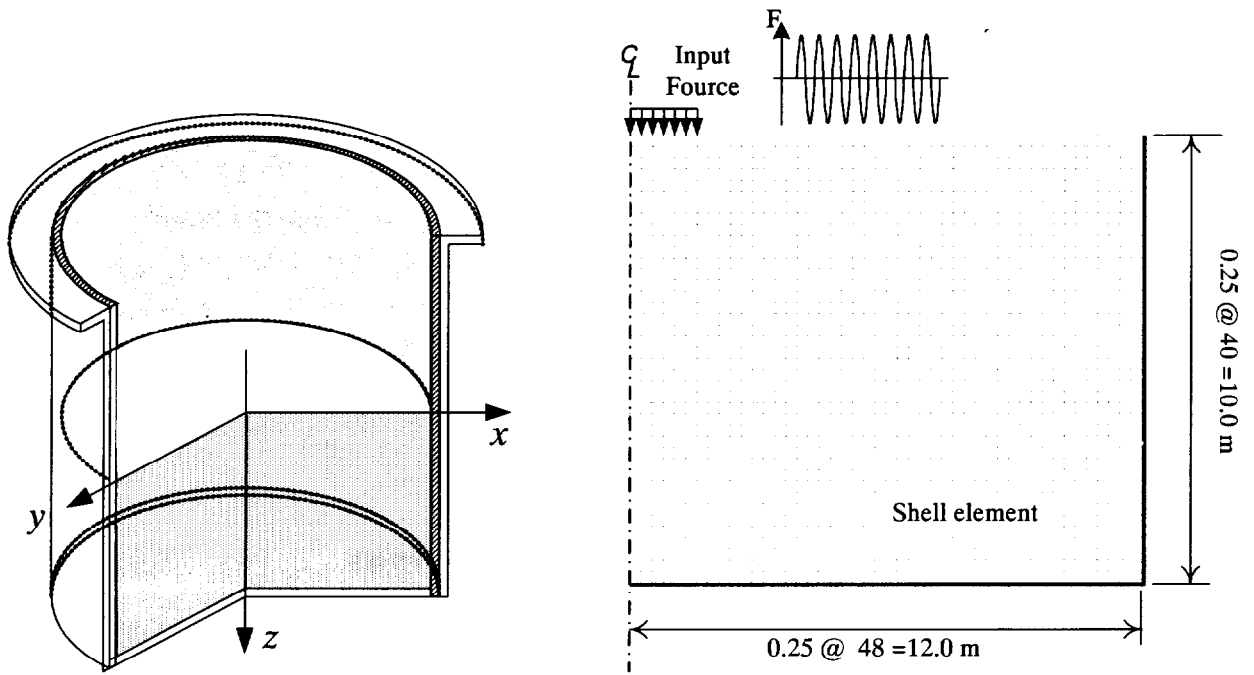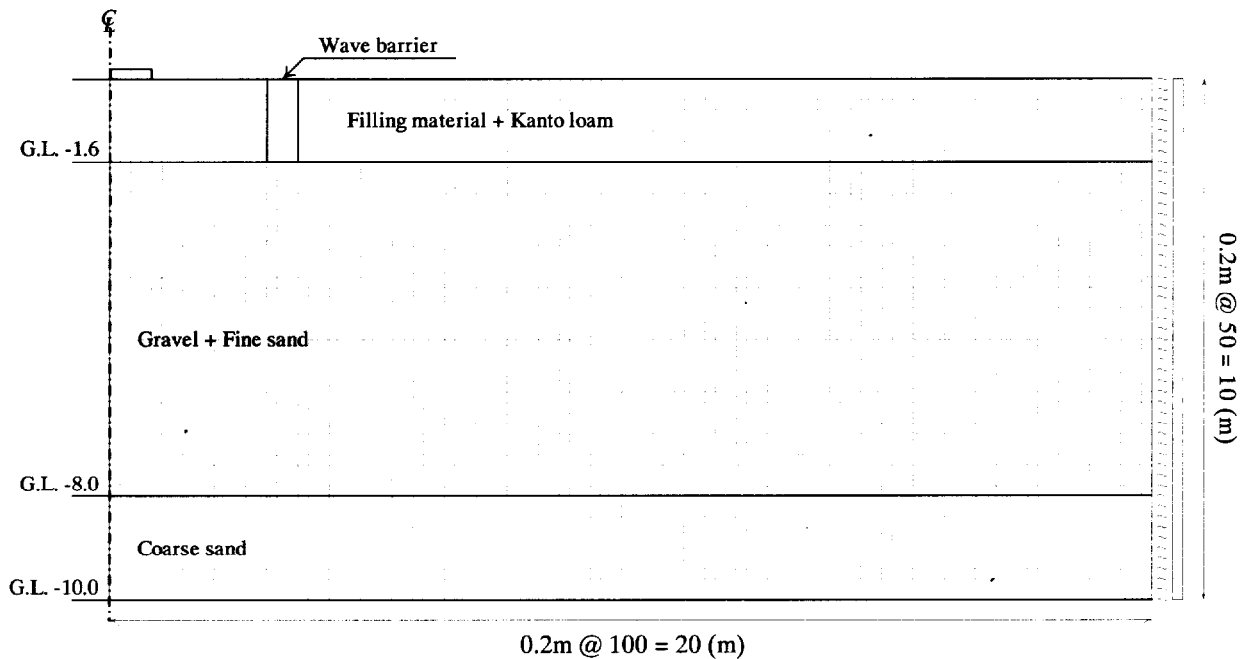

(b) Vibration Testing System

Figure A.1 Finite element mesh with boundary condition regarding centrifuge model test

Table A.1 Geomaterial parameters used in FE analysis regarding centrifuge model test

	Shear modulus G (MN/m^2)	Poisson's ratio v	Dry unit weight γ_d (kN/m^3)	Damping constant h
Toyoura sand	17.9	0.23	15.4	0.05
Aluminium	25.6×10^3	0.34	26.5	0.01
Acryl	12.1×10^2	0.35	11.8	0.01
EPS	11.1×10^{-1}	0.10	0.12	0.05

Figure A.2 Finite element mesh with boundary condition regarding field test

Table A.2 Geomaterial parameters used in FE analysis regarding field test

	Shear modulus G (MN/m^2)	Poisson's ratio v	Dry unit weight γ_d (kN/m^3)	Damping constant h
Filling material & Kanto loam	46.1	0.40	17.64	0.05
Gravel & Fine sand	304.0	0.40	18.62	0.05
Coarse sand	288.0	0.40	18.62	0.05
EPS 20	300.0	0.40	9.40	0.02
EPS 40	150.0	0.40	7.06	0.02
EPS60	50.0	0.40	4.66	0.02

ning, it may be helpful to analyze those using simple models. Thus two dimensional finite element analyses were conducted under the axisymmetric condition in the analysis here. Geomaterial parameters used in the analysis are listed in Table A.2. The analysis model of experimental site is shown in Fig. A.2. The size of an element considered was 0.2 × 0.2m. Here, the area of loading square in the FE analysis is adjusted so that it is proportionately that same as in the field test (D1.5 m × W1.5 m).

A.4 ANALYTICAL RESULTS AND DISCUSSIONS

A.4.1 Centrifuge model tests

(1) Multiple ball- dropping system

The amplitude variation of the calculated and observed waves with distance from vibration source is plotted on a log-log scale in Fig. A.3. In this figure, the amplitudes of calculated wave is modified for the geometrical spreading of surface wave. The amplitude attenuation of the calculated and the observed results are in good agreement. Comparison of the calculated and the observed vertical waveforms is shown in Fig. A.4. As to the first wave, the calculated waveforms approximately agree with the observed one. However, there are noticeable discrepancies between the calculated and the observed waveforms after the first wave, which might be due to the dispersion of observed wave in relation to surface wave as these is difference in the stress field. Tues, it could be said from this point that the predicted waveforms using numerical analysis would differ from the experimental results.

The effect of wave barriers in relation to the embedded depths and materials in reducing the vibration was also examined, using FE analysis. Comparison of the numerical results and experimental results are shown in Fig. A.5. It shows how the maximum acceleration decreases with distance from the vibration source for various barrier materials (Aluminium, Acryl, and EPS) with different embedded depths. Also, the cases without a barrier were shown. In the case of the stiff
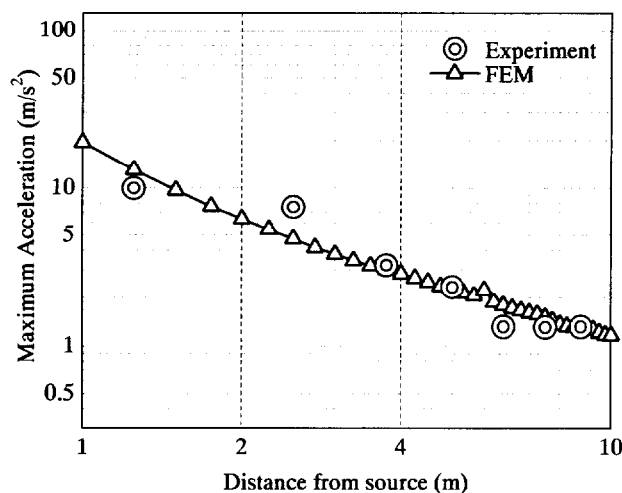

Figure A.3 Amplitude variation of the calculated and observed acceleration with distance from the vibration source (log-log scale)
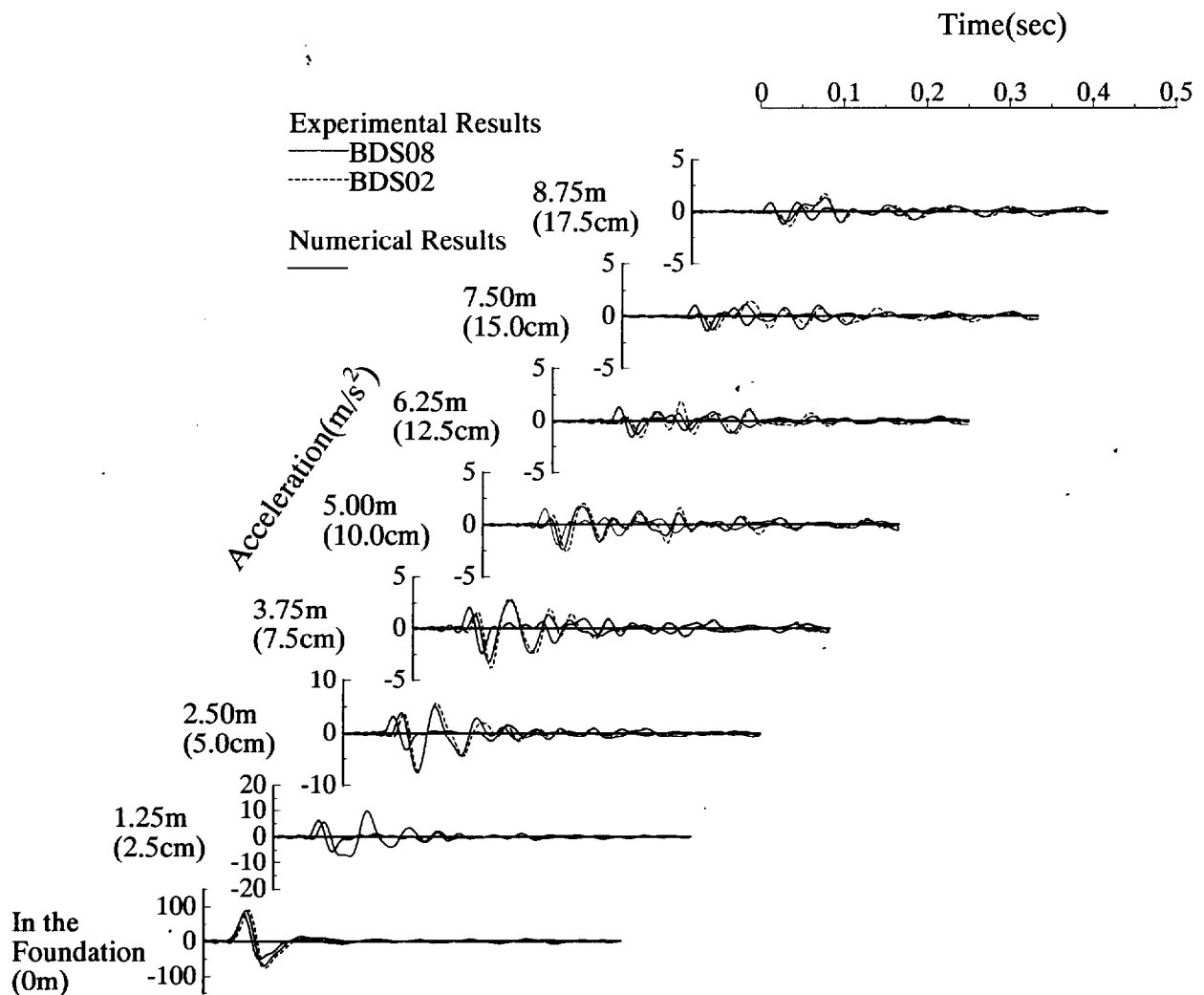
Figure A.4 Comparisons of experimental and numerical waveform on the surface ground

barriers (Aluminium and Acryl), the values of maximum acceleration obtained from numerical analysis are about tenfold lower than those of experimental data. In other words, numerical analyses for the case of stiff barriers seem to give overestimated vibration reduction values. In contrast to this, in the case of softer barrier (EPS), the values of maximum acceleration obtained from the numerical analyses and experimental data are in good agreement. Turning now to the attenuation curves of stiff and soft barriers, the attenuation curves, of numerical analyses are similar to those of experimental data. In other words, it is observed that the magnification of vibration amplifies on the barrier in the case of softer barrier. However, in the case of stiff barriers, it is observed that the magnification of vibration amplifies in front of the barrier and reduces on the barrier. The influences of normalized depth, D/λ and various barrier materials on amplitude ratio, R_A for locations at 5.00 m from source for both numerical and experimental results are compared in Fig. A.6 (See Fig. 4.34(b)). In comparison to experimental results, all numerical analysis results show lower values of amplitude ratio R_A. In the case of stiffer barriers, the numerical analysis results are especially different from the experimental results. In other words, experimental results show a marked effect of the barrier becoming more pronounced at deeper depth. In contrary, numerical results show the effec-
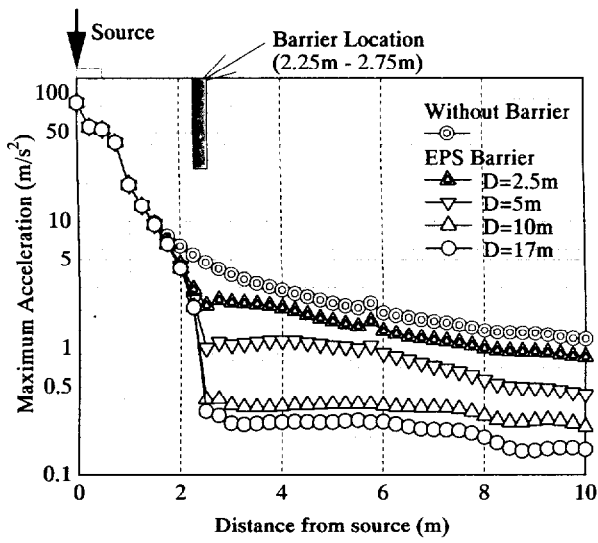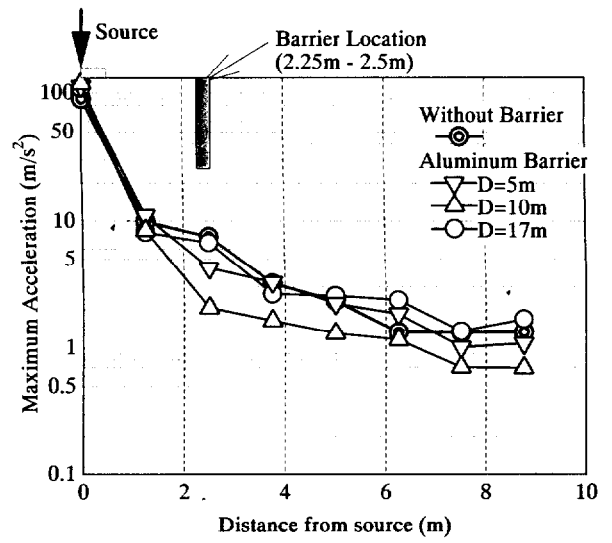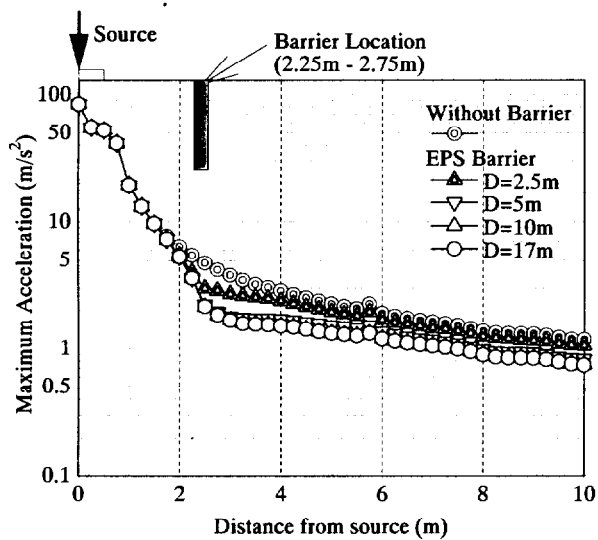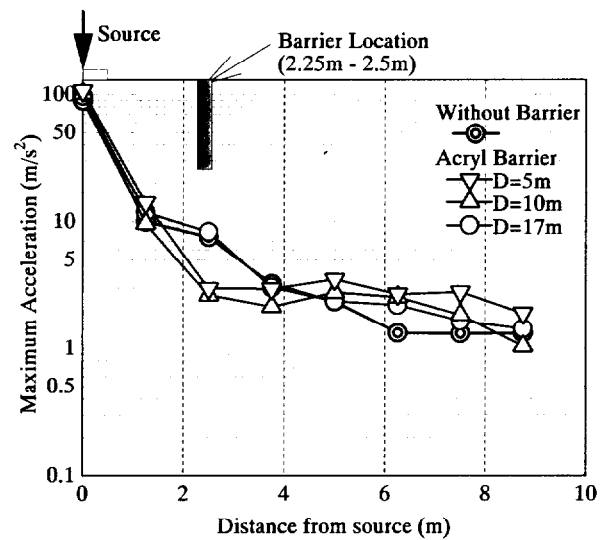
(i) Numerical results   (ii) Experimental results

(a) Aluminium barrier

(i) Numerical results   (ii) Experimental results

(b) Acryl barrier

(i) Numerical results   (ii) Experimental results
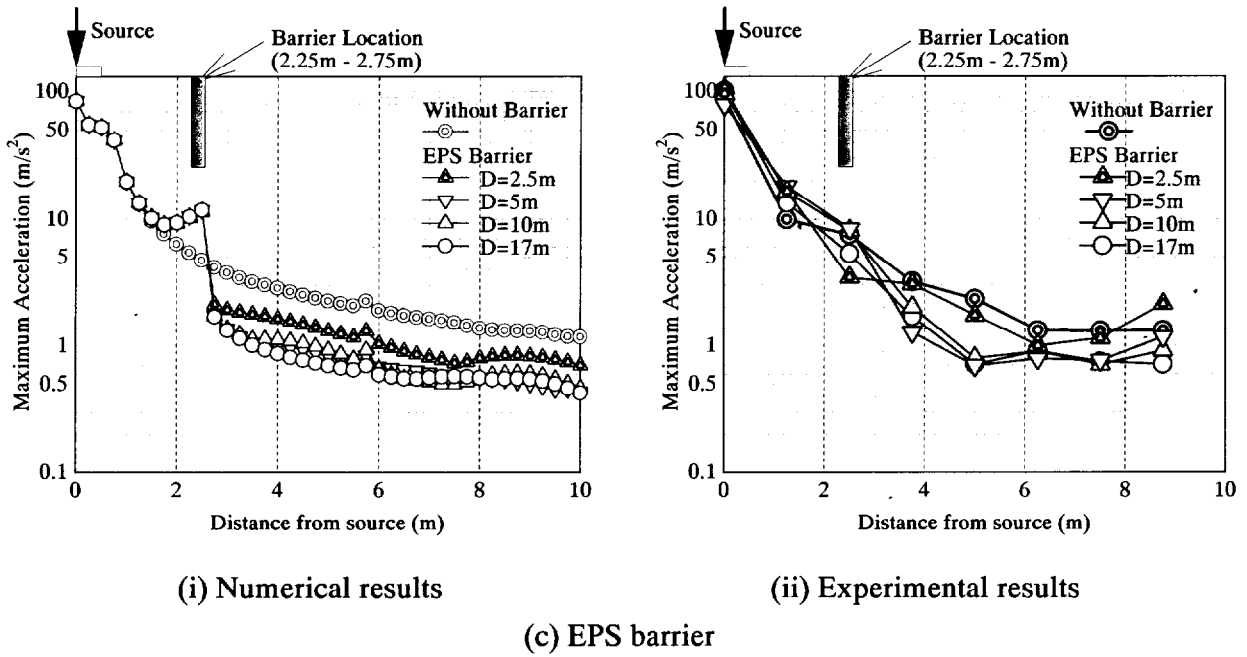
(c) EPS barrier

Figure A.5 The maximum acceleration decreases with distance from the vibration source for various barrier materials with different embedded depths.
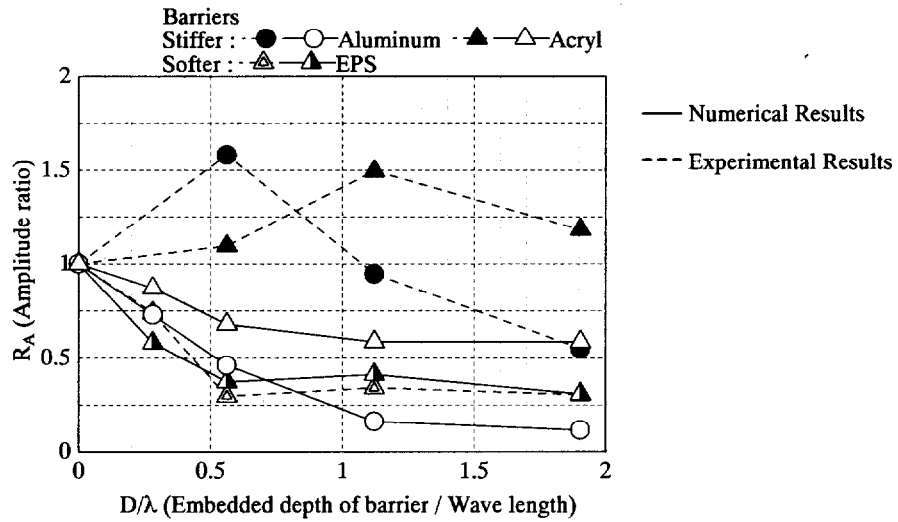

Figure A.6 Change in amplitude ratio R_A to embedded depth of barrier / wavelength D/λ for different barriers together with experimental results

tiveness in screening the vibration when these barriers are installed at a shallow depth. On the other hand, the effectiveness òf softer barrier in both experimental results and numerical results are the same for a wide range of D/λ. From stand point of predicting vibration reduction at the specific location, it can be said that the numerical analysis with softer barrier can predict the effectiveness in screening the vibration.

(2) Centrifugal Vibration Testing System

Figure A.7 shows attenuation of the root-mean-square acceleration with distance from vibration source for each input frequency. These figures show not only the experimental data but also the theoretical attenuation line predicted by Eq. (2.2) (Bornitz, 1931) along with the numerical data. As to predicted line, the solid black line represented attenuation of surface wave (n = 0.5), and the dashed and single-dotted gray line represented attenuation of body wave (n = 2). Although root-mean-square acceleration of numerical analysis results show considerable variations, these figures show some interesting associations. That is the numerical data almost fit with the experimental data and the theoretical attenuation line representing surface wave.

As for the effect of wave barrier on the reduction of vibration using FE analysis, Figs A.8 and A.9 show how the root-mean-square acceleration decreases with distance from the vibration source for two barrier materials; Aluminium (Fig. A. 8) and EPS (Fig. A. 9), with different embedded depths and with various input frequencies. Also data for the case without a barrier are also shown. As for Aluminium barrier, it is clear from this figure and Fig 5.16 that the calculated amplitude reduction in the deeper depth of wave barrier appears to be quite higher than the experimental results. In other words, Aluminium barrier becomes effective only when depth of wave barrier is larger. As for EPS barrier, there are two characteristic observations in accordance with the input frequencies. On one hand, in the case of higher frequencies (25 to 40 Hz), the calculated amplitude reduction appears to be higher than that using aluminium barrier, even if the length of barrier is shallow. On the other hand, in the case of lower frequencies (5 to 20 Hz), the calculated results really do not show any effect of barrier on the reduction vibration. Despite of the fact that the experimental results do not show any effect of barrier in reducing vibration, the numerical results clearly indicate that the Aluminium barrier in all frequencies and the EPS barrier in the high frequencies become effective. Moreover, in the case of input frequency which is more than 20 Hz, the magnification of vibration in front of the barrier and the reduction of vibration on the barrier are observed in the calculated results which are different from experiment results. Difference of amplification behavior behind and on the barrier in the numerical results and experimental results, might be due to slight difference in the consideration of lateral discontinuity in layer or at some boundary conditions in the experimental and numerical analysis conditions.
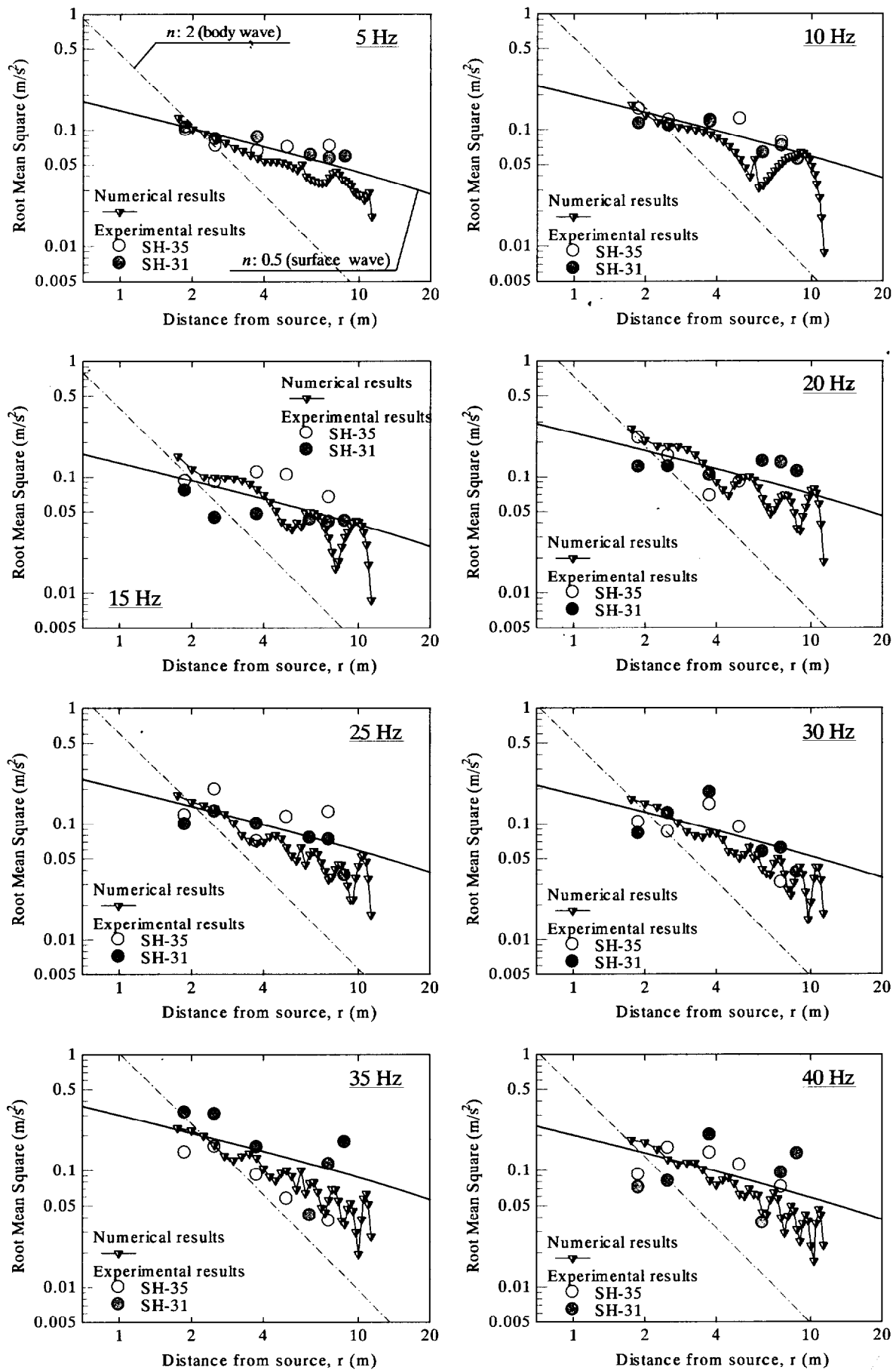
Figure A. 7 Attenuation of the root-mean-square acceleration with distance from vibration source together with experimental results
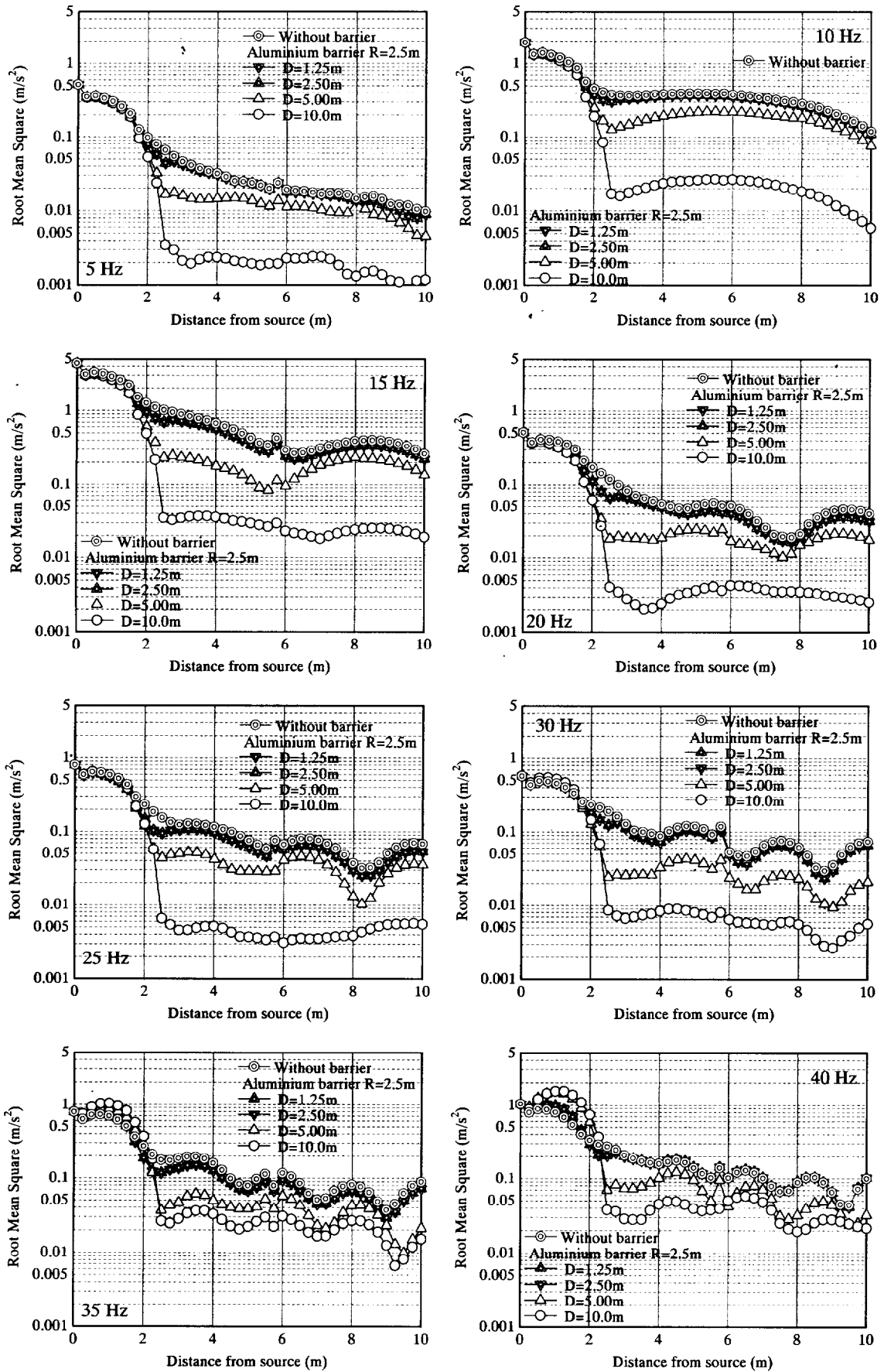
Figure A.8 Attenuation of the root-mean-square acceleration with distance from vibration source
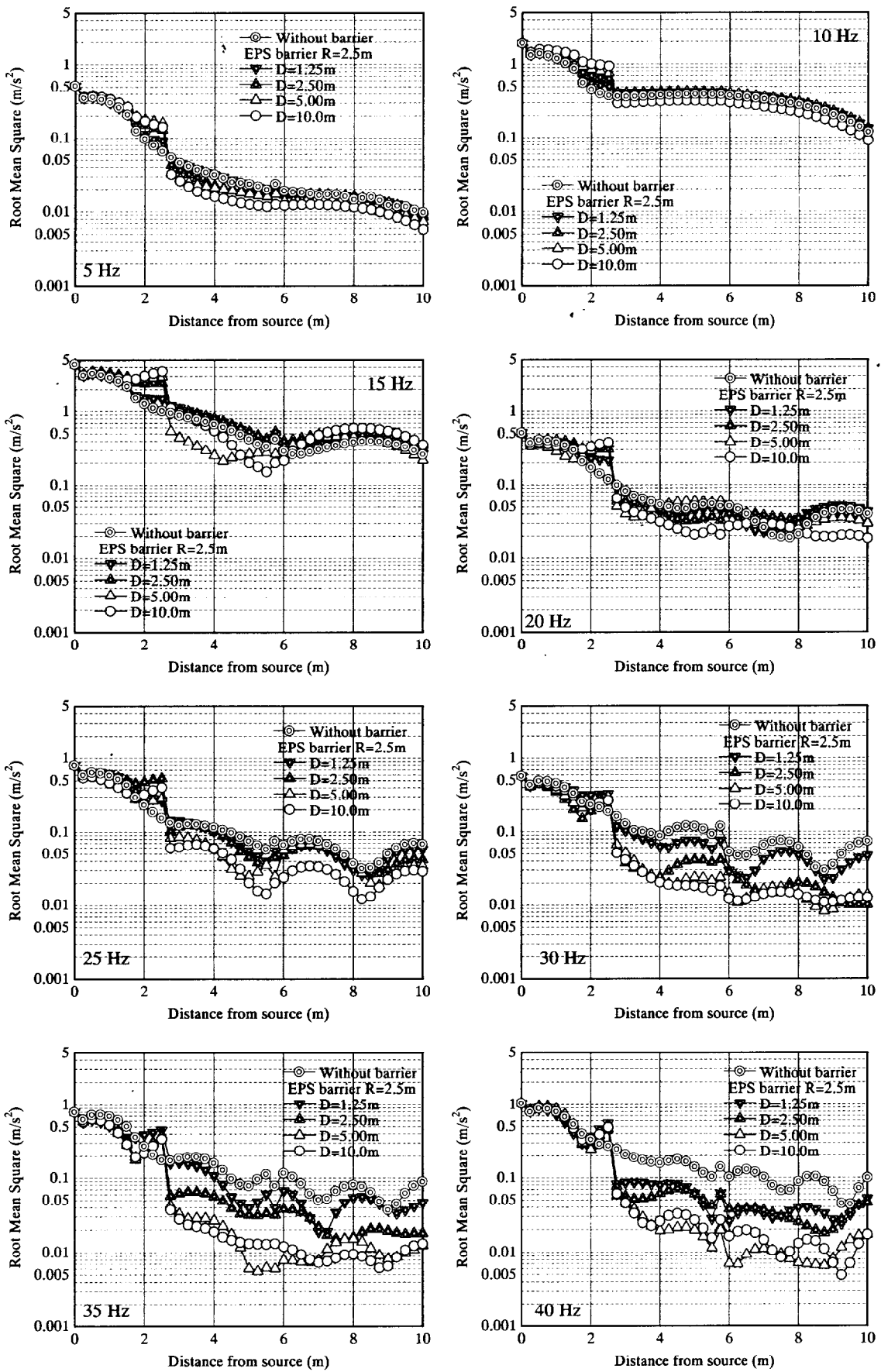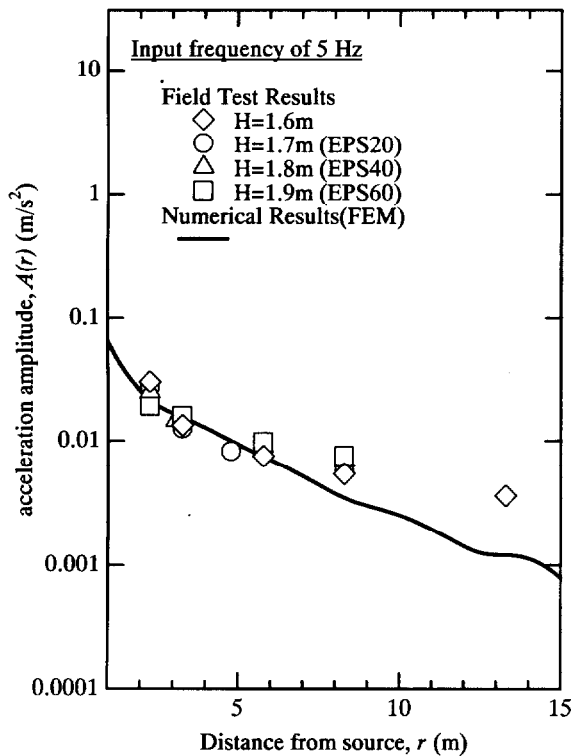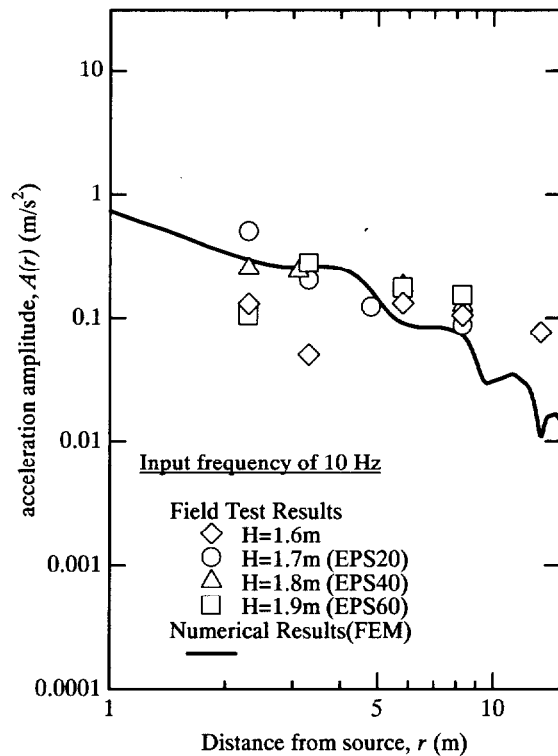for various embedded depths for the case of Aluminium barrier

Figure A.9 Attenuation of the root-mean-square acceleration with distance from vibration source for various embedded depths for the case of EPS barrier

A.4.2 Field tests

The calculated amplitudes and the observed amplitudes are summarized in Fig. A.10. The propagation of ground vibration from vibration exciter in the case of field test is very complicated in comparison to those shown in the centrifuge model test results in Chapters 4 and 5. Particularly, the ground vibration shows complicated wave propagation phenomena at different kinds of layers, in different soil conditions and its surrounding. However, the amplitude attenuations of the observed and calculated results are found to be consistent in this figure. Figure A.11 show the calculated vibration amplitudes with and without wave barrier, for various input frequencies and various wave barriers (EPS20, EPS40, and EPS60). In order to facilitate the comparison of the test data, the vibration amplitudes are normalized by the value of calculated input accelerometer. Figure A. 12 shows the effect of wave barrier on reduction of vibration. The reduction efficiency is expressed in term of the relative vibration reduction level, L_{rv}. Behind the barriers, a substantial reduction of the amplitudes can be observed in both the measured and the calculated cases. It is found that calculated results have a tendency to disperse the relative vibration reduction level. However, if the mean values are considered the points from the numerical analysis results are in good agreement with the experimental results.
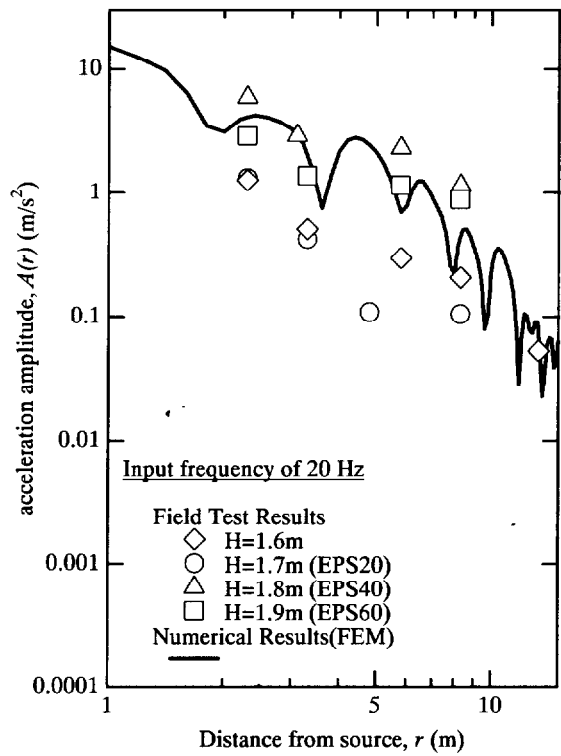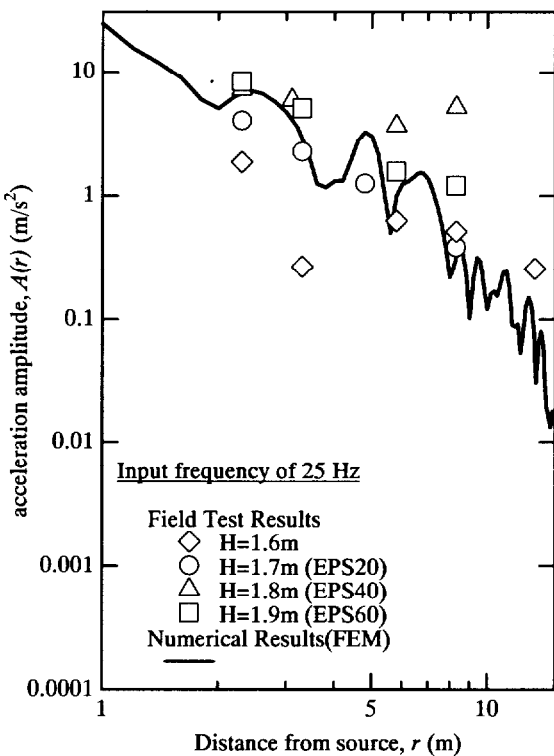

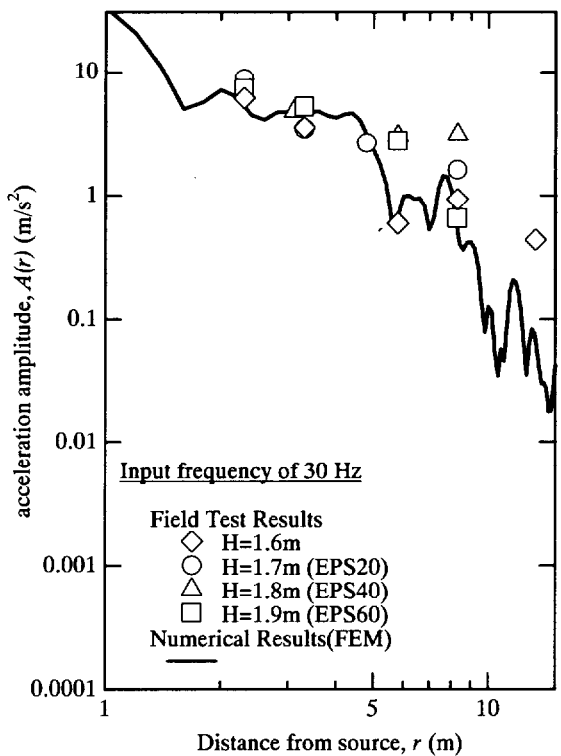(i) Input frequency of 5 Hz   (ii) Input frequency of 10 Hz
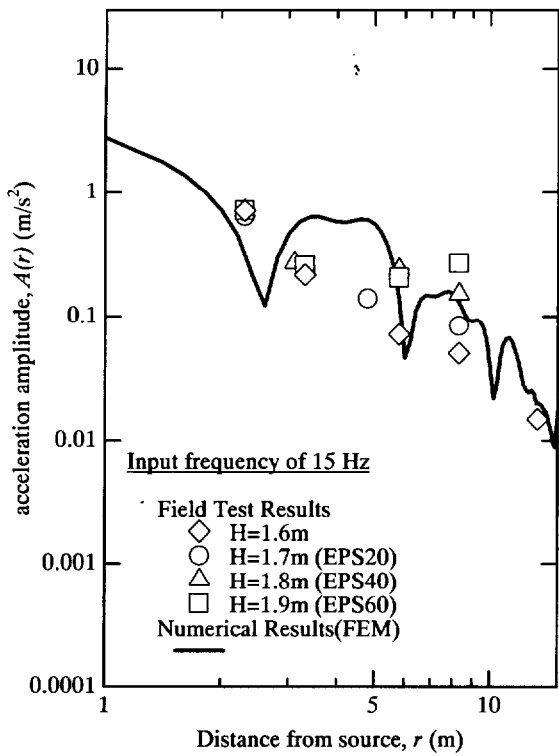
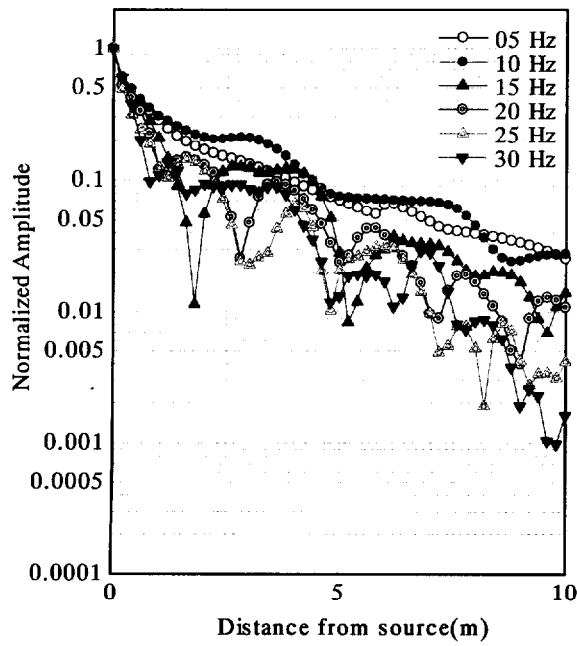(iii) Input frequency of 15 Hz

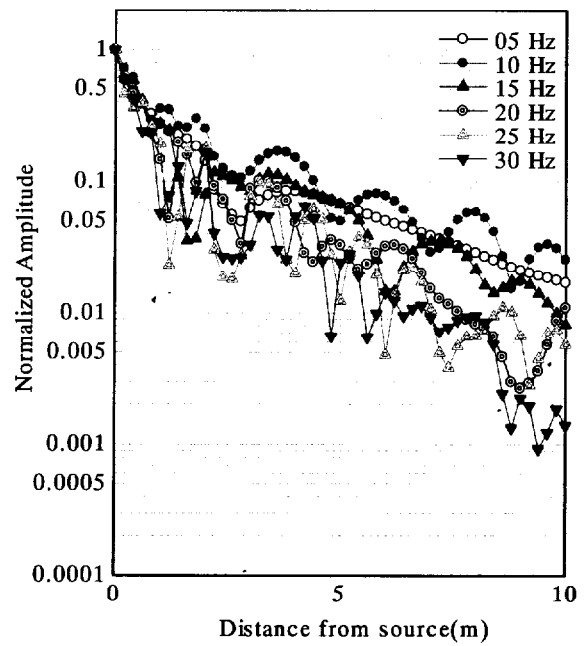(iv) Input frequency of 20 Hz

(v) Input frequency of 25 Hz
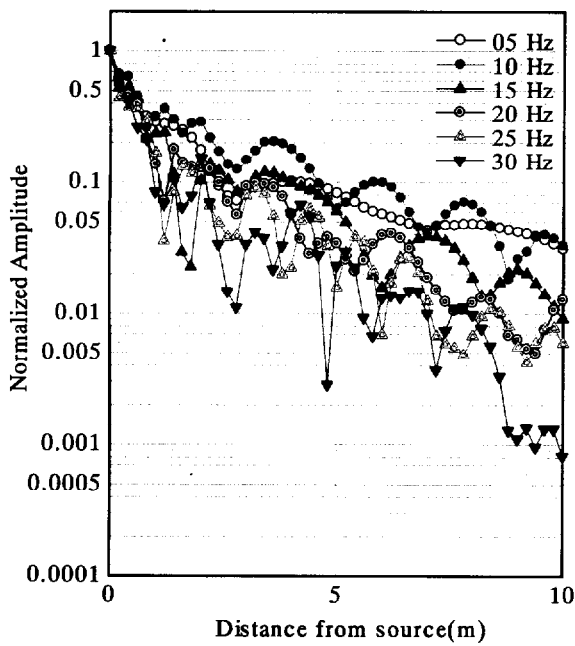
(vi) Input frequency of 30Hz

Figure A.10 Attenuation of the root-mean-square acceleration with distance from vibration together with experimental results
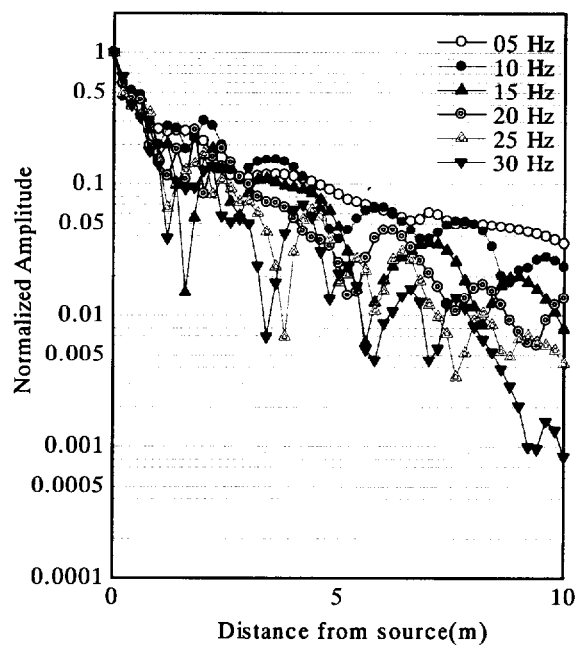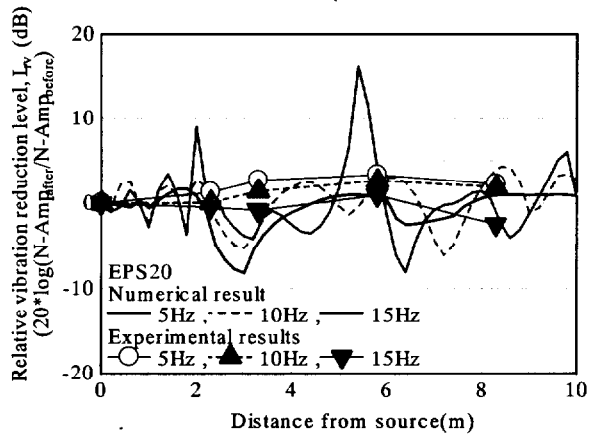
(i) without barrier
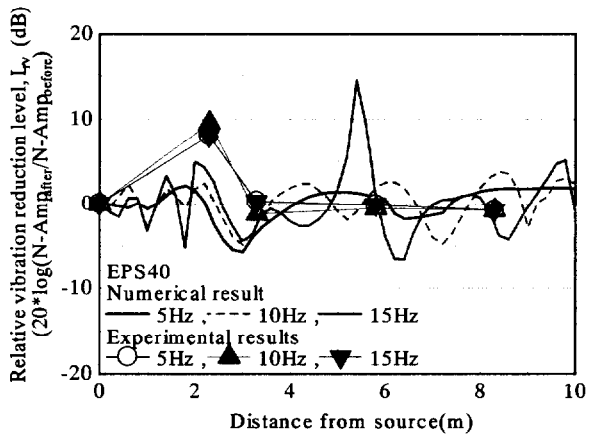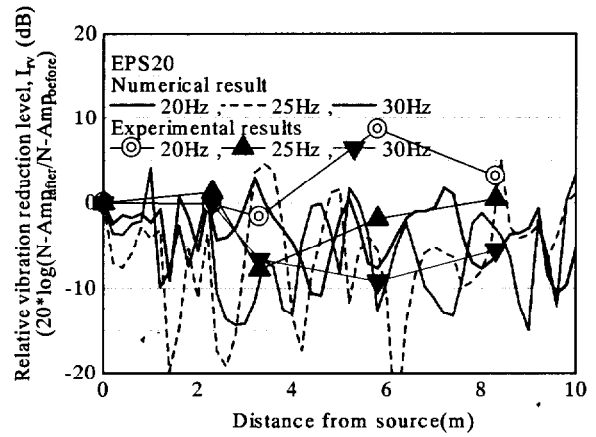
(ii) with EPS20 barrier

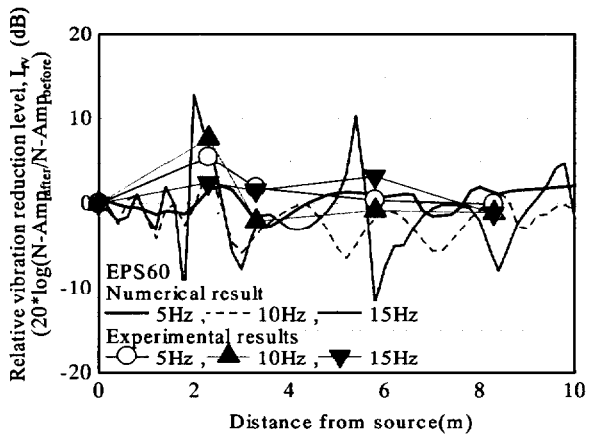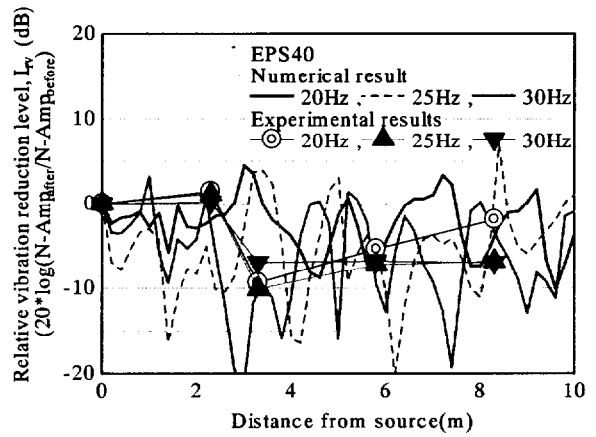(iii) with EPS40 barrier

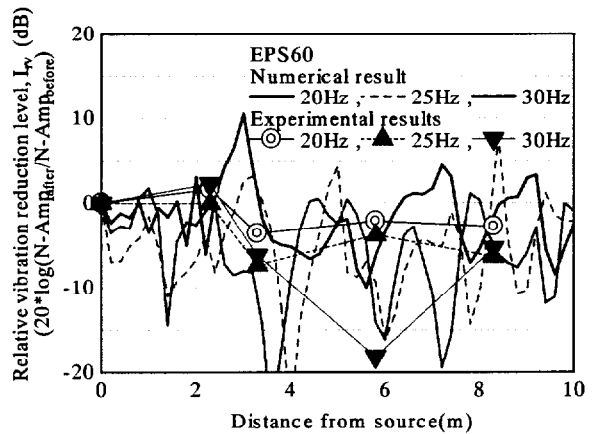(iv) with EPS60 barrier

Figure A.11 Amplitude-decay curves

Figure A.12 Attenuation of the relative reduction level with distance from vibration source for various barriers together with experimental results

A.5 SUMMARY

In order to estimate wave propagation and vibration reduction installing the wave barrier by numerical analysis, the consistency between the results of centrifuge model / field test and the results of numerical analysis was described in this appendix. The major consequences of interest are as follows;

1. Centrifuge model test

- In the case of the impact point loading, the amplitude attenuation of the calculated and the observed results are in good agreement. However, there are noticeable discrepancies between the calculated and the observed waveforms after the first wave. It could be said from this point that the predicted waveforms using numerical analysis would differ from the experimental results.

- In the case of the cyclic loading, although root-mean-square acceleration of numerical results shows considerable variations, numerical data almost fit with the experimental data and the theoretical attenuation line of surface wave.

- With regard to the effect of wave barrier on the reduction of vibration using FE analysis, there is a tendency for each material to find opposite behavior. Numerical analyses for the case of stiff barriers (Aluminium and Acryl) seem to give overestimated vibration reduction value. In contrast to this, in the case of softer barrier (EPS), the values obtained from the numerical analyses and experimental data are in good agreement. From stand point of predicting vibration reduction at the specific location, it can be said that the numerical analysis with softer barrier can predict the effectiveness in screening the vibration.

2. Field test

- As for wave propagation without barrier using FE analysis, the amplitude attenuation suggests a general tendency to share similarities between the observed and calculated results.

- With reference to the effect of wave barrier in reducing the vibration using FE analysis, it is found that calculated results have a tendency to disperse the relative vibration reduction level. However, if the mean values are considered the point from the calculated curves are in good agreement with the observed data.

As far as amplitude attenuation in the case of without barrier is concerned, calculated results approximately agree with the observed results. However, when it comes to investigate the effect of wave barrier on the reduction of vibration, the mechanism of wave propagation phenomena and numerical technique of boundary condition await future studies.

A.6 REFERENCES

Lysmer, J., Udaka, T., Tsai, C. -F., and Seed, H. B. (1975): "FLUSH a computer program for approximate 3-D analysis of soil-structure interaction problems," *Earthquake Engineering Research Center*, Report No. EERC 75-30, College of Engineering, University of California, Berkeley, CA.

Yoshioka, O., and Ashiya, K. (1990): "Attenuation properties of vibrator-induced ground vibrations passing through sheet pile in earth," *Railway Technical Research Institute Report (RTRI Report)*, Vol. 4, No. 8, pp. 51-58 (in Japanese).